Mécanismes de développement des cellules épendymaires : origine et lignage des cellules épendymaires dans le cerveau des mammifères

Marie Daclin

THÈSE DE DOCTORAT

de l'Université de recherche Paris Sciences et Lettres
PSL Research University

Préparée à l'Institut de Biologie de l'Ecole Normale Supérieure de Paris, France

Mechanisms of Ependymal Cell Development

Mécanismes de Développement des Cellules Ependymaires

Origine et Lignage des Cellules Ependymaires dans le Cerveau des Mammifères

Ecole doctorale n°158

Cerveau, Cognition et Comportement

Spécialité NEUROBIOLOGIE DU DEVELOPPEMENT

COMPOSITION DU JURY :

Mme. METIN Christine
Institut du Fer à Moulin,
Présidente

M. RAINETEAU Olivier
Stem Cell and Brain Research Institute,
Rapporteur

M. TISSIR Fadel
UCL Institut de Neurosciences,
Rapporteur

M. LIVET Jean
Institut de la Vision,
Examinateur

M. BAFFET Alexandre
Institut Curie,
Examinateur

Soutenue par Marie DACLIN
Le 28 juin 2018

Dirigée par **Nathalie SPASSKY**

Unité CNRS UMR8197 / Inserm U1024
Equipe : Rôle des Cils dans le Développement

ENS | PSL

Mecanisms of Ependymal Cell Development

Origin and Lineage of Ependymal Cells in the Mammalian brain

Marie DACLIN

PhD Thesis

Thesis Director: Dr. Nathalie SPASSKY

Institut de Biologie de l'Ecole Normale Supérieure, Paris, France

Paris Sciences et Lettres

Doctoral School of Université Pierre et Marie Curie ED3C: Cerveau, Cognition et Comportement

Laboratory unit CNRS UMR8197 / Inserm U1024

Team of Cilia Biology and Neurogenesis

Public Defense intended on Thursday, June 28th 2018

Composition of the jury:

President: Dr. Christine METIN

Reviewer: Dr. Fadel TISSIR

Reviewer: Dr. Olivier RAINETEAU

Examiner: Dr. Jean LIVET

Examiner: Dr. Alexandre BAFFET

Supervisor: Dr. Nathalie SPASSKY

À Sylvie, Véronique et Marc

À Pascal

« Dans la vie, rien n'est à craindre, tout est à comprendre »

Marie Curie

TABLE OF CONTENTS

ABSTRACTS

ENGLISH ABSTRACT

In the Mammalian brain, ependymal cells are post-mitotic glial cells lining the walls of all ventricular cavities. They form a monolayer of polarized cells at the interface between the brain and the cerebrospinal fluid (CSF). Their motile cilia are dynamic cytoskeleton structures anchored to basal bodies at the apical cell surface. Motile cilia beat synchronously to tightly orient the flow of CSF throughout the ventricles. Defects in cilia or ciliated cells are known to cause series of serious disorders such as hydrocephalus, ciliopathies or tumorigenesis. Moreover, ependymal cells insure critical absorptive and secretory functions between the brain and the CSF and are thus essential to maintain homeostasis of neural circuits and proper brain integrity. Interestingly, they also take a crucial part in the adult neurogenic niche located in the subventricular zone (SVZ) of rodents. They surround the adult neural stem cells (NSCs) so that ependymal cells and adult NSCs form pinwheel-like structures. This specific organization facilitates the propulsion of CSF by ependymal cells on the primary cilium of adult NSCs, and therefore maintains neurogenesis. NSCs in the adult brain are a subtype of astrocytes. Both astrocytes and ependymal cells originate from embryonic NSCs so-called radial glial cells around embryonic day 15.5 (E15.5). However, little is known about the detailed lineage of these cells during brain development and neurogenesis even though their role has proven paramount. In this project, we address the origins of ependymal cells and astrocytes in an effort to reach better understanding of brain development. We first show that ependymal progenitors do not migrate after their last division. This allows us to apprehend ependymal cell lineage through *in vivo* electroporation and recently developed lineage-tracing techniques. We find by these approaches that ependymal cells can be generated through both symmetric and asymmetric cell divisions during brain development. We uncover that asymmetric cell division of

ependymal progenitors also gives rise to astrocytes in the SVZ. Most interestingly, we identify these astrocytes as actual NSCs of the adult neurogenic niche. On the whole, this study provides major insights in ependymal cell lineage and highlights a new role of ependymal cell development in participating to adult neurogenesis. In the long term, these findings might help in raising new therapeutic perspectives for neurodevelopmental disorders.

FRENCH ABSTRACT

Les cellules épendymaires multiciliées sont des cellules gliales post-mitotiques qui recouvrent les parois des cavités ventriculaires du cerveau des Mammifères. Elles forment une monocouche de cellules polarisées à l'interface entre le cerveau et le liquide céphalo-rachidien (LCR). Leurs cils motiles constituent des structures dynamiques de cytosquelette qui viennent s'ancrer à des corps basaux à la surface cellulaire apicale. Ces cils battent de manière synchronisée afin d'orienter avec précision le flux de LCR dans les ventricules cérébraux. Des défauts dans la structure des cellules ciliées ou des cils eux-mêmes donnent lieu à de graves phénotypes et maladies tels que l'hydrocéphalie, les ciliopathies et le cancer. Les cellules épendymaires assurent également des fonctions critiques d'absorption et de sécrétion entre le cerveau et le LCR. Cela en fait des acteurs essentiels au maintien de l'homéostasie des circuits neuraux ainsi qu'à la préservation de l'intégrité du cerveau. Par ailleurs, elles prennent part à la niche neurogénique adulte située dans la zone sous-ventriculaire (SVZ) chez les rongeurs. Elles encerclent les cellules souches neurales adultes de manière à ce que cellules épendymaires et cellules souches forment une structure de « pinwheel » (en forme de moulin, de roue). Cette organisation bien spécifique facilite la propulsion du LCR par les cellules épendymaires sur les cils primaires des cellules souches, ce qui permet la neurogénèse adulte. Les cellules souches neurales du cerveau adulte sont un sous-type d'astrocytes. Les astrocytes ainsi que les cellules épendymaires sont produites par les cellules souches embryonnaires du cerveau appelées cellules de glie radiaire, au stade

embryonnaire E15.5. Bien que le rôle majeur de ces deux types de cellules ait été démontré, le lignage détaillé de ces deux types cellulaires reste à ce jour mal connu. Nous étudierons ici les origines des cellules épendymaires et des astrocytes pour mieux comprendre les mécanismes de développement du cerveau, mais aussi dans la perspective d'ouvrir de nouvelles pistes thérapeutiques pour les maladies neuro-développementales à plus long terme. D'une part, nous avons établi que les progéniteurs épendymaires ne migrent pas après leur dernière division. Cela nous permet d'appréhender le lignage épendymaire par la méthode d'électroporation *in utero,* ainsi que par des méthodes de suivi de lignage développées récemment. Ces approches ont montré que les cellules épendymaires pouvaient être générées par division symétrique et asymétrique au cours du développement du cerveau. Nos résultats ont aussi révélé que la division asymétrique des progéniteurs épendymaires donnait naissance à des astrocytes dans la SVZ. Nous avons de plus identifié ces astrocytes comme étant les cellules souches neurales de la niche neurogénique adulte. Ainsi, ces travaux constituent un progrès significatif dans la compréhension du lignage épendymaire, et révèlent que le développement des cellules épendymaires joue un rôle d'importance dans le maintien de la neurogénèse adulte.

ACKNOWLEDGEMENTS

Je dédie ma thèse à Sylvie, Véronique et Marc. Merci infiniment de m'accompagner sans réserve dans tous mes projets et mes choix avec autant d'amour et de confiance.

Je dédie aussi ma thèse à Pascal, la personne qui me rend la plus heureuse en ce monde.

***

One thing I've learned during these three years is that a PhD is everything but a lonely experience. Beyond the amazing scientific training I have received, I have also been very lucky to be surrounded by fantastic people with astonishing human qualities; that is why I have a lot to be thankful for.

My gratitude goes to Nathalie Spassky, who has welcomed me in her lab. Thank you Nathalie for your guidance and for investing so much energy in me all along these years. Thank you for your patience and for sharing so many scientific theories and reflexions with me. You have undoubtedly passed onto me your passion and enthusiasm for science. Thank you for providing me with help and assistance in the lab, I am very grateful that you allowed me to achieve my PhD.

Thank you Gonzalo for working alongside with me on these projects. I am incredibly lucky to have met you, because you are as an amazing scientist as you are a great and generous friend. I am glad I had the opportunity to work side by side with you. I am also in your eternal debt for sharing your unique interpretation of great songs with us. No doubt that one of them in particular, filmed in an elevator, will remain a classic!

Thank you Pauline for making life in the lab so pleasant. Your original ideas and efficiency to optimize experiments have inspired me more than you can imagine. Your practical mind has brought huge benefits on this project and taught us a lot. Thank you for always being available as a colleague but as a friend too. With you and Gonzalo, I could never imagine a better team to work with.

Thank you Alexia for being my office neighbour during more than 3 years! Thank you for always being so enthusiastic and full of initiatives. Thank you for tirelessly helping and advising me both on scientific and personal concerns. Your driving energy is essential to the cheerful atmosphere of the 7th floor that we all benefit from. Thank you for bringing up mind-blowing conversational topics during afterworks, for bringing extreme workout exercise into our life (and hereby introducing me to my physical limits), for generously sharing with us your most vital ownings (mouse disguise, red lipstick, music playlists, movies, etc.), for being the best interpret of Disney

songs and the best dancer of Madison. I could not imagine life in the lab without you mocking my chocolate addiction. Thank you for being a fantastic friend to me in all circumstances, your care is priceless to me.

Thank you Olivier for joining our team. Your kindness, motivation and positive spirit are a real inspiration! Thank you for sharing valuable scientific interests and exciting ideas, and for planning great afterworks, week-ends and lab-retreats with us. Thank you for being my running coach as well as for feeding me cookies on the side.

Thank you Marion for being the most generous, listening and kind person I know. You have helped me during my PhD in so many ways that listing them all would just take a whole other thesis. You have taught me so much on how to improve experimental techniques, dissections, how to experiment on mice and how to get better organized. Thank you for helping me with ordering, genotyping and maintaining transgenic mice in good health and many other experiments during these years. I know I could not have finished my PhD without you.

Thank you Shihav for providing a huge and valuable contribution in all bioinformatic aspects of this project. Your help and your expertise are most appreciated and have made this project possible.

Thank you also to all the other members of the Spassky lab: Alice, Nathalie D, Adel, Aurélien, Ronaël, Raphaël and Ayush. From both scientific and personal perspectives, you have each generously offered your help at all times unreservedly and mentored me in your own special way. Your humour, care, trust and respect are most precious to me. Thank you for the amazing atmosphere in the lab, my PhD will remain a unique positive experience thanks to you.

Thank you Alex and Ioana, for I had the chance to spend some valuable time with each of you individually. These privileged moments mean a great deal to me, just as you two lovely people do.

Thank you to the other 7th floor Shenanigans! I am very grateful for countless joyful afterworks we spent together, which made life so beautiful. Isabel, thank you for inspiring me both from scientific and personal points of view. Abdoul, thank you for your valuable help at work and your sense of humour, it makes up for all the chocolate you stole from our lab (yes, it is *finally* written down!). Fan Di, Orthis, and Franck, thank you for your help and for being great friends during my PhD.

Thank you to all the people from the 7th floor at IBENS (from the teams of Sonia Garel, Jean-François Brunet and Xavier Morin) for constant scientific advice and help, and for maintaining such a nice atmosphere at work.

Thank you to all the people of IBENS who have contributed to my PhD project as well: from the administration, the imaging platform and the animal facility, especially Amandine. Thank you Caroline for teaching and helping me with my mice surgeries in the L2 platform. I know for a fact that experiments do not succeed as well without your good vibes.

I address my gratitude to our collaborators: Jean Livet, Solène Clavreul, Karine Loulier and Auguste Genovesio.

Thank you to Olivier Raineteau, Fadel Tissir, Alexandre Baffet, Jean Livet and Christine Métin for accepting to be part of the jury of my PhD.

Thank you Magdalena Renner and Jürgen Knoblich (IMBA, Vienna, Austria), Timm Schlegelmilch and Francesca Peri (EMBL, Heidelberg, Germany) and Pierre Pouget (ICM, Paris, France) for supervising my previous internships. I am most grateful for I have learned a lot during each internship, and all of you have encouraged me to pursue my education with a PhD.

***

Enfin, merci à mon entourage, famille et amis, pour votre affection et votre soutien inconditionnels. J'ai conscience qu'avoir autant de proches aussi exceptionnels est une chance rare.

Virgilia, tu as ma plus immense gratitude. Aux moments les plus critiques de ma thèse, tu m'as encouragée, tu m'as redonné confiance, tu n'as jamais cessé un instant d'être à mes côtés. J'ai une chance incroyable d'avoir une amie aussi extraordinaire que toi. Marion, toi aussi tu as été celle sur qui j'ai pu compter, non seulement durant ces trois années de thèses mais durant toute ma vie, et je t'en suis infiniment reconnaissante. Les conseils et encouragements que tu m'as dispensés sont d'une valeur inestimable à mes yeux.

Un immense merci à Sophie, mais aussi à Catherine et à Laëtitia d'avoir été et d'être aussi formidables. Votre appui dans les bons comme les mauvais moments de ces trois ans (mais pas seulement) compte énormément pour moi. Merci Serge pour ton mentorat en recherche, et ce depuis si longtemps. Je te suis particulièrement reconnaissante car tu m'as transmis cette curiosité pour les sciences et la recherche lorsque tu t'y es engagé toi-même (peut-être même inconsciemment), et tu es resté un modèle pour moi toutes ces années.

Eric, merci infiniment de m'avoir insufflé la curiosité et le goût des sciences dès mon plus jeune âge, par des histoires, des sorties au musée, de l'aide aux devoirs (et ce contre vents et marées !), et surtout des discussions passionnées autour de la presqu'île de Gâvres. Merci encore Eric, Maï et Madeleine pour votre tendresse, votre patience à mon égard, et merci et de n'avoir jamais douté de moi, y compris lorsque j'ai entrepris ma thèse.

Nad, merci d'être mon guide et ma bonne étoile tout au long de ma vie, j'ai une chance inouïe d'avoir une marraine aussi exceptionnelle. Ta présence durant la préparation de ma thèse m'a considérablement aidée.

Pierre, merci d'avoir répondu présent et de m'avoir généreusement offert une assistance technique aussi efficace et qui s'est révélée indispensable à mon travail de thèse. S'il y a bien un point sur lequel je regrette de ne pas te ressembler, c'est bien ton talent informatique. Pour le reste… (!)

Anne, Nicole et Patrick merci pour votre présence et votre bonne humeur quotidiennes, vous m'accompagnez durant toute ma vie, la thèse n'y faisant pas exception, et je ne sais comment vous remercier pour votre immense contribution à mon bonheur.

Merci Sylvie, Baptiste, et Aude de m'avoir autant soutenue pendant ma thèse ; vous compter parmi les membres de ma famille me rend infiniment heureuse.

Alexis, je te remercie pour ta bonne humeur et ton soutien durant ces trois ans, c'est vraiment un plaisir de t'avoir pour beau-frère !

Pierre-Emmanuel, merci pour tes précieuses recommandations durant mon parcours, et ce depuis le début de mes études supérieures. Merci pour ta gentillesse, le temps que tu m'as accordé, et la confiance que tu as placée en moi avant même tout autre chercheur !

Merci à mes deux filleuls Pierre et Madeleine ; voir quelles belles personnes vous devenez me remplit de joie !

Mes remerciements et toute mon affection vont évidemment aussi à Alexandra et Jérémy ainsi que tous mes amis que je ne peux pas tous citer mais qui ont été là tout au long de ces trois années de thèse pour me donner le sourire !

Pour finir, j'adresse toute ma gratitude et mon respect à Michel Campano, Frédéric Michel, Ingrid Jamin, Maxime Plaize et Thierry Bigot sans qui ce travail n'aurait pu être achevé. Merci à vous pour tout votre investissement. Merci également à Jean-Guilhem Xerri pour l'aide que tu m'as apportée.

INTRODUCTION

CHAPTER 1: BRAIN DEVELOPMENT

I- FORMATION OF THE MAMMALIAN NEURAL TUBE[1, 2]

1) Neural induction

After fertilization, the mammalian oocyte is totipotent, which means that it can give rise to all the different cell types of the organism. First, it divides to give rise to 2 then 4 apparently identical cells. The cleavage plan crosses the entire cells at this primitive phase. Soon, the cells forming the embryo will acquire a more specialized potency to give rise to distinct though various structures. At this early developmental stage, the embryo is called Blastocyst and forms two different structures: an inner cell mass which contains pluripotent cells and therefore will form the embryo itself, surrounded by a layer of outer cells that will contribute to the future placenta and extra-embryonic membranes. The Blastocyst is implanted within the wall of the uterus and starts to elongate. Then, as embryogenesis proceeds, gastrulation begins. It is a phase of intense cellular movement and reorganization of the embryo. Cells engage further in differentiation pathways and three basic layers are observed: the ectoderm, the mesoderm and the endoderm. At this stage, the cells are multipotent; one cell can only give rise to some specific discrete cell types. The mesoderm involutes in a cavity named blastocoel inside the embryo, in order to re-localize right beneath the ectoderm and induce the ectoderm above into a neural plate. This internalization is clearly visible at the surface of the elongated embryo since it forms a primitive streak and a primitive pit. During neurulation, the neural plate rolls up into a tube so-called the neural tube (Figure 1 and 2)[3].

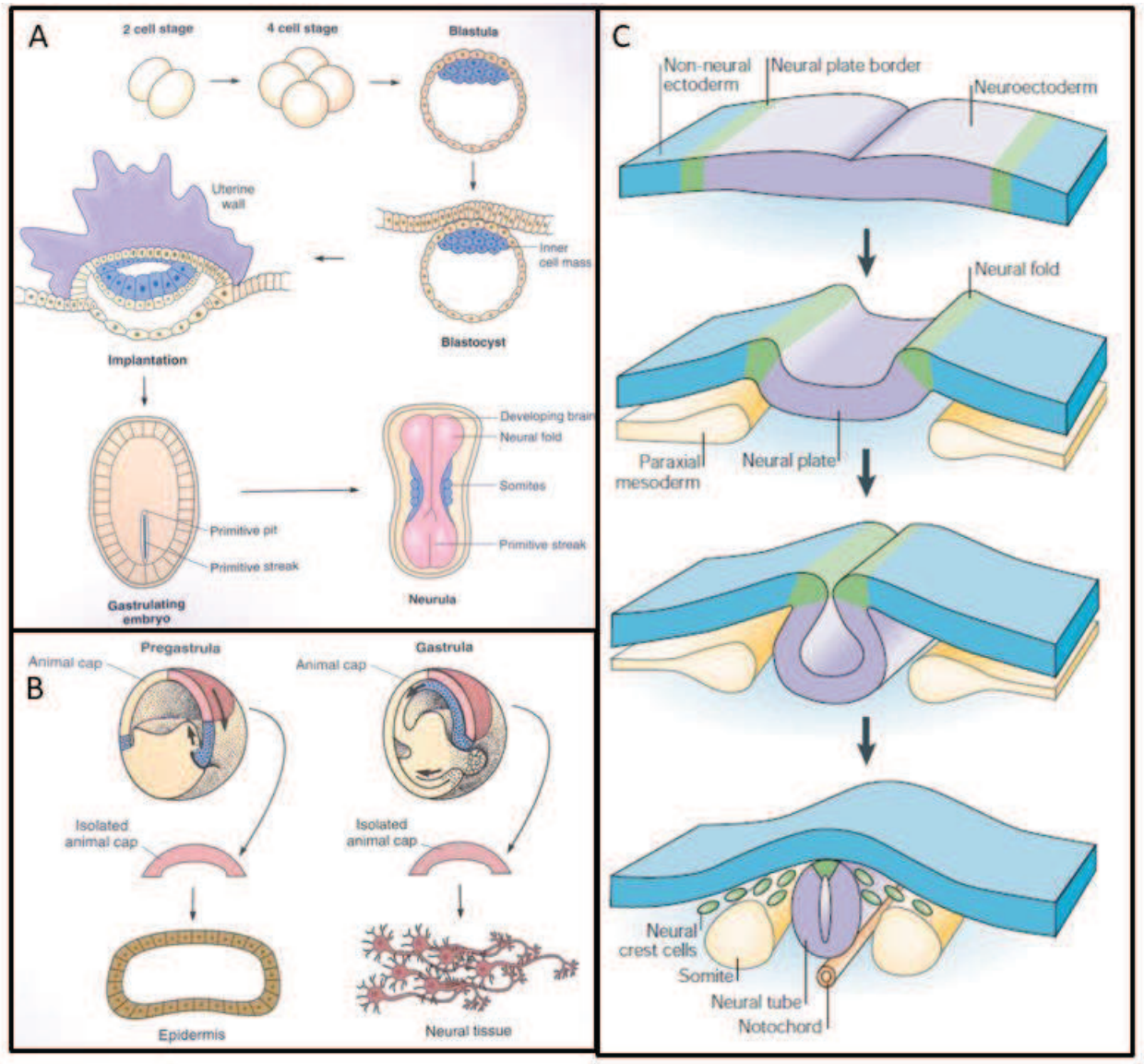

Figure 1: Scheme of the development of the neural tube.
A- Development of the human embryo. **B**- Gastrulation specifies neural tissue from the ectoderm (here Amphibian model system). **C**- Formation of the neural tube from the neural plate. Adapted from Sanes et al. 2011 and Gammill and Bronner-Fraser 2003[1,4].

The neural tube originates the brain and spinal cord in the Mammalian nervous system. At the region of the fusion of the neural tubes, a population of cells called the neural crest migrates away. Meanwhile, the mesoderm right underneath the neural tube assembles in a structure named the notochord. In Vertebrates, the region of the neural tube defines the dorsal-ventral polarity, with the neural tube being on the dorsal side of the embryo. The cavity inside the neural tube develops into a complex ventricular system filled with liquid called the cerebrospinal fluid (CSF).

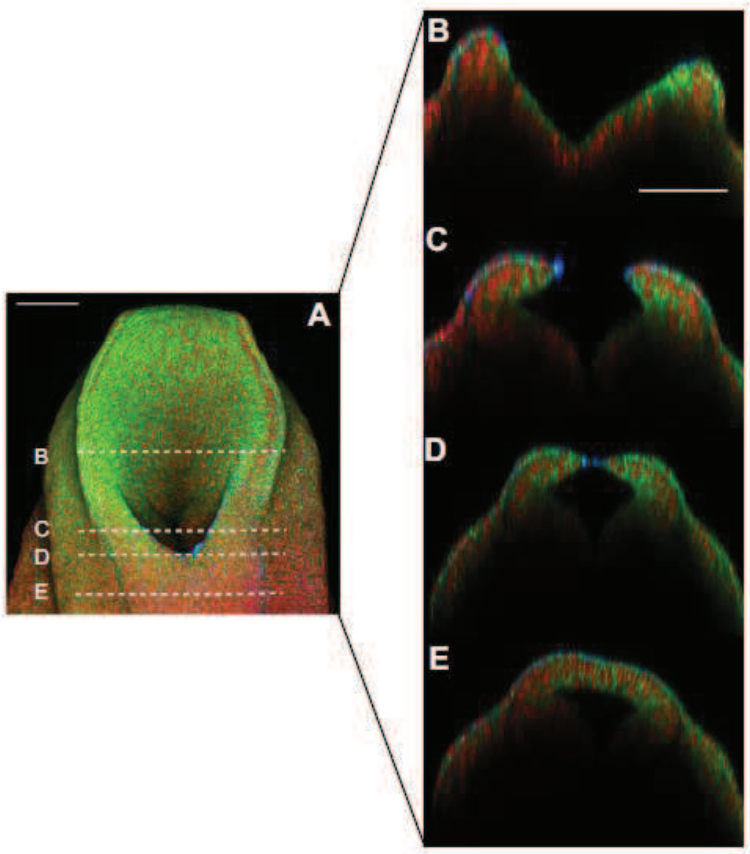

Figure 2: Closure of the mouse neural tube.
A- Wholemount staining using CellMask (green) to label cell membranes, phalloidin (blue) to label F-actin and DAPI (red) to label nuclei. **B to E-** Optical sectioning across different levels. From Nikolopoulou et al., 2017[3].

From a molecular perspective, neural induction is triggered by the repression of the Bone Morphogenic Proteins (BMP) pathway in the ectoderm by secreted factors from the mesoderm[5]. By default, BMP signalling is active in the ectoderm. More specifically, BMP is part of the wider family of Transforming Growth Factor β (TGFβ) and binds to a heterodimeric transmembrane receptor of ectodermic cells. The two subunits (I and II) of the receptor assemble in the presence of their ligand and an intracellular signal is transduced. When active, the subunit II of the TGFβ receptor is a kinase and phosphorylates the subunit I. The phosphorylated receptor is able to recruit Smad proteins and phosphorylate them as well. The Smad complex of proteins is then translocated inside the cell nucleus and binds to genes (Figure 3).

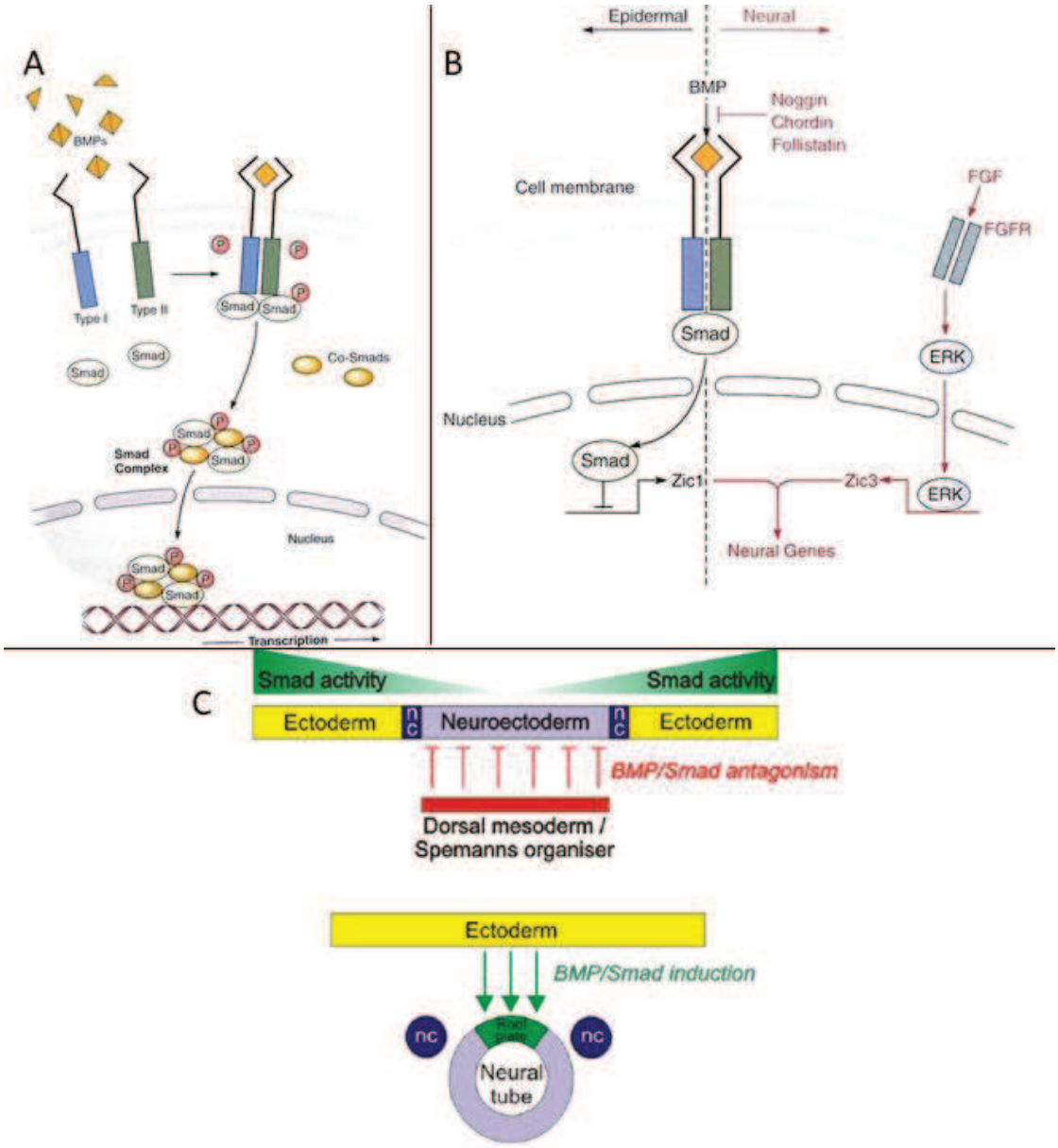

Figure 3: Scheme of the BMP signalling pathway.

A- BMP signalling mechanism. **B- and C-** BMP and its repressors regulate epidermal and neural fate. From Sanes et al. 2011 and Hegarty et al. 2013 [1.5]

Notably, Smad complex represses the activity of pro-neural transcription factors Zic1 and Zic3. Eventually, active BMP signalling cascade of the ectoderm differentiates into epidermis. Nevertheless, in the ectodermic region in contact with the mesoderm, BMP signalling is repressed by Noggin, Chordin and Follistatin factors secreted by the mesoderm. The expression of Zic1 and Zic3 transcription factors thus results in the activation of pro-neural genes. Sox genes are also regulated by the BMP signalling pathway and play a role in the

development of the neural tube. The Fibroblast Growth Factor (FGF) signalling is another neural inducer: the association of FGF with its homo-dimeric receptor which activates ERK pathway. In turn, ERK is translocated inside the nucleus to activate the expression of Zic3 and promote neural differentiation. Interestingly, the antagonism of BMP signalling is necessary and sufficient for neural induction in Vertebrates.

2) Regionalization of the nervous system

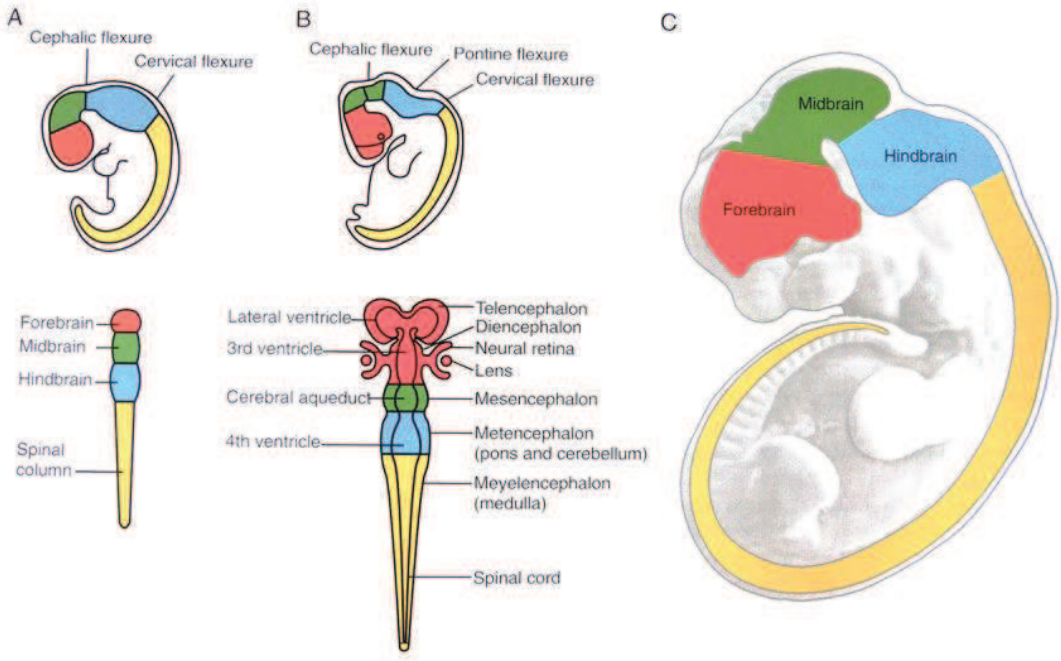

Figure 4: Scheme of different embryonic stages in Vertebrates.
A- Three vesicles stage of embryonic development. **B-** Five vesicle stage of embryonic development. **C-** Brain divisions reported to the overall organization of the embryo. From Sanes et al., 2011[1].

In the Vertebrate embryo, only the enlarged most rostral region of the neural tube will eventually give rise to the brain, while the spinal cord will arise from the longest remaining part of the neural tube. First, the future brain is composed by three vesicles: the forebrain (or prosencephalon) which will develop into prominent paired cerebral hemispheres, the midbrain (or mesencephalon) and

the hindbrain (or rhombencephalon) which will give rise to the caudal regions of the brain stem. Later during development, the prosencephalon will divide in two more vesicles: the telencephalon and the diencephalon which generated the thalamus, hypothalamus and the optic vesicles (in turn, optic vesicles become the retina and the pigmented epithelial layers of the eyes). In the meantime, the hindbrain subdivides in the metencephalon which will generate the pons and the cerebellum and the myelencephalon which will constitute the medulla in the adult. At this stage, the nervous system is composed of five vesicles (Figure 4).

Historically, the polarity of the rhombencephalon was first addressed because of its striking analogies with the anterior-posterior polarity of *Drosophilae melanogaster* (a.k.a. fruit fly)[1]. In principle, the rhombencephalon is segmented in rhombomeres clearly separated from one another and linked to each other via axons projecting as cranial nerves in different segments of the hindbrain[6]. The differentiation of these so-called rhombomeres is allowed thanks to the expression of Homeobox genes (Hox genes) in the *Drosophila* and in the Vertebrates. Briefly, the position of each Hox gene on the chromosome can be correlated to the development of a corresponding rhombomere in the same order according to the anterior-posterior axis[1,7,8]. Each rhombomere contains motoneurons which assemble in a cranial nerve leading to specific muscles from an area of the cranio-facial region, allowing chewing movements and oculomotricity for instance. However, this very basic and simple organization of Hox genes allowing anterior-posterior polarity stops at the anterior boundary of the metencephalon. The regionalization of the telencephalon lies on more complexes interweaved mechanisms based on the expression of transcription factors specific to the 6 prosomeres[1,9]. Notably, the expression of the transcription factor *Emx1* is responsible for the development of the anterior half of the cerebral hemispheres, while *Emx2* has been identified in the posterior half of the cerebral hemispheres. Similarly, the pattern of expression of other transcription factors have allowed to distinguish six prosomeres numbered caudal to rostral within the prosencephalon: P1 is adjacent to the mesencephalon,

P2 and P3 form the diencephalon, and the telencephalon is composed of P4, P5 and P6. Logically, the more advanced the development is, the more combinations of transcription factors will be required for complex neural structures to differentiate (Figure 5).

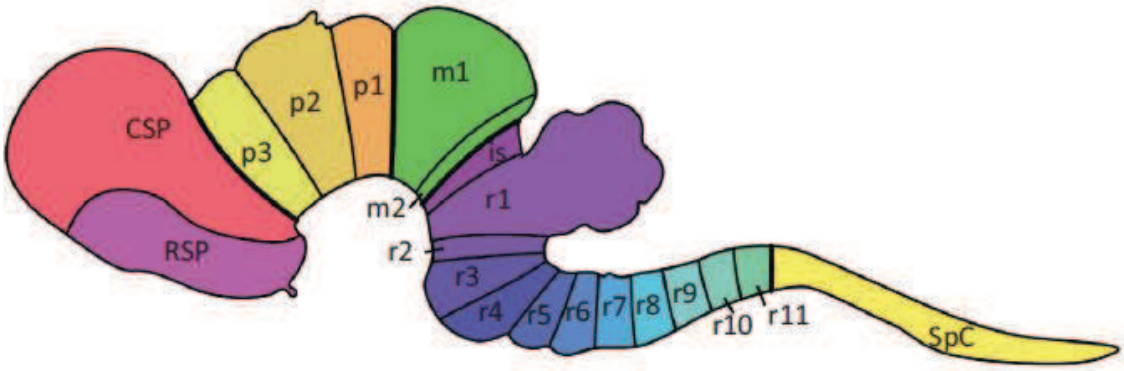

Figure 5: Map of the embryo showing the location of Prosomeres and Rhombomeres. From Puelles et al.,2013 [10]

The expression of *Sonic Hedgehog* (*Shh*) protein is necessary and sufficient for the acquisition of a dorsal-ventral polarity by the neural tube[1,11]. Interestingly, what we can call the neural differentiation "by default" gives rise to dorsal structures in the neural tube, whereas this additional *Shh* factor is required for the development of more ventral neural structures. *Shh* is secreted by the notochord which is located underneath the ventral side of the neural tube. The concentration of *Shh* received by the cells of the neural tube thus follows a gradient which is responsible for the dorsal-ventral polarization of the neural tube.

One of the characteristic of Mammals is undoubtedly the possession of an extremely complex and prominent cerebral cortex[1,12]. It is accountable for sophisticated mental functions such as decision-making, planning and anticipating, and has been classified into approximately fifty cortical areas, which reflects its high level of complexity. From a developmental point of view, the cerebral cortex derives from the anterior part of the telencephalon, and the delimitation of the different cortical regions is driven by the pattern of expression

of various transcription factors. Two of the main actors of cortical development are *Pax6* and *Emx2*. Remarkably, they are expressed through two opposite gradients: *Pax6* is more concentrated at the lateral-anterior part on the cortex, whereas *Emx2* is more concentrated at the more medial-posterior cortical region. Members of the FGFs family are essential to regulate the activity of these transcription factors.

3) Ventricular system and cerebrospinal fluid[13,14]

Closure of the neural tube allows delimitation of a cavity that will eventually give rise to all brain ventricles (Figure 6). The ventricular system is complex and regionalizes concomitantly with the development of the neural tube: the fourth ventricle is generated in the rhombencephalon, the lateral ventricles arise within the telencephalon, and the third ventricle is located in the diencephalon. Choroid plexuses appear subsequently to the formation of the ventricles, and secrete around two thirds of the CSF in the Human. They are composed of ependymal cells arranged in granular meningeal protrusions within cerebral ventricles. The remaining fraction of CSF is secreted by subarachnoid cells and ependymal cells. Importantly, choroid plexuses receive innervation from cholinergic and sympathetic autonomic systems, which can respectively increase or reduce CSF secretion. CSF renewal is circadian and its entire volume is renewed several times a day (four to five times in the young adult human brain). This intense turnover rate implies that CSF is essentially re-absorbed by cranial arachnoid granulations in the internal jugular system.

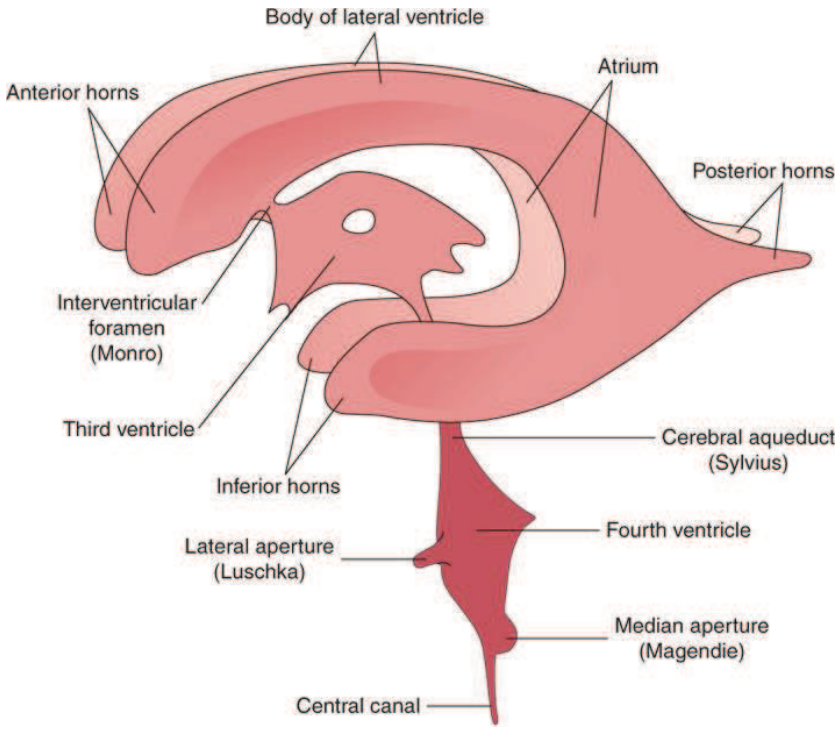

Figure 6: Ventricular system. From Timor-Tritsch et al. 2012[15].

The CSF is warrant of critical hydromechanical protection of the entire nervous system. The flow of CSF is unidirectional and pulsatile, according to the systolic impulse of choroid arteries initiated by heart beats. Multiciliated ependymal cells lining the ventricular walls also contribute to the orientation and propulsion of CSF through coordinate ciliary function, as we will study hereafter (cf Chapter II part I.3 and part II). CSF produced by the choroid plexus in the lateral ventricles circulates in a rostrocaudal direction. It flows from the lateral ventricles by the interventricular foramina to the third ventricle, then travels through the cerebral aqueduct (which develops within the mesencephalon of the neural tube) to reach the fourth ventricle. Finally, it accesses meningeal subarachnoid spaces via the median aperture (so-called foramen of Magendie) and the lateral apertures (so-called foramen of Luschka). In caudal regions, CSF can also be found in the central canal of the spinal cord. Interestingly, most of the CSF is actually contained in the cranial and spinal arachnoid spaces, while the rest of it is located in cerebral ventricles.

II- GENERATION OF NEURONS AND GLIA

The mammalian brain hosts two distinct cell populations: neurons and glial cells. For long, neurobiologists have mainly focused their studies on neurons, while glial cells remained widely mysterious. Yet, neuronal and glial cells are now known to be present in equal proportions in the human brain[16]. In 1846, Rudolf Virchow first discovered a population of "supporting cells" in the brain, which were later identified as glial cells[17]. Historically, the first main hypothesis stated that neurons and glial cells derived from distinct types of progenitors during brain development. Only in the early 1900s did Wilhelm His prove this hypothesis wrong by demonstrating that neurons and glial cells shared a common origin[17]. Subsequent researches have then brought to light a more detailed timeline of brain development, indicating that neuronal and glial progenitor cells' fate was determined depending on both space and time cues in the developing brain.

In the early developmental neuroepithelium, neural stem cells (NSCs) were first identified as neuroepithelial cells (NCs) (Figure 7)[12]. It is now known that NCs amplify their pool of progenitors by symmetric cell division (SCD). All neurons derive from NCs. Originally, these cells emerge from the neural plate to form a pseudostratisfied neuroepithelium in the early neural tube. They are highly bipolar polarized cells, anchoring both at the basal lamina and at the lumen of the neural tube. They are connected to each other via Adherens junctions[12]. At embryonic stage E9-E10, once the rodent neural tube is fully closed, these cells will start to express astroglial markers such as BLBP (brain lipid-binding protein), GLAST (astrocyte-specific glutamate transporter), and TN-C (Tenascin-C) and neurofilament proteins as GFAP (glial fibrillary acidic protein), Nestin and Vimentin, therefore switching their identity to Radial Glial Cells (RGCs)[17] (Figure 7). The possibility that NCs could directly give rise to neurons through asymmetric cell division (ACD) was raised[18].

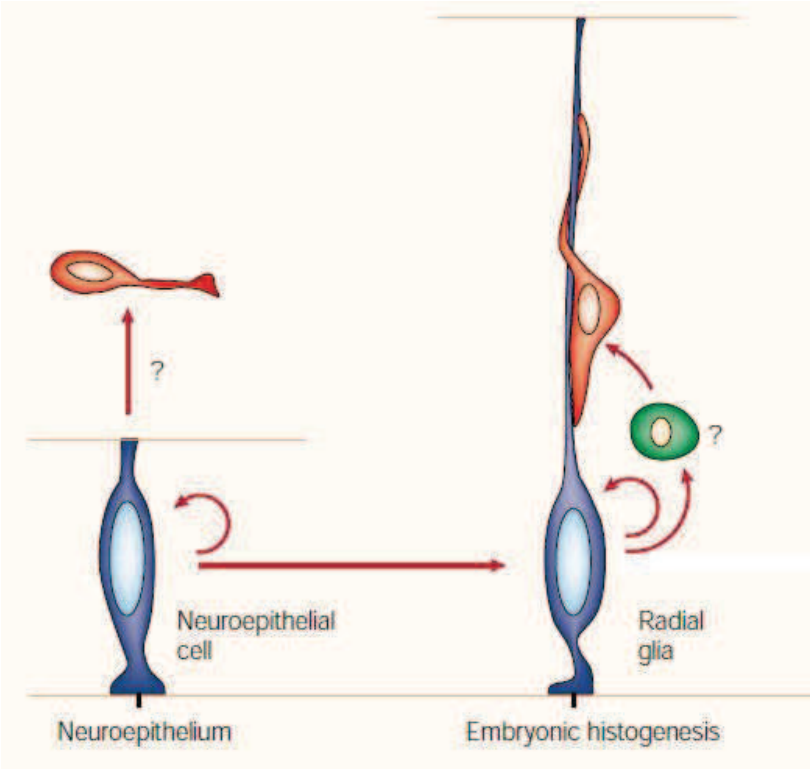

Figure 7: Scheme of Neuroepithelial cell versus Radial glial cell. Adapted from Alvarez-Buylla et al., 2001[19].

1) Radial glial cells

RGCs are so-called because of their very peculiar morphology, which was first described by Ramon y Cajal in 1890 (Sur l'origine et les ramifications des fibres nerveuses de la moelle embryonnaire. Anat Anz 5:85–95 and 111–119). These observations were made thanks to a staining method uncovered by Camillo Golgi and based on silver impregnation of the nervous tissue. RGCs anchor both at the basal pia of meninges and the apical ventricular wall and thus have a bipolar very elongated shape. In 1935, Sauer was able to show that both NCs and RGCs undergo interkinetic nuclear migration (INM): their nucleus migrates radially in the ventricular-subventricular zone (VZ-SVZ) depending on the phase of the cell cycle (Figure 8)[20]. This INM is crucial for neurogenesis regulation since it exposes the nucleus to a gradient of Notch that will determine its fate[21]. RGCs divide both symmetrically and asymmetrically in the most apical region of the VZ-SVZ, so as to renew their pool of NSCs and give rise to more differentiated daughter cell types. Their progeny will migrate towards the cortex along their basal process.

Henceforth, RGCs are not only NSCs; they also ensure major scaffolding role of the developing brain structure. (For Review, see[22,23]).

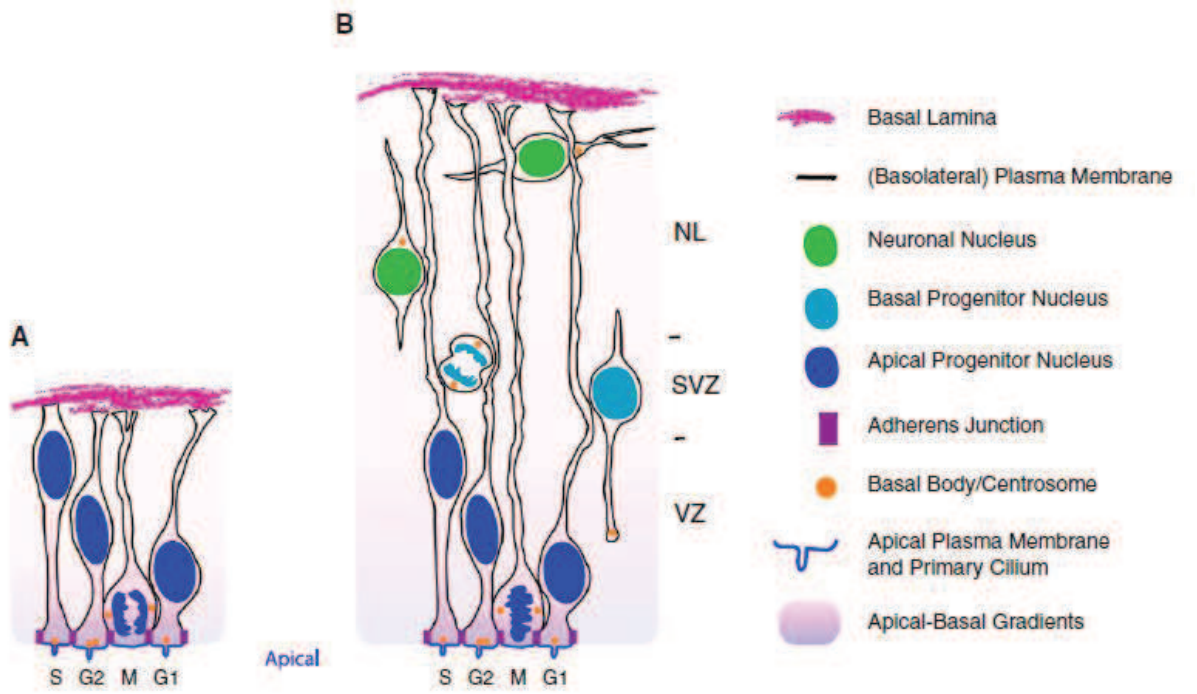

Figure 8: Interkinetic migration of neural progenitors
A- For Neuroepithelial cells. **B-** For Radial Glial Cells. From Taverna and Huttner, 2010[23].

Similarly as almost all human cells, RGCs anchor a primary cilium at their apical plasma membrane. This organelle is often named "sensory cilium" since it is capable of mechanic, molecular or chemical signals detection from the CSF and hence harbours important molecular traffic. Its structure involves cytoskeleton proteins, yet it is a immotile cilium measuring 0.5 to 2 µm in length and 200-300 nm of diameter[24,25]. It is nucleated by the centrosome, more specifically via centrosome mother centriole. It has a "9+0" axoneme organisation, where 9 doublets of microtubule (cytoskeleton tubular polymers of tubulin) are arranged in an empty cylinder. The primary cilium is retracted during cell division so that each daughter cell inherits a centriole (which then becomes mother centriole and duplicates in S phase) and a primary cilium can be formed again. Pericentriolar proteins such as PCM1 have been identified as key stabilizers of the centrioles nucleating primary cilia. They are involved in the recruitment of ciliary plasma

membrane cargo proteins from the Golgi, or else loading cargo proteins on the axoneme[26,27]. Primary cilium has also been extensively studied for its implications in brain development through the Hedgehog, Intraciliary/Intraflagellar transport (IFT), Wnt and mTOR signalling pathways [28,29,30,31,32,33]. IFT proteins gather motor transport proteins moving along microtubules of the axoneme: kinesin proteins were described as anterograde motors, while dynein proteins were identified as retrograde motors. Primary cilia are specialized in calcium signalling, which includes crosstalks with the HH signalling pathway[24].

2) Neurogenic and gliogenic phases of cortical development

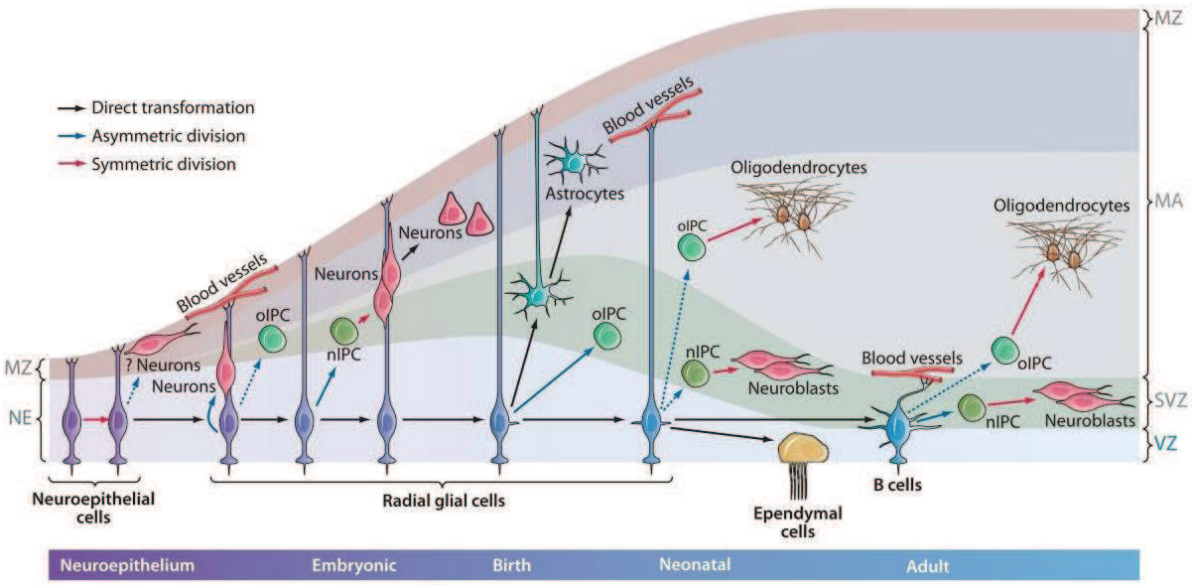

Figure 9: Scheme of brain development.
MA, mantle; MZ, marginal zone; NE, neuroepithelium; nIPC, neurogenic progenitor cell; oIPC, oligodendrocytic progenitor cell. From Kriegstein and Alvarez-Buylla 2011[22].

We can differentiate two main phases in cortical development: a neurogenic phase and a gliogenic phase (Figure 9).

First, RGCs undergo a neurogenic phase during which they mainly perform ACDs, either by direct or indirect production of neurons through intermediate progenitors (IPs or IPCs). Newly born IPs and neurons migrate basally during

neurogenesis, which results in considerable thickening of the cortex as they accumulate according to a tightly controlled map. The cortex is endowed with a complex architecture: neurons distribute according to both laminar and columnar patterns, based on clonal and developmental stage criteria. Clonal neuronal populations use basal processes of RGCs as scaffolding structures to migrate radially. They organize in six distinct layers generated according to an inside-out pattern depending on their date of birth during corticogenesis (Figure 10). The inner sixth layer is composed of earliest-born neurons whereas the last-born neurons will concentrate in the outer first cortical layers. Altogether, clonal populations of neurons form columnar functional units where deep-layer neurons were produced prior to superficial-neurons during corticogenesis[12,34,35]. Interestingly, cortical domains of neurons with distinct functional properties appear early during corticogenesis and are able to impact later developmental stages[36].

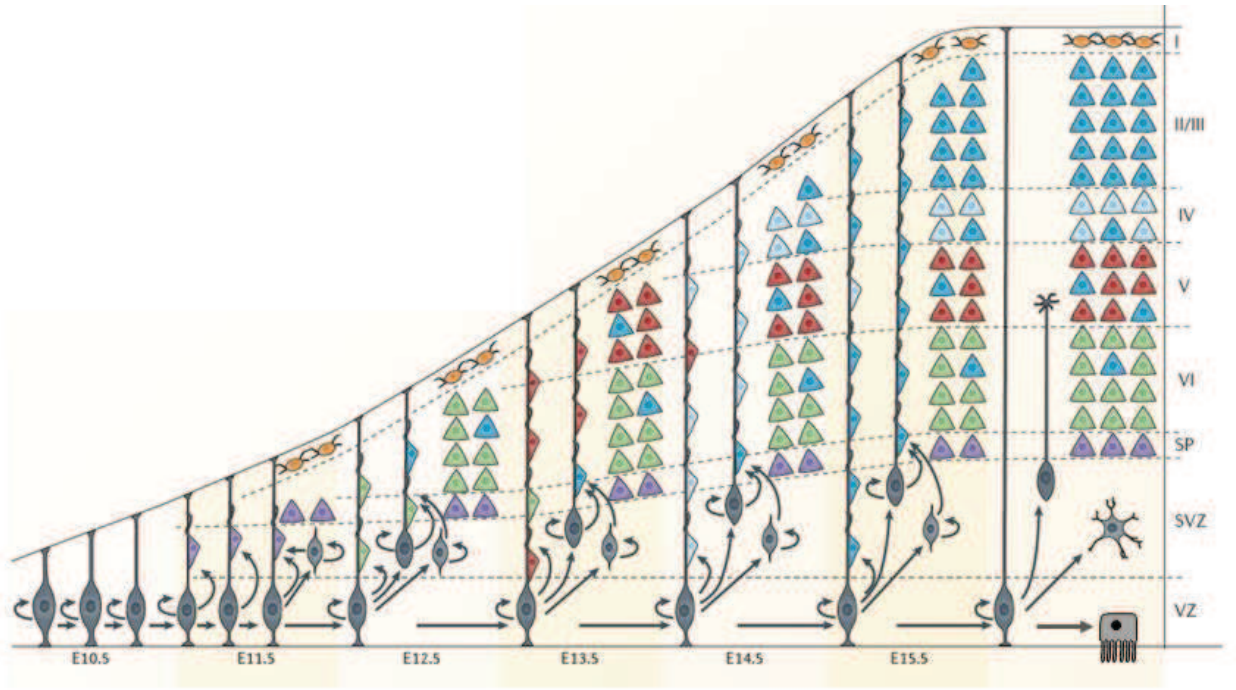

Figure 10: Scheme of the development of the six cortical layers.
Adapted from Greig et al., 2013, [37]

Only later during brain development will RGCs give rise to glial cell types through a gliogenic phase: astrocytes[38], oligodendrocytes (through IPs)[39] and ependymal cells[40,12]. Notably, microglia is generated by extra-embryonic primitive myeloid progenitors in the rodent yolk sac before colonizing the brain[41]. Glia and neurons of the peripheral nervous system don't derive from RGCs either, but from neural crests progenitors. dendrocyte progenitors) through three competitive production waves[39]. Noteworthy however, oligodendrocytes can also derive from B1 cells in the normal or injured adult rodent brain[42].

In this work, we investigate the development of ependymal cells. They are post-mitotic multiciliated glial cells lining up the walls of all ventricular cavities. BrdU injections at embryonic stages in the mouse revealed that they differentiate from RGCs which last divided between E14.5 and E16.5[40]. The development of ependymal multiciliated cells will be described more thoroughly in Chapter 2 Part III of this study.

Astrocytes were found to be the largest population among glial cells in the central nervous system (CNS). They ensure critical homeostasis maintenance of neural circuits via absorption of nutrients, maintenance of extracellular ion balance, reinforcement of the blood-brain-barrier and post-traumatic cellular repair and scarring functions. Lineage-tracing studies have revealed that astrocytes were produced by multiple sources. Initially, they arise from embryonic RGCs[38], either directly or indirectly through prior differentiation into IPs. Within the first three postnatal weeks in the rodent brain, they undergo a wave of 6 to 8 fold self-expansion. This massive local expansion is due to the symmetric cell division of differentiated astrocytes to amplify their own population and integrate in the pre-existing glial network[43]. They also pursue their local proliferation in the adult brain throughout life[44]. What mechanisms drive the different origins and lineages of astrocytes depending on the brain region and developmental/postnatal stage? Answering this interrogation still requires further investigations. Most intriguingly, Doetsch et al. have described a subtype of astrocytes (also known of B1 cells) which retain neurogenic features in the adult rodent brain[45]. These adult

NSCs are also descending from RGCs and remain in direct contact with the lateral ventricles within the adult VZ-SVZ[46].

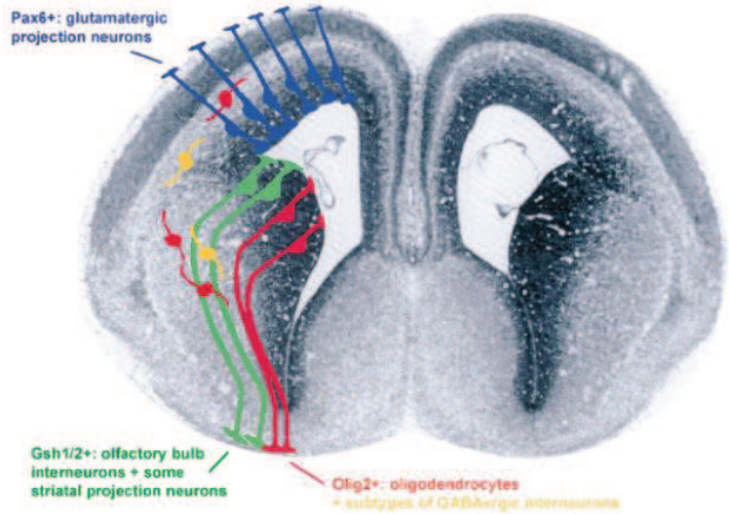

Figure 11: Scheme of RGC heterogeneity.
From Kriegstein and Götz 2003[47].

On the whole, RGCs are able to generate a large diversity of cell types during embryogenesis (Figure 11). Far from being homogeneous, RGC population is highly heterogeneous and regionally organized. RGC retain distinct hallmarks and receive various environmental signals in a region-dependant manner with high level of complexity. For instance, differential expression of Olig2, Gsh1/2 and Pax6 can be used to distinguish subtypes of RGCs with progeny that varies both in terms of daughter cell types and spatial location[47].

III- RADIAL GLIA LINEAGE-TRACING IN THE BRAIN, AN OVERVIEW

1) Lineage-tracing techniques[48]

Neuroscientists have faced the challenges of characterizing brain development for many years now. Confrontation to this degree of complexity has soon required the elaboration of original labelling techniques to mark cells. As our brain understanding improves, the stringency of lineage tracing methods needs to be highly increased. Ultimately, to address further levels of details in brain

functioning, neurobiologists are bound to combine various methods to still track more cell lineages in live tissues and fulfil their ambition.

a- Dye-mediated labelling techniques

At first, basic labelling methods were discovered that allowed staining of cells without killing them. The cells could all be stained regardless of their identity, but as these methods are quite easy to apply from an experimental practical point of view, biologists keep using them on a daily basis. We can cite quite a few without giving an exhaustive list. Dye-mediated technique consists on staining living cells with a carbocyanine lipophilic molecule: DiO or DiI. They emit intense fluorescence and possess long carbon chains that enable them to incorporate into the cell plasma membrane[49]. For instance, it was used in 1989 to study the stage of migration of neural crest cells towards the wing bud in the chick[50]. To target more specifically cycling cell populations, BrdU (bromodeoxyuridine) was used. It is a fluorescent synthetic analog of thymidine which is integrated in cell DNA during S-phase (replication phase). Daughter cells then inherit BrdU-labeling through cell division. Other nucleoside analogs have been unravelled since BrdU first came to use (EdU, CldU and IdU). If cells derived from initially BrdU positive ancestors keep on dividing, BrdU-labeling will dilute at each generation of cells. After numerous cell divisions, it becomes undetectable, unless it is reintroduced in the cell environment. This allows to pinpoint dividing cells at a specific moment (during development for instance). For example, BrdU was used at different developmental stages to label cycling RGCs in the embryonic rodent brain. This method allowed to determine that the last division of RGCs that will differentiate into ependymal cells occurs between E14.5 and E16.5, following which ependymal cells become postmitotic[40]. One drawback of this technique is that the revelation process of these molecules requires specific toxic treatment that can only be applied (with caution) on fixed tissues. Conveniently, commercial societies now produce them in the form of kits that are relatively inexpensive. Last, horseradish peroxidase (HRP) and fluorescent dextran polysaccharides can be used as unspecific cell tracers. They are large molecules which must be

injected directly into the cytoplasm of the cell(s) of interest and cannot exit the cytoplasm because of their size. HRP must be revealed through colorimetric enzymatic reaction and is not compatible with live experiments, whereas dextran can be coupled to various fluorophores.

b- Unspecific genetic labelling

Genetic markers are more specific cell lineage tracers. They can be introduced in the living tissues by two techniques: either electroporation or viral infection. In principle, electroporation consists on injecting a plasmid at close proximity with the targeted cells before applying an electric current (that is viable for the organism or the cells). Electric chocks permeabilize the plasma membrane by creating pores, which allow the DNA to penetrate the cell. As DNA is negatively charged, it will enter the cells that are closer to the positive electrode, whereas it will be repulsed from the negative electrode. Logically, electrodes have to be properly oriented to target the region of interest (Figure 12). To track cell lineage, reporter fluorescence must be induced specifically in electroporated cells. Fine-tuning of the concentration of the injected plasmids is required to study cell-autonomous effects, or region-dependant phenotypes. Nevertheless, *in vivo* electroporation is only compatible for cells located in regions nearby cavities to allow plasmid injection. Unless combined with other lineage tracing techniques (such as transgenic animals), electroporation of mere fluorescent plasmids will not integrate into the cell DNA, nor will it target specific cells. To introduce cell-discrimination in the electroporation method, biologists have designed a tremendously large variety of fluorescent plasmids, including plasmids composed of a fluorescent protein sequence driven by a cell-type-specific promoter. Conveniently, plasmid synthesis and amplification can be easily performed in a laboratory, with minimal equipment and at a relatively low cost. Many studies show that both *in utero* and postnatal electroporation methods allow to efficiently apprehend the role of many cell types including ependymal multiciliated cells and newly born neurons of the postnatal olfactory bulb[51,52,53,54,55,56].

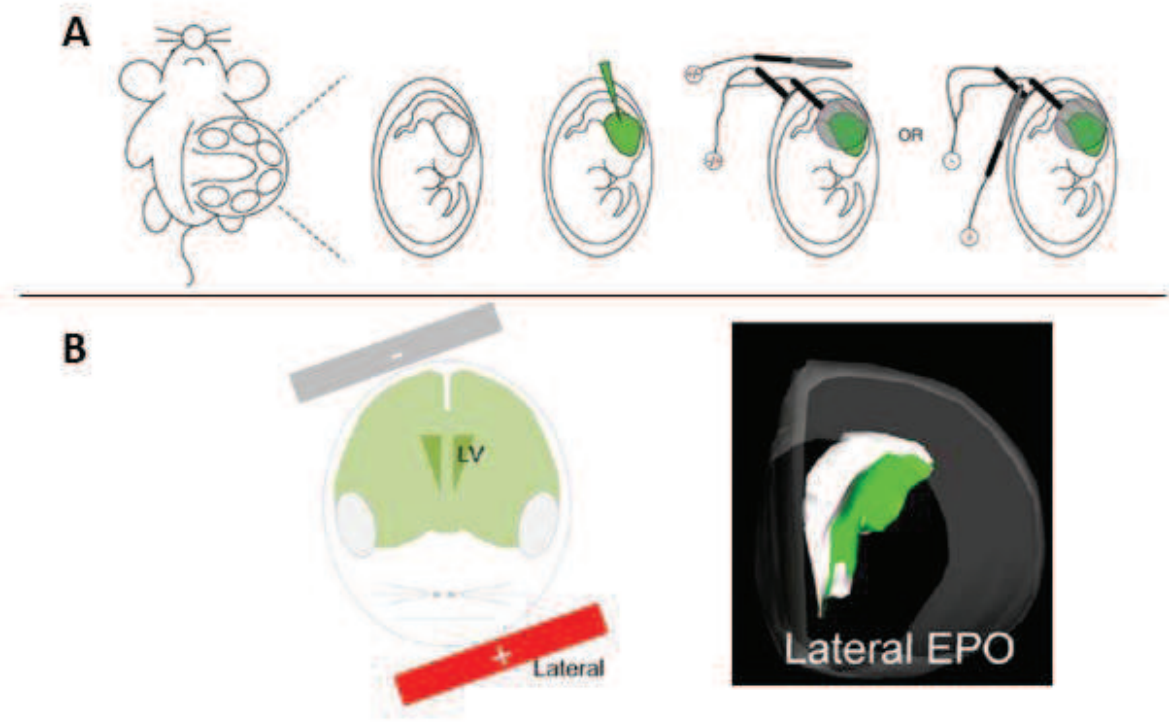

Figure 12: Electroporation technique.
A- *In utero* electroporation. **B-** Postnatal electroporation of the Lateral wall of the LV. Adapted from Dal Maschio et al., 2012[57] and Fernandez et al. 2011[54].

Infection with viruses is another genetic tool to study cell lineage, especially when combined to others lineage-tracing techniques. Viruses infect every cell types and integrate very stably into the genome of the host cell using the machinery of the host. To follow cell-lineage, it is important that synthesized viruses should be designed without replication machinery elements in such a way that only the cells which were initially infected will transmit the virus to their progeny. There are several types of viruses endowed with distinct cues: retroviruses (lentiviruses LV and Moloney murine leukemia viruses MMLV), adeno-associated viruses (AAV), and rabies viruses. It is also possible to couple viral infection with another lineage-tracing technique to label specific cell types. Unlike the electroporation technique, regulating the number of cells infected with a virus is very complex. Virus production is also a rather long and fastidious process that can only be launched in specific conditions of security, confinement and waste-disposal which require adequate and expensive equipment.

Fortunately, private companies are constantly expending the number of viruses commercially available.

c- Specific genetic labelling by recombinase

The first technique of specific genetic labelling depends on three elements: a recombinase, a reporter gene element, and a site-specific recombinase. These can be expressed in the cells through many means (electroporation, generation of transgenic animals, etc.). Expression of the recombinase can be cell-specific when driven by a cell-specific promoter. This enzyme can only bind to a SSR which sequence is within in the cell DNA (either integrated its genome or carried by a plasmid inside the cell). Two such systems have already been described: the Cre-lox and the Flp-FRP systems.

The Cre recombinase is an enzyme isolated from bacteriophage P1. It can only bind to loxP SSR in order to exert its activity. At high doses, it is toxic, except when fused to an estrogenic binding-domain. The Flp recombinase has been extracted from the yeast *Saccharomycaes cerevisae.* It is active when associated to FRP SSR of the DNA[58]. Despite its possible toxicity, the Cre recombinase is much more efficient than Flp recombinase, that's why it is preferably used for mammalian model systems, whereas the Flp-FRP is rather used for *Drosophilae melanogaster.*

The recombinase genetic technique is very robust because it is permanent, integrated in the cell and inherited by cell descendants. While high doses of recombinase allow extensive recombination to target a whole cell population, low doses of recombinase facilitate sparse recombination events to optimize clonal analysis.

Reporter genes are various and allow numerous strategies to make the recombination even more stringent and specific. To do so, it is possible to have reporter genes encoding multiple fluorescent proteins (GFP, RFP, mCherry, etc.). More specifically, recombination can be conditioned if reporter genes include the

expression of enzymes (β-galactosidase, luciferase, alkaline phosphatase) or if the reverse sequence of the gene of interest flanked by SSRs was cloned for instance.

Inducible Cre-recombinase has also been engineered via Cre recombinase gene fusion with an estrogenic receptor (Cre-ER). In this situation, the Cre recombinase is expressed only in presence of an activator of the estrogenic receptor: Tamoxifen. Unfortunately, injection of tamoxifen in pregnant mice has been shown to increase abortion frequency and early postnatal death of pups. Therefore, developmental studies using inducible recombination strategies at embryogenic stages are not trivial.

d- Specific genetic labelling by Brainbow technique

Clonal strategies have been elaborated in an effort to target specific cells at a clonal scale. Remarkably, the Brainbow technique bases on the Cre-lox recombination system described above to allow aleatory and conditional expression of three fluorescent proteins in a cell-autonomous way[59]. Several parameters can be adjusted so as to modulate the number of possible colours adopted by cells such as the number of copies of the transgenes, the dose of Cre recombinase, the targeted cellular compartment (cytoplasm, membrane or nucleus)[60]. Stabilization of the labelling can be obtained through genetic integration of the Brainbow transgenes by transposase activity. The Brainbow technique can be applied by electroporation, even so conditional transgenic Brainbow animals have also been generated. Interestingly, Brainbow lineage-tracing strategy offers a very wide variety of colours obtained by independent aleatory recombination events. This can be both an asset and an issue, because generating numerous colours allows differentiating many clones, but also requires the use of a high-resolution microscope equipped with specific fluorescence filters, and complex discriminative image analysis methods.

e- Specific genetic labelling by mosaic strategies

The first mosaic developmental analysis was achieved by cell transplantations. Technically, these graft experiments were not suitable for single cell clonal lineage tracking. More adapted techniques were developed using genetic tools to overcome this technical difficulty. One of them is the mosaic analysis with a repressible cell marker (MARCM), which is based on the Flp-FRP recombination system (Figure 13A). A genetic construct is designed in which one allele contains a specific cell marker upstream from the mutation of interest, while the other allele possesses the repressor gene of the previous allele. Thanks to the activity of Flp recombinase, the repressor gene will end up on the same chromosome (though different allele) as the cell marker and the mutant gene. Interchromosomal segregation phenomenon will then cause the daughter cell to hold the two mutant alleles, while the two repressor alleles will be segregated in another daughter cell. As a consequence, the mutant genes and cell markers can be expressed in the cell, since they are apart from their repressor. This useful tool has even been made more complex through the mean of twin-spot MARCM (Figure 13B).

The second technique is the mosaic analysis with double cell markers (MADM) (Figure 13C and D)[61]. Its principle is quite similar to MARCM although it occurs through Cre recombinase activity. The N-terminal part of the GFP gene and the C-terminal part of RFP gene are on the same allele, with a Cre SSR in-between. The other allele contains the N-terminal part of the RFP gene upstream from a Cre SSR and the C-terminal part of the GFP gene. After replication, Cre-mediated recombination will result in the segregation of the GFP N and C-terminal parts on the same allele, and the RFP N and C-terminal parts on a different allele in G2 phase. Cell mitosis will ultimately result in one GFP positive daughter cell (green), one RFP positive daughter cell (red), one GFP and RFP positive daughter cell (yellow), and one color-less daughter cell containing unrecombinated alleles with parts of GFP and RFP genes. Importantly, Cre-mediated recombination in cells during G0 or G1 phases will be GFP and RFP positive (yellow), preventing any interpretation these yellow clones with this technique. This strategy allows the

clonal identification of cell lineage only when the recombination process occurs in sparse cells prior to a mitotic event. Opposite to the Brainbow approach, the clonal analysis through mosaic analysis technique is limited to two colours and thus requires sparse recombination to be able to distinguish in-between clones. Furthermore, its recombination process is less efficient than the Brainbow method.

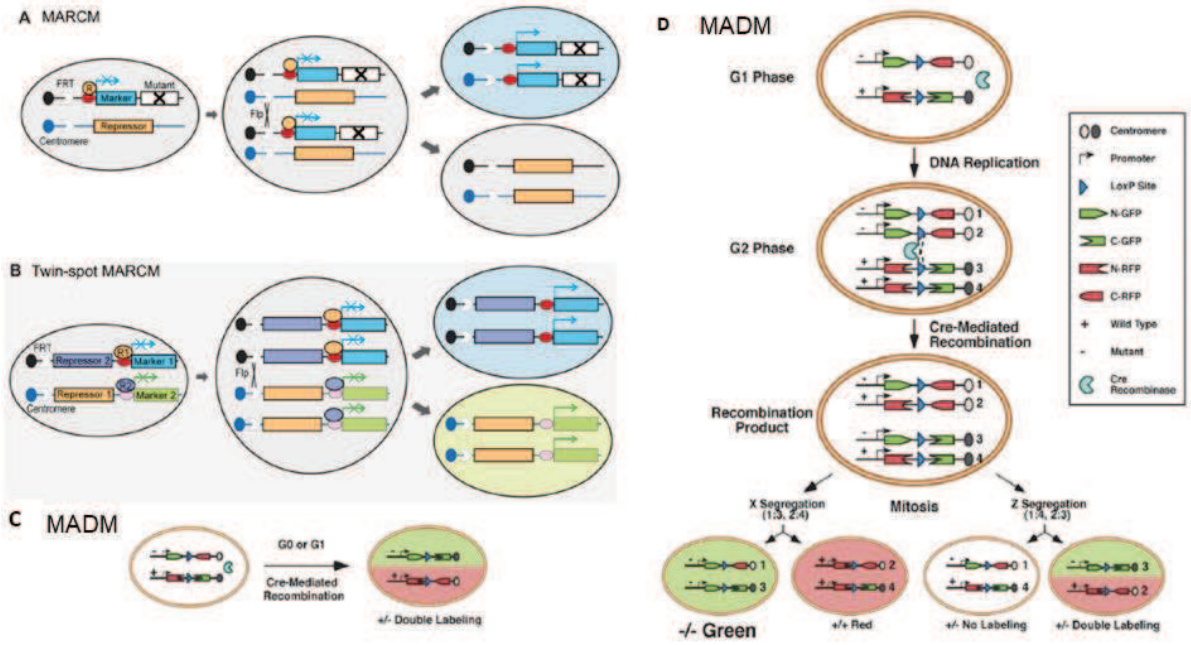

Figure 13: Mosaic analysis strategies.
A- Mosaic analysis with a repressible marker (MARCM). **B-** Twin-spot MARCM. C-Mosaic analysis with a double marker (MADM) when recombination occurs at G0 or G1 phase. D- MADM when recombination occurs in G2 phase. Adapted from Solek and Ekker 2012[48] and Zong et al. 2005[61]

2) Lineage-tracing studies of RGC progeny

For the last decades, biologists have worked twice as hard to elucidate plasticity and differentiation phenomena in stem cells. Further understanding of regenerative and embryogenic processes has laid crucial foundations for the surge of cell therapies. Aside from their function of scaffolding, RGCs are the major source of neuronal and glial cells during brain development. Comprehension of their lineage specification mechanisms is thus paramount. To what extent do external cues influence RGC fate? Are RGCs subdivided in distinct

populations of progenitors which yield distinct cell types? How is fate-decision driven in RGCs? What mechanisms underlie asymmetric versus symmetric cell division? Here, we review major advances on RGC lineage during brain development.

The lineage of cortical neurons still remains elusive. Many studies have shed light on intrinsic properties that are decisive for cellular fate specification. Oblique or vertical orientation of the mitotic spindle is notably suspected to influence neural progenitors towards ACD[62]. In line with this, data published by Bultje et al. provides substantial elements in favour of a potentially important role of the orientation of the subcellular cleavage furrow in ACD events[63]. They notably show that the dynamic distribution of mPar3 (a protein involved in cell polarity) in RGCs is necessary for ACD through differential regulation of Notch signalling in their progeny. All in all, the possible existence of a correlation between fate determination and the orientation of the mitotic spindle is supported by many studies in *Drosophilae* as well as in some Vertebrates (e.g. in the chick), but remains uncertain in Mammalian model systems[64,62].

Several components of the MTOC have also been examined for their potential influence on neurogenesis, since they could bear responsibility for asymmetric segregation of molecular cues underlying ACD. Accordingly, it was shown that depletion of the subdistal appendages protein Ninein from the mother centriole (daughter centrioles lack these proteins in normal conditions) disrupted asymmetric segregation of mother centrioles in neural progenitors. ACD is ultimately impaired and leads to premature loss of neural progenitors. This report suggests that centriolar asymmetry is thus essential for the maintenance of neural progenitors during ACD[65]. Conversely, later experiments of Insolera et al. have demonstrated that neurogenesis could be maintained in absence of centrioles[66]. They observe that RGCs lack centrioles and are no longer localized within the VZ in Sas4 protein-depleted mice. Protein Sas4 is necessary for centriole biogenesis. It was found that centriole-deprived RGCs retain delayed mitotic activity even though their mitotic spindle is disoriented. This results in

p53-dependant neuronal cell death and microcephaly, which can both be rescued by concomitant removal of p53 in Sas4 depleted mice. The authors hereby propose that centrioles are necessary to ensure proper localization of RGCs in the VZ, but not essential for the production of neurons. They assume that centrioles play a critical role in neuronal migration as well as in the establishment of complex cortical laminar structure. Collectively, these works suggest that centrioles are not essential for proliferation and differentiation maintenance in RGCs. Instead, RGCs possess an intrinsic program allowing them to perform neurogenesis outside of the VZ and independently of their cleavage plan and cellular morphology. This further underscores the existence of an important plasticity of RGCs *in vivo*.

Transcription factors are indisputably heavily involved in fate determination. Surprisingly, a very elegant mosaic clonal analysis realised by Gao et al. has revealed that although the expression of the transcription factor Otx1 is predominant in early progenitors and postnatal deep-layer neurons, depletion of Otx1 in progenitors reduces both deep-layer and superficial-layer neuronal output[67]. This suggests that the transcription factor Otx1 has a cell-autonomous effect on the production of deep-layer and superficial-layer neurons during corticogenesis. This result strongly contradicts previous postulates on the fate-restriction of RGCs and gives a more complex perspective of brain cell-lineage. Namely, cell-lineage during brain development would be the result of a cocktail of transcription factors which differential expression will eventually lead to different neuronal populations. According to this theory, the embryonic pattern of expression of transcription factors in RGCs does not reflect on post-mitotic neurons, but they are rather uncorrelated. Besides, this study also emphasizes that RGCs follow a deterministic program; they undergo SCD prior to ACD to give rise to nascent neurons and thereby exhaust their proliferative capacity. At later embryonic stages, the large majority of RGCs (5 out of 6) will entirely complete their proliferation by a last neurogenic SCD. However, the remaining fraction of RGCs is responsible for the production of glial cells subsequent to the neurogenic

phase. Each RGC will thus give rise to a pre-defined number of neurons which can be predicted (approximately 5 or 6 neurons), and possible glial cells. These findings are hence subject to discrepancy since they contrast with previous reports by Franco et al. who submitted a model of fate-restricted RGCs[68].

In addition to similar intrinsic programmes, neurons exhibit a cell-lineage bias on a more functional aspect too. Yu et al. have then compared the number of synapses between neurons belonging to the same clonal population and neurons derived from distinct progenitors. They show that synapses are established preferentially between sister neuronal cells, thereby reinforcing the concept of microcircuit within cortical functional units in the brain[66].

The main difficulty is to examine whether neural progenitors are fate-restricted or multipotent. Fate-restriction of progenitors entails that they will specify into a cell identity based essentially on their intrinsic determinants. On the contrary, multipotency of neural progenitors implies that their fate-decision also relies on external and environmental signalling factors. In many cases, reviewing the literature tends to suggest that both these theories are accurate: the fate decision of neural progenitors seems to be influenced by the combination of both intrinsic programmes and extrinsic signals[69]. Cortical layers of neurons are produced at different developmental stages according to inside-out waves of neuronal output, although these waves widely overlap with each other. Neuronal subtypes exhibit striking similarities with adjacent neurons which belong to the same particular cortical layer and were produced concomitantly during corticogenesis. This suggests that their progenitors might share common properties. Accordingly, it has been shown that the birthdate of neural progenitors influences their plasticity, even though it can be reversed. Later-born progenitors become more restrictive in their state of competence than early-born progenitors: when transplanted into later-produced upper-layers, early-born progenitors are capable of producing neurons specific to the upper-layers. Nevertheless, when later-born progenitors are transplanted into deeper cortical layers, they can only be induced to produce early-born neurons in very specific conditions[70]. These

data collectively highlight the presence of specific external molecular signals within each cortical layer "niche", which will interplay with intrinsic programmes in cells to determine their fate. Remarkably, extrinsic molecular signals do not limit to conferring specific cell identities within cortical layers, but also contribute to correct brain and nervous system regionalization on a more global scale (to only name few: Shh, Wnt, FGF, EGF, Nodal, retinoids, etc)[71]. We can henceforth legitimately interpret that intrinsic properties of neural progenitors act together with competing external molecular cues of cortical layers so as to specify cell fate.

Yet, this question remains highly controverted. For example, two concurrent scientific teams have examined the origin of projection neurons via lineage-tracing studies using *Fezf2* transcription factor without reaching agreement. Interestingly, *Fezf2* is expressed in early cortical progenitors and deep-layer neurons. The team of Dr Müller has first stated that Cux+ neurons were produced from fate-restricted *Fezf2*+ progenitors in 2012[68]. In 2013 however, the team of Dr Chen has diverged from this theory and affirmed that all *Fezf2*+ progenitors are not fate-restricted but multipotent stem cells. Namely, some of *Fezf2*+ progenitors can give rise not only to down-layer neurons at early developmental stages but also to upper-layer neurons as well as oligodendrocytes and astrocytes later during corticogenesis[72]. Two years later, the debate is still open as each team discloses inconsistencies in the conclusions previously obtained by his competitor[73,74]. Both these theories are viable and yet place neurobiologists in opposite perspectives on the way they tackle brain development and the strategies to cure neurodevelopmental pathologies. Additional investigations are still required to unravel cell-lineage issues in the brain.

IV- ADULT NEUROGENESIS

For a long time, neuroscientists were convinced that neurons were exclusively produced at embryonic stages and could not be replaced afterwards. Nowadays, prominent progress was achieved regarding our knowledge about brain plasticity, even so open questions are still pending. In an effort to reach further comprehension of the brain complexity, two neurogenic regions have been uncovered in the adult rodent brain during the past decades. One is located in the subependymal granular zone near the striatum and gives rise to neurons colonizing the hippocampus throughout adult life, the second is located within the VZ-SVZ and gives rise to neurons of the olfactory bulb[75,76,77,78,45]. Logically, neurogenesis in the hippocampus aims at maintaining a constant potential for memory renewal. Although the reason why neurogenesis occurs in the hippocampus can instinctively be presumed, we still fail to understand the causes of neuronal replacement within olfactory bulbs. Yet, hypothesis have been emitted that neuronal renewal in olfactory bulbs could allow adult rodents to retain the capacity to process new smells throughout their whole life [79,80]. In theory, olfaction is a sensory detector heavily participating to vital functions in rodents, enabling them to flee when confronted to predators, or to find food and shelter, or else to identify peers. The olfactory bulb sends projections to the hippocampus that is known for his implication in memory processes. This has led to the hypothesis that adult neurogenesis in the olfactory bulb promotes odour memory and discrimination in rodents[79]. As a consequence, it is crucial that rodents should be able to learn and recognize new smells as they encounter them during life.

We will hereafter focus more thoroughly on the other adult neurogenic niche of the SVZ that has been mentioned previously[45]. Neurons arising from the adult stem cells of the SVZ neurogenic niche can exclusively be found in the olfactory bulb. Importantly, data seem to suggest that this adult neurogenic niche does not exist in the human brain. Understanding of the mechanisms underlying adult

neurogenesis in this niche is yet decisive to apprehend brain functioning in physiological as well as pathological conditions.

How is adult neurogenesis occurring within the SVZ? An increasing number of research teams evaluate solving this issue as a top priority, and related high-profile articles are continuously published. Adult NSCs are born from embryonic RGCs in the SVZ along lateral brain ventricles during brain development[45,81]. Between E13.5 and E15.5, RGCs specify in so-called B1-cells by acquiring astroglial properties in the SVZ where they will remain throughout the entire life[81,82,83]. They are mostly quiescent until postnatal stages where they activate so as to generate neuroblasts[81] (Figure 14).

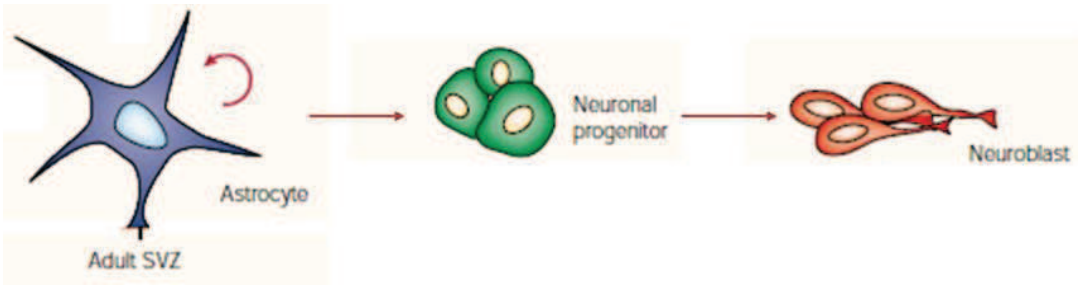

Figure 14: Simplified scheme of neuroblasts production in the adult brain.
Adapted from Alvarez-Buylla et al., 2001 [19]

Very recently, the team of Dr Alvarez-Buylla has shown that adult neural stem cells could perform symmetric cell division to renew their own pool of progenitors, but also to generate transient amplifying cells that will later on differentiate into neurons. They also found that this process is decreasing with age[84]. After division in the subventricular zone, immature neuroblasts migrate through the brain along a closely-regulated track named rostral migratory stream (RMS) towards the olfactory bulbs, where they differentiate into mature neurons. Indeed, these emerging cells will steadily replace local GABAergic and dopaminergic interneurons (mostly granule cells and periglomerular cells)[17,85,86]. Most surprisingly, the production of neuroblasts according to this pathway is very efficient, since around 30 000 neuroblasts exit the SVZ and enter the RMS per day[87,79]. The migration of neuroblasts is not following RGC basal processes.

Instead, neuroblasts undergo radial migration followed by tangential migration. This long-distance migration is in chain and harboured by tubular structures composed of a specific subtype of astrocytes[87,79,88]. During their migration, immature neurons have a morphology that is shared by all migrating neurons in general: they possess processes directed towards the direction of migration[87]. More recent studies have brought formal evidences that the origin of interneurons subtypes was region-dependant in the adult SVZ (Figure 15). Detailed fate-mapping of NSCs microdomains was set based on the expression of transcription factors to further comprehend the origin of previously unknown subtypes of interneurons (Emx1, Dlx 5/6, Nkx6.2, Zic e.g.)[89,90,91,92,93,94].

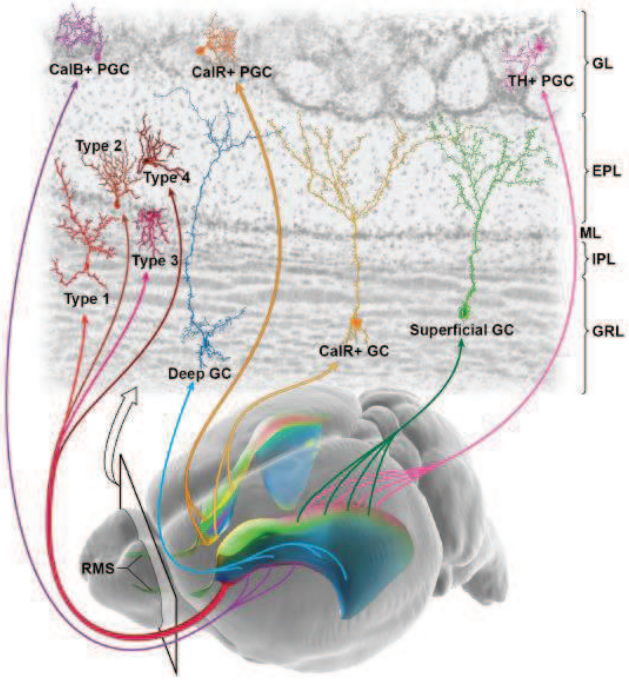

Figure 15: Regional organization of adult NSCs of the SVZ.
From Lim and Alvarez-Buylla 2014 [89].

1) Composition of the SVZ neurogenic niche

We have previously insisted on the fundamental role of NSCs, or B1-cells, in neuronal generation in the adult SVZ. The different members implicated in adult neurogenesis hence form a well-organized niche within the SVZ.

Like RGCs, B1-cells are endowed with a primary cilium at their apical surface which is in contact with the CSF. This primary cilium is sensory and functions like an antenna to detect molecular and physical signals. B1-cells also retain a long basal process from their RGCs ancestors, although it is not anchored to the pial surface but to blood vessels instead[95]. Neuroblasts derive from B1-cells NSCs in the adult SVZ and colonize the olfactory bulb where they finally differentiate into mature interneurons[96]. Surrounding B1-cells, ependymal multiciliated cells (sometimes called E1-cells) organize in pinwheels or rosettes[95] (Figure 16). Their pinwheel layout conveniently brings the CSF in contact with the primary cilium of adult neural stem cells (adult NSCs also known as B1-cells)[95]. The CSF contains molecular factors required for neurogenesis maintenance, and these factors will be directly carried to the B1-cells thanks to ependymal ciliary beating. The composition of the CSF changes throughout life, and therefore impacts on adult neurogenesis[45,97]. This supports the hypothesis that ependymal motile ciliary beating efficiently provides NSCs with molecular determinants of the CSF that are critical for proper neurogenesis. Additionally, adult Tg737^{orpk} transgenic mice with defective ciliogenesis causing immotile ependymal cilia and hydrocephalus have altered CSF flow. In these mutant mice, neuroblasts migration to the adult olfactory bulb is defective. The ependymal flow is hence necessary for the establishment of chemorepulsive gradients guiding neuroblasts migration in the adult SVZ. This leaves no doubt that ependymal flow is essential for adult neurogenesis[98]. Ependymal cells also antagonize BMP signalling by Noggin expression, which favours neurogenesis at the expanse of proliferation[99]. Noteworthy, ependymal-like cells equipped with only two cilia (E2-cells) have been identified as part of the niche too[95].

There is now substantial evidence of the contribution of other actors to the adult germinal niche of the SVZ. Notably, proliferating IPCs are retained in the adult subventricular niche close to blood vessels (also called transit amplifying cells)[17,96]. Vascular endothelial cells participate in the neurogenic niche by promoting self-renewal of adult NSCs[100], whereas astrocytes rather lead NSCs

(undifferentiated astrocytes) to differentiate into neurons[83]. A role of microglia in adult neurogenesis of the SVZ has also been brought to light; It was shown that a reduced number of microglia significantly altered the neuronal production capacity of adult NSCs within the niche[101,96].

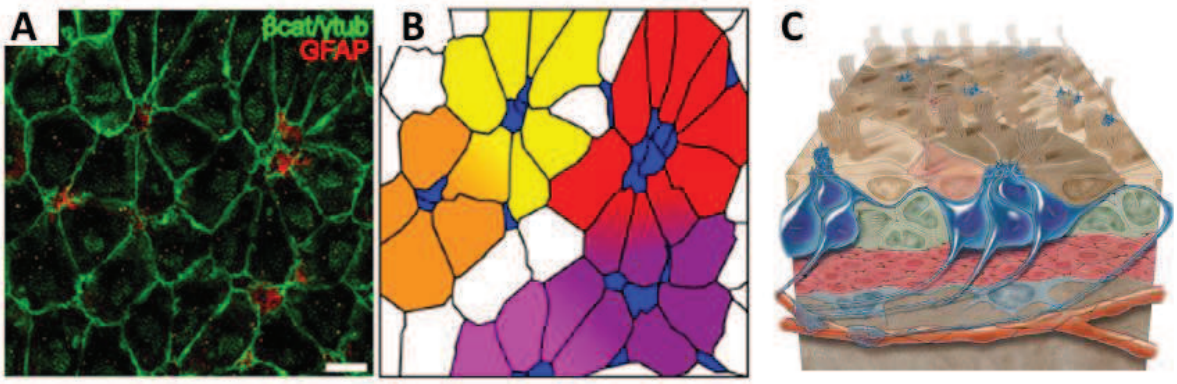

Figure 16: Adult Stem Cell Niche.
A- Immunostaining of β-catenin and γ-tubulin (green) and GFAP (red) of the lateral wall of the **LV. B-** Representative scheme of pinwheels of the staining in A with B1-cells (blue) and ependymal cells (purple, yellow, orange and red). **C-** Scheme of the pinwheel model of the adult neural stem cell niche. Adapted from Mirzadeh et al. 2008[95].

Importantly, neurons are not the only cell population to be generated through NSC differentiation. Indeed, the niche also exhibit gliogenic features; Oligodendrocytes arise from B1-cells in particular through Wnt/β-catenin signalling pathway, as it was pointed out[42,96,102].

2) Molecular mechanisms of adult neurogenesis

Molecular mechanisms driving adult neurogenesis of neurons in the olfactory bulb are a combination of intrinsic and extrinsic factors cooperating to modulate the balance between proliferation and differentiation. We are only listing few of these mechanisms hereafter, as an illustration of the high degree of complexity of the interactions constituting the niche (Figure 17).

Intrinsic programmes gather several signalling mechanisms. High levels of cell cycle regulators including Retinoblastoma and E2F families coordinate proliferation in progenitors within the niche[103]. Similarly, defects in Ephrin

signalling in progenitors affect proper proliferation and severely impair the migration of neuroblasts[104]. Soluble amyloid precursor sAPP down-regulation can affect proliferation in NSCs too, given that they possess EGF-receptors of sAPP[105]. Furthermore, genetic deletion of mCD24 (small glycosylated GPI-anchored protein) in mice causes increased neurogenesis in their olfactory bulb[106]. Pax6 is also essential for the production of olfactory dopaminergic interneurons[107].

Extrinsic factors depend on the microenvironment of cells, as well as their exposure to hormones, neurotransmitters and growth factors. They underlie both cell differentiation and survival. A key-role of BMP signalling pathway in the maintenance of the balance between proliferation and neurogenesis was mentioned above. BMP signalling in NSCs enhances the maintenance of the pool of progenitors via extensive proliferation, but can be countered by the antagonistic action of Noggin from adjacent ependymal cells. In the latter case, ependymal cells increase neurogenic events and impair progenitor pool maintenance[99]. Interestingly, deletion of Smad4 in adult NSCs drastically decreases neuronal output in the same way as Noggin infusion[108]. In NSCs, Smad4 negatively regulates BMP signalling in a region-dependant fashion, which results in the expression of Olig2 transcription factor in their descendants. Olig2 positive cells will then differentiate into oligodendrocytes in the corpus callosum by repressing the expression Pax6 in the progeny of NSCs[108,109]. In line with this, Mash1 is also required for oligodendrocytes and neuronal specification[110]. Growth factors PEDF (Pigment epithelium-derived factor) and PDNF (parasite-derived neurotrophic factor) promote B1-cells proliferation, whereas BDNF (brain-derived neurotrophic factor) has the opposite effects and rather increases neurogenesis[111,112,113]. Hedgehog signalling and Galectin-1 carbohydrate-binding protein were also found to be involved in the maintenance of proliferation of NSCs[114,115]. More specifically, Hedgehog molecular pathway allows the maintenance of the progenitor pool, the production of IPs (also called transit amplifying cells) and indirectly the migration of neuroblasts[114]. A role of

transcription factors has also been disclosed: NSCs secrete GABA that binds to GABA-A receptors of neuroblasts and decreases their migratory speed locally.

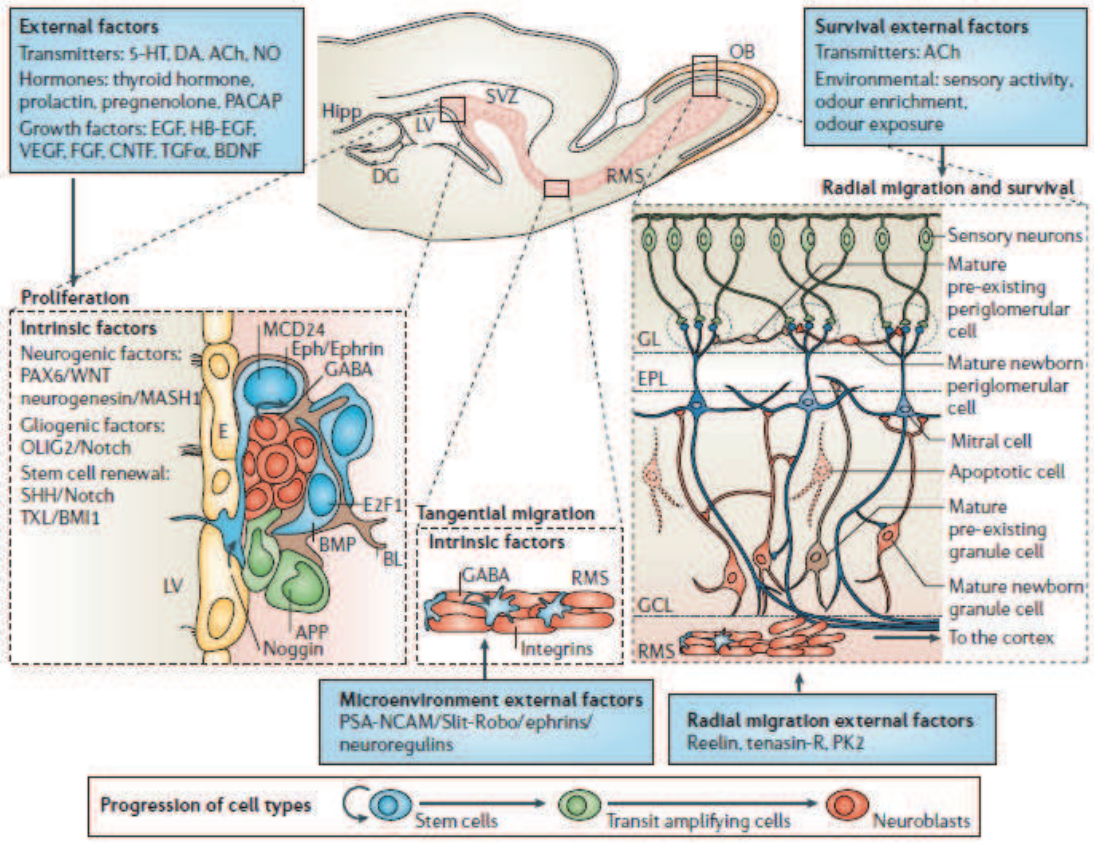

Figure 17: Scheme of molecular signalling driving adult neurogenesis in the SVZ.
From Lledo and Grubb 2006[79].

3) Plasticity of adult NSCs

The discovery of adult neurogenic niches in the brain has brought renewed interest to neural stem cells and their plasticity. Very intriguingly, a contemporary publication[116] has underlined the potency of NSCs to produce nascent endothelial cells by mere cell signalling in spite of their neuronal or glial progenitor identity. Proximity with endothelial cells can therefore convey endothelial identity to stem cells through their exposure to endothelial factors in spite of prior fate-commitment of stem cells towards neuronal or glial lineage. This result was most unexpected since stem cell plasticity had only been achieved

by cell-fusion at this time (2004). Cell-fusion consists on the acquisition of certain specific cellular determinants by another cell type via cell-fusion rather than exterior cellular signalling mediation. This work first raised the possibility that stem cells could enter distinct differentiation pathways depending on their environment and independently of cell-fusion mechanisms. It can be considered as a milestone for research in stem cell and regenerative medicine because it has considerably broadened the spectrum of stem cell plasticity. So far, these findings prompt to uncover original methods and genetic tools to address cell-lineage. Among others, the team of Dr Schaffer has taken up this challenge by generating an *in vitro* high-throughput microarrays technology to recapitulate heterotypic cell populations of the adult stem cell niche. This enables to study the effect of cell-cell communication and competing signals on the fate-decision *in vitro*. They conclude that there is a hierarchy between the molecular signals that modulates adult neurogenesis[117].

CHAPTER 2: MULTICILIATED EPENDYMAL CELLS

I- PRESENTATION OF MULTICILIATED CELLS

Epithelia of multiciliated cells form protective sheaths of mammalian organs. They exclusively participate in the efficiency of the reproductive, respiratory, and nervous systems. Their apical cell surface anchors 30 to 300 motile cilia organized in a ciliary tuft which confers to multiciliated cells important physical features fulfilling very specific vital functions (Figure 18 and Figure 19).

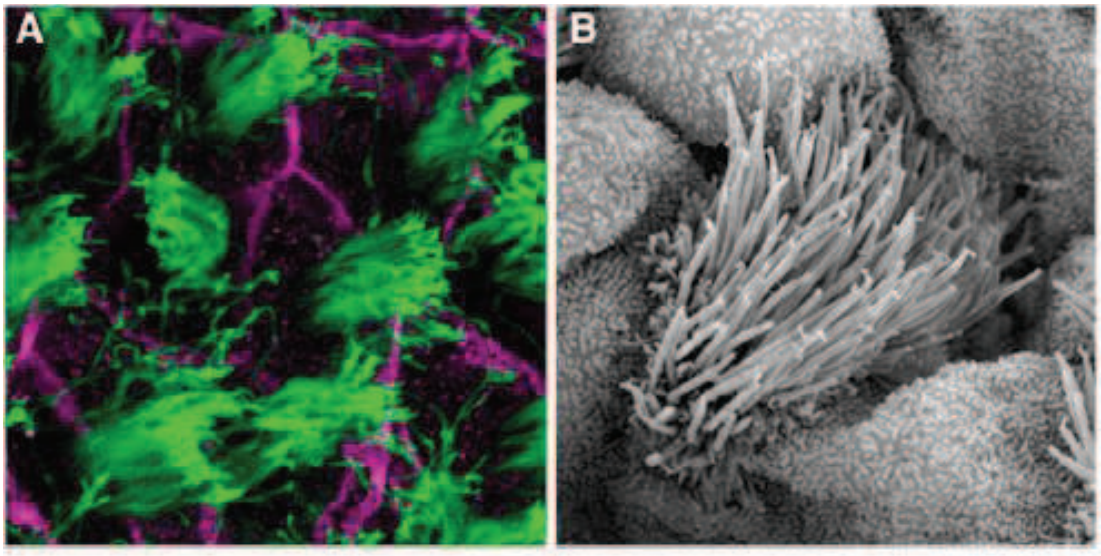

Figure 18: Multiciliated cells.
A-Mouse ependymal multiciliated cells stained with acetylated tubulin (green) and beta-catenin (magenta) **B-** Scanning electron micrograph of mouse tracheal multiciliated cells. From Brooks and Wallingford 2014[118].

1) Multiciliated cells of the respiratory system

Secretory cells, basal cells, and multiciliated cells all line the walls of respiratory tracts. Cilia are found in the upper airways which include nasal cavities, paranasal sinuses, Eustachian tubes and middle ear, and in the lower respiratory tract that goes from the trachea to the terminal bronchioles. Multiciliated cells are highly protective cells in charge of pathogens capture and mucus clearance. Consistently, their integrity is vital. The entire apical surface of multiciliated cells is covered with 100 to 200 cilia to maximize their effectiveness. Ciliary beating

together with coughing and swallowing participate in exiting the mucus from the respiratory tract to the pharynx in order to prevent infections. Mucociliary multiciliated cells are produced by transdifferentiation of basal and secretory cells[119,120]. Along the tracts towards the part of the respiratory tract, the diameter of the airways and multiciliated cell density are progressively reduced. The ciliary length is also decreased from 5-7µm in the trachea to 2-3µm in the 7th airway division[121]. The airways do not solely contain mucus, because the cilia of multiciliated cells are in fact separated from the mucus *per se* by a periciliary layer (PCL) of liquid. Because it is made of mucopolysaccharides and engulfs toxic chemicals, pathogens and small debris, the mucus is highly viscous as compared with the PCL of liquid which only contains mucins. The PCL of liquid thus facilitates ciliary beating and prevents the actual gel-like mucus to be trapped by cilia. Hydration/viscosity of the mucus and ciliary beating are interrelated via calcium and cAMP signalling cascade. Only thanks to this two-phase system called the "Gel on Brush" model can we explain certain respiratory diseases that previous models failed to explain[122,123].

2) <u>Multiciliated cells of the reproductive system</u>[122]

Logically, proper ciliary function takes a significant part in maintaining fertility, although other parameters also come into play (hormones, muscle contraction, etc.). To date, the main role of multiciliated cells in the female reproductive tract that has been described is oocyte transportation within the Fallopian tubes (so-called oviducts for non-human species)[124]. Investigations still fail to explain the presence of cilia in some parts of the reproductive system: in the uterus for instance, it was hypothesized that cilia could transport material secreted by glandular cells. Ciliary beating frequency is modulated by hormonal cycles; it increases during ovulation to facilitate oocyte transportation[125]. The proportion of multiciliated cells is region-dependant[126], and it is decreased by pregnancy and steroid contraception. Transport of the oocyte is enabled through its interaction with the glycocalix present at the tip of the cilia[127]. Conveniently, long-term sperm storage is possible for Mammalian species since their ovulation period is

not necessarily concomitant with copulation[128]. After intercourse, multiciliated cells among other cells allow sperm storage in the female tracts up to 6 days prior ovulation[122].

Multiciliated cells are in charge of sperm motility in the male reproductive system. They favour the transport of spermatozoa from the testis where they are produced, to the epididymis where they exit the testicle. Accordingly, the density of multiciliated cells increases through this path. Cilia beat in the direction opposite to fluid and sperm transportation, permitting reabsorption of fluid by non-ciliated cells to concentrate sperm. The concentration of sperm increases along the efferent ducts so that only sufficiently concentrated sperm will be able to circumvent ciliary activity and exit the efferent ducts. Collectively, proper sperm concentration, ciliary beating and tightly regulated gradient of pressure act together to ensure male fertility. [122,119,129,130].

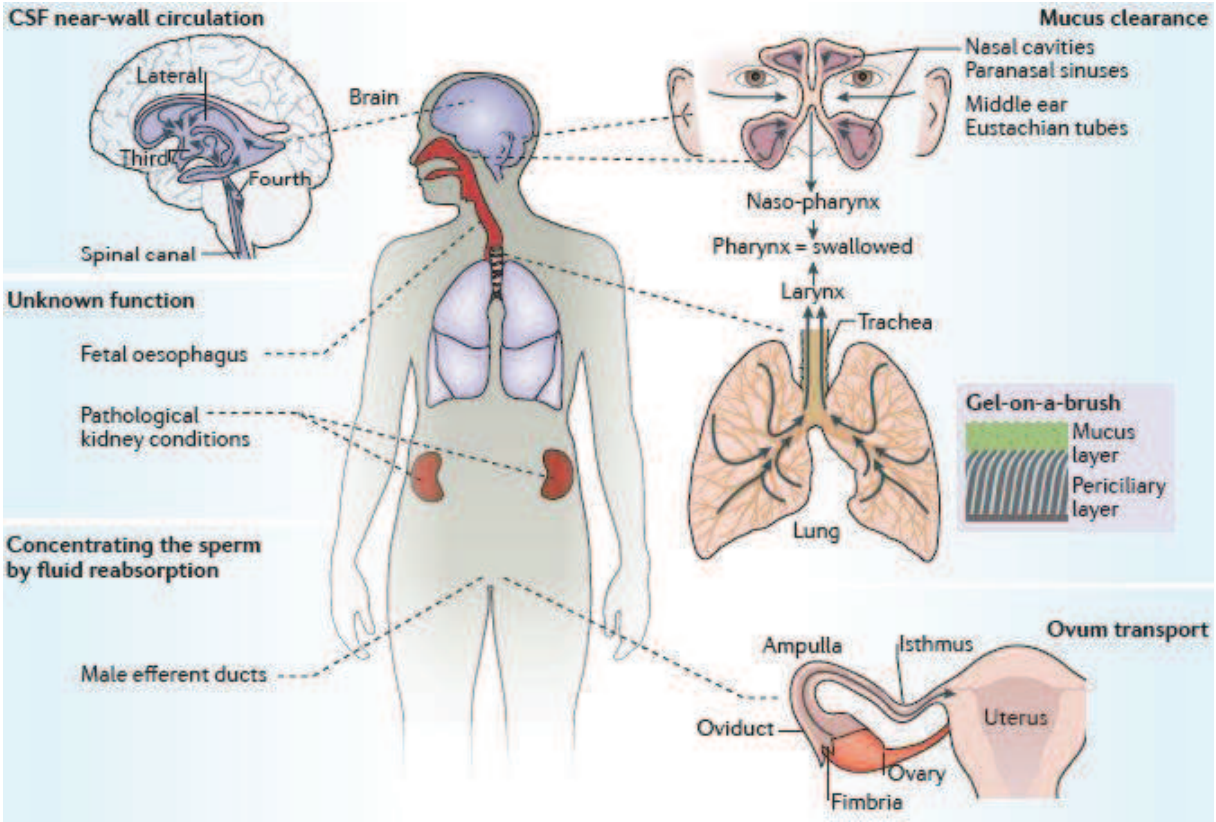

Figure 19: Multiciliated cells endorse various functions.
From Spassky and Meunier 2017[122].

3) Multiciliated ependymal cells

In the present work, we focus more particularly on ependymal multiciliated cells which line along the walls of all brain ventricles. Their strategic location at the interface between the CSF of ventricles and the brain enables them to endorse secretive and absorptive functions, which have proven necessary to maintain proper brain homeostasis[131]. Their multiple motile cilia beat synchronously to tightly control the flow of CSF through brain ventricles, therefore allowing biochemical communication between neural cells. Unlike respiratory cilia, ependymal cilia do not cover the entire apical surface. They cluster in an off-centered ciliary bundle. The position of the ciliary tuft on ependymal cells is defined by translational polarity[32]. The CSF ensures several vital functions. First as a liquid, it amortizes physical chocks, thus securing the brain and protecting it from neural damages. It also endorses crucial signalling functions which make it a leading actor of brain development and homeostasis[132,98]. Although CSF propulsion is mainly caused by heart beats, ependymal multiciliated cells also participate in orienting the CSF stream through rapid coordinate beating of their multiple motile cilia.

Defects in ependymal cells or their motile cilia can cause severe disorders, such as hydrocephalus phenotypes[119]. Hydrocephalus consists on an accumulation of CSF in the cerebral ventricles, so much that cerebral ventricles enlarge and dangerously compress brain tissues against the skull. This phenotype is due to impaired ependymal ciliary beating that prevents proper CSF circulation within cerebral ventricles. Eventually, the lack of CSF flow causes the acqueduct of Sylvius to close to the extent that CSF in the third cerebral ventricle can no longer reach the fourth cerebral ventricle. Cilia abnormalities in human are not sufficient to cause hydrocephalus but contribute to it. As we have previously mentioned, the ependymal flow of CSF ependymal cells is essential for the maintenance of neural circuits in the adult brain too, since it allows the proper migration of neuroblasts. Given this critical role of ependymal cells in the maintenance of

neural circuits, we can legitimately assess that mal-functioning ependymal cells might engender other neural disorders. Unfortunately, ependymal cells are still widely under-studied, and corroborating this hypothesis would require further investigations.

Unlike mature multiciliated ependymal cells from ventricular walls which are postmitotic[40], biciliated ependymal cells of the spinal cord retain stemness potency. They exhibit the capacity to self-renew in homeostatic conditions and act as neural stem cells after spinal cord injury. They can give rise to oligodendrocytes and abundant astrocytes which will be recruited to the site of injury to start the scarring process, according to the literature[133]. Nevertheless, more recent data published opposite findings, supporting a minimum contribution of ependymal cells scar formation subsequent to spinal cord injury[134]. This puts at question the well-established identity of ependymal cells as a major source of neural stem cells in the spinal cord. All in all, this controversy suggests that further investigations should be provided.

II- EPENDYMAL MOTILE CILIA

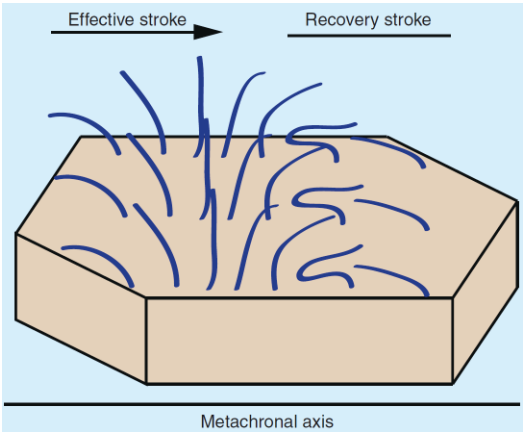

Figure 20: Schematic of ciliary beating of motile cilia.
From Brooks and Wallingford, 2014[118].

Motile cilia are much conserved organelles through animal species although their structure can vary among distinct multiciliated cell types. They widely used among microorganisms, mainly for their own motion in a liquid environment through fluid propulsion. Conversely, in Mammalian, they are organized in ciliary tufts and beat along a unidirectional plan (from 5 to 35 Hz) to form metachronal waves in order to regulate and better orient liquid or objects (pathogens, oocyte, etc.) circulation[122] (Figure 20). Because of their motility, cilia were the first organelle to ever be described in 1674-1675[135].The "9+2 structure" of motile cilia consists on an axoneme composed of 9 doublets of microtubules arranged in circle around two singlet microtubules. Each axoneme is nucleated by a basal body docked at the plasma membrane. The cilium is attached to the basal body thanks to a cytoskeleton-based structure called a ciliary rootlet. A basal body derives from one of the two centrioles of a cell centrosome (Figure 21).

Remarkably, some of their signalling pathways including intraciliary/intraflagellar transport (IFT) or planar cell polarity (PCP) signalling resemble the ones of the primary cilia, as they are responsible for ciliogenesis in general. Each motile cilium is anchored at a basal body which is a short centriole-derived cylindrical structure docked at the apical membrane of multiciliated cells. Together, Centrin-2 (Cen2), protein of centriole 5 (POC5) are bound to polyglutamylated tubulin to form a basal body and recruit Cep164 (distal appendage protein) to anchor at the apical membrane and grow the cilium[122,136,137,138,139,140]. Basal bodies have an oriented asymmetric structure because of their basal foot, and their orientation is coordinated with one another in order to allow proper ciliary function[141]. This basal foot is considered a major microtubule-organizing center (MTOC) in multiciliated cells. Interestingly, genetic depletion of microtubule-associated basal feet caps components (outer dense fiber protein 2 Odf2, γ-tubulin and galectin-3) prevents proper alignment of basal bodies with each other[141,142,143,144,145].

In ependymal multiciliated cells more specifically, basal bodies are clustered towards the downstream flow at the cell surface[146], whereas in airway multiciliated cells, they are evenly distributed on the entire apical surface.

The beating process is biphasic and initiated by energy-consuming ATPase dynein motor proteins triggering neighbouring axonemes to slide onto one another. This causes the cilium to bend fast and thus propel the liquid vigorously before slowly recovering its initial uptight position in the direction opposite to the fluid flow. While the initial fluid propulsion stroke is powerful and very rapid, the recovery stroke is much slower (Figure 20).

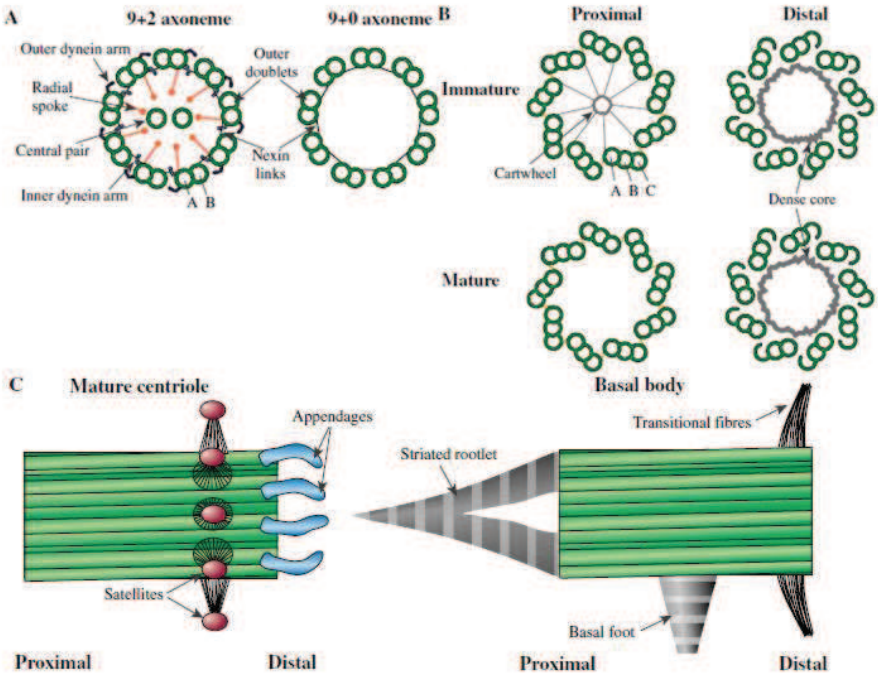

Figure 21: Representative scheme of cilia, centriole and basal body structure. **A-** Structure of a transverse section of motile (left) and immotile (right) axonemes. **B-** Structure of a transverse section of centrioles. C- Longitudinal view of centriole and basal body and their connected elements. From Dawe et al. 2006[147].

Other cytoskeleton components also contribute to the proper orientation of all basal bodies within the cell: Myosin II is responsible for the unipolar migration of basal bodies in clusters[132], and actin is recruited at the subapical part of

multiciliated cells to allow even distribution of adjacent basal bodies[144]. As for the interplay of motile cilia with extracellular environment, voluminous proteins such as G-protein-coupled receptors (GPCRs) are incapable of entering the cilium through simple diffusion even though much smaller proteins can. They require specific mechanisms and proteins located in the transition zone, at the proximal end of the cilium.

III- EPENDYMAL CELL DEVELOPMENT

Ependymal multiciliated cells of the rodent brain derive from a subpopulation of RGCs, as it was mentioned previously. These RGCs perform their last division between E14.5 and E16.5 prior to the onset of the expression of genes promoting ciliogenesis[40]. BrdU injections at successive embryonic stages in mice also revealed that ependymal cells located at the caudal part of the lateral wall of the lateral ventricle develop earlier than more rostral ependymal cells. These results indicate that the ependymal cell development and maturation is region dependent, they begin caudally and progress in a wave-like pattern along the caudal-rostral axis[40]. Ependymal cells then pursue their maturation during late embryogenic stages and the first postnatal week. They are post-mitotic cells which do not divide nor renew throughout life under physiological conditions[40].

1) Specification of ependymal multiciliated cells

It has been shown that Notch 1 expression was lower in multiciliated cells than in neighbouring cells in human airways and *Xenopus laevis* embryonic epidermis[148]. Furthermore, Notch expression is known to inhibit ciliogenesis and is considered as a marker of undifferentiated cells (such as NSCs for instance). To summarize, Notch signalling is activated signal of via the association of transmembrane protein Notch with the Delta-like transmembrane protein (Dll) located on an

adjacent cell. This paracrine signal will cause the release of Notch intracellular domain (NICD) by γ-secretase proteolytic cleavage. NICD is then translocated inside the nucleus where it interacts with DNA-binding proteins to induce the expression of transcription factors and recruit co-activators (such as Mastermind protein for instance)[149]. Notch expression can be downregulated by lateral inhibition, preventing the expression of stemness genes[150]. However, Notch is involved in numerous differentiation pathways and does not limit to the mediation of ependymal cell progenitors; In human airways, micro-RNAs miR-34 and miR-449 were highlighted as inhibitors of the Notch-Dll pathway, therefore promoting ciliogenesis[148,151]. Besides, Notch downregulation in human embryonic stem cells leads to motor neurons generation[152]. Conclusively, Notch down-regulation or inhibition is necessary although insufficient to commit stem cells towards ependymal cell-fate fate. In other words, Notch is a major actor of the differentiation of RGCs prior to their fate-commitment.

How is cell fate specified towards ciliogenesis in multiciliated cells? Elucidating fate-committing mechanisms of stem cells towards multiciliated cells (so-called specification mechanisms) is paramount in order to comprehend ciliopathies and for obvious therapeutic purposes. In this perspective, recent investigations have shed light on GemC1 (a.k.a. Lynkeas) protein. In the mouse brain, GemC1 is homologous to the Geminin protein and acts upstream of Multicilin (or McIdas) to launch ciliation transcriptional programmes[153,154]. GemC1, Multicilin and Geminin all belong to the Geminin superfamily owing to their common coiled-coil domain. Remarkably, the coiled-coil regions of GemC1 and Geminin are less similar with each other than the coiled-coil regions of Geminin and Multicilin. GemC1 possess a C-terminal region resembling the C-terminal region of Multicilin unlike Geminin[155].

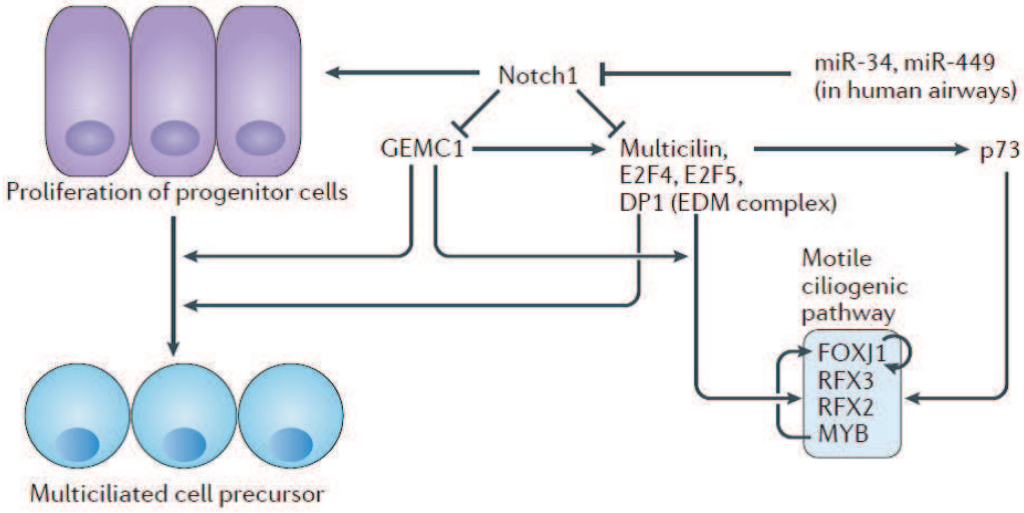

Figure 22: Molecular pathways of Ciliation.
From Spassky and Meunier 2017[122].

What are the molecular mechanisms of Geminin superfamily proteins to initiate multiciliated cell specification? (Figure 22)

Importantly, Notch is an antagonist of Multicilin. Multicilin promotes centriole biogenesis that is necessary to start ciliogenesis via E2F cell cycle regulators[156]. Multicilin is located in the nucleus where it can activate genes that are critical for ciliogenesis, such as FoxJ1 (Forkhead box J1) transcription factor[157]. Alternatively, GemC1 can also directly trigger FoxJ1 activation driving multiciliogenesis [154,153,158,159]. FoxJ1 is a core actor of motile cilia generation in a large variety of multiciliated cells[160,161,162,163] . Interestingly, multiciliated cells are formed in mouse FoxJ1 null mutant mouse. Nonetheless, studies have demonstrated that centriole duplication occurs normally in these mutant mice. In spite of this, centrioles cannot dock to the apical plasma membrane of multiciliated cells and become basal bodies in because Rho-A-mediated apical actin enrichment is defective. This indicates that FoxJ1 is not involved in the fate-decision making of progenitors towards multiciliated cell fate but rather acts subsequent to lineage-commitment during late ciliogenesis in multiciliated cells[164]. Additional works also provided evidence that FoxJ1 is necessary and sufficient to drive motile cilia biogenesis by inducing the expression of genes of

the multiciliogenesis pathway in the *Xenopus* and Zebrafish[165]. In the lungs, Myb transcription factor is expressed subsequent to cell cycle exit in progenitors and initiates multiciliogenesis by promoting FoxJ1 expression in these cells[158].

a. *Role of Geminin Superfamily in the cell cycle*

The role of GemC1 was first uncovered in the cell cycle. It is strategically located at the origins of replication to act on DNA replication in *Xenopus* egg extract. To fulfil this function, it associates initially with checkpoint and replication factor TopBP1 protein. This interaction enables GemC1 to bind chromatin at the onset of replication and form pre-replication complexes. Only afterwards can GemC1 reach an active phosphorylated state through its interaction with Cdc45 and Cdk2-Cyclin 2, therefore initiating DNA replication[166].

Geminin, GemC1 and Multicilin are all part of the Geminin coiled-coil superfamily. Accordingly, the central coiled coil part of Multicilin and Geminin allows their association. This interaction reduces the affinity of Geminin for Cdt protein. In proliferating cells, Geminin inhibits Cdt by binding to it during S and G2 phases of the cell cycle. This results in preventing supernumerary rounds of DNA replication by Cdt. Conversely, Multicilin is expressed in some regions of the developing brain where it can bind with Geminin and thus orient the cell fate towards differentiation. In sum, these data highlight the role of Geminin in cellular fate decisions by controlling the balance between cell proliferation and differentiation[155].

b. *Role of GemC1 in ciliogenesis*

Recent studies have demonstrated a critical role of GemC1 in the development of RGCs into ependymal cells in the mammalian developing brain (Figure 23)[159,167,168]. Along with Multicilin, GemC1 begins to be expressed in undifferentiated RGCs of the periventricular zone around E16. Later during embryogenesis, FoxJ1 expression begins in ependymal progenitors where it

colocalizes with GemC1 and Multicilin until the first postnatal week. While S100β is also expressed in these cells, Tuj1 neuronal marker is not. These results are clear evidence that GemC1 and Multicilin are specific markers of ependymal fate-committed RGCs. This raises the possibility that GemC1/Multicilin signalling pathway could be accountable for fate-decision and lineage-commitment of RGCs long before the actual onset of ependymal differentiation[159,40].

This role appears to be conserved in other types of multiciliated cells through organs (airway) as well as species (zebrafish)[153,169,170].

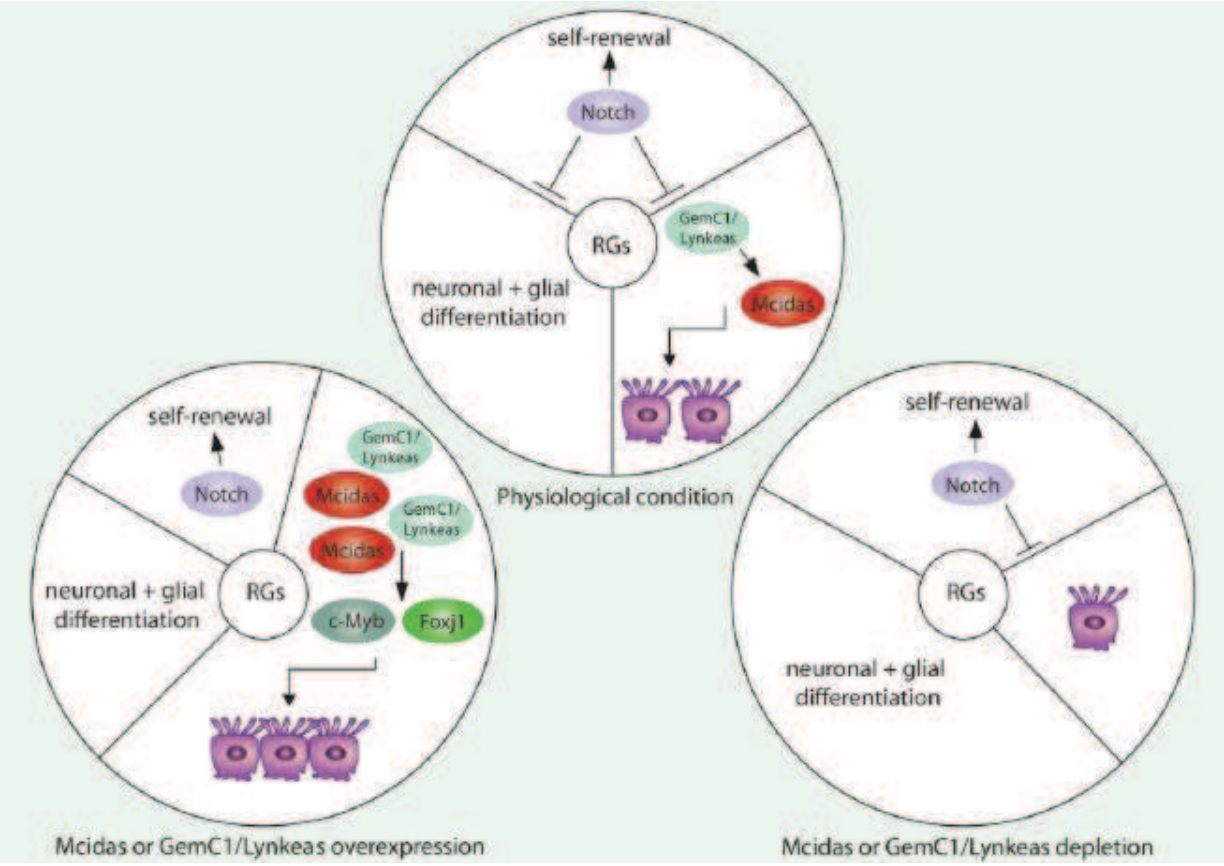

Figure 23: Schematic specification of RGCs in the Mammalian developing brain.
From Kyrousi et al. 2016[167]

2) Maturation of ependymal multiciliated cells

Like RGCs, early ependymal progenitors originally have a centrosome nucleating a primary cilium. A centrosome is an organelle composed of two centrioles arranged orthogonally and it is well known as a crucial regulator of the cell cycle and the main MTOC. A centriole is a cytoskeleton cylinder of nice triplets of microtubules organised in a cartwheel-like structure. The mother centriole can be easily recognised by the distal appendages surrounding it and can nucleate a primary cilium in most cells, unlike the daughter centriole. Noteworthy, many proteins called pericentriolar material (PCM) can be found akin the centrosome (e.g. ninein, pericentrin and γ-tubulin).

How do ependymal progenitors amplify their centrioles to grow numerous motile cilia? (Figure 24) As they mature, ependymal progenitors undergo large-scale centriole production to generate all the basal bodies that will anchor each motile cilium. A recent study in the laboratory has shown that massive centriole biogenesis occurs through a two distinct pathways: the centriolar deuterosome-independent and the deuterosome-dependant mechanisms. This highlights the existence of a centrosome asymmetry, where the mother centriole is responsible for the nucleation of the primary cilium in cycling progenitors of multiciliated cells, and the daughter centriole for the nucleation of motile cilia in differentiating progenitors of multiciliated cells through the deuterosome-dependant pathway[171]. The earliest ependymal progenitor can be identified by its centrosome prior to the onset of centriole amplification. In the deuterosome-dependant pathway, centriole amplification *per se* starts when the daughter centriole initiates the formation of deuterosomes in its direct contact. Deuterosomes nucleate the growth of several procentrioles. They express the deuterosome protein Deup1 which can therefore be used as a marker for deuterosomes. Once formed, a deuterosome connected to its procentrioles will detach from the daughter centriole in the cytoplasm to allow formation of new deuterosomes, but remains in its proximity: this is known as the “halo stage”. Then procentrioles grow all around deuterosomes (or the mother and daughter

centrioles for the centriolar deuterosome-independent pathway) as they mature: this is the "flower stage". At this stage, the mother and daughter centrioles directly nucleate procentrioles too. Last, centrioles are released into the cytoplasm to mature and dock at the apical plasma membrane prior to motile cilia growth. Mature docked centrioles are eventually called basal bodies.

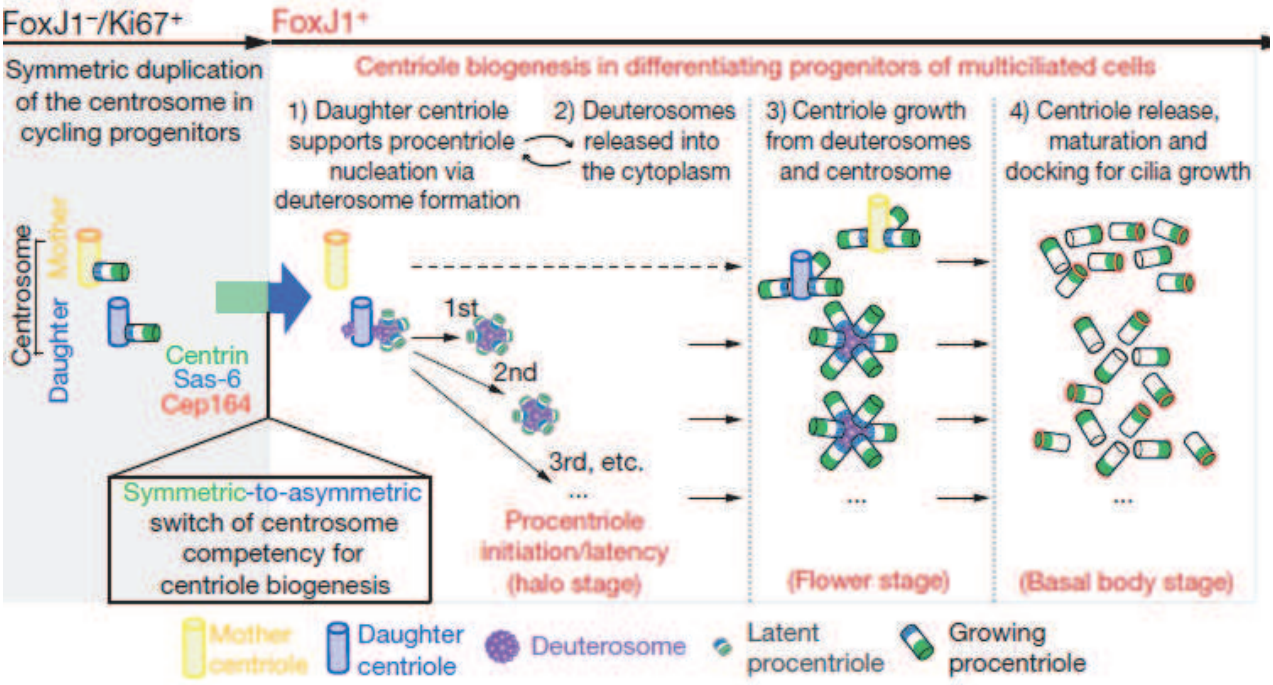

Figure 24: Centriole amplification mechanism.
From Al Jord et al. 2014[171]

As ciliogenesis begins, scattered randomly-oriented basal bodies of a multiciliated cell tend to re-distribute in clusters and all orient in the same direction *in vivo* with respect to the tissue polarity. In line with this, adjacent multiciliated cells usually also develop simultaneously within a local region of ventricular walls. These two levels of polarity are characteristic cues of ependymal multiciliated cells. The orientation of the ciliary beating is called "rotational polarity", while the planar asymmetric localization of clusters of basal bodies at the apical cell surface is named "translational polarity"[122]. The establishment of rotational and translational polarities is critical to ensure proper cilia maturation.

In mouse ependymal cells, rotational and translational polarities are driven by signalling mechanisms. Nevertheless, while both polarities are established through PCP signalling, the mechanisms are different. The common orientation of all basal bodies within a multiciliated cell (a.k.a. rotational polarity) is Celsr1-dependant, whereas the asymmetric position of the patch of basal bodies on the apical cell surface for several cells at the tissue-level (a.k.a translational polarity) is due to the intervention of Celsr2 and 3[172]. Interestingly, proteins Celsr 1, 2 and 3 are all necessary for proper localization of Vangl2 and Fzd3 at the plasma membrane[173]. Since Fzd3 is part of Dishevelled (Dsh) signalling, its localization at the plasma membrane is also crucial for the well-functioning Wnt signalling. Studies have also shown that the protein Vangl2 is expressed in both immature and mature ependymal cells at the apical membrane and along cilia. Remarkably, the transient localization of at the posterior apical surface of ependymal cells (corresponding to the upstream side of CSF flow) is necessary for their differentiation since it is required for the ciliary alignment response to CSF flow[174,172]. These results highlight the importance of hydrodynamic forces and PCP coupling in ependymal cell development.

The role of the primary cilium of RGCs in PCP signalling has also been characterized[146]. Namely, primary cilia retain mechanosensory proteins polycystic kidney disease 1 and 2 (Pkd1 and Pkd2) that are first required for proper establishment of translational polarity in ependymal progenitors. By extension, it has been hypothesized that the primary cilium might be able to detect hydrodynamic forces in CSF in RGCs or immature ependymal cells via Pkd1 and Pkd2[172,32].

On the whole, PCP signalling drives both tissue-level polarity and intracellular polarity in all Vertebrate multiciliated cells more generally (Figure 25)[32]. Tissue-level polarity relies on the asymmetric distribution of PCP proteins within the intracellular cortex of multiciliated cells. Henceforth, PCP signalling is critical for ciliogenesis in all ciliated cells and more specifically impacts the establishment of both rotational and translational polarities in ependymal cells[172]. Ultimately, only

the flawless spatiotemporal coordination of ependymal cells will result in a global efficient regulation of the CSF flow throughout adult brain ventricles.

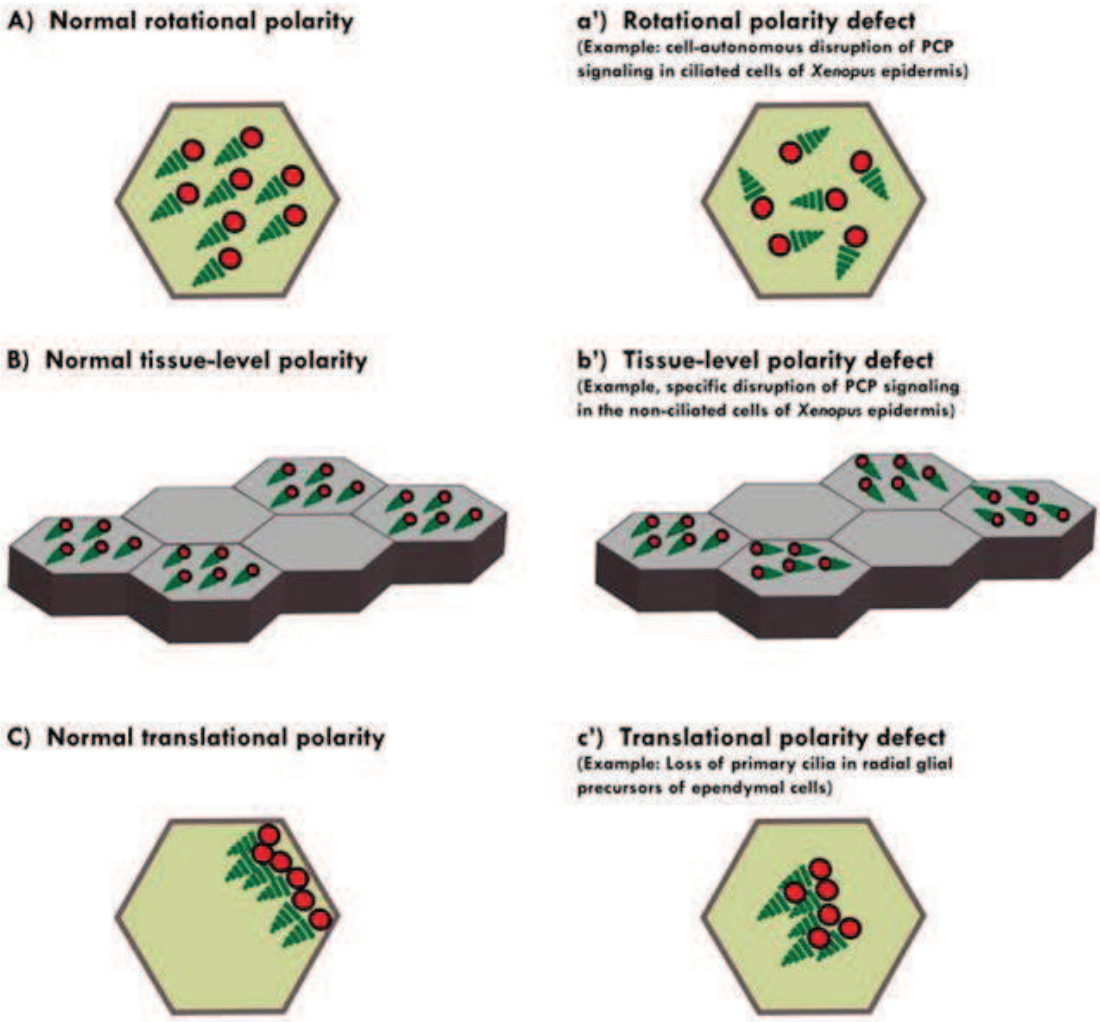

Figure 25: Explicative scheme of the rotational and the translational polarity. Rootlets are represented in green and basal bodies in red. From Wallingford 2011[175].

OBJECTIVES

We have introduced pre-existing theories and concepts underlying neural development, and more particularly the development of multiciliated ependymal cell. These data set crucial foundations for new biological questions and discoveries in this research field, and prompt to reach further levels of understanding of neural development.

In light of these notions, our work is focused on the production of ependymal cells during neural development. We tune complementary clonal lineage approaches: Brainbow and MADM, and complex experimental techniques such as *in utero* electroporation to fulfil precise objectives:

- First, we study ependymal progenitors to understand whether they migrate away from the location where their last division has occurred or if they stay where they were produced.
- Second, we determine whether ependymal cells are produced through symmetric or asymmetric cell division during embryogenesis, and what other(s) cell type(s) is/are produced concomitantly during gliogenesis.
- Last, we also tackle fate-decision mechanisms in RGC using factors promoting or disrupting ependymal cell production.

Results

Research Article

Submitted Manuscript

ADULT NEURAL STEM CELLS AND MULTICILIATED EPENDYMAL CELLS SHARE A COMMON LINEAGE

Gonzalo Ortiz Alvarez[1]*, Marie Daclin[1]*, Asm Shihavuddin[1,5], Pauline Lansade[1], Aurélien Fortoul[1], Marion Faucourt[1], Solène Clavreul[2], Stavros Taraviras[3], Simon Hippenmeyer[4], Jean Livet[2], Alice Meunier[1], Auguste Genovesio[1] and Nathalie Spassky[1]

AFFILIATIONS

[1]Cilia biology and neurogenesis, Institut de biologie de l'Ecole normale supérieure (IBENS), Ecole normale supérieure, CNRS, INSERM, PSL Université Paris 75005 Paris, France

[2]Sorbonne Université, INSERM, CNRS, Institut de la Vision, F-75012 Paris, France

[3]Department of Physiology, Medical School, University of Patras, 26504 Rio, Patras, Greece

[4]Institute of Science and Technology Austria, Am Campus 1, 3400 Klosterneuburg, Austria

[5]Present address: Department of Applied Mathematics and Computer Science, Technical University of Denmark (DTU), Kgs. Lyngby, Denmark

AUTHOR LIST FOOTNOTES

*Equal contribution

Corresponding author and lead contact e-mail address: nathalie.spassky@ens.fr

SUMMARY

Adult neural stem cells (NSCs) (B1 cells) and post-mitotic multiciliated ependymal cells (E cells) are glial cells that compose the neurogenic niche in the mammalian brain. Although both cells originate from radial glial cells (RGCs) at late embryonic stages, the mechanism of their production is unknown. By clonal analysis of large numbers of RGCs using MAGIC markers and single-cell resolution of progenitor division patterns and fate with MADM, we show that the vast majority of B1 and E cells originate from bipotent progenitors. We also demonstrate that the Geminin family members, initially identified as regulators of DNA replication can modify the relative numbers of B1 and E cells in the resulting clones. These results suggest that the cell fate decision of gliogenic progenitors in the ventricular-subventricular zone (V-SVZ) of the lateral ventricles is controlled by regulators of DNA replication.

INTRODUCTION

Neurons and glial cells are continuously produced throughout life. During embryogenesis, neurons are first produced from radial glial cells (RGCs), which then become gliogenic (Gao et al., 2014). A subpopulation of astrocytes (type B1) located in the ventricular-subventricular (V-SVZ) region of the lateral ventricle retain stem cell properties in the adult, i.e., self-renewal and multilineage differentiation (Doetsch et al., 1999). These cells contact the lateral ventricle (LV) and have a long basal process ending on blood vessels (Shen et al., 2008; Tavazoie et al., 2008). Their apical contact, from which a primary cilium grows from the centrosome, is surrounded by another type of glial cell, the multiciliated ependymal cell, and form a pinwheel structure at the ventricular surface (Mirzadeh et al., 2008). Ependymal cells form a multiciliated epithelium at the brain-ventricle interface. The coordinated beating of their cilia contributes to cerebrospinal fluid (CSF) dynamics, which is crucial for the exposure of type B1 cells to trophic and metabolic signals and to clear toxins and waste from the brain (Spassky and Meunier, 2017). Proper functioning of adult neurogenesis thus depends on the production and positioning of the controlled number of ependymal cells and type B1 astrocytes composing the neurogenic niche.

Type B1 astrocytes and ependymal cells are both derived from RGCs between E13.5 and E15.5 and progressively acquire identical phenotypic markers (Sox2, Sox9, Nestin, CD133) (Ferri et al., 2004; Mirzadeh et al., 2008; Sun et al., 2017), suggesting common developmental mechanisms for these cells. In addition to their distinct morphologies and functions in the adult neurogenic niche, one major difference between these cells is that type B1 astrocytes are reactivable quiescent cells, while multiciliated ependymal cells are postmitotic under homeostasis throughout life (Fuentealba et al., 2015; Furutachi et al., 2015; Shah et al., 2018; Spassky et al., 2005). It is totally unknown how these cells acquire their common characteristics/distinct identities and functions. One way to address this question would be to study their lineage and determine whether they are derived from distinct individual early-specified RGCs, as recently shown for olfactory bulb interneurons (Fuentealba et al., 2015).

The Geminin superfamily consists of three members: Geminin, McIdas and GemC1, which were initially characterized for their role in DNA replication control (Balestrini et al., 2010; McGarry and Kirschner, 1998; Pefani et al., 2011). More recently, GemC1 and McIdas were identified as master regulators of multiciliogenesis (Arbi et al., 2016; Boon et al., 2014; Kyrousi

et al., 2015; Ma et al., 2014; Stubbs et al., 2012; Terré et al., 2016; Zhou et al., 2015) and Geminin as a regulator of neural cell fate and is highly expressed in cycling type B1 cells in the adult SVZ (Khatri et al., 2014; Sankar et al., 2016).

Here, we exploited high resolution lineage-tracing techniques, namely the MAGIC Markers (Loulier et al., 2014) and MADM strategies (Gao et al., 2014) in the mouse brain to show that type B1 astrocytes and ependymal cells share a common RGC progenitor. These RGCs first produce type B1 astrocytes through both symmetric and asymmetric divisions. In addition, ependymal cells are produced through a terminal symmetric division. We also examined the role of antagonist regulators of DNA replication (GemC1 and Geminin) in the lineage progression. We show that GemC1 promotes premature symmetric division of RGCs producing ependymal cells at the expense of astrocytes, whereas Geminin favors symmetric divisions producing type B1 astrocytes. Altogether, we show that ependymal cells and type B1 astrocytes share a common lineage, in which type B1 cells are produced first followed by a majority of ependymal cells. This dynamic can be modulated by the Geminin family members.

RESULTS

1) Ependymal cells originate from locally-differentiated RGCs

Multiciliated ependymal cells are generated from RGCs around E15 (Spassky et al., 2005). To determine how these cells develop, we performed a single injection of EdU at E15.5 and studied the relative positions of EdU^+ ependymal cells on the ventricular walls at P15. EdU^+ ependymal cells were often juxtaposed or close to each other (Supplementary Figure 1A-B). To quantitatively assess their spatial distribution, we performed a nearest-neighbor distance (NND) analysis on the data sets. The NNDs among EdU^+ ependymal cells were significantly shorter than in simulated random data sets, suggesting that ependymal cells born at the same time remain in the same area (Supplementary Figure 1C). To further test this possibility, we employed a genetic fate-tracing strategy. We crossed the Ai14 transgenic mouse line, which expresses tdTomato after Cre-dependent excision of a “floxed-stop” cassette (Madisen et al., 2010), with Emx1-Cre, Gsh2-Cre or Nkx2.1-Cre transgenic mice, which mainly express Cre in the dorsal/medial, lateral and ventral regions of the lateral ventricles, respectively (Figure 1A-C). At P10, almost all ependymal cells were tdT^+ in Cre-expressing ventricular walls (Figure 1D-

Figure 1

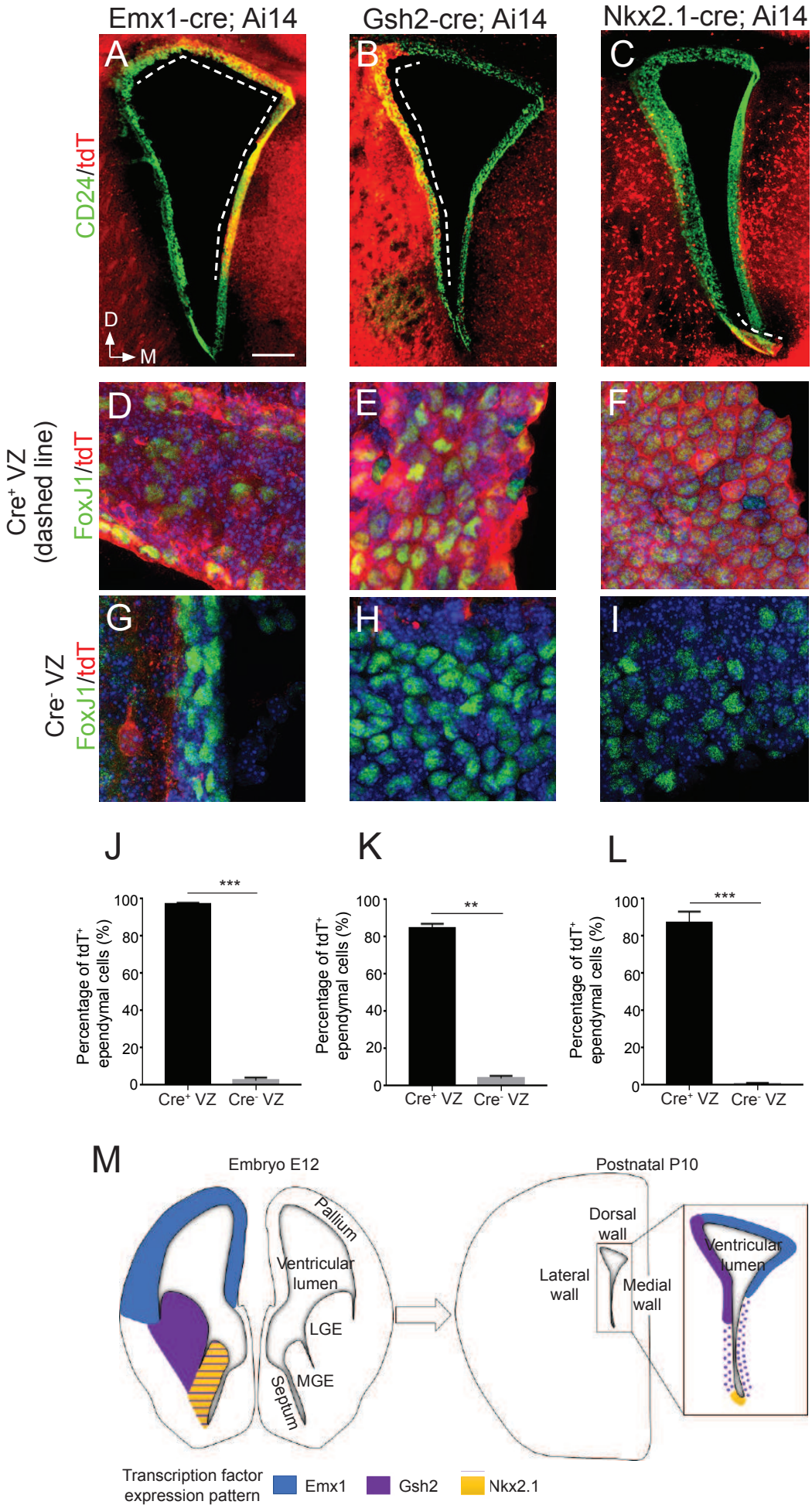
Emx1-cre; Ai14
Gsh2-cre; Ai14
Nkx2.1-cre; Ai14
A
B
C
CD24/tdT
D
M
D
E
F
Cre+ VZ (dashed line)
FoxJ1/tdT
G
H
I
Cre- VZ
FoxJ1/tdT
J
K
L
***
**
***
Percentage of tdT+ ependymal cells (%)
100
80
60
40
20
0
Cre+ VZ
Cre- VZ
M
Embryo E12
Postnatal P10
Pallium
Ventricular lumen
LGE
MGE
Septum
Dorsal wall
Lateral wall
Medial wall
Ventricular lumen
Transcription factor expression pattern
Emx1
Gsh2
Nkx2.1

Figure 1. Ependymal cell progenitors are produced locally along the brain ventricles.

(A-C) Representative images of coronal sections of Emx1-Cre; Ai14 (A), Gsh2-Cre; Ai14 (B) and Nkx2.1-Cre; Ai14 (C) forebrain at P10, immunostained with the CD24 (green) and DsRed (tdT, red) antibodies. $CD24^{+}tdT^{+}$ ependymal cells are only observed in the Cre-expressing domains in each mouse line (indicated by a dashed line). (D-I) Representative high magnification images of the Emx1-Cre; Ai14 (D, G), Gsh2-Cre; Ai14 (E, H) and Nkx2.1-Cre; Ai14 (F, I) coronal sections immunostained with FoxJ1 (green) and DsRed (tdT, red) antibodies in the Cre^{+} domains (D, E, F) or Cre^{-} domains (G, H, I), respectively. In the Cre^{+} domains, almost all ependymal cells are tdT^{+}, whereas very few cells are double-labeled in the Cre^{-} domains in each mouse line. (J-L) Quantification of tdT^{+} ependymal cells in different areas of the ventricular zone from n=4 mice from each of the three transgenic mouse lines. Error bars indicate the SEM. p-values were determined with the Mann-Whitney test; ** = $p \leq 0.01$ and *** = $p \leq 0.001$. (M) Schematic of the expression patterns of each transcription factor in the mouse forebrain at E12 and model of the spatial origin of ependymal cells at P10. D, dorsal; M, medial. The scale bar represents 200 μm (A-C) and 10 μm (D-I).

F), whereas they were tdT$^-$ in Cre negative regions (Figure 1G-I), showing that ependymal cells do not migrate out of their site of origin during maturation (Figure 1J-M). We observed similar results in all caudo-rostral regions examined. Together, these results show that ependymal cells are produced locally and do not migrate long distances from their site of origin.

2) *In utero* electroporation (IUE) labels ependymal cells and type B1 astrocytes in the V-SVZ

Given that ependymal cells develop locally from RGCs, we labeled their progenitors at E14.5 in the Lateral Ganglionic Eminence (LGE) by electroporation *in utero* and traced their lineage at later stages. We first verified that cells targeted by IUE are cycling by injecting EdU at E13.5 or E14.5. The next day, 78±2% of electroporated cells were indeed EdU$^+$ (Supplementary Figure 2), confirming that cycling cells are preferentially transfected by IUE and that progenitor fate can be traced by this technique, as previously shown (Loulier et al., 2014; Stancik et al., 2010).

We then characterized the progeny of cells electroporated at E14.5 with the H2B-GFP plasmid by immunostaining the V-SVZ at P10-P15 with FoxJ1 and Sox9 antibodies to distinguish ependymal cells (FoxJ1$^+$Sox9$^+$) from other glial cells (FoxJ1$^-$Sox9$^+$) (Sun et al., 2017) (Figure 2A-B). We observed that around two thirds of GFP$^+$ cells were ependymal cells, whereas most of the remaining FoxJ1$^-$ cells were Sox9$^+$ astrocytes (Figure 2C). We also performed FOP and GFAP staining to distinguish ependymal cells (multiple FOP$^+$ basal bodies/GFAP$^-$) from astrocytes (FOP$^+$ centrosome/GFAP$^+$). Most electroporated cells close to the ventricular surface were either GFAP$^-$ ependymal cells containing multiple FOP$^+$ basal bodies or GFAP$^+$ astrocytes with one FOP$^+$ centrosome (Figure 2D). A ventricular contact emitting a primary cilium was also observed on GFP$^+$ astrocytes (Doetsch et al., 1999). The GFP$^+$ astrocytes often had an unusual nuclear morphology with envelope invaginations, as recently reported (Cebrián-Silla et al., 2017). Noteworthy, neuroblasts with their typical migratory morphology were observed deeper in the tissue and at a distance from the electroporated area in the direction of the olfactory bulb (data not shown).

To further test whether some of the astrocytes originating from the electroporated RGCs could act as adult neural stem cells (type B1 astrocytes), we permanently labeled RGCs and their progeny with a transposable *Nucbow* vector at E14.5 (nuclear MAGIC markers, Loulier et al., 2014) and administered EdU through the animals' drinking water for 14 days starting at

Figure 2

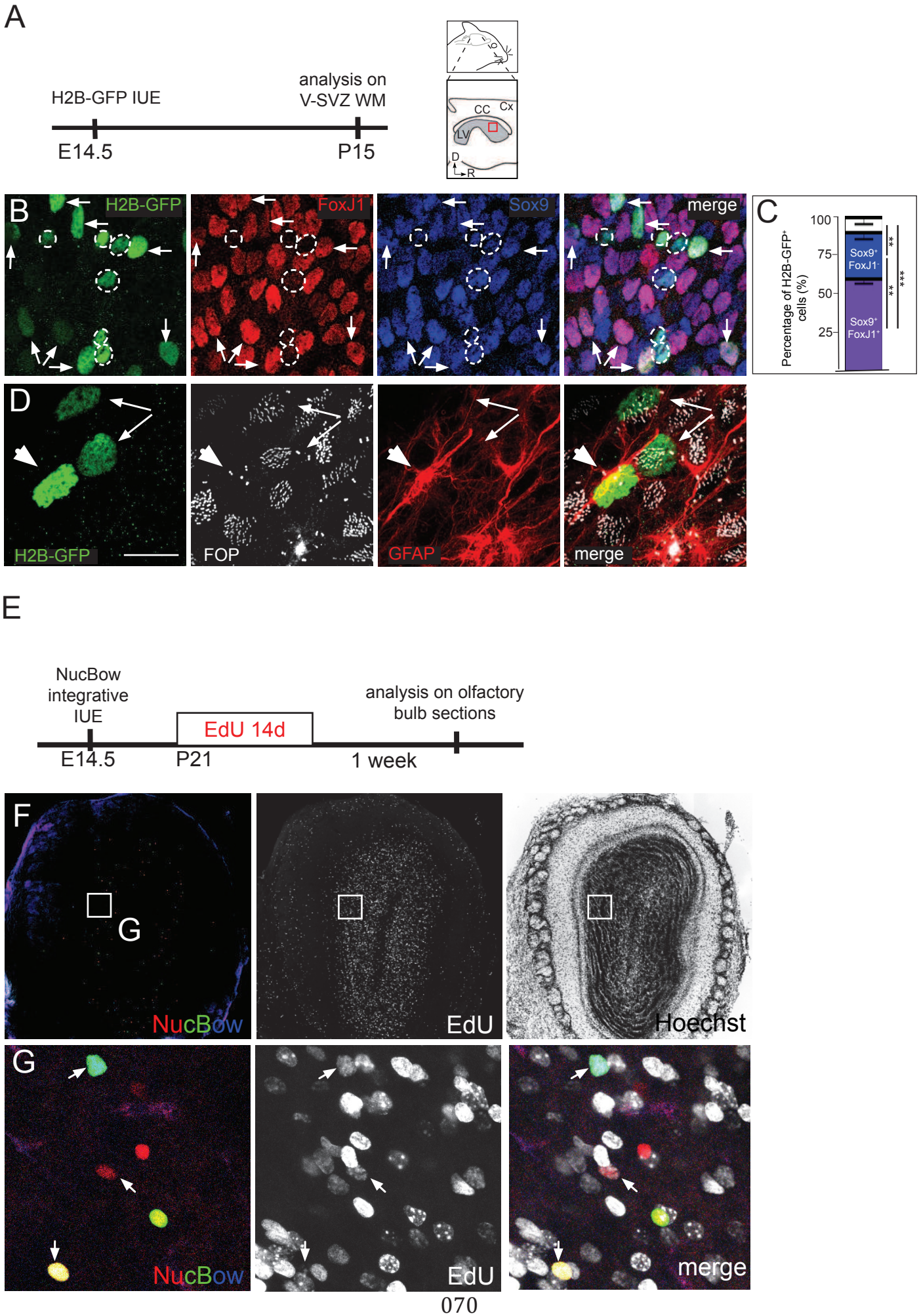
A
H2B-GFP IUE
E14.5
analysis on
V-SVZ WM
P15
CC
Cx
LV
D
R
B
H2B-GFP
FoxJ1
Sox9
merge
C
Percentage of H2B-GFP+ cells (%)
100
75
50
25
Sox9+ FoxJ1-
Sox9+ FoxJ1+
**
**
***
D
H2B-GFP
FOP
GFAP
merge
E
NucBow integrative IUE
E14.5
EdU 14d
P21
analysis on olfactory bulb sections
1 week
F
G
NucBow
EdU
Hoechst
G
NucBow
EdU
merge

Figure 2: Radial Glial Cells generate ependymal cells and adult neural stem cells (type B1 astrocytes)

(A) Experimental schema for (B-D): the H2B-GFP-expressing plasmid was electroporated *in utero* at E14.5 and analyzed on SVZ WM at P15. CC, corpus callosum; Cx, Cortex; LV, lateral ventricle; R, Rostral and D, Dorsal. (B, D) P15 V-SVZ wholemounts were double immunostained with FoxJ1 (red) and Sox9 (blue) antibodies (B) or FOP (white) and GFAP (red) antibodies (D). (B) $GFP^+FoxJ1^+Sox9^+$ ependymal cells are indicated by arrows and $GFP^+FoxJ1^-Sox9^+$ astrocytes are outlined in white. (D) GFP^+GFAP^- ependymal cells with multiple FOP^+ dots are indicated by arrows and a GFP^+GFAP^+ astrocyte with a FOP^+ centrosome is indicated by an arrowhead.

(C) Percentage of astrocytes ($Sox9^+FoxJ1^-$), ependymal cells ($Sox9^+FoxJ1^+$) and others ($Sox9^-FoxJ1^-$) among H2B-GFP^+ electroporated cells. Analyses were done on n=3 animals; a total of 441 cells were counted. Error bars represent the SEM. p-values were determined with the two-proportion Z-test; ***p≤0.001, **p≤0.01.

(E) Experimental schema for (F-G): Nucbow plasmids (^{PB}*CAG-Nucbow* along with the PiggyBac transposase and the self-excising Cre recombinase) were electroporated *in utero* at E14.5 and received EdU (through drinking water) for 14 days starting at P21. (F, G) Coronal sections of the olfactory bulb (OB) were prepared 1 week after the last day of EdU administration. (G) High magnification image of (F) to show that some $Nucbow^+$ interneurons in the OB are EdU^+.

The scale bar represents 40 µm (B), 15 µm (C), 520 µm (F) and 180 µm (G).

P21 (Figure 2E). One week after the end of EdU administration, EdU$^+$Nucbow$^+$ neurons were observed on each olfactory bulb section, showing that cells derived from electroporated RGCs at E14.5 are adult neural stem cells that give rise to olfactory bulb neurons (Figure 2F-G).
These results show that electroporation of RGCs at E14.5 labels multiciliated ependymal cells and adult neural stem cells (type B1 astrocytes) that are retained in the V-SVZ at adult stages.

3) Lineage-tracing using MAGIC Markers show that ependymal cells derive from symmetric and asymmetric divisions of RGCs

We then took advantage of the large panel of distinct colors produced by the MAGIC Markers approach to trace and analyze the lineage of ependymal cells. The V-SVZ of P15-P20 brains electroporated with the Nucbow vector at E14.5 were immunostained with the ependymal marker FoxJ1 in far red, and colors were automatically analyzed to avoid any eye bias (Figure 3A-C). Briefly, FoxJ1 staining was first used as a reference for the ventricular surface and 25 µm-thick 3D image stacks of the ventricular whole-mounts were segmented as previously described (Shihavuddin et al., 2017). Nucbow$^+$ cells were then sorted as FoxJ1$^+$ or FoxJ1$^-$ (Supplementary Figure 3, Figure 3D). To define the criteria for sister cells, 2 independent researchers manually picked 49 pairs of cells with similar Nucbow colors (Supplementary Figure 4A). Both their color content (saturation, value and hue in the RGB tridimensional space) and their 3D spatial distances were computed (Supplementary Figure 4B-C). The maximum difference found for each of these parameters was chosen as a threshold for the automatic analysis of all Nucbow$^+$ cells in each brain (Figure 3E, Supplementary Figure 4D-G). This automatic analysis of all cells from 6 electroporated brains (a total of 7668 Nucbow$^+$ cells were analyzed and 418 clones of more than 2 cells) showed that 80% of clones (with at least one Nucbow$^+$FoxJ1$^+$ cell) contained 6 or less cells, suggesting that most ependymal cells were derived from 3 or less cell divisions (Figure 3F-G, Supplementary Figure 5A-F). We excluded the largest clones (7 to 32 cells) as we noted that they were often labeled with the most frequent labels in the dataset (corresponding to primary colors red, green, blue), suggesting that merging of juxtaposed clones expressing the same label had occurred (Supplementary Figure 5G).
Among the 323 clones with fewer than 6 cells, around half contained only 2 cells, suggesting that, at E14.5, most clones were generated from one terminal cell division of RGCs (n=6 mice,

Figure 3

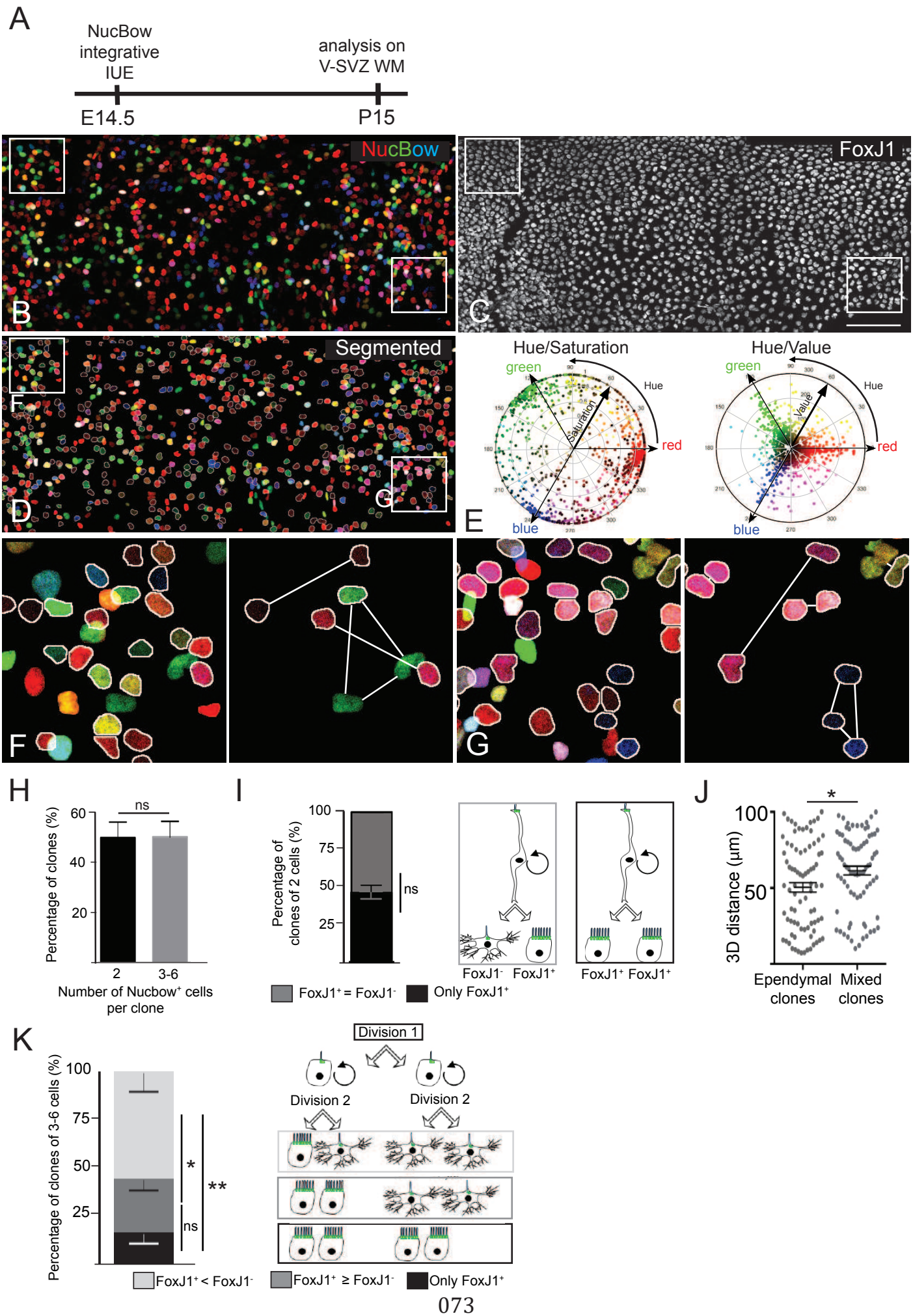
A
NucBow integrative IUE
E14.5
analysis on V-SVZ WM
P15
NucBow
B
FoxJ1
C
Segmented
D
F
G
Hue/Saturation
Hue/Value
green
blue
red
Hue
Saturation
Value
E
F
G
H
Percentage of clones (%)
ns
2
3-6
Number of Nucbow+ cells per clone
I
Percentage of clones of 2 cells (%)
ns
FoxJ1- FoxJ1+
FoxJ1+ FoxJ1+
FoxJ1+ = FoxJ1-
Only FoxJ1+
J
3D distance (µm)
*
Ependymal clones
Mixed clones
K
Percentage of clones of 3-6 cells (%)
*
**
ns
Division 1
Division 2
Division 2
FoxJ1+ < FoxJ1-
FoxJ1+ ≥ FoxJ1-
Only FoxJ1+

Figure 3: Clonal analysis of ependymal cell with MAGIC Markers reveals both symmetric and asymmetric divisions of RGCs

(A) Experimental schema: Nucbow plasmids were electroporated *in utero* at E14.5 and analyzed at P15-20. (B-D) Representative Z-projected image of an *en-face* view of the V-SVZ (B) immunostained at P15 with anti-FoxJ1 antibody (C). (D) Segmented image of (B-C) obtained using FoxJ1 staining as reference (see methods and Supplementary Figures 3-5). FoxJ1^{+}Nucbow^{+} cells are outlined in white. (E) Circular Hue-Saturation and Hue-Value plots of all Nucbow^{+} cells from (D). (F-G) High magnification images of the insets in (D) showing examples of clones: 2 ependymal doublets and 1 triplet containing 1 ependymal cell and 2 FoxJ1^{-} cells (F) and 3 ependymal doublets, 1 ependymal triplet and 1 triplet containing 1 ependymal cell and 2 FoxJ1^{-} cells (G). (H) Percentages of clones containing 2 or 3-6 Nucbow^{+} cells. Error bars represent the SEM of n= 163 clones of 2 cells and n=160 clones of 3-6 cells; p-values were determined by the Mann-Whitney test; ns, p>0.05. (I) Percentages of clones of 2 Nucbow^{+} cells containing 1 (mixed clones, in grey) or 2 (ependymal clones, in black) FoxJ1^{+} cells. Error bars represent the SEM of n=82 ependymal clones and n=81 mixed clones from 6 independent experiments; p-values were determined by the Mann-Whitney test; ns, p>0.05. (J) 3D distances between the cells composing ependymal or mixed clones of 2 cells. Error bars represent the SEM of n=82 ependymal clones and n=81 mixed clones from 6 independent experiments; p-values were determined by the Mann-Whitney test; *p≤0.05. (K) Percentages of clones of 3-6 Nucbow^{+} cells containing only FoxJ1^{+} cells (black), more or equal number of FoxJ1^{+} compared to FoxJ1^{-} cells (dark grey) or more FoxJ1^{-} cells (light grey) per clone. Error bars represent the SEM of n=160 clones of 3-6 cells; p-values were determined by the Mann-Whitney test; **p≤0.01; *p≤0.05; ns p>0.05. The scale bar represents 100 µm (B-D) and 22 µm (F-G).

Figure 3H). These 2-cell clones were composed of 1 or 2 FoxJ1^{+} cells, showing that the terminal division could be either symmetric or asymmetric (Figure 3I). Interestingly, the 3D distance between cells was higher in mixed clones (clones composed of ependymal and non-ependymal cells) compared to pure ependymal clones (Figure 3J), showing that FoxJ1^{-} cells were deeper in the SVZ compared to FoxJ1^{+} cells in the VZ.

Clones containing 3 to 6 cells were generated through 2 or 3 cell divisions, the last of which was either only symmetric (clones containing FoxJ1^{+} cells only), or both symmetric and asymmetric (clones containing FoxJ1^{+} and FoxJ1^{-} cells). Interestingly, a majority of these clones contained more FoxJ1^{-} cells than FoxJ1^{+} cells suggesting that symmetric divisions giving rise to 2 FoxJ1^{-} cells might have occurred in these clones (Figure 3K).

Lineage-tracing experiments of RGCs using the MAGIC Markers strategy thus show that ependymal cells originate from either one terminal symmetric division giving rise to 2 ependymal cells, or 1 asymmetric division giving rise to 1 ependymal and 1 FoxJ1^{-} cell.

4) Mosaic Analysis with Double Markers (MADM) of V-SVZ gliogenesis reveals that E and B1 cells share a common lineage

To obtain more insight into the cellular mechanisms and the sequence of symmetric versus asymmetric divisions producing each clone, we used the MADM system coupled with IUE of Cre recombinase at E13.5 or E14.5 (Figure 4A; Gao et al., 2014). In electroporated cells, Cre recombinase mediates interchromosomal recombination, which reconstitutes cytoplasmic enhanced GFP (EGFP, green) or tandem-dimer Tomato (tdTomato, red). If recombination occurs in the G2 phase of the cell cycle, and each red or green chromosome segregates in each daughter cell (X segregation), the two descendent lineages will be permanently labelled in green or red by MADM events (Figure 4B). Analysis of cell number and identity will thus allow direct assessment of the division pattern (symmetric versus asymmetric) and cell fate decision of the original dividing progenitors. Otherwise, if recombination occurs in G0/G1, or if both red and green chromosomes segregate in the same cell (Z segregation), recombined cells appear yellow and will be excluded from the analysis (Figure 4B). We thus induced Cre activity through IUE in MADM pregnant mothers at E13.5 or E14.5 and analyzed V-SVZ at P15-P20 after immunolabelling of centrioles combined with MADM cytoplasmic staining to identify the cell types composing each clone (Figure 4C). This approach allowed a clonal study of green-

Figure 4

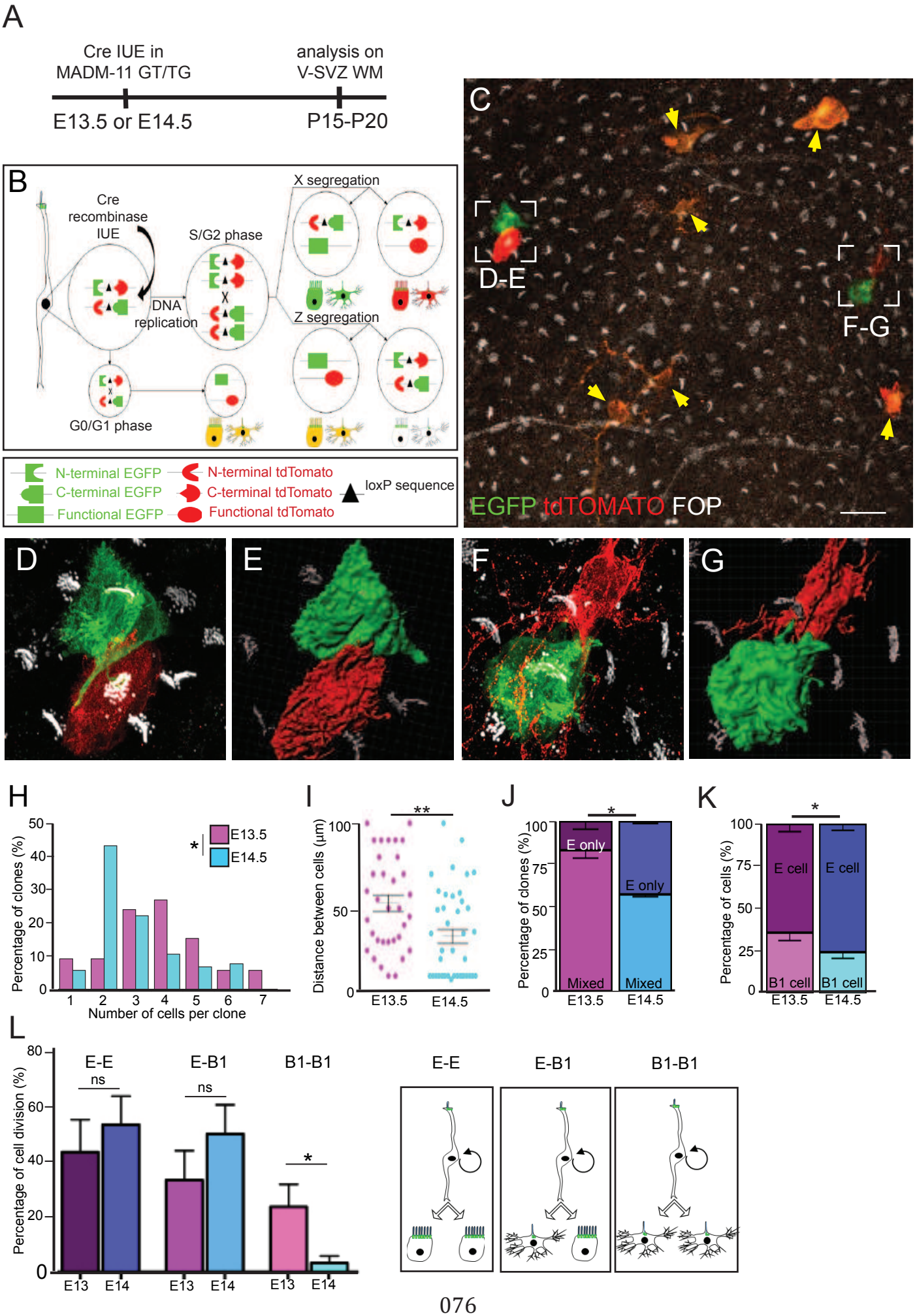
A
Cre IUE in MADM-11 GT/TG
analysis on V-SVZ WM
E13.5 or E14.5
P15-P20
B
Cre recombinase IUE
S/G2 phase
DNA replication
X segregation
Z segregation
G0/G1 phase
N-terminal EGFP
C-terminal EGFP
Functional EGFP
N-terminal tdTomato
C-terminal tdTomato
Functional tdTomato
loxP sequence
C
D-E
F-G
EGFP tdTOMATO FOP
D
E
F
G
H
Percentage of clones (%)
E13.5
E14.5
Number of cells per clone
I
Distance between cells (µm)
E13.5
E14.5
J
Percentage of clones (%)
E only
Mixed
K
Percentage of cells (%)
E cell
B1 cell
L
Percentage of cell division (%)
E-E
E-B1
B1-B1
ns
E13
E14

Figure 4: MADM reveals the presence of ependymal-ependymal and ependymal-astrocyte divisions at E13.5 and E14.5

(A) Experimental schema: Cre plasmid was electroporated *in utero* in *MADM-11*$^{TG/GT}$ at E13.5 or E14.5 and V-SVZ WM were analyzed at P15-20.

(B) Schematic representation of Cre-mediated MADM-clone induction in dividing RGCs. A G2-X event results in clones of red and green labeled cells and a G2-Z event generates double-labeled (yellow) and unlabeled clones of cells. Recombination occurring in the G0/G1 phases of the cell cycle leads to double-labeled (yellow) cells.

(C-G) Airyscan confocal image of a P15 MADM-labeled V-SVZ whole-mount electroporated with a CRE-expressing plasmid at E14.5. Ventricular wall was stained with EGFP (green), tdTomato (red) and FOP (white) antibodies. Double labeled yellow cells issued from a G2-Z recombination event are indicated by yellow arrowheads. Ependymal-ependymal (D-E) and ependymal-astrocyte (F-G) clones of two sister cells are shown at high magnification (D, F) and in a 3D view (E, G). See also Supplementary movies 1, 2.

(H) Percentage of all clones generated from *in utero* electroporation with Cre at E13.5 or E14.5 according to the number of cells per clone (n=6 and 16 animals at E13.5 and E14.5, respectively); p-values were determined with the Chi^2 test for trend; *p≤0.05.

(I) Average distance between cells composing the clones. Error bars represent the SEM of 29 and 44 clones at E13.5 and E14.5, respectively; p-values were determined with the Mann-Whitney test; **p≤0.01

(J) Percentage of all clones generated from E13.5 or E14.5 containing ependymal cells only or a mixed population of ependymal (E) and astrocytes (B1) cells. Error bars represent the SEM of 29 and 44 clones at E13.5 and E14.5, respectively; p-values were determined with the two-proportion Z-test; *p≤0.05.

(K) Percentage of E and B1 cells in all clones generated from E13.5 or E14.5. Error bars represent the SEM of 117 and 134 cells at E13.5 and E14.5, respectively; p-values were determined with the two-proportion Z-test; *p≤0.05.

(L) Percentage of E-E, E-B1 and B1-B1 cell divisions in all clones generated from E13.5 or E14.5. Error bars represent the SEM of 24 and 54 cell divisions at E13.5 and E14.5, respectively; p-values were determined with the Mann-Whitney test; *p≤0.05.

The scale bar represents 30 μm (C).

red clones because the efficiency of recombination was low in these mice (mean number of clones per animal=5) and most recombined cells were double-labeled (yellow) (Figure 4C). Cells were considered a clone if their spatial distance was less than 100 μm, as previously defined by the Nucbow lineage-tracing experiments. Red or green cells located in the electroporated region of the V-SVZ were either multiciliated ependymal cells (E) characterized by a few short processes and multiple FOP^+ basal bodies in their cytoplasm associated with long cilia, or astrocytes (type B1) the cell body of which and multiple long processes were deeper in the SVZ. These astrocytes contained a centrosome that occasionally contacted the ventricular surface. When the cells of a clone were in close proximity, their cell body or processes often contacted each other, suggesting that they might maintain communication at adult stage (Figure 4C-G; Supplementary movies 1 and 2). We observed very few red or green cells alone (clone of 1 cell in Figure 4H) or larger monochrome clones, if any, in the V-SVZ, suggesting that asymmetric divisions giving rise to one ventricular and one non-ventricular cell were rare in these experiments. In contrast, the majority of red-green clones contained two cells when Cre was electroporated at E14.5, which is in line with our findings above showing that most RGCs divided once to produce glial cells in the V-SVZ. At E13.5, RGCs also produced V-SVZ cells, but the majority divided twice since most clones contained 3 to 4 cells (Figure 4H). The distance between the cells in a clone was higher at E13.5 compared to E14.5, showing that cells disperse as cell divisions proceed (Figure 4I). Both the proportion of mixed clones (containing both E and B1 cells; Figure 4J) and the number of type B1 astrocytes (Figure 4K) in the clones decreased at E14.5 compared to E13.5, suggesting that fewer type B1 astrocytes are produced compared to ependymal cells. Alternatively, type B1 astrocytes might be produced at earlier stages compared to ependymal cells. Noteworthy, the distribution of astrocytes (B1) and ependymal cells (E) in each clone revealed that astrocytes were produced at a lower rate than ependymal cells and that symmetric divisions producing 2 astrocytes (B1-B1) occurred more frequently at E13.5 than at E14.5 (Figure 4L; Supplementary Table 1).

Together, these results show that ependymal cells and astrocytes are sister cells produced through symmetric (B1-B1 or E-E) and asymmetric (E-B1) divisions of RGCs at mid-gestation in the mouse forebrain. To gain more insight into the molecular regulation of RGC differentiation into type B1 astrocytes or ependymal cells, we perturbed these divisions with members of the Geminin superfamily, initially described as regulators of DNA replication (Balestrini et al., 2010; Pefani et al., 2011). Two members of this family (Mcidas and GemC1) were recently

identified as master regulators of multiciliated ependymal cell fate (Kyrousi et al., 2015), while the other member Geminin was not yet studied.

5) GemC1 expression induces premature ependymal cell differentiation at the expense of type B1 cells.

Overexpression of GemC1 through IUE at E13.5 (data not shown) or E14.5 dramatically increased ependymal cell differentiation at the expense of SVZ cells, as previously shown (Supplementary Figure 6A-D; Kyrousi et al., 2015). Interestingly, since B1 cells were absent, pinwheels were not observed in densely GemC1-electroporated regions (Supplementary Figure 6E-F) compared to neighboring areas in which GemC1 electroporation was sparse (Supplementary Figure 6G). Overexpression of GemC1 together with the induction of Cre activity through IUE in MADM embryos at E14.5 did not change the size of the clones compared to controls, suggesting that most RGC were already undergoing their last division at that stage (Chi^2 test for trend between E14.5 and E14.5GemC1: not significant $p>0.1$; compare Figure 4H and 5C). In contrast, when IUE was performed at E13.5, the clones were smaller compared to controls suggesting that GemC1 induced premature exit from the cell cycle at that stage (Chi^2 test for trend between E13.5 and E13.5GemC1: $^{**}p\leq0.01$; compare Figure 4H and 5C). Consistently, the average distance between cells in the GemC1 clones at E13.5 was smaller than in controls (compare Figure 4I and 5D, Mann-Whitney test; $^{**}p\leq0.01$) and similar to E14.5GemC1 (Figure 5D). Furthermore, overexpression of GemC1 at E13.5 or E14.5 promoted the ependymal fate, since the numbers of both pure ependymal clones and ependymal cells in the clones were dramatically increased compared to controls (two-proportion Z-test between controls and GemC1: $^{***}p\leq0.001$; compare Figures 4J-K and 5E-F). Notably, although astrocytes were occasionally produced through symmetric divisions in controls, they were exclusively generated through asymmetric divisions of ependymal cells after GemC1 overexpression at E13.5 or E14.5. Indeed, no pairs of astrocytes were detected after GemC1 overexpression (Figure 6F; Supplementary Table 2).

6) Geminin expression favors the generation of type B1 cells

Figure 5

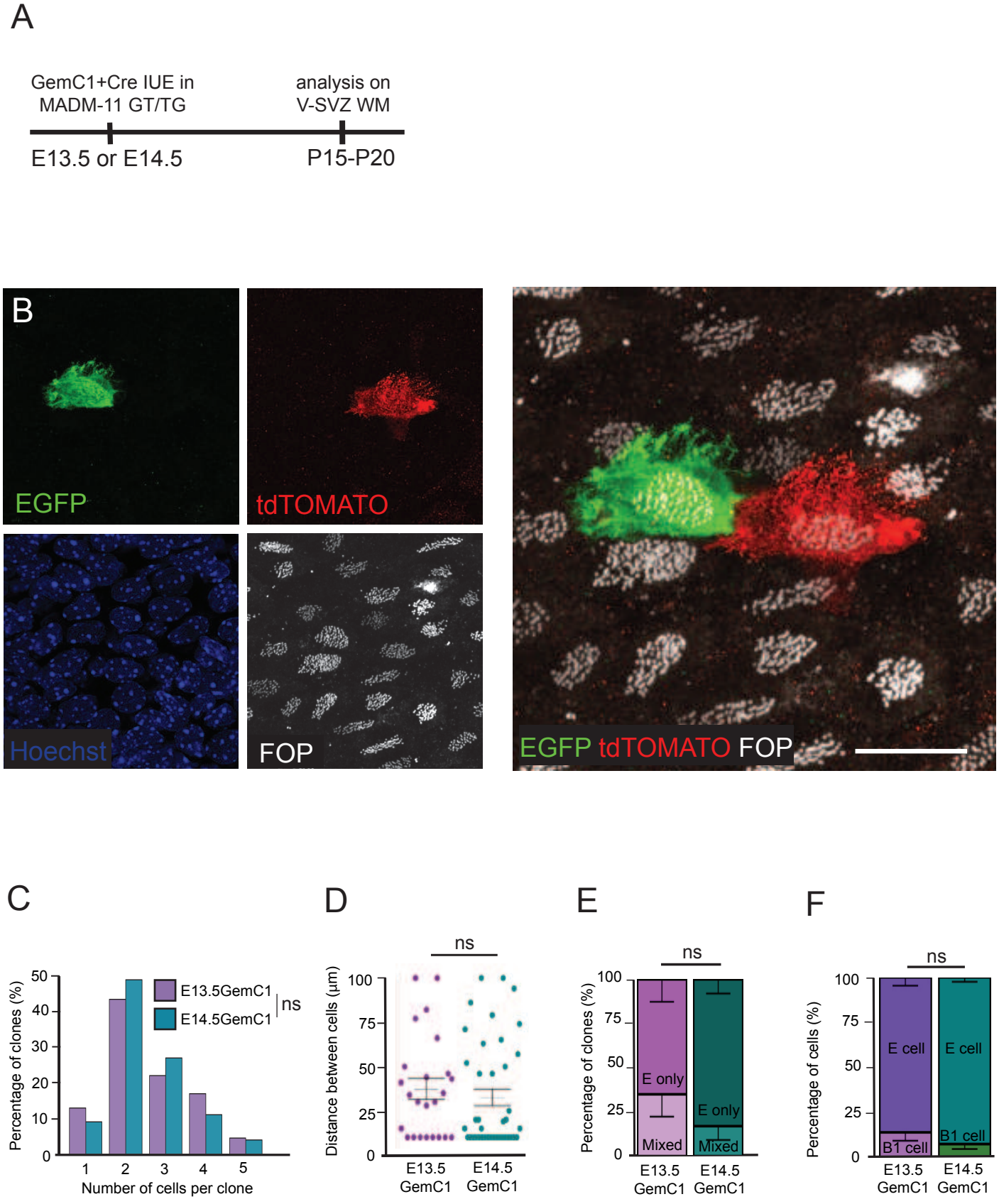
A
GemC1+Cre IUE in MADM-11 GT/TG
analysis on V-SVZ WM
E13.5 or E14.5
P15-P20
B
EGFP
tdTOMATO
Hoechst
FOP
EGFP tdTOMATO FOP
C
Percentage of clones (%)
E13.5GemC1
E14.5GemC1
ns
Number of cells per clone
D
ns
Distance between cells (µm)
E13.5 GemC1
E14.5 GemC1
E
ns
Percentage of clones (%)
E only
Mixed
E13.5 GemC1
E14.5 GemC1
F
ns
Percentage of cells (%)
E cell
B1 cell
E13.5 GemC1
E14.5 GemC1

Figure 5: GemC1 favors the formation of pure ependymal clones at both E13.5 and E14.5

(A) Experimental schema: GemC1 and Cre plasmids were co-electroporated *in utero* in *MADM-11*$^{TG/GT}$ at E13.5 or E14.5 and V-SVZ WM were analyzed at P15-20.

(B) Airyscan confocal image of a P15 MADM-labeled V-SVZ whole-mount immunostained with EGFP (green), tdTomato (red) and FOP (white) antibodies showing a clone of 2 ependymal cells.

(C) Percentage of all clones generated from co-electroporation with Cre and GemC1 at E13.5 or E14.5 according to the number of cells per clone (n=4 and 9 animals at E13.5 and E14.5, respectively); p-values were determined with the Chi^2 test for trend; ns, p>0.05.

(D) Average distance between cells composing the clones generated from the co-electroporation of Cre and GemC1 at E13.5 or E14.5. Error bars represent the SEM of 20 and 41 clones at E13.5 and E14.5, respectively; p-values were determined with the Mann-Whitney test; ns, p>0.05.

(E) Percentage of all clones generated from the co-electroporation of Cre and GemC1 at E13.5 or E14.5 containing ependymal cells only or a mixed population of ependymal cells and B1 cells. Error bars represent the SEM of 20 and 41 clones, respectively; p-values were determined with the two-proportion Z-test; ns, p>0.05.

(F) Percentage of E and B1 cells in all clones generated from the co-electroporation of Cre and GemC1 at E13.5 or E14.5. Error bars represent the SEM of 57 and 110 cells at E13.5 and E14.5, respectively; p-values were determined with the two-proportion Z-test; ns, p>0.05.

The scale bar represents 50 µm.

Geminin physically interacts with GemC1 and Mcidas (Caillat et al., 2013, 2015), but its role during ependymal cell generation is still unknown. We thus tested the influence of Geminin overexpression on the fate of RGCs through IUE with Cre in MADM pregnant mothers at E14.5 (Figure 6A-B). Notably, a majority of the clones contained type B1 astrocytes characterized by an apical contact with a primary cilium and cytoplasmic extensions contacting blood vessels (Figure 6B; Supplementary movie 3; Supplementary Table 3). The size of the clones was similar to that of controls, suggesting that Geminin does not act on the rate of cell division in RGCs (Chi^2 test for trend between E14.5 and E14.5Geminin: not significant, $p>0.1$; compare Figure 4H and 6C). Interestingly, the proportion of mixed clones and the number of type B1 astrocytes were not significantly increased after Geminin overexpression (two-proportion Z-test between controls and Geminin: not significant $p>0.1$; compare Figures 4J-K and 6D-E; Figure 6F). However, Geminin overexpression at E14.5 led to the formation of clones containing only B1 cells, which was never observed in controls (Figure 6D). Consistently, the number of symmetric divisions producing 2 astrocytes (B1-B1) increased significantly after Geminin overexpression at E14.5 compared to controls (Figure 6F; Supplementary Table 3). Altogether, these results show that ependymal cells and astrocytes are sister cells produced through symmetric or asymmetric divisions, the balance of which is modulated by the level of expression of Geminin family genes.

DISCUSSION

By using a Cre-lox fate mapping technique and complementary MAGIC Markers- and MADM-based clonal analysis approaches, our study reveals how glial cells are produced in the V-SVZ during development. First, our results proved that ependymal cells are derived from RGCs all along the embryonic neuroepithelium (pallium, Lateral and Medial Ganglionic Eminences) and differentiate locally, this is, ependymal progenitors born in a specific area of the VZ do not migrate long distances to colonize other areas of the neuroepithelium (Figure 1). We then show that ependymal cells and B1 type astrocytes appear at the end of neurogenesis mainly through E-B1 asymmetric or E-E symmetric divisions of RGCs. B1-B1 symmetric divisions were less frequent and always combined with E-E or E-B1 divisions (Figure 7). These glial cells have a low migratory capacity and often contact each other, even at the adult stage. Our study thus demonstrates that multiciliated ependymal cells and adult neural stem cells, ultimately forming the adult neurogenic niche, are sister cells that share a common origin. We also

Figure 6

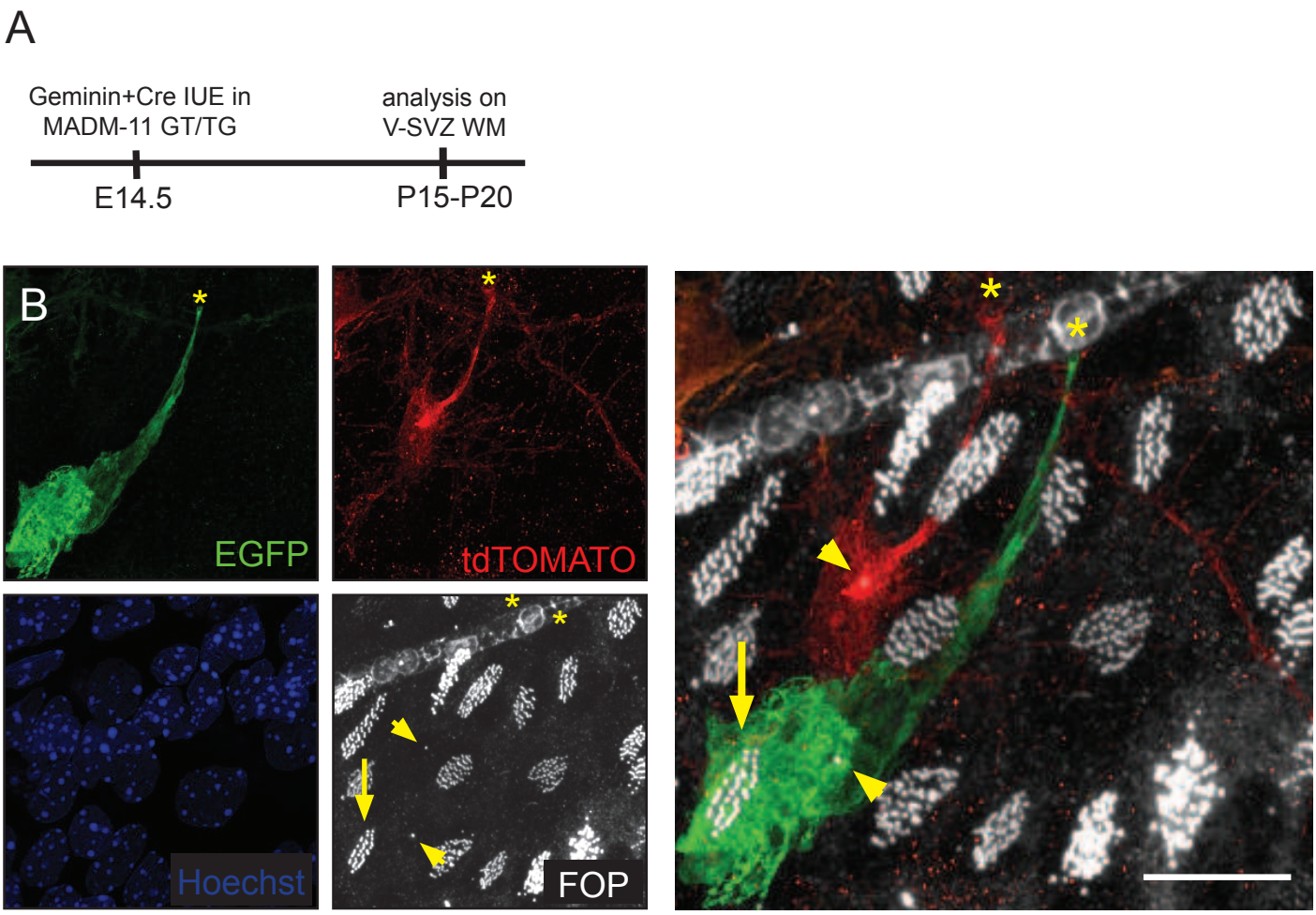
A
Geminin+Cre IUE in MADM-11 GT/TG
analysis on V-SVZ WM
E14.5
P15-P20
B
EGFP
tdTOMATO
Hoechst
FOP
C
E14.5Geminin
Percentage of clones (%)
Number of cells per clone
D
E only
Mixed
B1 only
Percentage of clones (%)
E14.5 Geminin
E
67
E cells
33
B1 cells
Percentage of cells (%)
E14.5 Geminin
F
E-E
E-B1
B1-B1
ns
*
***
**
Percentage of cell division (%)
Ctrl
GemC1
Geminin

Figure 6: Geminin favors the formation of B1 cell-containing clones at E14.5

(A) Experimental schema: Geminin and Cre plasmids were co-electroporated *in utero* in *MADM-11*$^{TG/GT}$ at E14.5 and V-SVZ WM were analyzed at P15-20.

(B) Airyscan confocal image of a P15 MADM-labeled V-SVZ whole-mount immunostained with EGFP (green), tdTomato (red) and FOP (white) antibodies showing a clone containing 1 GFP$^+$ ependymal cell (arrow), and two B1 cells (one GFP$^+$ and one tdT$^+$, arrowheads). Note that both B1 cells contain a centrosome at the ventricular surface (arrowheads) and they extend a process toward a blood vessel (yellow asterisks). See also Supplementary movie 3.

(C) Percentage of all clones generated from the co-electroporation of Cre and Geminin at E14.5 according to the number of cells per clone (n=13 animals); p-values of E14.5 control and Geminin were determined with the Chi^2 test for trend; ns, p>0.05 (compare with Figure 4H).

(D) Percentage of all clones generated from the co-electroporation of Cre and Geminin at E14.5 and containing either B1 cells only, or ependymal cells only, or a mixed population of ependymal cells and B1 cells. Error bars represent the SEM of 107 clones; p-values were determined with the two-proportion Z-test; ns, p>0.05 for ependymal and mixed clones and *p≤0.05 for clones containing B1 cells only (compare with E14.5 in Figure 4J).

(E) Percentage of E and B1 cells in all clones generated from the co-electroporation of Cre and Geminin at E14.5. Error bars represent the SEM of 335 cells; p-values were determined with the two-proportion Z-test; ns, p>0.05 (compare with E14.5 in Figure 4K).

(F) Percentage of E-E, E-B1 and B1-B1 cell division in clones generated from E14.5 in controls, or after overexpression of GemC1 or Geminin. Error bars represent the SEM of 16, 9 and 13 independent animals electroporated with Cre, Cre+GemC1 or Cre+Geminin, respectively; p-values were determined with the Mann-Whitney test; ***p≤0.001, **p≤0.01, *p≤0.05 and ns, p>0.05.

The scale bar represents 50 µm.

provide evidence that these cells are sequentially produced, with the bulk of B1 astrocytes being produced just before the bulk of ependymal cells. Interestingly, their respective numbers are precisely regulated by the Geminin-family members. Geminin overexpression, a gene whose expression is higher in cycling B1 cells (Khatri et al., 2014), favors B1-B1 symmetric divisions and increases the final total number of these cells (Figure 6D-E). On the contrary, overexpression of its antagonist, GemC1, leads to more terminal E-E divisions, as well as an increase in the final number of ependymal cells (Figure 5E-F). One could thus hypothesize that the sequential expression of Geminin family members could be responsible for the temporal differences in glia production, and that the defined proportions of E and B1 cells (with a two-fold presence of E cells with respect to B1 cells, Mirzadeh et al., 2008) could be established by the balance of these genes. These findings raise the question of the fate-decision mechanisms driving RGCs towards symmetric or asymmetric cell division. An analogous question was addressed by others concerning neural versus glial cell generation. Interestingly, it was shown that the number of neurons produced by RG is predictable, suggesting that RGCs can perform a gliogenic division only when they have exhausted their capacity to proliferate (Gao et al., 2014). Similarly, we found that RGCs generate more mixed clones and more astrocytes when they are electroporated at E13.5 than at E14.5 (Figure 4J-K). This supports the hypothesis that astrocytes are produced earlier than ependymal cells. One might hypothesize that RGCs first give rise to astrocytes until they exhaust their proliferative capacity and yield two ependymal cells through symmetric cell division at later developmental stages. Importantly, while ependymal cells become post-mitotic (Spassky et al., 2005), most V-SVZ astrocytes can be reactivated in the adult (Obernier et al., 2018). Altogether, this suggests that RGCs first produce quiescent daughter cells with the potential to enter the cell cycle again (type B1 astrocytes), then post-mitotic ependymal cells. Interestingly, the description of distinct pathways of glial production via symmetric or asymmetric division unveils the existence of two separate fate decision-making mechanisms, which occur subsequently to the last division of RGCs. This indicates that ependymal versus astrocyte specification might be dependent on the correct segregation of organelles (i.e. centrioles or mitochondria), which have been shown to influence neural stem cell self-renewal and fate decisions (Khacho et al., 2016; Wang et al., 2009). Noteworthy, Geminin superfamily members were initially described as regulators of DNA replication. It would thus be of interest to determine whether fate decisions in RGCs are driven by DNA replication events following re-entry into the cell cycle.

Figure 7

A

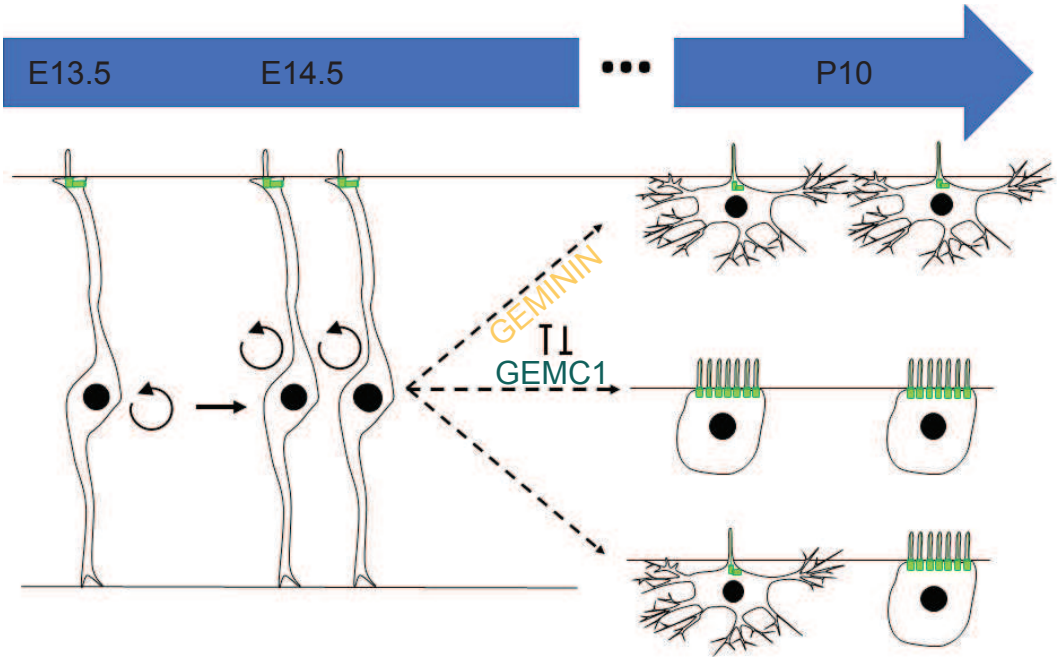

	%	
GEMININ	Control	GEMC1
12	3	0
40	47	84
48	50	16

Figure 7. Ependymal cells and B1 astrocytes form one common lineage regulated by Geminin family members.

(A) Model of adult NSCs and multiciliated ependymal cells generation. RGCs give rise to type B1 cells through symmetric divisions (rare event: 3%) or asymmetric divisions (frequent event 50%) and to multiciliated ependymal cells through symmetric divisions (frequent event: 47%). The antagonistic Geminin family members, Geminin and GemC1, can modulate the cell fate decision. Geminin overexpression favors symmetric divisions giving rise to type B1 astrocytes. On the contrary, GemC1 overexpression triggers symmetric divisions giving rise to ependymal cells. The percentage of E-E, E-B1 and B1-B1 divisions are indicated for IUE at E14.5 in a control situation and upon GemC1 or Geminin overexpression, respectively.

ACKNOWLEDGMENTS

We thank all members of the Spassky laboratory for comments and discussion. We thank X. Morin for the pCAAGS-H2B-GFP and pCAGGS-Cre plasmids. We thank A.-K. Konate and R. Nagalingum for administrative support and the IBENS Animal Facility for animal care. We thank the IBENS Imaging Facility, with grants from Region Ile-de-France (NERF 2011-45), Fondation pour la Recherche Médicale (FRM) (DGE 20111123023), and Fédération pour la Recherche sur le Cerveau Rotary International France (2011). The IBENS Imaging Facility and the team received support from Agence Nationale de la Recherche (ANR) Investissements d'Avenir (ANR-10-LABX-54 MEMO LIFE, ANR-11-IDEX-0001-02 PSL* Research University). The Spassky laboratory is supported by INSERM, CNRS, École Normale Supérieure (ENS), ANR (ANR-17-CE12-0021-03), European Research Council (ERC Consolidator grants 647466 and 649117), Cancéropôle Ile-de-France (2014-1-PL BIO-11-INSERM 121). G.O.A. and M.D. received fellowships from the Labex MEMOLIFE and the French Ministry of Higher Education and Research, respectively.

AUTHOR CONTRIBUTIONS

N.S. designed, funded and supervised the research. G.O.A., M.D., P.L., A.F., M.F., S.C., J.L. and N.S. designed experiments and performed the research. G.O.A., M.D., P.L., A.F., A.S., A.M., A.G. and N.S. analyzed the data. S.T., S.H. provided resources. G.O.A., M.D. and N.S. wrote the manuscript with inputs from all authors.

DECLARATION OF INTERESTS

The authors declare no competing financial interests

REFERENCES

Arbi, M., Pefani, D., Kyrousi, C., Lalioti, M., Kalogeropoulou, A., Papanastasiou, A.D., Taraviras, S., and Lygerou, Z. (2016). GemC1 controls multiciliogenesis in the airway epithelium. EMBO Rep. *17*, 400–413.

Balestrini, A., Cosentino, C., Errico, A., Garner, E., and Costanzo, V. (2010). GEMC1 is a TopBP1-interacting protein required for chromosomal DNA replication. Nat. Cell Biol. *12*, 484–491.

Boon, M., Wallmeier, J., Ma, L., Loges, N.T., Jaspers, M., Olbrich, H., Dougherty, G.W., Raidt,

J., Werner, C., Amirav, I., et al. (2014). MCIDAS mutations result in a mucociliary clearance disorder with reduced generation of multiple motile cilia. Nat. Commun. *5*, 4418.

Caillat, C., Pefani, D.-E., Gillespie, P.J., Taraviras, S., Blow, J.J., Lygerou, Z., and Perrakis, A. (2013). The Geminin and Idas Coiled Coils Preferentially Form a Heterodimer That Inhibits Geminin Function in DNA Replication Licensing. J. Biol. Chem. *288*, 31624–31634.

Caillat, C., Fish, A., Pefani, D.-E., Taraviras, S., Lygerou, Z., and Perrakis, A. (2015). The structure of the GemC1 coiled coil and its interaction with the Geminin family of coiled-coil proteins. Acta Crystallogr. Sect. D Biol. Crystallogr. *71*, 2278–2286.

Cebrián-Silla, A., Alfaro-Cervelló, C., Herranz-Pérez, V., Kaneko, N., Park, D.H., Sawamoto, K., Alvarez-Buylla, A., Lim, D.A., and García-Verdugo, J.M. (2017). Unique Organization of the Nuclear Envelope in the Post-natal Quiescent Neural Stem Cells. Stem Cell Reports *9*, 203–216.

Doetsch, F., Caillé, I., Lim, D.A., García-Verdugo, J.M., and Alvarez-Buylla, A. (1999). Subventricular Zone Astrocytes Are Neural Stem Cells in the Adult Mammalian Brain. Cell *97*, 703–716.

Ferri, A.L., Cavallaro, M., Braida, D., Di Cristofano, A., Canta, A., Vezzani, A., Ottolenghi, S., Pandolfi, P.P., Sala, M., DeBiasi, S., et al. (2004). Sox2 deficiency causes neurodegeneration and impaired neurogenesis in the adult mouse brain. Development *131*, 3805–3819.

Fuentealba, L.C., Rompani, S.B., Parraguez, J.I., Obernier, K., Romero, R., Cepko, C.L., and Alvarez-Buylla, A. (2015). Embryonic Origin of Postnatal Neural Stem Cells. Cell *161*, 1644–1655.

Furutachi, S., Miya, H., Watanabe, T., Kawai, H., Yamasaki, N., Harada, Y., Imayoshi, I., Nelson, M., Nakayama, K.I., Hirabayashi, Y., et al. (2015). Slowly dividing neural progenitors are an embryonic origin of adult neural stem cells. Nat. Neurosci. *18*, 657–665.

Gao, P., Postiglione, M.P., Krieger, T.G., Hernandez, L., Wang, C., Han, Z., Streicher, C., Papusheva, E., Insolera, R., Chugh, K., et al. (2014). Deterministic progenitor behavior and unitary production of neurons in the neocortex. Cell *159*, 775–788.

Gorski, J.A., Talley, T., Qiu, M., Puelles, L., Rubenstein, J.L.R., and Jones, K.R. (2002). Cortical excitatory neurons and glia, but not GABAergic neurons, are produced in the Emx1-expressing lineage. J. Neurosci. *22*, 6309–6314.

Hadjantonakis, A.-K., and Papaioannou, V.E. (2004). Dynamic in vivo imaging and cell tracking using a histone fluorescent protein fusion in mice. BMC Biotechnol. *4*, 33.

Hippenmeyer, S., Youn, Y.H., Moon, H.M., Miyamichi, K., Zong, H., Wynshaw-Boris, A., and Luo, L. (2010). Genetic Mosaic Dissection of Lis1 and Ndel1 in Neuronal Migration. Neuron *68*, 695–709.

Kessaris, N., Fogarty, M., Iannarelli, P., Grist, M., Wegner, M., and Richardson, W.D. (2006). Competing waves of oligodendrocytes in the forebrain and postnatal elimination of an embryonic lineage. Nat. Neurosci. *9*, 173–179.

Khacho, M., Clark, A., Svoboda, D.S., Azzi, J., MacLaurin, J.G., Meghaizel, C., Sesaki, H., Lagace, D.C., Germain, M., Harper, M.E., et al. (2016). Mitochondrial Dynamics Impacts Stem Cell Identity and Fate Decisions by Regulating a Nuclear Transcriptional Program. Cell Stem Cell *19*, 232–247.

Khatri, P., Obernier, K., Simeonova, I.K., Hellwig, A., Hölzl-Wenig, G., Mandl, C., Scholl, C., Wölfl, S., Winkler, J., Gaspar, J.A., et al. (2014). Proliferation and cilia dynamics in neural stem cells prospectively isolated from the SEZ. Sci. Rep. *4*, 3803.

Kyrousi, C., Arbi, M., Pilz, G.-A., Pefani, D.-E., Lalioti, M.-E., Ninkovic, J., Götz, M., Lygerou, Z., and Taraviras, S. (2015). Mcidas and GemC1/Lynkeas are key regulators for the generation of multiciliated ependymal cells in the adult neurogenic niche. Development.

Loulier, K., Barry, R., Mahou, P., Le Franc, Y., Supatto, W., Matho, K.S., Ieng, S., Fouquet, S., Dupin, E., Benosman, R., et al. (2014). Multiplex cell and lineage tracking with combinatorial labels. Neuron *81*, 505–520.

Ma, L., Quigley, I., Omran, H., and Kintner, C. (2014). Multicilin drives centriole biogenesis via E2f proteins. Genes Dev *28*, 1461–1471.

Madisen, L., Zwingman, T.A., Sunkin, S.M., Oh, S.W., Zariwala, H.A., Gu, H., Ng, L.L., Palmiter, R.D., Hawrylycz, M.J., Jones, A.R., et al. (2010). A robust and high-throughput Cre reporting and characterization system for the whole mouse brain. Nat. Neurosci. *13*, 133–140.

McGarry, T.J., and Kirschner, M.W. (1998). Geminin, an inhibitor of DNA replication, is degraded during mitosis. Cell *93*, 1043–1053.

Mirzadeh, Z., Merkle, F.T., Soriano-Navarro, M., Garcia-Verdugo, J.M., and Alvarez-Buylla, A. (2008). Neural stem cells confer unique pinwheel architecture to the ventricular surface in neurogenic regions of the adult brain. Cell Stem Cell *3*, 265–278.

Mirzadeh, Z., Doetsch, F., Sawamoto, K., Wichterle, H., and Alvarez-Buylla, A. (2010). The subventricular zone en-face: wholemount staining and ependymal flow. J. Vis. Exp.

Morin, X., Jaouen, F., and Durbec, P. (2007). Control of planar divisions by the G-protein regulator LGN maintains progenitors in the chick neuroepithelium. Nat. Neurosci. *10*, 1440–1448.

Obernier, K., Cebrian-Silla, A., Thomson, M., Parraguez, J.I., Anderson, R., Guinto, C., Rodas Rodriguez, J., Garcia-Verdugo, J.-M., and Alvarez-Buylla, A. (2018). Adult Neurogenesis Is Sustained by Symmetric Self-Renewal and Differentiation. Cell Stem Cell *22*, 221–234.e8.

Ollion, J., Cochennec, J., Loll, F., Escudé, C., and Boudier, T. (2013). TANGO: a generic tool for high-throughput 3D image analysis for studying nuclear organization. Bioinformatics *29*, 1840–1841.

Pefani, D.-E., Dimaki, M., Spella, M., Karantzelis, N., Mitsiki, E., Kyrousi, C., Symeonidou, I.-E., Perrakis, A., Taraviras, S., and Lygerou, Z. (2011). Idas, a Novel Phylogenetically Conserved Geminin-related Protein, Binds to Geminin and Is Required for Cell Cycle Progression. J. Biol. Chem. *286*, 23234–23246.

Sage, D., Neumann, F.R., Hediger, F., Gasser, S.M., and Unser, M. (2005). Automatic tracking of individual fluorescence particles: application to the study of chromosome dynamics. IEEE Trans. Image Process. *14*, 1372–1383.

Sankar, S., Yellajoshyula, D., Zhang, B., Teets, B., Rockweiler, N., and Kroll, K.L. (2016). Gene regulatory networks in neural cell fate acquisition from genome-wide chromatin association of Geminin and Zic1. Sci. Rep. *6*, 37412.

Schindelin, J., Arganda-Carreras, I., Frise, E., Kaynig, V., Longair, M., Pietzsch, T., Preibisch, S., Rueden, C., Saalfeld, S., Schmid, B., et al. (2012). Fiji: an open-source platform for biological-

image analysis. Nat. Methods *9*, 676–682.

Shah, P.T., Stratton, J.A., Stykel, M.G., Abbasi, S., Sharma, S., Mayr, K.A., Koblinger, K., Whelan, P.J., and Biernaskie, J. (2018). Single-Cell Transcriptomics and Fate Mapping of Ependymal Cells Reveals an Absence of Neural Stem Cell Function. Cell *173*, 1045–1057.e9.

Shen, Q., Wang, Y., Kokovay, E., Lin, G., Chuang, S.-M., Goderie, S.K., Roysam, B., and Temple, S. (2008). Adult SVZ Stem Cells Lie in a Vascular Niche: A Quantitative Analysis of Niche Cell-Cell Interactions. Cell Stem Cell *3*, 289–300.

Shihavuddin, A., Basu, S., Rexhepaj, E., Delestro, F., Menezes, N., Sigoillot, S.M., Del Nery, E., Selimi, F., Spassky, N., and Genovesio, A. (2017). Smooth 2D manifold extraction from 3D image stack. Nat. Commun. *8*, 15554.

Smith, A.R., Ray, A., Smith, and Ray, A. (1978). Color gamut transform pairs. ACM SIGGRAPH Comput. Graph. *12*, 12–19.

Spassky, N., and Meunier, A. (2017). The development and functions of multiciliated epithelia. Nat. Rev. Mol. Cell Biol. *18*, 423–436.

Spassky, N., Merkle, F.T., Flames, N., Tramontin, A.D., García-Verdugo, J.M., and Alvarez-Buylla, A. (2005). Adult ependymal cells are postmitotic and are derived from radial glial cells during embryogenesis. J. Neurosci. *25*, 10–18.

Stancik, E.K., Navarro-Quiroga, I., Sellke, R., and Haydar, T.F. (2010). Heterogeneity in ventricular zone neural precursors contributes to neuronal fate diversity in the postnatal neocortex. J. Neurosci. *30*, 7028–7036.

Stubbs, J.L., Vladar, E.K., Axelrod, J.D., and Kintner, C. (2012). Multicilin promotes centriole assembly and ciliogenesis during multiciliate cell differentiation. Nat. Cell Biol. *14*, 140–147.

Sun, W., Cornwell, A., Li, J., Peng, S., Osorio, M.J., Aalling, N., Wang, S., Benraiss, A., Lou, N., Goldman, S.A., et al. (2017). SOX9 Is an Astrocyte-Specific Nuclear Marker in the Adult Brain Outside the Neurogenic Regions. J. Neurosci. *37*, 4493–4507.

Tavazoie, M., Van der Veken, L., Silva-Vargas, V., Louissaint, M., Colonna, L., Zaidi, B., Garcia-Verdugo, J.M., and Doetsch, F. (2008). A Specialized Vascular Niche for Adult Neural Stem Cells. Cell Stem Cell *3*, 279–288.

Terré, B., Piergiovanni, G., Segura-Bayona, S., Gil-Gómez, G., Youssef, S.A., Attolini, C.S., Wilsch-Bräuninger, M., Jung, C., Rojas, A.M., Marjanović, M., et al. (2016). GEMC1 is a critical regulator of multiciliated cell differentiation. EMBO J. *35*, 942–960.

Wang, X., Tsai, J.-W., Imai, J.H., Lian, W.-N., Vallee, R.B., and Shi, S.-H. (2009). Asymmetric centrosome inheritance maintains neural progenitors in the neocortex. Nature *461*, 947–955.

Xu, Q., Tam, M., and Anderson, S.A. (2008). Fate mapping Nkx2.1-lineage cells in the mouse telencephalon. J. Comp. Neurol. *506*, 16–29.

Zhou, F., Narasimhan, V., Shboul, M., Chong, Y.L., Reversade, B., and Roy, S. (2015). Gmnc Is a Master Regulator of the Multiciliated Cell Differentiation Program. Curr. Biol. *25*, 3267–3273.

MATERIALS AND METHODS

Mouse lines

Mice were bred and the experiments were performed in conformity with French and European Union regulations and the recommendations of the local ethics committee. The date of the vaginal plug was recorded as embryonic day (E) 0.5 and the date of birth as postnatal day (P) 0. Emx1-Cre (JAX stock #005628, Gorski et al., 2002), Gsh2-Cre (a gift from the laboratory of N. Kessaris, Kessaris et al., 2006) and Nkx2.1-Cre (JAX stock #008661, Xu et al., 2008) transgenic animals were crossed with R26:tdTomato$^{mT/mT}$ animals (Ai14, Madisen et al., 2010). MADM$^{GT/+}$ and MADM$^{TG/+}$ transgenic animals were a gift from the laboratory of S. Hippenmeyer (Hippenmeyer et al., 2010). Heterozygous mice were crossed to obtain homozygous MADM$^{GT/GT}$ and MADM$^{TG/TG}$ animals. These homozygous mice were then mated to obtain MADM$^{GT/TG}$ embryos. Expression of the Cre Recombinase in MADM$^{GT/TG}$ embryos was achieved by *in utero* electroporation of pcX-Cre plasmid (1µg/µl, Morin et al., 2007) at E13.5 or E14.5. All transgenic mice lines were kept as B6D2F1/J or C57/Bl6 background. For the other experiments, RjORL:SWISS mice were used because of their fertility and their maternal instinct.

EdU administration and detection

To determine the cell cycle stage at the time of electroporation, 50 mg/kg body weight (8 mg/ml stock, dissolved in filtered PBS) of EdU (Fisher Scientific, cat. no. 11590926) was administered to pregnant mice by intraperitoneal injection 2 hours before and 2 hours after *in utero* electroporation. To assess the neurogenic potential of SVZ astrocytes, EdU was administered for 14 days through the drinking water (1 mg/ml) of P21 electroporated litters. EdU incorporation was detected using the Click-iT™ EdU Alexa Fluor imaging kit (ThermoFisher Scientific C10339 for Alexa Fluor™ 594 staining or C10340 for Alexa Fluor™ 647 staining), according to manufacturer's protocol. Briefly, fixed coronal sections were permeabilized in blocking solution with 0.1% Triton X-100 and 10% fetal bovine serum in PBS for 1h. After washing with PBS, sections were incubated for 1 hour with the Click-iT™ reaction cocktail, protected from light. The sections were washed again and incubated overnight at 4°C with the primary antibodies. After incubation with the secondary antibody

for 2 hours and Hoechst staining, slices were mounted with Fluoromount-G (Southern Biotech cat. no. 0100-01) mounting medium.

In utero electroporation

In utero electroporation of mouse embryos was performed at E13.5 and E14.5. Pregnant females were injected subcutaneously with buprenorphine (0.1 mg/kg) 15 minutes prior to surgery. They were subsequently anaesthetized by isoflurane inhalation, the abdominal cavity opened and the uterine horns exposed. With a thin glass capillary (Harvard Apparatus 30-0019), 1µl of plasmid in filtered PBS was injected together with FastGreen (0.025%, Sigma F7252) into the lateral ventricles of the embryo. The final concentrations of plasmids were 1 µg/µl ^{PB}*CAG-Nucbow*, 0.5 µg/µl *CAG-hypBase*, 0.1 µg/µl *CAG-seCre* (Loulier et al., 2014), 1 µg/µl *CAG-H2B-GFP* (a gift from the laboratory of X. Morin, Hadjantonakis and Papaioannou, 2004), 1µg/µl pCAGGS -Cre (a gift from the laboratory of X. Morin, Morin et al., 2007), or 1µg/µl pCAGGS-GemC1 or pCAGGS-Geminin (gifts from the laboratory of S. Taraviras, Kyrousi et al., 2015).

Immediately after injection, four 50ms 35V pulses were applied to embryos at 950 ms intervals with an electroporator (CUY21 EDIT, Nepagene). Finally, the embryos were carefully placed back into the abdominal cavity and left to develop before sacrifice.

Tissue collection and immunostaining

When the immunostaining and analyses were to be performed on coronal sections, the mice, previously anesthetized with a mixture of 100 mg of ketamine and 10 mg of xylazine per kg of body weight, were perfused transcardially with 4% PFA. After overnight fixation of the dissected brain in 4% PFA at 4°C, 80 µm-thick floating sections were cut on a vibratome.

Wholemounts of the lateral walls of the lateral ventricles were dissected (Mirzadeh et al., 2010) and fixed for 15 minutes in 4% PFA at room temperature. Samples were incubated for 1h in blocking solution (1X PBS with 0.1-0.2% Triton-X100 and 10% fetal bovine serum) at room temperature. Wholemounts and floating sections were incubated overnight at 4°C in the primary antibodies diluted in blocking solution. The next day, they were stained with species-specific Alexa Fluor secondary antibodies (Invitrogen) and Hoechst solution protected from light for 2h at room temperature. Finally, the wholemounts were redissected to keep only the thin lateral walls of the lateral ventricle (Mirzadeh et al., 2010)

which were mounted with Vectashield mounting medium (H-1000, Sigma), for Nucbow-positive samples, or Fluoromount-G mounting medium (Southern Biotech cat. no. 0100-01), for other stainings. Fluoromount-mounted slides were stored at 4°C; Vectashield-mounted slides were stored at -20°C to avoid color fading. The primary antibodies used were CD24 (1:200, BD Pharmingen, cat. no. 557436), FoxJ1 (1:500, eBioscience, cat. no. 14-9965-82), GFP (1:1600, Aves, cat. no. GFP-1020), Dsred (1:400, Clonetech, cat. no. 632496), Sox9 (1:1200, Millipore, cat. no. AB5535), FOP (1:600, Abnova, cat. no. H00011116-MO1), ZO1 (1:100, Life Technologies, cat.no. 402200) and GTU88 (1:500, Sigma, cat.no. T6557).

Imaging

Fixed slices or lateral ventricle wholemounts were examined with an upright Zeiss Axio Observer.ZI epifluorescence microscope, using an Apochromat 63 x 1.4 NA objective and a Zeiss Apotome with an H/D grid.

Confocal image stacks were collected with a 40 x 1.3 NA objective on Olympus FV1000 and FV1200 microscopes or with a 40 x 1.4 NA oil objective on an inverted LSM 880 Airyscan Zeiss microscope with 440, 515, 560 and 633 laser lines to excite, independently, Cerulean, mEYFP, mCherry and Alexa 647/Cy5,

Image and Statistical Analysis

Quantification, image and statistical analyses were performed with Fiji (Schindelin et al., 2012), Matlab (Mathworks, USA), Excel, and GraphPad Prism software.

Automatic MAGIC Markers image analysis

For clarity, mCherry, EYFP and Cerulean Nucbow signals are represented as red, green and blue (RGB) values. 1) **Local apical layer extraction*:*** to maintain consistency among datasets, only cells within 25 µm of the apical surface were considered using the SME projection tool on the FoxJ1-stained cell nuclei (Shihavuddin et al., 2017). 2) **Segmentation of ependymal cells stained with FoxJ1:** the 3D volume occupied by each cell nucleus was delineated using FoxJ1 far red staining. RGB information was extracted from the segmented mask using the following steps implemented as a FIJI macro: Noise was reduced in a preprocessing step using 3D Gaussian filtering, where the sigma values of the Gaussian kernel was set to 1/3rd of the estimated mean nuclear radius in 3D. This was followed by Log3D filtering (Sage et al.,

2005) to select objects corresponding to nuclear size; the local 3D maximum was then detected to determine the center of each cell nucleus. 3D-seeded watershed segmentation was performed from these maxima to accurately detect the nuclear border in 3D. This 3D segmentation mask was used to compute the volume and the mean color of each nucleus. 3) **Segmentation of non-ependymal cells**: After elimination of FoxJ1-positive ependymal cells, only FoxJ1-negative non-ependymal cells remained in the 25µm apical layer. Since there is no specific marker for these cells, they were characterized by their color information as follows: **Projection:** projection of the Nucbow color channels was maximized to obtain a 2D representation of all labeled non-ependymal cells. **Color gradient extraction:** In order to accentuate nuclear borders, the image gradient was computed from the sum of the intensities of the three RGB channels. The gradient image was further filtered with adaptive Gaussian filtering to improve the signal to noise ratio. The adaptive filter augments smoothing where the image gradient is weak and decreases smoothing where the gradient is high, in order to preserve nuclear edges. **Watershed segmentation**: Local maxima were extracted from the inverted smoothed gradient response to retrieve one maximum per nucleus. The seeded watershed transform was then used (Ollion et al., 2013) to detect cells in 2D. 4) **Color normalization*:*** RGB channels were rescaled linearly from 0 and the 99th percentile of their intensity distribution to ensure alignment of their relative intensity (1% of the most saturated cells were therefore excluded from the analysis of each sample). 5) **Determination of clonal lineage*:*** To identify the cell lineage, each cell was characterized by the median R G B values and their spatial location in 3D X, Y, Z. RGB values were converted to their equivalent in the HSV (Hue, Saturation, Value) color space as described in Loulier et al., 2014. This conversion was performed in MATLAB with the HEXCONE model proposed by Smith et al., 1978.

Supplementary Figure 1

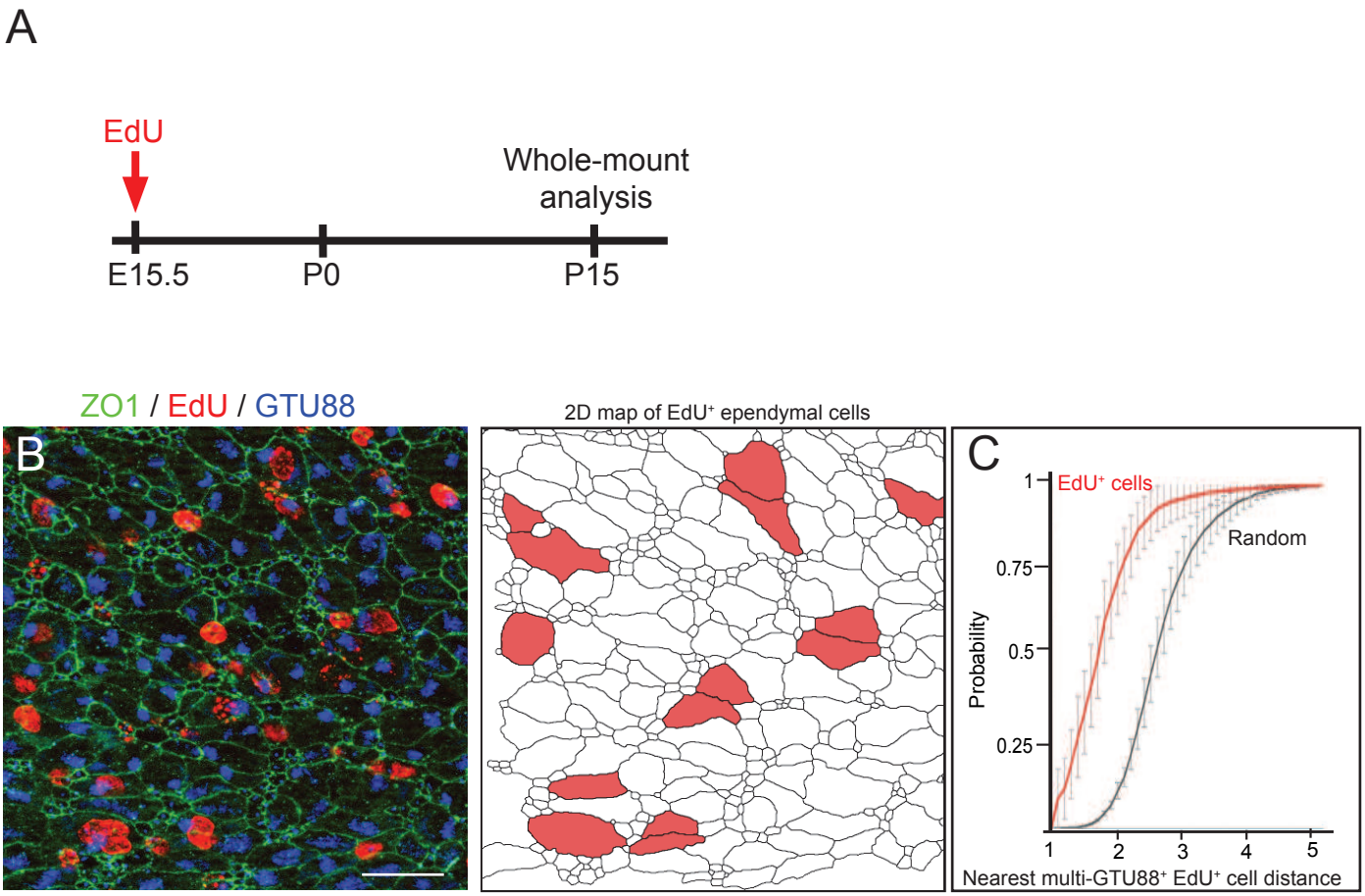

Supplementary Figure 1: Ependymal cells derived from E15.5 progenitors are closer than random at P15

(A) Experimental schema for (B): Timed-pregnant female mice received one injection of EdU at E15.5 and wholemounts of the V-SVZ of the offspring were analyzed at P15.

(B) Triple immunolabeling with ZO1 (green), EdU (red) and GTU88 (basal body marker, blue) and 2D map of EdU^+ ependymal cells. SME projection was used to extract a 2D image of the surface in the vicinity of the apical layer of the 3D stack. Watershed segmentation was then performed on 2D image, using local maxima of the adaptive gaussian-smoothed input image as seeds. The segmented cells were then classified in EdU^+ (red) or EdU^- (white) ependymal cells with a rule-based classifier applied to texture features computed from each single segmented cell. (C) Nearest neighbor distance analysis of EdU^+ ependymal cells (with multiple $GTU88^+$ basal bodies) in the P15 V-SVZ injected with EdU at E15.5. According to the average amount and proportion of EdU^+ cells observed in 24 images obtained from 5 different mouse brains, 500 artificial images were generated, each containing a regular hexagonal grid of 345 cells with a 0.065 probability of being randomly EdU^+. From there, a distribution of the distance of the closest EdU^+ cell from each EdU^+ cell was obtained with the distance defined as the number of cells between two EdU^+ cells. A mean of the 500 cumulative distributions are represented by the black curve in panel (C) with the standard deviation. The red curve represents the same computed results made on the real dataset of 25 images. Data are presented as the mean ± SD. The p-value was determined with the non-parametric Kolmogorov-Smirnov test for 2 samples; $p \leq 0.0001$. The scale bar represents 25 µm.

Supplementary Figure 2

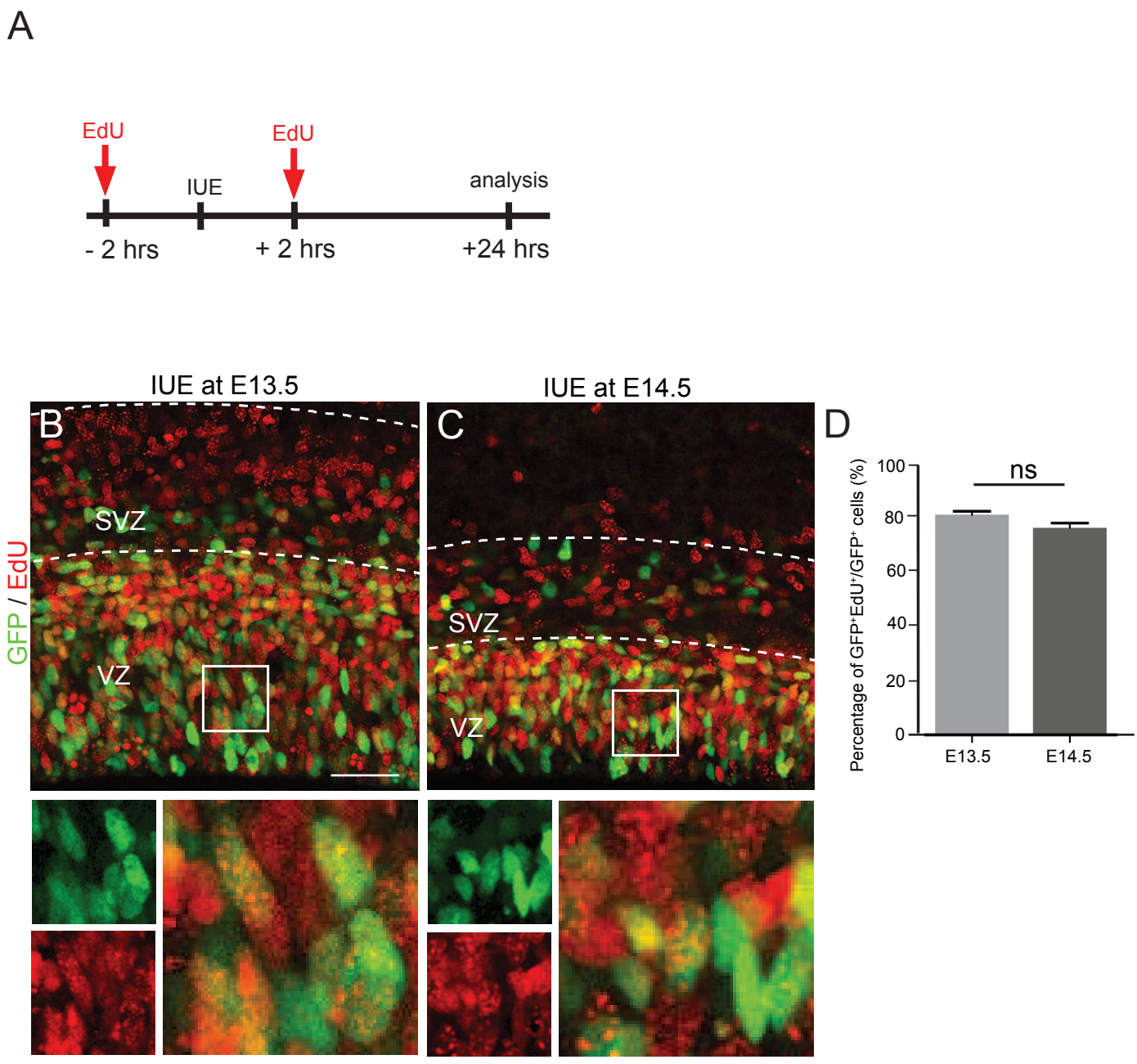

Supplementary Figure 2: *In utero* electroporation targets proliferating radial glia progenitors

(A) Experimental schema for (B): Timed-pregnant female mice received a single injection of EdU 2 hours before and after *in utero* electroporation of H2B-GFP at E13.5 (B) or E14.5 (C) and coronal sections of the forebrain were analyzed 24 hours later.

(B-C) EdU labeling on coronal sections of the H2B-GFP^{+} brains, 24 hours after the electroporation.

(D) Percentage of GFP^{+}EdU^{+} among all GFP^{+} cells one day after the electroporation at E13.5 or E14.5. Data are presented as the mean ± SEM. The p-value was determined by the Mann-Whitney test; ns, p>0.05, n=3 experiments. VZ, ventricular zone; SVZ, subventricular zone. The scale bar represents 75 µm.

Supplementary Figure 3

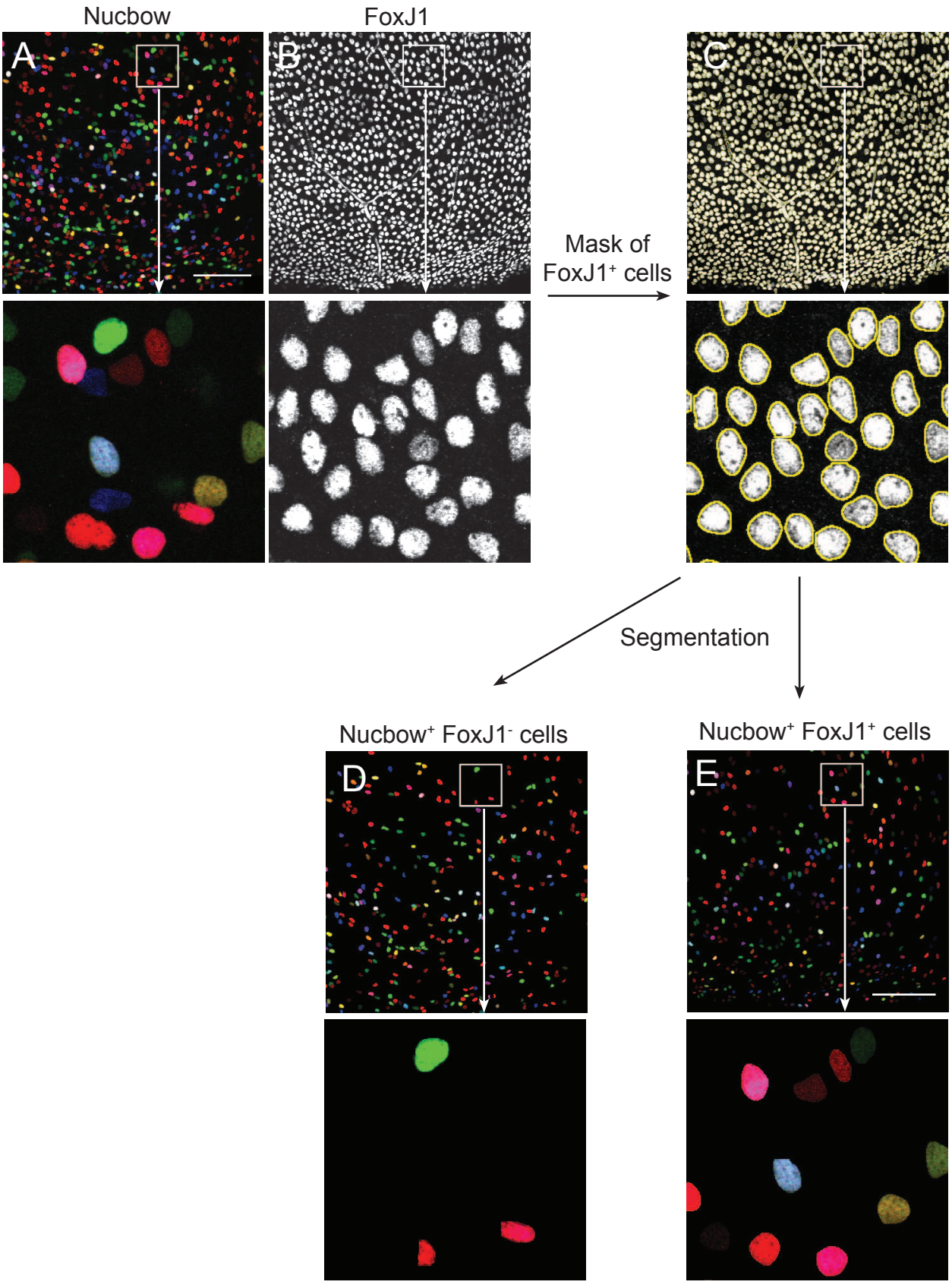

Supplementary Figure 3: Methodology for the detection of FoxJ1^{+} and FoxJ1^{-} Nucbow^{+} cells

(A-B) Representative raw images of an *en-face* view of the V-SVZ electroporated at E14.5 with ^{PB}*CAG-Nucbow* along with the PiggyBac transposase and the self-excising Cre recombinase (A) and immunostained at P15 with FoxJ1 antibody (B). (C) 25 µm 3D-segmentation of FoxJ1^{+} cells outlined in yellow using Gaussian smoothing, Log3D filtering and 3D watershed segmentation implemented as a FIJI macro (see methods). (D-E) Segmented images of Nucbow^{+}FoxJ1^{-} and Nucbow^{+}FoxJ1^{+} cells, respectively. The scale bar represents 300 µm.

Supplementary Figure 4

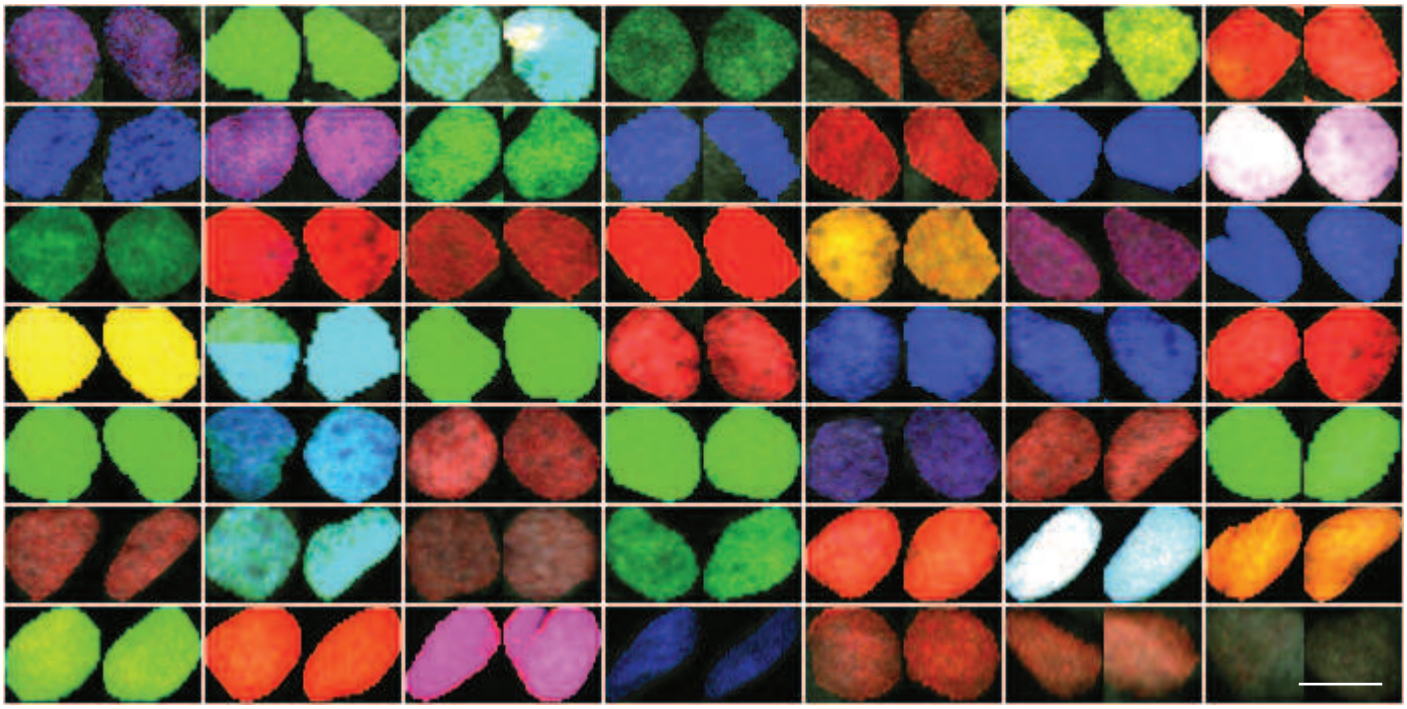

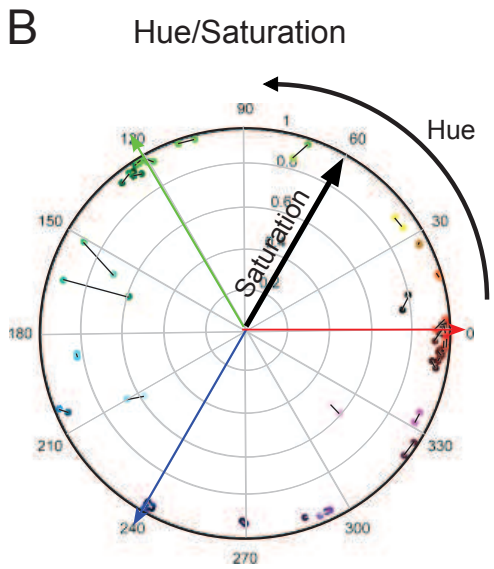

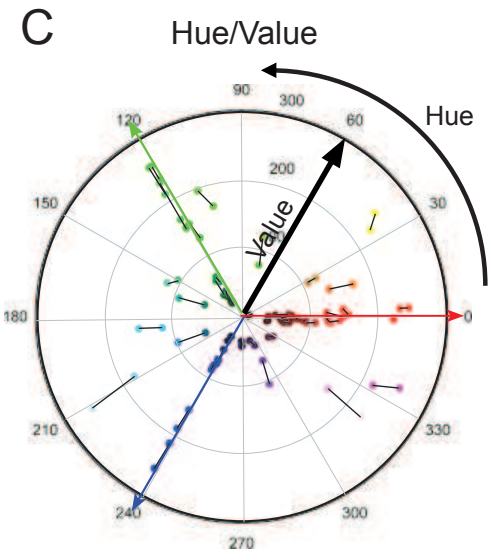

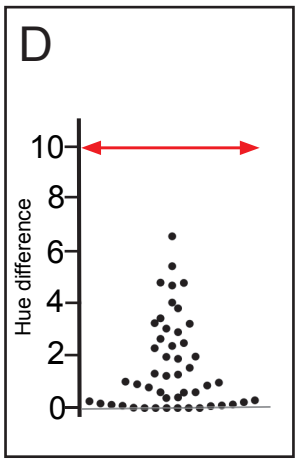

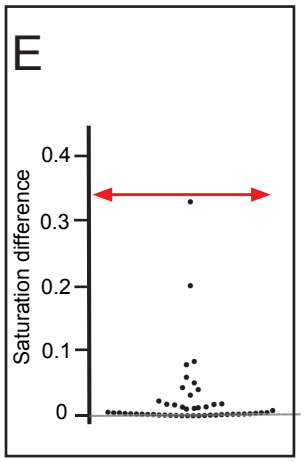

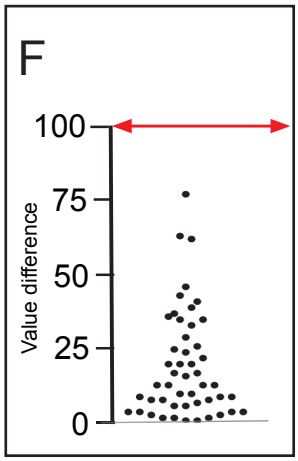

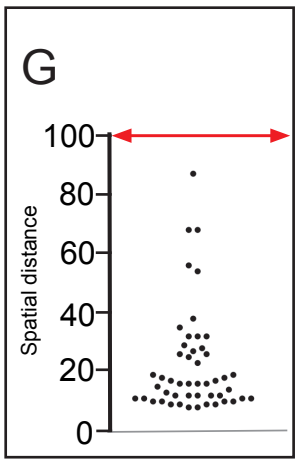

Supplementary Figure 4: Color analysis of manually selected Nucbow^{+} clones

(A) 49 couples of cells were manually selected by 2 independent researchers from 4 different electroporated brains with ^{PB}*CAG-Nucbow* along with the PiggyBac transposase and the self-excising Cre recombinase at E14.5. (B-C) Circular Hue-Saturation (B) and Hue-Value (C) plots of manually selected Nucbow^{+} cells shown in (A). (D-G) Hue, Saturation, Value differences and spatial distance between each cell of the manually selected Nucbow^{+} clones shown in (A). The red arrows indicate the thresholds chosen for the automatic analysis. The scale bar represents 15 µm.

Supplementary Figure 5

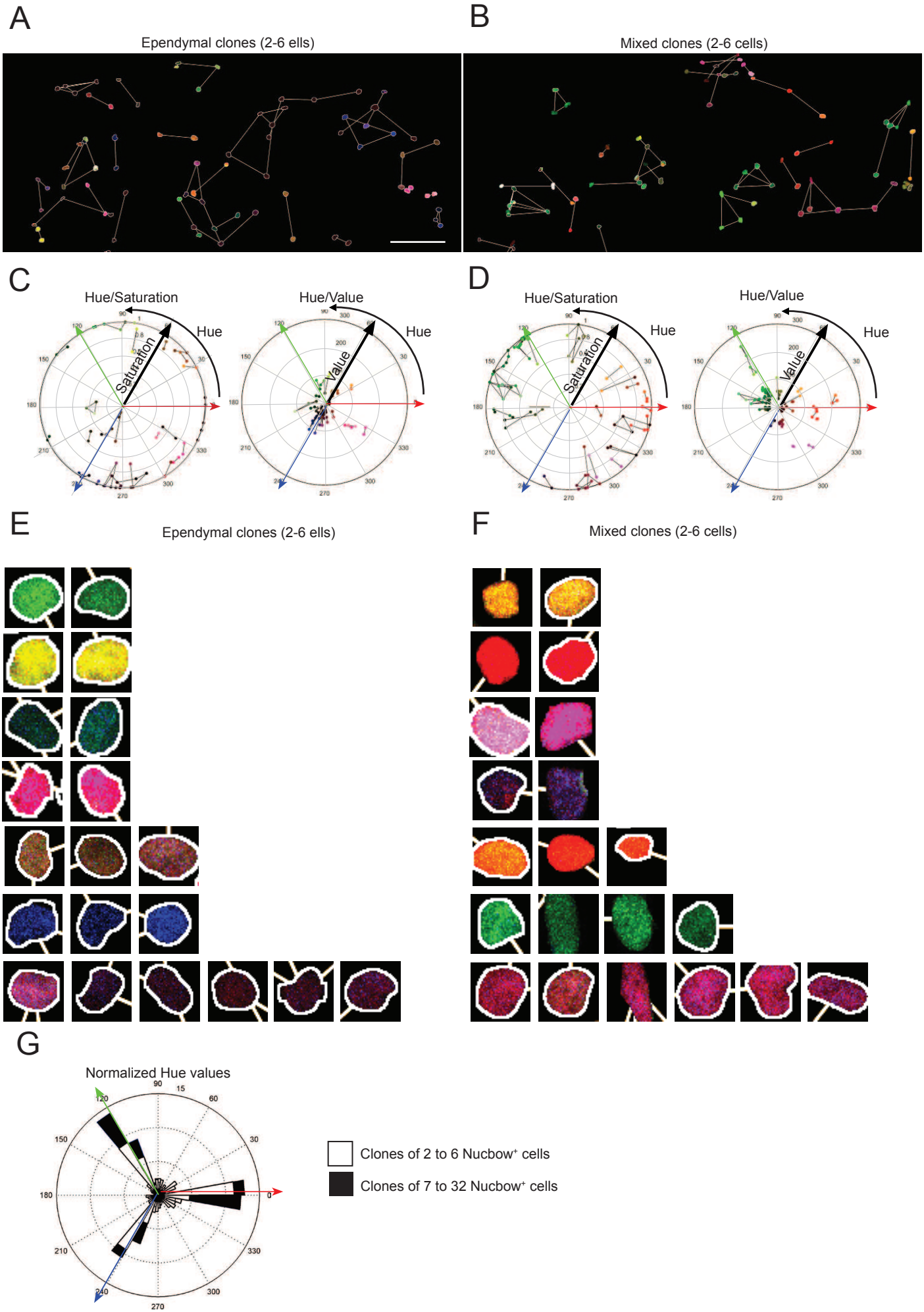

Supplementary Figure 5: Color analysis of Nucbow^{+} clones

(A-B) Map of Nucbow^{+} clones containing 2 to 6 ependymal cells (A) or a mixed population of FoxJ1^{+} and FoxJ1^{-} cells (B). (C-D) Circular Hue-Saturation and Hue-Value plots of all depicted Nucbow^{+} cells from (A-B), respectively. (E-F) Examples of ependymal cell clones formed by 2, 3 or 6 FoxJ1^{+} cells (E) and clones containing at least one FoxJ1^{+} cell formed by 2, 3, 4 or 6 cells. In all maps, FoxJ1^{+}Nucbow^{+} cells are outlined in white. (G) Normalized circular histogram of Hue values of cells contained in clones of 2 to 6 cells (small clones, white) or clones of 7 to 32 cells (big clones, black). Cells from big clones are more frequent around primary colors compared to cells from small clones (Kolmogorov-Smirnov test, p=0.001). The scale bar represents 100 μm (A-B, E-F).

Supplementary Figure 6

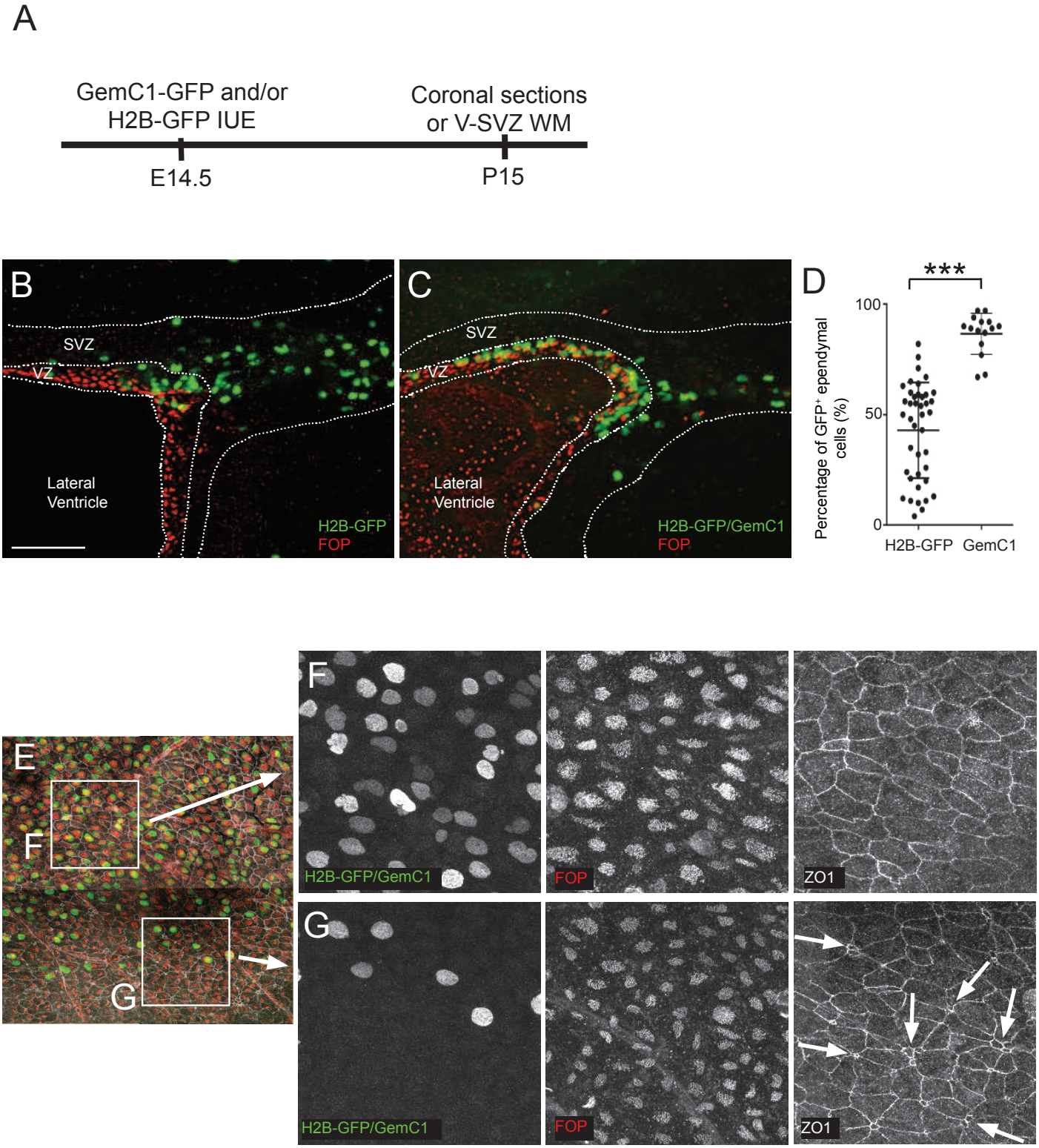

Supplementary Figure 6: GemC1 expression induces ependymal cell differentiation at the expense of B1 cells

(A) Experimental schema: GemC1 and/or H2B-GFP plasmids were electroporated *in utero* at E14.5 and V-SVZ WM or coronal sections were analyzed at P15.

(B-C) Confocal image of coronal sections of the forebrain at P15 immunostained with GFP and FOP antibodies (red), previously electroporated with H2B-GFP (B) or GemC1 and H2B-GFP (C). Ependymal cells are identified by the co-localisation with the basal body marker FOP. VZ: ventricular zone; SVZ: Subventricular zone.

(D) Percentage of GFP^+FOP^+ ependymal cells among all GFP^+ cells. Data are presented as the mean ± SEM. The p-value was determined by the Mann-Whitney test; ***p≤0.001, n=3.

(E) Confocal image of the V-SVZ WM at P15 immunostained with GFP (green), the basal body marker FOP (red) and ZO1 (white) antibodies. (F-G) High magnification images of the insets in (E) showing that pinwheel structures are absent when most cells express GemC1 (F) whereas pinwheels (arrows in G) are present in regions weakly electroporated with GemC1.

The scale bar represents 50 µm in (B-C) and 200 µm in (E).

Supplementary Movie 1: 3D analysis of a pure ependymal (ependymal-ependymal) clone at P15 following Cre expression in a MADM-embryo at E14.5 (related to Figure 4)

Supplementary Movie 2: 3D analysis of a mixed (ependymal-type B1 astrocyte) clone at P15 following Cre expression in a MADM- embryo at E14.5 (related to Figure 4)

Supplementary Movie 3: 3D analysis of a mixed (ependymal-type B1 astrocyte) clone at P15 following Geminin and Cre expression in a MADM- embryo at E14.5 (related to Figure 6)

Table S1: MADM lineage tracing after Cre expression at E13.5 or E14.5 (related to Figure 4)

E13.5 Cre

		Composition of clones		
Clone ID	Clone Size	Green cell	Red cell	Clone type
1B-3	1	B		B
1C-3	1	B		B
1C-1	1	E		E
1A-5	2	E	B	M
3A-2	2	E	B	M
1C-6	2	B	E	M
1A-7	3	B	EE	M
1B-4	3	E	BB	M
1A-3	3	EE	B	M
1B-7	3	B	EE	M
1B-8	3	EB	E	M
3A-1	3	EB	E	M
1A-6	3	E	EE	E
1B-9	3	E	EE	E
5B-1	4	EE	BB	M
1A-11	4	E	EBB	M
1C-4	4	B	EEB	M
1C-5	4	EB	BB	M
3A-3	4	EBB	E	M
1B-2	4	EEB	B	M
3A-4	4	E	BBB	M
1A-8	4	EE	EE	E
1B-5	4	EEE	E	E
1A-4	5	EEEB	E	M
1A-12	5	EEEB	E	M
1C-2	5	EEB	EE	M
3B-3	5	EB	EEB	M
1B-6	5	BBB	EE	M
3B-2	6	EEBB	EE	M
1A-10	6	EEEEB	E	M
1A-9	7	EEEEB	EE	M
1B-1	7	EEB	EBBB	M

E14.5 Cre

		Composition of clones		
Clone ID	Clone Size	Green cell	Red cell	Clone type
19B-1	1		E	E
23B-4	1		E	E
15C-1	1		E	E
6B-1	2	E	B	M
14A-2	2	B	E	M
10B-3	2	B	E	M
13A-2	2	E	B	M
13B-1	2	E	B	M
15B-1	2	E	B	M
15C-2	2	E	B	M
15C-3	2	B	E	M
15C-4	2	E	B	M
22C-1	2	B	E	M
23B-2	2	B	E	M
9B-1	2	E	E	E
9B-3	2	E	E	E
12B-1	2	E	E	E
13A-1	2	E	E	E
14A-1	2	E	E	E
14A-4	2	E	E	E
14A-5	2	E	E	E
14A-6	2	E	E	E
19A-2	2	E	E	E
23B-1	2	E	E	E
8B-4	3	B	BE	M
12A-1	3	B	BE	M
12C-1	3	EB	E	M
14A-7	3	EE	B	M
19A-1	3	B	EE	M
23B-3	3	B	EE	M
15B-2	3	BB	E	M
15B-8	3	EB	E	M
19B-2	3	EB	E	M
14A-3	3	E	EE	E
15B-4	3	E	EE	E
10B-1	4	BB	EB	M
10B-2	4	BB	EE	M
15B-5	4	EB	EE	M
12C-2	4	EE	EE	E
12C-4	4	EE	EE	E
15B-7	5	EBB	EB	M
9B-2	5	EEE	EE	E
15B-6	5	EEE	EE	E
6B-2	6	EEE	EEB	M
12C-3	6	EEEE	EE	E
15B-9	6	EEEE	EE	E
6B-3	6	EEE	EEE	E

Supplementary Table 1: MADM lineage tracing after Cre expression at E13.5 or E14.5 (related to Figure 4)

Cre activity was induced through IUE in MADM embryos at E13.5 or E14.5 and red-green clones were analyzed on V-SVZ at P15-P20. B=Type B1 astrocytes; E=Ependymal cells; M=Mixed clones; E= Ependymal clones.

Table S2: MADM lineage tracing after GemC1 and Cre expression at E13.5 and E14.5 (related to Figure 5)

E13.5 Cre GemC1

		Composition of clones		
Clone ID	Clone Size	Green cell	Red cell	Clone type
21B-5	1		E	E
21B-6	1	E		E
21B-7	1	E		E
21B-2	2	E	B	M
21B-3	2	B	E	M
21C-5	2	B	E	M
22A-2	2	B	E	M
21A-4	2	E	E	E
22A-1	2	E	E	E
21B-4	2	E	E	E
21C-2	2	E	E	E
21C-6	2	E	E	E
22A-3	2	E	E	E
21C-1	3	E	EB	M
21A-1	3	E	EE	E
21A-5	3	EE	E	E
21C-3	3	EE	E	E
21C-4	3	E	EE	E
21A-2	4	EEB	E	M
21B-1	4	EB	EB	M
21A-6	4	EEE	E	E
21A-7	4	EE	EE	E
21A-3	5	EE	EEEE	E

E14.5 Cre GemC1

		Composition of clones		
Clone ID	Clone Size	Green cell	Red cell	Clone type
25C-1	1		E	E
25C-2	1		E	E
25A-3	1	E		E
25A-6	1	E		E
25C-3	2	B	E	M
25A-10	2	E	B	M
28A-7	2	E	B	M
25A-2	2	E	E	E
25A-5	2	E	E	E
25A-7	2	E	E	E
25A-8	2	E	E	E
25A-9	2	E	E	E
26B-2	2	E	E	E
26B-3	2	E	E	E
26B-3'	2	E	E	E
27A-1	2	E	E	E
28A-1	2	E	E	E
28A-2	2	E	E	E
28A-3	2	E	E	E
28A-4	2	E	E	E
28B-1	2	E	E	E
29A-1	2	E	E	E
29A-5	2	E	E	E
29B-1	2	E	E	E
29B-3	2	E	E	E
29B-5	2	E	E	E
25C-4	3	EB	B	M
26B-3"	3	E	EB	M
26A-3	3	B	EE	M
26B-4	5	EEEB	E	M
25A-4	3	EE	E	E
25A-6	3	EE	E	E
26A-1	3	E	EE	E
28A-6	3	E	EE	E
29A-3	3	E	EE	E
29A-4	3	EE	E	E
29A-6	3	E	EE	E
29B-4	3	EE	E	E
29A-2	3	E	EE	E
27A-2	4	EE	EE	E
28A-5	4	EEE	E	E
29A-7	4	EE	EE	E
29B-2	4	EEE	E	E
26A-2	4	EE	EE	E
26B-1	5	EE	EEE	E

Supplementary Table 2: MADM lineage tracing after Cre and GemC1 overexpression at E13.5 or E14.5 (related to Figure 5)

GemC1 overexpression together with Cre activity was induced through IUE in MADM embryos at E13.5 or E14.5 and red-green clones were analyzed on V-SVZ at P15-P20. B=Type B1 astrocytes; E=Ependymal cells; M=Mixed clones; E= Ependymal clones.

Table S3: MADM lineage tracing after Geminin and Cre expression at E14.5 (related to Figure 6)

E14.5 Cre Geminin

Clone ID	Clone Size	Composition of clones		Clone type
		Green cell	Red cell	
341-1-2	1		B	B
360-1-2	1	B		B
362-5-17	1	E		E
362-5-17'	1		E	E
362-5-15	1		E	E
376-4-21	1		B	B
378-4-3	1		B	B
378-4-7	1	E		E
378-4-9	1	E		E
378-5-3	1		E	E
378-3-	1		E	E
378-3-	1		E	E
378-3-	1		E	E
378-3-	1		E	E
378-3-	1		E	E
378-3-	1		E	E
378-3-	1		E	E
378-3-	1		B	B
378-3-	1		B	B
378-3-	1		B	B
378-3-	1	B		B
378-3-	1	B		B
378-3-	1	B		B
378-3-	1	B		B
378-3-	1	B		B
378-3-	1	B		B
335-1-2	2	B	B	B
376-4-19	2	B	B	B
376-4-25	2	B	B	B
376-5-8	2	B	B	B
376-5-12	2	B	B	B
376-6-4	2	B	B	B
378-3-8	2	B	B	B
378-4-2	2	B	B	B
378-4-8	2	B	B	B
378-4-26	2	B	B	B
360-1-1	2	E	E	E
376-4-4	2	E	E	E
376-4-8	2	E	E	E
376-4-9	2	E	E	E
376-4-11	2	E	E	E
376-4-12	2	E	E	E
376-5-2	2	E	E	E
376-5-10	2	E	E	E
378-3-1	2	E	E	E
378-3-7	2	E	E	E
378-4-5	2	E	E	E
378-4-11	2	E	E	E
378-4-13	2	E	E	E
341-3-2	2	B	E	M
359-2-2	2	E	B	M
359-1-1	2	B	E	M
360-1-3	2	E	B	M
362-5-1	2	B	E	M
362-5-3	2	E	B	M
362-5-10	2	B	E	M
376-4-13	2	B	E	M
376-4-23	2	B	E	M
376-4-24	2	E	B	M
376-4-28	2	E	B	M
376-5-3	2	B	E	M
376-5-4	2	E	B	M
376-5-9	2	B	E	M
376-6-2	2	E	B	M
378-3-4	2	E	B	M
378-3-6	2	E	B	M
378-4-1	2	E	B	M

Clone ID	Clone Size	Composition of clones		Clone type
		Green cell	Red cell	
378-4-12	2	E	B	M
378-4-16	2	E	B	M
378-4-21	2	E	B	M
378-4-24	2	E	B	M
378-5-2	2	E	B	M
378-5-4	2	B	E	M
359-2-1	3	E	EE	E
362-5-2	3	E	EE	E
360-1-4	3	E	EE	E
376-4-6	3	EE	E	E
376-4-16	3	EE	E	E
376-4-22	3	E	EE	E
376-5-14	3	EE	E	E
376-6-5	3	EE	E	E
378-4-6	3	EE	E	E
362-5-5	3	E	EB	M
335-1-1	3	EE	B	M
376-4-2	3	EE	B	M
376-4-15	3	B	EB	M
376-4-17	3	E	EB	M
376-4-20	3	EB	B	M
376-4-26	3	EB	B	M
376-5-13	3	BB	E	M
376-6-8	3	B	EE	M
378-3-2	3	EB	B	M
378-4-4	3	E	EB	M
378-4-15	3	EE	B	M
376-4-5	4	EE	EE	E
376-4-10	4	EE	EE	E
376-6-6	4	EE	EE	E
376-6-7	4	E	EEE	E
378-4-18	4	EE	EE	E
378-4-25	4	EE	EE	E
362-5-14	4	EE	EE	E
376-5-1	4	EB	EE	M
376-5-5	4	BEE	B	M
376-5-11	4	E	EEB	M
376-4-3	4	E	EEB	M
376-6-1	4	EB	EB	M
378-3-3	4	EB	EB	M
378-3-5	4	EE	BB	M
378-4-14	4	EE	EB	M
378-4-17	4	BB	EE	M
378-4-19	4	EB	EE	M
378-4-22	4	EEB	E	M
378-5-1	4	EE	EB	M
361-6-1	4	EE	EB	M
360-1-5	4	EEB	B	M
362-5-4	4	EE	BB	M
362-5-6	4	BB	EB	M
362-5-7	4	B	EEE	M
362-5-9	4	EBB	B	M
362-5-8	5	EE	EEE	E
362-5-18	5	EEEE	E	E
376-6-3	5	EEE	EE	E
362-5-11	5	EEE	EB	M
362-5-12	5	EEB	EB	M
376-5-6	5	BB	EEE	M
376-5-7	5	BBE	BB	M
376-4-1	5	EB	EBB	M
378-4-20	6	EEE	EEE	E
378-4-10	6	EEB	EEE	M
378-4-23	6	EEB	EBB	M
376-4-18	6	EEEBB	B	M
376-4-18bis	7	EEB	EEEE	M
376-4-14	7	EEEEB	EE	M

Supplementary Table 3: MADM lineage tracing after Cre and Geminin overexpression at E14.5 (related to Figure 6)

Geminin overexpression together with Cre activity was induced through IUE in MADM embryos at E14.5 and ref-green clones were analyzed on V-SVZ at P15-P20. B=Type B1 astrocytes; E=Ependymal cells; M=Mixed clones; E=Ependymal clones.

CONCLUSIVE REMARKS AND DISCUSSION

I- MULTICILIATED EPENDYMAL CELLS: ORIGINS AND ADULT NEUROGENESIS

1) Take-home messages (Figure 26)

- Ependymal progenitors do not migrate subsequent to their last division and lead to mature ependymal cells that remain in close proximity to each other in the ventricular region where they were produced in the wall of lateral ventricles.

- Multiciliated ependymal cells can be produced through symmetric or asymmetric cell division of radial glial cells during brain development.

- Both multiciliated ependymal cells and astrocytes can be produced either through ependymal-only or astrocytic-only production symmetric divisions or mixed ependymal-astrocytic production asymmetric division in the subventricular zone.

- The astrocytes produced together with ependymal cells are capable of generating new neurons in the adult brain. They are the adult neural stem cells (NSCs) of the subventricular zone also known as B1-cells.

- Multiciliated ependymal cells seem to be produced slightly later during development than B1 cells.

- Over-expression of GemC1 promotes premature ependymal cell differentiation via symmetric terminal cell division of radial glia at the expense of B1 cells production by asymmetric cell division.

- Over-expression of Geminin promotes B1 cells production through symmetric cell division of RGC.

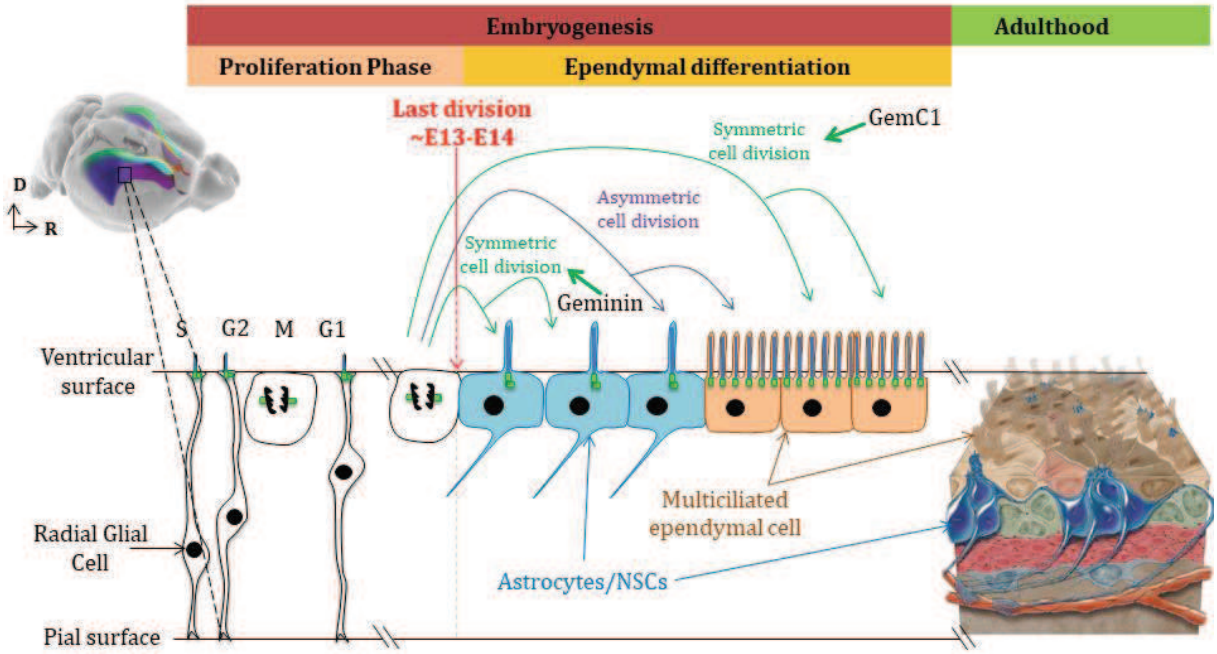

Figure 26: Schematic of the production of ependymal cells and astrocytes in the SVZ over time. *Adapted from Mirzadeh et al., 2008* [1]

2) Cell fate-decision of RGC

Collectively, our data reveal that RGC give rise to ependymal cells (E) and astrocytes/adult neural stem cells (A) at the end of neurogenesis mainly through E-E SCD or E-A ACD. To a lesser extent, they can also perform A-A SCD – though always in parallel with E-E and or E-A cell divisions. A crucial interrogation thus arises from these observations, addressing whether RGCs are programmed to execute a pre-determined number of divisions before committing towards ependymal fate. This theory is in line with other data provided by Gao et al., Namely, their results suggest that RGC exhaust their proliferative capacity earlier during development, before being able to perform one last gliogenic division[2]. Similarly, our study suggests that RGCs might differentiate into ependymal cells by default once they have exhausted their proliferative potency.

As a follow-up to our study and to answer this pending question, comparing the size of telomeres of ependymal progenitors at distinct developmental stages could be involved in the decision-making process. The fact that ependymal cells

originate from two distinct mechanisms (SCD and ACD) makes the verification of this hypothesis considerably complex. This suggests that the molecular machinery involved in ependymal cell fate commitment is highly complex, and might be different for SCD- and ACD-derived ependymal progeny.

Our results have shed light on the production of astrocytic cell subtype B1-cells. Nevertheless, we cannot exclude the presence of other GFAP+Sox9+ astrocytic populations which are not involved in adult neurogenesis. Further investigations using astrocytic cell subtype-specific markers are needed before we can answer this interrogation. As for different cell types (non-astrocytic and non-ependymal), there is little probability that they can be produced together with an ependymal cell via ACD because the proportion of unidentified electroporated cells (Sox9-FoxJ1-) on the lateral SVZ is very low. The observation of these unidentified cells is more likely due to experimental variability due to an uncomplete success of our immunostainings.

3) Ependymal cell specification

We provide evidence that ependymal cells can arise from RGC either through SCD or through ACD. This implies that ependymal cell production results from a complex mechanism and further raises the possibility that there are in fact two distinct ependymal cell subtypes, one being produced through SCD, one through ACD. Up until today, no difference in the expression of ependymal markers has been reported, and multiciliated ependymal cells are considered as one cell-type (except for biciliated ependymal cells, which we do not study here).

We and others have insisted on the crucial role of GemC1 in specifying RGCs towards ependymal fate[3]. However, overexpression of GemC1 by electroporation does not entirely inhibit the potency of RGCs to produce adult NSCs, as we observe from our data. This might be due to partly unsuccessful co-electroporation of GemC1 and other plasmids (Cre-recombinase or H2B-GFP reporter) in the cells. Past studies efficiently yielded results obtained through coelectroporation of multiple plasmids (including Brainbow plasmids),

suggesting that this hypothesis can be excluded; coelectroporation of several plasmids is an experimental robust and reproducible technique. This experimental bias is possible although very unlikely, as coelectroporation of several plasmids has proven very reliable and efficient in past studies[4,5]. We suggest that this can rather be explained by a potential dose-effect of GemC1. Electroporation of relatively low quantity of GemC1 plasmid in RGCs could be insufficient to influence their cell destiny. Unfortunately, the number of plasmid copies present in electroporated cells is highly variable and cannot be anticipated, therefore preventing further verification of this hypothesis using our model system. In addition, other molecular candidates need to be considered and tested. To identify these candidates, RNA sequencing of mature ependymal cells and undifferentiated precursors cultured *in vitro* could be performed in the laboratory, using an adapted protocol (well described in Al Jord et al., 2014[6]).

The present findings also prompt to address more precise timing of ependymal specification. More particularly, does ependymal fate-commitment occur before or after the last division of RGCs? This is still an open question. Our study suggests that fate decision occurs subsequent to the last division since it can be asymmetric and thereby produce an astrocyte. Then assessing the expression of GemC1 or other candidates prior to ependymal last division would be decisive to determine their possible implication in ependymal fate-commitment.

4) <u>The role of ependymal cells in adult neurogenesis</u>

Our images provide further insights on the interactions between ependymal cells and B1-cells first uncovered by Mirzadeh et al.[1]. In 2008, Mirzadeh has shown that ependymal cells organize as pinwheels all around B1-cells in the adult SVZ neurogenic niche. This pinwheel structure allows ependymal cells to locally propel CSF in direct contact with the primary cilium of B1-cells, and more globally to maintain the current of CSF so that newly born neuroblasts can properly migrate[1,7]. We now further complete these observations by showing that

B1-cells send cytoplasmic extensions from the depth of the SVZ tissue to the ependymal cells located above them (Part Results Figure 4E). This suggests that the role of ependymal cells in the adult niche does not limit to CSF flow maintenance. They could also contribute to adult neurogenesis through other yet-undisclosed molecular signalling cascades. Another interpretation of this interplay would be that our images were captured at P10. Given that mice do not reach adulthood and cellular maturity before P30, ependymal and B1-cells could act on their mutual maturation process completion still during early postnatal stages.

5) Technical limitations of clonal analysis methods

The Brainbow technique is a very useful tool to study a large number of clones which are located within close proximity of each other. The colour of the cell depends on the combination of the fluorescent proteins expressed. Two levels of randomization occur to drive this protein expression: the number of internalized copies of plasmids and the recombination process. The number of possible colours thus seems infinite and highly decreases the statistical probability that two adjacent cells could express the same combination of plasmids after recombination. However, we have observed on the hue/value/saturation plots that primary colours red green and blue were more frequently obtained than more complex colour (part Results Figure 2D). This indicates that recombination in the Brainbow technique is not absolutely random but rather biased. This experimental bias could be due to more stable expression of primary colours as compared with secondary or tertiary colours. Still, the level of difficulty to distinguish and analyse the colours is proportional to the number of colours that we obtain, which is high. Extract cell colours cues, define the stringency for clonal association and analyse all samples systematically without being influenced by human subjectivity require tuning of an automatic fine processing method. Ultimately, the automatic processing can include in the data a low proportion of errors which are highly difficult to avoid. Notably, the statistical data extracted from the analysis cannot take into account some cells due to technical issues. For

instance, we cannot anticipate the proportion of clones which died by apoptosis, clones that are out of the imaged field of view, clones that were damaged by the tissue dissection, etc. On the contrary, automatic analysis will not allow the distinction of cells that might coincidently express the same colour without being clones. Nevertheless, every statistical analysis includes a degree of uncertainty, and we are confident that our automatic processing method has overcome most of these complications.

To make the present results more robust, we have also used the MADM mosaic analysis technique and verified that our conclusions were confirmed. Some of the technical challenges that we faced using this method are the same as for Brainbow: apoptosis, field of view and tissue damage could not be anticipated in the quantifications. Besides, this technique only yields two analysable colours. This makes MADM technique complementary to Brainbow and thus an adequate tool for our second clonal study. Furthermore, the fluorescent proteins are expressed in the cytoplasm which allows better apprehension of the cellular morphology. We encountered other issues due to the limited number of colours obtained with this technique. Clonal lineage cannot be assessed with certitude in two configurations: first if distinct clones are in close proximity with each other, and second if a wide number of electroporated cells are nearby. Fortunately, these situations were very rare due to the fact that sister ependymal cells do not migrate subsequent to their production from their RGC ancestor. Additionally, we noticed that recombination was much more efficient in the Brainbow technique than in the MADM technique. As a consequence, a large amount of samples is required to draw robust conclusions with the MADM technique.

The clonal analysis techniques we use here are performed by electroporation, leading to sparse recombination. Therefore, these methods unfortunately do not allow assessing whether B1-cells and ependymal cells within the same pinwheel are systematically part of the same clonal population, since addressing this question requires the establishment of a clonal map of the entire ependymal population. Applying the Brainbow or the MADM techniques would thus not be

suited to label all ependymal cells due to the recombination bias mentioned previously and to the fact that fluorescent signals from ependymal cells at the ventricular surface and from underneath astrocytes would overlap and prevent proper analysis. Nonetheless, we can hypothesize that ependymal cells and their sister B1-cells would only belong to the same pinwheel if they remained literally adjacent during SVZ maturation. Given that only some cells are adjacent and could be part of the same pinwheel whereas many are separated by several other cells, we consider unlikely that B1-cells and ependymal cells being part of the same pinwheel is pre-determined. We assume it is only in the case of concomitant astrocytic and ependymal production occurring via late ACD that both these cells could be part of the same pinwheel. We believe that it is by physical and mechanical forces driving normal tissue expansion during development that cells are constrained to form pinwheel structures. Logically, if cells are produced earlier during development they should be localized further apart and have lower probability to be part of the same pinwheel, unlike cells produced by late cell division. To answer this question, we could use a Brainbow transgenic mouse as the ones used in previous papers instead of using the electroporation technique and stain the tight junctions separating ependymal cells using a ZO1 antibody[8,4]. According to this rationale, the probability for B1 and ependymal cells to be part of the same pinwheel would indeed be higher for clonal sister cells than for unrelated cells because we have shown that clonal descendants do not migrate very far from each other.

This hypothesis is supported by the results published by Mirzadeh et al.[1], who emphasize the existence of hotspots of B1-cells within the SVZ of the lateral ventricle, whereas ependymal cells are present on the entire ventricular walls[1] (Figure 27).

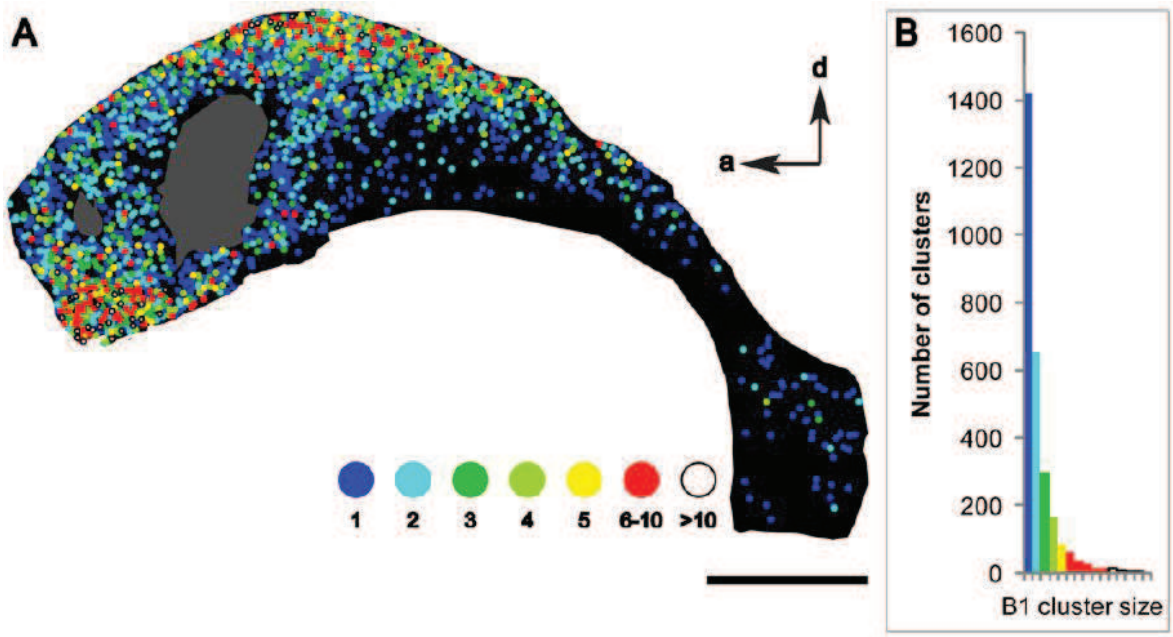

Figure 27: Illustration of the repartition of pinwheels on the lateral wall of the LV. **A-** Representative map of the number oh pinwheels. **B-** Distribution of the size of B1 cells clusters. *Adapted from Mirzadeh et al., 2008* [1]

This assumption requires to be tested. More specifically, confirming whether E-A ACD events occur more frequently nearby these hotspots whereas E-E SCD are preferentially taking place where there are fewer B1-cells is crucial. Unfortunately, the techniques we use in this project are not adapted to establish a connection between the spatial region of the SVZ and SCD vs ACD events because the variability of the electroporation region is inevitably high.

6) <u>The last division of ependymal cells</u>

To gain further insights on the last division of ependymal cells, we have attempted to film it on a high-resolution confocal microscope. Our aim is to reinforce our current results that ependymal cells and astrocytes can be generated through ACD and SCD. Here, we report preliminary observations which set ground for further attempts to image ependymal development but cannot be taken into account as definitive results yet. As this is a long process, we face many

technical limitations, a number of which we were able to overcome in our protocol. However, our preliminary findings suggest that filming the last division of ependymal progenitors is possible (Figure 28). Given that our observations are still at preliminary stage, further optimizing our live-imaging method will be necessary to solve the remaining difficulties.

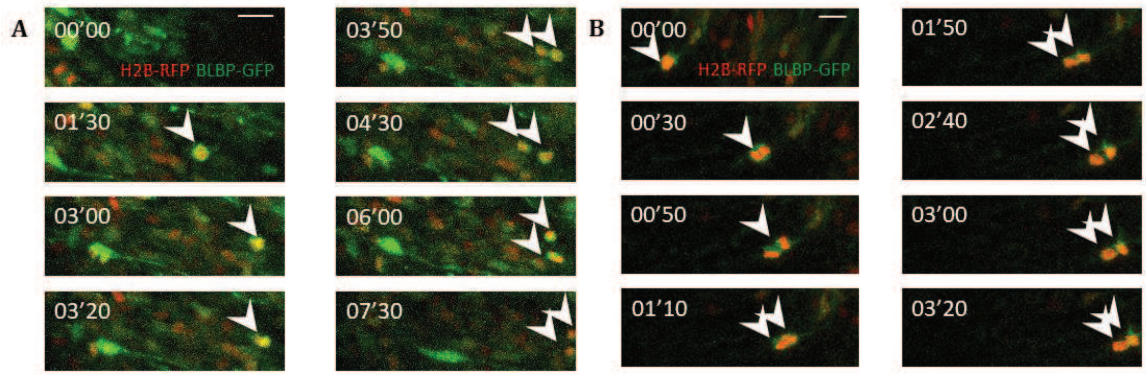

Figure 28: Live-imaging of cell division on the lateral wall of LV coronal slices. A and **B-** Electroporation of H2B-RFP nuclear and BLBP-GFP cytoplasmic plasmid (BLBP is a marker of RGCs) at E13.5 prior to slicing and imaging at E14.5 during around 15h. Arrowhead(s) point(s) first to a dividing cell and then to its two daughter cells. Scale bars: 20µm.

Unfortunately, we also observe that live samples degenerate fast in culture and start exhibiting signs of non-physiological events. We can thus not rely on the events recorded after the samples have been cultured for significant time. After lot of tuning and adaptations, we are capable of filming the last ependymal cell division but cannot yet differentiate SCD from ACD.

As a perspective to this experiment, we have generated FoxJ1::CreER;Tomato+/- inducible transgenic mice from the existing FoxJ1::CreER transgenic mouse[9], to detect differentiation process into multiciliated cells in cells thanks to the expression of FoxJ1 specific ependymal marker. First, an interesting approach could consist on electroporating the SVZ with a nuclear H2B-GFP plasmid at early developmental stages. 24 hours later, we put the samples (either live coronal slices of half or full brains or live explants of VZ-SVZ[10]) in culture with 4-OH-tamoxifen and start imaging. FoxJ1 being expressed subsequent to ependymal

last division is most inconvenient, since electroporation does not specifically target our cells of interest. Consequently, we are confronted to an ambitious challenge: electroporated cells are indistinguishable and we can only image them randomly until one happens to be an ependymal progenitor. We bypass this issue by co-electroporating GemC1 plasmid in the SVZ of transgenic mice. As we and others have seen, GemC1 promotes premature ependymal differentiation through SCD[3]. This will therefore increase our chance to image SCD. Yet, this method is unlikely to enable recording of ACD, since GemC1 overexpression pushes ependymal progenitors towards ependymal differentiation via SCD at the expense of ACD.

II- INSIGHTS ON THE MORPHOLOGY OF EPENDYMAL CELLS

As a perspective to the present project and to be able to film the ependymal last division, we believe that studying the morphology of ependymal cells is critical to understand the extent of their functions, and further unravel open interrogations such as the existence of several populations of ependymal cells. More particularly, we hypothesize that describing ependymal cell morphology might disclose pathways through which ependymal cells could impact adult neurogenesis. To verify this, we use the transgenic FoxJ1::CreER;Tomato+/- inducible mice that we have generated. Up until today, this transgenic animal has not been characterized in-depth. There is great need of studying FoxJ1::CreER;Tomato+/- mouse model system in order to exploit its full potential. Indeed, it allows apprehending the morphology of multiciliated cells in the brain with great level of details. Here, we propose several preliminary observations to tackle the characterization of this transgenic mouse more and describe ependymal cell morphology and further use this transgenic mouse to film the last ependymal cell division.

1) <u>The expression of FoxJ1 transcription factor in ependymal progenitors and cells is time-and region-dependant</u>

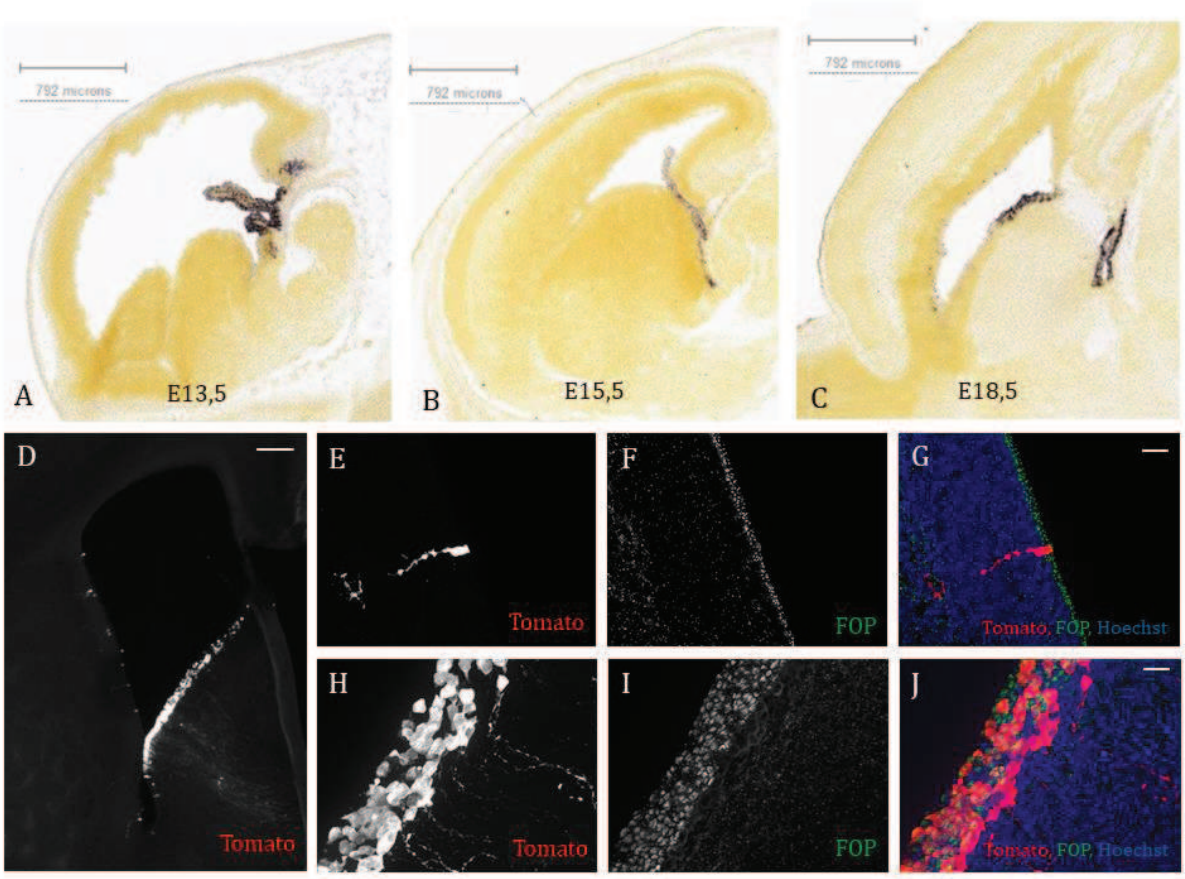

Figure 29: Transcription factor FoxJ1 expression pattern. A-to **C-** *in situ* hybridization of FoxJ1 on embryonic sagittal slices at E13.5, E15.5 and E18.5 respectively, from the Allen Brain Atlas available online. Scale bar: 192µm. **D-** to **J-** Immunostainings of the LV on coronal slice of E19.5 FoxJ1::CreER;Tomato+/- mouse brain subsequent to gavage of the pregnant mother with Tamoxifen at E16.5. Tomato+ FOP+ ependymal cell(s) of the lateral wall (**E-** to **G-**) and of the medial wall (**H-** to **J-**) of the LV at higher magnification. **D-** Scale bar: 100µm. **E-** to **J-** Scale bar: 20µm.

First, we have assessed the timing of the expression of FoxJ1 transcription factor thanks to online data of *in situ* hybridization from the Allen Brain Atlas (Figure A-B-C). We observe that FoxJ1 is expressed in the choroid plexus from E13.5, whereas it is not expressed in the walls of the LV at this stage (Figure A). The expression of FoxJ1 in the walls of the LV appears sparsely at E15.5 and progressively in more cells of the LV at E18.5 (Figure B-C).

Immunostainings of LV performed at E19.5 after gavage of the pregnant FoxJ1::CreER;Tomato+/- mouse mother at E16.5 reveal that Tomato+ ependymal cells identified by multiple FOP+ basal bodies appear first on the medial wall since they are more numerous at this stage, before reaching cells of the lateral wall of the, where we observe less cells (Figure D to J). Noteworthy, the morphology of Tomato+ ependymal cells seems to differ between Tomato+ ependymal cells depending on their location. Ependymal cells of the medial wall, appear cuboidal whereas Tomato+ ependymal cells of the lateral wall of the LV exhibit a long basal process, resembling the one of the RGC from which they derive. At this stage, this phenomenon could be explained by the differential and progressive differentiation of ependymal cells. More specifically, we can hypothesize that ependymal cells of the medial wall of the LV develop earlier during development than ependymal cells of the lateral wall of the LV, meaning that cells start expressing FoxJ1 earlier in the medial wall than in the lateral wall of the LV. In line with this rationale, the ependymal cells of the lateral wall of the LV retain a basal process similar to the one of RGCs from which they derive only because they are less mature than ependymal cells of the medial wall of the LV. Accordingly, the cuboidal morphology of ependymal cells of the medial wall could be explained because they are more mature and had time to retract their basal process. Importantly, we cannot exclude that this basal process could be extended *de novo* in maturing ependymal cells, although we rather hypothesize that it is retained from RGC ancestors since it appears the most parsimonious assumption. This should be investigated more in depth before reaching any conclusion or to establish a viable model.

2) <u>Ependymal cells are not cuboidal</u>

To verify this hypothesis, we have performed immunostainings of FoxJ1::CreER;Tomato+/- mice at P16 and P30 subsequent to gavage of the pregnant mother at E17.5 and P0 respectively. We observe that many cells, but not all, exhibit a basal process which resembles the one from their RGC ancestors.

This is in contradiction with our previous hypothesis, stating that the presence of a basal process in ependymal cells could reflect on their maturation stage.

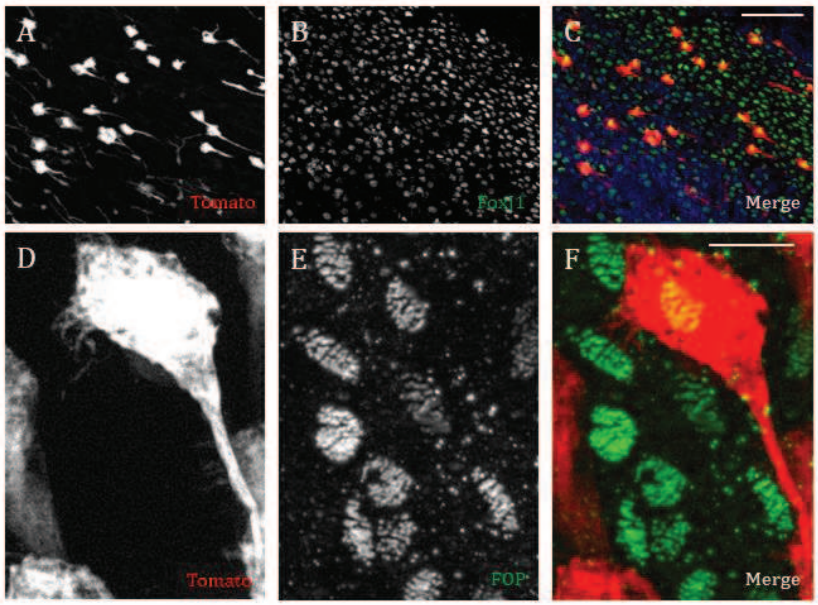

Figure 30: Ependymal cells are not cuboid and retain a long basal process at postnatal stages. A-to **C –**Immunostainings of Tomato+FOP+ ependymal cells on "en face" wholemounts of LV of FoxJ1::CreER;Tomato+/- mouse brain at P16 subsequent to gavage of the pregnant mother with Tamoxifen at E17.5. Scale bar 100 µm. **D-**to **F -** Immunostainings of Tomato+ FOP+ ependymal cell on "en face" wholemounts of LV of adult mouse brain (>P30) subsequent to subcutaneous injection of Tamoxifen at P0. Scale bar: 10µm.

Here, our observations tend to suggest that the stage of maturation of ependymal cells is not correlated to their morphology. We can thus assume that there might be two populations of ependymal cells based on morphological cues: one with a basal process and one cuboidal-shaped.

3) Non-ependymal FoxJ1 positive cells

One day after intraperitoneal injection of EdU and gavage of the FoxJ1::CreER;Tomato pregnant mouse with Tamoxifen at E14.5, we observe that the large majority of the Tomato+ cells of the pups are EdU- near the LV. Nevertheless, some cells are Tomato+ FoxJ1+ EdU+. This suggests that induction of Cre in FoxJ1::CreER;Tomato+/- mouse line label two populations of cells: a larger population of FoxJ1+ EdU- cells which do not proliferate anymore, and a very small population of FoxJ1+ EdU+ progenitor cells which keep on

proliferating at E15.5 (Figure 31A to K). The live-imaging studies of this transgenic mouse has shown us that FoxJ1 is expressed subsequent to the last division of ependymal cells and thus could not be involved in ependymal fate-decision in the RGC progenitors (cf Part I.6). Consequently, we can assess that the largest population of Tomato+FoxJ1+ population which is EdU- labels immature ependymal cells subsequent to the last division of their RGC ancestor. As for the smallest population of Tomtato+ FoxJ1+EdU+ cells, we hypothesize that they label progenitor cells which exhibit the morphology of astrocytes. . Noteworthy, this is in line with previous results showing that FoxJ1 transcription factor is not specific to ependymal cells only, but can also label an astrocytic population[11]. This astrocytic population is distinct form the adult NSCs we have studied because these were FoxJ1- whereas the one we observe here are FoxJ1+.

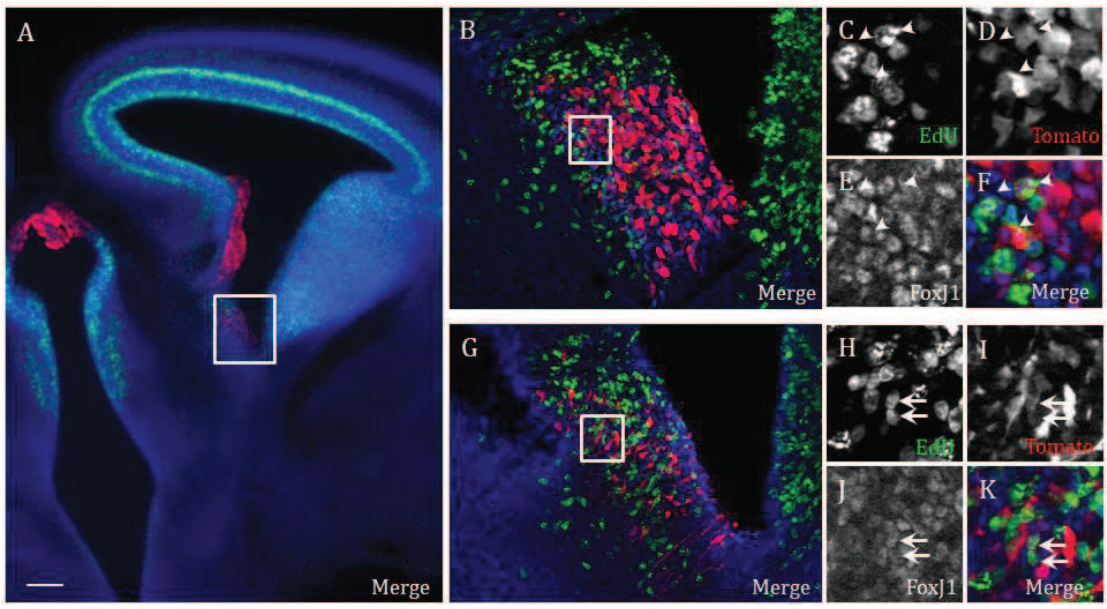

Figure 31: Non-ependymal cells proliferating cells are FoxJ1+. Immunostainings of the LV on coronal slice of E15.5 FoxJ1::CreER;Tomato+/- mouse brain subsequent to EdU intraperitoneal injection and gavage of the pregnant mother with Tamoxifen at E14.5. Scale bar: 200µm. **B-** to **F-** Deeper z position of the region of interest (ROI) at the ventral tip **C-** to **F-** higher magnification. Arrowheads point to EdU+ Tomato+ FoxJ1+ cells. **G-** to **K-** More Superficial z position of the ROI at the ventral tip H- to K- higher magnification. Arrows point to EdU+ Tomato+ FoxJ1+ cells.

Most interestingly, we observe that some neurons and astrocytes are Tomato+ at P16 when Cre recombinase is induced in FoxJ1::CreER;Tomato+/- pups by tamoxifen subcutaneous injection at birth (Figure A to D). Altogether, these preliminary observations also confirm our previously described results showing that ependymal cells and NSC/astrocytes are produced together during brain development. Remarkably, some Tomato+ astrocytic cells are located very far from the LV (Figure 32C-D) which suggest that not only adult astrocytic NSCs are Tomato+ in this transgenic mouse. This further prompts to address whether NSCs are the only astrocytic population produced together with ependymal cells during brain development.

We have also performed immunostaingings of FoxJ1::CreER;Tomato+/- mice at birth after gavage of their pregnant mother with Tamoxifen at E17.5. Our preliminary observations have brought to light a population of cells which seem to migrate out of the choroid plexus (Figure 32E and F). We hypothesize that these cells are in migration because they have the typical morphology of migrating cells: their soma is preceeded by a long cytoplasmic extension, and all cell seem to be oriented in the same direction. The presence of these cells raises numerous questions, and yet we do not know where these cells migrate to and what is their function.

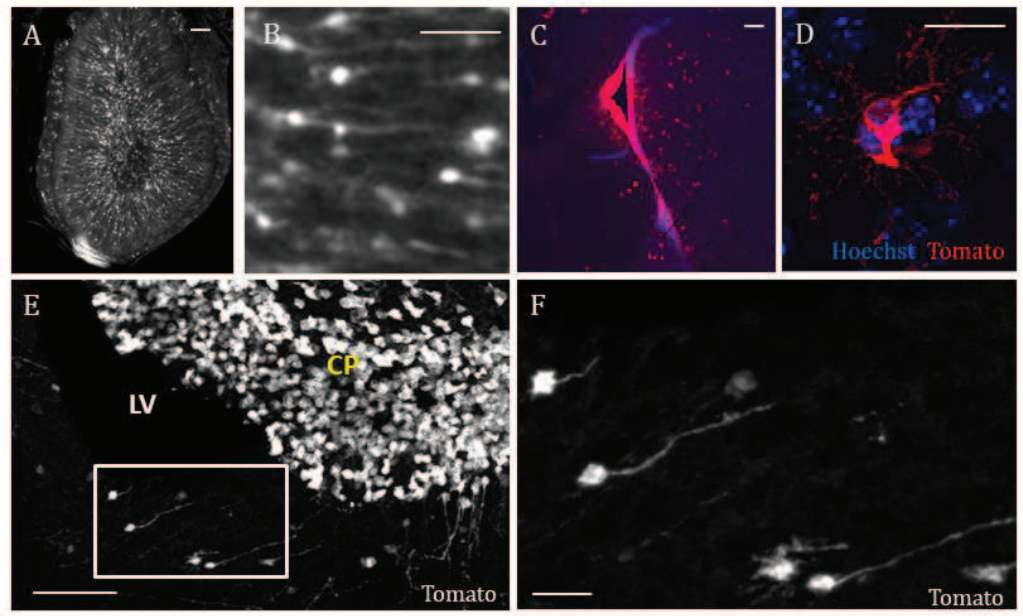

Figure 32: Some Tomato+ cells are also non-ependymal cells. A-to **D-** Immunostainings of the LV on coronal slice at P16 of FoxJ1::CreER;Tomato+/- mouse brain subsequent to gavage of the pregnant mother with Tamoxifen at E19.5. **A-** Tomato+ neurons of the olfactory bulb. Scale bar: 200µm. **B-** Higher magnification of the Tomato+ neurons of the olfactory bulb. Scale bar: 100µm. **C-** Low magnification of the LV. Astrocytes can be spotted near the LV but not only at the wall of the LV. Scale bar: 200µm. **D-** Higher magnification of an astrocyte near the LV. Scale bar: 20µm. **E-F-** Immunostainings of the LV on coronal slice of E19.5 FoxJ1::CreER;Tomato+/- mouse brain subsequent to gavage of the pregnant mother with Tamoxifen at E17.5. **E-** Scale bar: 100µm. **F-** Scale bar: 25µm. LV: Lateral Ventricle. CP: Choroid Plexus.

On the whole, this work sets grounds for future investigations to elucidate all the interrogations emerging from our preliminary observations.

SUPPLEMENTARY METHODS

Gavage intraperitoneal Tamoxifen of FoxJ1::CreER;Tomato+/- mice: from 0.05mg/g to 0.1 mg/g of the pregnant mouse and Progesterone 0.05 mg/g of mouse. Tamoxifen and Progesterone are diluted in corn oil.

Subcutaneous injection of Tamoxifen and Progesterone (same doses, dilution in corn oil, double the volume of dilution).

Antibodies:

Dsred (1:400, Clonetech, cat. no. 632496)
FOP (1:600, Abnova, cat. no. H00011116-MO1)
FoxJ1 (1:500, eBioscience, cat. no. 14-9965-82)

The rest of the material and methods are identical to the part Material and Methods of the Result part.

ABBREVIATIONS

ACD: Asymmetric cell division

CNS: Central nervous system

GPCR: G-protein-coupled receptor

INM: Interkinetic nuclear migration

IP: Intermediate progenitor

MTOC: Microtubule-organising center

NC: Neuroepithelial cell

NSC: Neural stem cell

PCL: Periciliary layer

PCP: Planar cell polarity

RGC: Radial glial cell

RMS: Rostral migratory stream

SCD: Symmetric cell division

V-SVZ: ventricular-subventricular zone

BIBLIOGRAPHY

INTRODUCTION

1. Sanes, D. H., Reh, T. A. & Harris, W. A. Development of the Nervous System: Third Edition. *Dev. Nerv. Syst. Third Ed.* 1–341 (2011).

2. Catala, M. From conception to the child. *Child's Nerv. Syst.* **15,** 613–619 (1999).

3. Nikolopoulou, E., Galea, G. L., Rolo, A., Greene, N. D. E. & Copp, A. J. Neural tube closure: cellular, molecular and biomechanical mechanisms. *Development* **144,** 552–566 (2017).

4. Gammill, L. S. & Bronner-Fraser, M. Neural crest specification: Migrating into genomics. *Nat. Rev. Neurosci.* **4,** 795–805 (2003).

5. Hegarty, S. V., O'Keeffe, G. W. & Sullivan, A. M. BMP-Smad 1/5/8 signalling in the development of the nervous system. *Prog. Neurobiol.* **109,** 28–41 (2013).

6. Lumsden, A. & Keynes, R. Segmental patterns of neuronal development in the chick hindbrain. *Nature* **337,** 424–8 (1989).

7. Krumlauf, R. Hox Genes and the Hindbrain. A Study in Segments. *Curr. Top. Dev. Biol.* **116,** 581–596 (2016).

8. Carpenter, E. M., Goddard, J. M., Chisaka, O., Manley, N. R. & Capecchi, M. R. Loss of Hox-A1 (Hox-1.6) function results in the reorganization of the murine hindbrain. *Development* **118,** 1063–1075 (1993).

9. Cecchi, C., Mallamaci, A. & Boncinelli, E. Otx and Emx homeobox genes in brain development. *J. Poult. Sci.* **44,** 663–668 (2000).

10. Puelles, L., Harrison, M., Paxinos, G. & Watson, C. A developmental ontology for the mammalian brain based on the prosomeric model. *Trends Neurosci.* **36,** 570–578 (2013).

11. Belgacem, Y., Hamilton, A., Shim, S., Spencer, K. & Borodinsky, L. The Many Hats of Sonic Hedgehog Signaling in Nervous System Development and Disease. *J. Dev. Biol.* **4,** 35 (2016).

12. Florio, M. & Huttner, W. B. Neural progenitors, neurogenesis and the evolution of

the neocortex. *Development* **141,** 2182–94 (2014).

13. Sakka, L., Coll, G. & Chazal, J. Anatomy and physiology of cerebrospinal fluid. *Eur. Ann. Otorhinolaryngol. Head Neck Dis.* **128,** 309–316 (2011).

14. Korzh, V. Development of brain ventricular system. *Cell. Mol. Life Sci.* (2017). doi:10.1007/s00018-017-2605-y

15. Timor-Tritsch, I., Monteagudo, A. & Del Rio, M. Normal two-and three-dimensional neurosonography of the prenatal brain. (2012).

16. Azevedo, F. A. C. *et al.* Equal numbers of neuronal and nonneuronal cells make the human brain an isometrically scaled-up primate brain. *J. Comp. Neurol.* **513,** 532–541 (2009).

17. Kriegstein, A. & Alvarez-buylla, A. The Glial Nature of Embryonic and Adult Neural Stem Cells. *Annu. Rev. Neurosci.* 149–184 (2011). doi:10.1146/annurev.neuro.051508.135600.The

18. Huttner, W. B. & Brand, M. Asymmetric division and polarity of neuropithelial cells. *Curr. Opin. Neurobiol.* **7,** 29–39 (1998).

19. Alvarez-Buylla, A., García-Verdugo, J. M. & Tramontin, A. D. A unified hypothesis on the lineage of neural stem cells. *Nat. Rev. Neurosci.* **2,** 287–293 (2001).

20. Sauer, F. C. Mitosis in the neural tube 1934Sauer FC.pdf. 377–405 (1934).

21. Del Bene, F., Wehman, A. M., Link, B. a. & Baier, H. Regulation of Neurogenesis by Interkinetic Nuclear Migration through an Apical-Basal Notch Gradient. *Cell* **134,** 1055–1065 (2008).

22. Kriegstein, A. & Alvarez-buylla, A. The Glial Nature of Embryonic and Adult Neural Stem Cells. *Annu. Rev. Neurosci.* 149–184 (2011). doi:10.1146/annurev.neuro.051508.135600.The

23. Taverna, E. & Huttner, W. B. Neural progenitor nuclei IN motion. *Neuron* **67,** 906–914 (2010).

24. Delling, M., DeCaen, P. G., Doerner, J. F., Febvay, S. & Clapham, D. E. Primary cilia

are specialized calcium signalling organelles. *Nature* **504,** 311–4 (2013).

25. Paridaen, J. T. M. L., Huttner, W. B. & Wilsch-Bräuninger, M. *Analysis of primary cilia in the developing mouse brain*. **127,** (2015).

26. Nachury, M. V. *et al.* A Core Complex of BBS Proteins Cooperates with the GTPase Rab8 to Promote Ciliary Membrane Biogenesis. *Cell* **129,** 1201–1213 (2007).

27. Kim, J. C. *et al.* The Bardet-Biedl protein BBS4 targets cargo to the pericentriolar region and is required for microtubule anchoring and cell cycle progression. *Nat. Genet.* **36,** 462–470 (2004).

28. Goetz, S. C. & Anderson, K. V. The Primary Cilium: A Signaling Center During Vertebrate Development. *Nat. Rev. Genet.* **11,** 331–344 (2010).

29. Huangfu, D. & Anderson, K. V. Cilia and Hedgehog responsiveness in the mouse. *Proc. Natl. Acad. Sci.* **102,** 11325–11330 (2005).

30. Corbit, K. C. *et al.* Vertebrate Smoothened functions at the primary cilium. *Nature* **437,** 1018–1021 (2005).

31. Baudoin, J. P. *et al.* Tangentially Migrating Neurons Assemble a Primary Cilium that Promotes Their Reorientation to the Cortical Plate. *Neuron* **76,** 1108–1122 (2012).

32. Meunier, A. & Azimzadeh, J. Multiciliated cells in animals. *Cold Spring Harb. Perspect. Biol.* **8,** 1–22 (2016).

33. Guemez-Gamboa, A., Coufal, N. G. & Gleeson, J. G. Primary Cilia in the Developing and Mature Brain. *Neuron* **82,** 511–521 (2014).

34. Rakic, P. Specification of Cerebral Cortical Areas. *Science (80-.).* **241,** 170–176 (1988).

35. Noctor, S. C., Flint, A. C., Weissman, T. A., Dammerman, R. S. & Kriegstein, A. R. Neurons derived from radial glial cells establish radial units in neocortex. *Nature* **409,** 714–720 (2001).

36. Bellion, A., Wassef, M. & Métin, C. Early differences in axonal outgrowth, cell

migration and GABAergic differentiation properties between the dorsal and lateral cortex. *Cereb. Cortex* **13,** 203–214 (2003).

37. Greig, L. C., Woodworth, M. B., Galazo, M. J., Padmanabhan, H. & Macklis, J. D. Molecular logic of neocortical projection neuron specification, development and diversity. *Nat. Rev. Neurosci.* **14,** 755–69 (2013).

38. Noctor, S. C., Martinez-Cerdeño, V., Ivic, L. & Kriegstein, A. R. Cortical neurons arise in symmetric and asymmetric division zones and migrate through specific phases. *Nat. Neurosci.* **7,** 136–144 (2004).

39. Kessaris, N. *et al.* Competing waves of oligodendrocytes in the forebrain and postnatal elimination of an embryonic lineage. *Nat. Neurosci.* **9,** 173–179 (2006).

40. Spassky, N. *et al.* Adult ependymal cells are postmitotic and are derived from radial glial cells during embryogenesis. *J. Neurosci.* **25,** 10–18 (2005).

41. Ginhoux, F. *et al.* NIH Public Access. *Science (80-.).* **330,** 841–845 (2010).

42. Menn, B. *et al.* Origin of Oligodendrocytes in the Subventricular Zone of the Adult Brain. *J. Neurosci.* **26,** 7907–7918 (2006).

43. Ge, W. P., Miyawaki, A., Gage, F. H., Jan, Y. N. & Jan, L. Y. Local generation of glia is a major astrocyte source in postnatal cortex. *Nature* **484,** 376–380 (2012).

44. Ge, W. & Jia, J. Review Local Production of Astrocytes in the Cerebral Cortex. 1–7 (2015). doi:10.1016/j.neuroscience.2015.08.057.Local

45. Doetsch, F., Caille, I., Lim, D. A., Garcı, J. M. & Alvarez-buylla, A. Subventricular Zone Astrocytes Are Neural Stem Cells in the Adult Mammalian Brain. *Cell* **97,** 703–716 (1999).

46. Fuentealba, L. C. *et al.* Embryonic Origin of Postnatal Neural Stem Cells. *Cell* **161,** 1644–1655 (2015).

47. Kriegstein, A. R. & Götz, M. Radial glia diversity: A matter of cell fate. *Glia* **43,** 37–43 (2003).

48. Solek, C. M. & Ekker, M. Cell lineage tracing techniques for the study of brain

development and regeneration. *Int. J. Dev. Neurosci.* **30,** 560–569 (2012).

49. Axelrod, D. Carbocyanine dye orientation in red cell membrane studied by microscopic fluorescence polarization. *Biophys. J.* **26,** 557–573 (1979).

50. Serbedzija, G. N., Bronner-Fraser, M. & Fraser, S. E. A vital dye analysis of the timing and pathways of avian trunk neural crest cell migration. *Development* **106,** 809–816 (1989).

51. Saito, T. & Nakatsuji, N. Efficient gene transfer into the embryonic mouse brain using in vivo electroporation. *Dev. Biol.* **240,** 237–246 (2001).

52. Tabata, H. & Nakajima, K. Efficient in utero gene transfer system to the developing mouse brain using elecroporation: visualizatio of neuronal migration in the developing cortex. *Neuroscience* **103,** 8 (2001).

53. Walantus, W., Castaneda, D., Elias, L. & Kriegstein, A. In Utero Intraventricular Injection and Electroporation of E15 Mouse Embryos. *J. Vis. Exp.* 2007 (2007). doi:10.3791/239

54. Boutin, C., Diestel, S., Desoeuvre, A., Tiveron, M. C. & Cremer, H. Efficient in vivo electroporation of the postnatal rodent forebrain. *PLoS One* **3,** 1–6 (2008).

55. Barnabé-Heider, F. *et al.* Genetic manipulation of adult mouse neurogenic niches by in vivo electroporation. *Nat. Methods* **5,** 189–196 (2008).

56. Fernández, M. E., Croce, S., Boutin, C., Cremer, H. & Raineteau, O. Targeted electroporation of defined lateral ventricular walls: a novel and rapid method to study fate specification during postnatal forebrain neurogenesis. *Neural Dev.* **6,** 13 (2011).

57. dal Maschio, M. *et al.* High-performance and site-directed in utero electroporation by a triple-electrode probe. *Nat. Commun.* **3,** 960 (2012).

58. Properties, G. The 2 pm Circle Plasmid of. *Yeast* **4,** (1988).

59. Livet, J. *et al.* Transgenic strategies for combinatorial expression of fluorescent proteins in the nervous system. **450,** (2007).

60. Loulier, K. *et al.* Multiplex Cell and Lineage Tracking with Combinatorial Labels. *Neuron* **81,** 505–520 (2014).

61. Zong, H., Espinosa, J. S., Su, H. H., Muzumdar, M. D. & Luo, L. Mosaic analysis with double markers in mice. *Cell* **121,** 479–492 (2005).

62. Lancaster, M. A. & Knoblich, J. A. Spindle orientation in mammalian cerebral cortical development. *Curr. Opin. Neurobiol.* **22,** 737–746 (2012).

63. Bultje, R. S. *et al.* Neuron. **63,** 189–202 (2009).

64. Peyre, E. & Morin, X. An oblique view on the role of spindle orientation in vertebrate neurogenesis. *Dev. Growth Differ.* **54,** 287–305 (2012).

65. Wang, X. *et al.* Nature. *October* **461,** 947–955 (20009).

66. Yang, G., Sau, C., Lai, W., Cichon, J. & Li, W. HHS Public Access. **344,** 1173–1178 (2015).

67. Gao, P. *et al.* Deterministic progenitor behavior and unitary production of neurons in the neocortex. *Cell* **159,** 775–788 (2014).

68. Franco S. J. Science. **337**, 746-749 (2012).

69. McConnell, S. & Kaznowski, C. Cell cycle dependence of laminar determination in developing neocortex. *Science (80-.).* **254,** 282–285 (1991).

70. Molyneaux, B. J., Arlotta, P., Menezes, J. R. L. & Macklis, J. D. Neuronal subtype specification in the cerebral cortex. *Nat. Rev. Neurosci.* **8,** 427–437 (2007).

71. Rallu, M., Corbin, J. G. & Fishell, G. Parsing the prosencephalon. *Nat. Rev. Neurosci.* **3,** 943–951 (2002).

72. Guo C., et al. Neuron 80(5):1167-74 (2013)

73. Eckler, M. J. *et al.* Cux2-Positive Radial Glial Cells Generate Diverse Subtypes of Neocortical Projection Neurons and Macroglia. *Neuron* **86,** 1100–1108 (2015).

74. Gil-Sanz, C. *et al.* Lineage Tracing Using Cux2-Cre and Cux2-CreERT2 Mice. *Neuron* **86,** 1091–1099 (2015).

75. Altman, J. & Das, G. D. Autoradiographic and histologicalevidence of postnatal hippocampal neurogenesis in rats. *J. Comp. Neurol.* **124,** 319–335 (1965).

76. Kaplan, M. S. & Hinds, J. W. Neurogenesis in the adult rat: electron microscopic analysis of light radioautographs. *Science* **197,** 1092–4 (1977).

77. Kornack, D. R. & Rakic, P. Continuation of neurogenesis in the hippocampus of the adult macaque monkey. *Proc. Natl. Acad. Sci. U. S. A.* **96,** 5768–73 (1999).

78. Kuhn, H. G., Dickinson-Anson, H. & Gage, F. H. Neurogenesis in the dentate gyrus of the adult rat: age-related decrease of neuronal progenitor proliferation. *J Neurosci* **16,** 2027–2033 (1996).

79. Lledo, P. M., Alonso, M. & Grubb, M. S. Adult neurogenesis and functional plasticity in neuronal circuits. *Nat. Rev. Neurosci.* **7,** 179–193 (2006).

80. Lledo, P. M. & Valley, M. Adult olfactory bulb neurogenesis. *Cold Spring Harb. Perspect. Biol.* **8,** (2016).

81. Fuentealba, L. C. *et al.* Embryonic Origin of Postnatal Neural Stem Cells Article Embryonic Origin of Postnatal Neural Stem Cells. 1644–1655 (2015).

82. Garcia, A. D. R., Doan, N. B., Imura, T., Bush, T. G. & Sofroniew, M. V. GFAP-expressing progenitors are the principal source of constitutive neurogenesis in adult mouse forebrain. *Nat. Neurosci.* **7,** 1233–1241 (2004).

83. Song, S. H., Stevens, C. F. & Gage, F. H. Astroglia induce neurogenesis from adult neural stem cells. **417,** 39–44 (2002).

84. Obernier, K. *et al.* Adult Neurogenesis Is Sustained by Symmetric Self-Renewal and Differentiation. *Cell Stem Cell* **22,** 221–234.e8 (2018).

85. Imayoshi, I. *et al.* Roles of continuous neurogenesis in the structural and functional integrity of the adult forebrain. *Nat. Neurosci.* **11,** 1153–1161 (2008).

86. Petreanu, L. & Alvarez-Buylla, A. Maturation and death of adult-born olfactory bulb granule neurons: role of olfaction. *J. Neurosci.* **22,** 6106–6113 (2002).

87. Lois, C. & Alvarez-buylla, A. Long-Distance Neuronal Migration in the Adult

Mammalian Brain Author (s): Carlos Lois and Arturo Alvarez-Buylla Published by : American Association for the Advancement of Science Stable URL : http://www.jstor.org/stable/2885135 Accessed : 26-06-2016 18. *Science (80-.).* **264,** 1145–1148 (1994).

88. Gage, F. H. Linked references are available on JSTOR for this article : Mammalian Neural Stem Cells. **287,** 1433–1438 (2016).

89. Lim, D. A. & Alvarez-buylla, A. Adult neural stem cells stake their ground. **37,** 1–9 (2014).

90. Merkle, F. T. *et al.* Adult neural stem cells in distinct microdomains generate previously unknown interneuron types. *Nat. Neurosci.* **17,** 207–14 (2014).

91. Ventura, R. E. & Goldman, J. E. Dorsal Radial Glia Generate Olfactory Bulb Interneurons in the Postnatal Murine Brain. *J. Neurosci.* **27,** 4297–4302 (2007).

92. Kohwi, M. *et al.* A Subpopulation of Olfactory Bulb GABAergic Interneurons Is Derived from Emx1- and Dlx5/6-Expressing Progenitors. *J. Neurosci.* **27,** 6878–6891 (2007).

93. Vergano-Vera, E. *et al.* Generation of GABAergic and dopaminergic interneurons from endogenous embryonic olfactory bulb precursor cells. *Development* **133,** 4367–4379 (2006).

94. Merkle, F. T., Mirzadeh, Z. & Alvarez-Buylla, A. Mosaic organization of neural stem cells in the adult brain. *Science* **317,** 381–384 (2007).

95. Mirzadeh, Z., Merkle, F. T., Soriano-Navarro, M., Garcia-Verdugo, J. M. & Alvarez-Buylla, A. Neural Stem Cells Confer Unique Pinwheel Architecture to the Ventricular Surface in Neurogenic Regions of the Adult Brain. *Cell Stem Cell* **3,** 265–278 (2008).

96. Ihrie, R. a & Álvarez-Buylla, A. NIH Public Access. **70,** 674–686 (2011).

97. Silva-Vargas, V., Maldonado-Soto, A. R., Mizrak, D., Codega, P. & Doetsch, F. Age-Dependent Niche Signals from the Choroid Plexus Regulate Adult Neural Stem Cells. *Cell Stem Cell* **19,** 643–652 (2016).

98. Sawamoto, K. *et al.* New Neurons Follow theFlow of Cerebrospinal Fluidin the Adult Brain. **629,** 1–4 (2006).

99. Lim, D. A. *et al.* Noggin antagonizes BMP signaling to create a niche for adult neurogenesis. *Neuron* **28,** 713–726 (2000).

100. Shen, Q. *et al.* F1000Prime recommendations of: Endothelial cells stimulate self-renewal and expand neurogenesis of neural stem cells. *Sci. (New York)* **304,** 1338–1340 (2004).

101. Harrison, J. F. *et al.* Altering DNA base excision repair: use of nuclear and mitochondrial-targeted N-methylpurine DNA glycosylase to sensitize astroglia to chemotherapeutic agents. *Glia* **55,** 1416–1425 (2007).

102. Azim, K. *et al.* Persistent wnt/??-catenin signaling determines dorsalization of the postnatal subventricular zone and neural stem cell specification into oligodendrocytes and glutamatergic neurons. *Stem Cells* **32,** 1301–1312 (2014).

103. Yoshikawa, K. Cell cycle regulators in neural stem cells and postmitotic neurons. *Neurosci.Res.* **37,** 1–14 (2000).

104. Conover, J. C. *et al.* Disruption of Eph / ephrin signaling affects migration and proliferation in the adult subventricular zone. *Nat. Neurosci* **3,** 1091–1097 (2000).

105. Caille, I. Soluble form of amyloid precursor protein regulates proliferation of progenitors in the adult subventricular zone. *Development* **131,** 2173–2181 (2004).

106. Belvindrah, R., Rougon, G. & Chazal, G. Increased neurogenesis in adult mCD24-deficient mice. *J Neurosci* **22,** 3594–3607 (2002).

107. Kohwi, M. Pax6 Is Required for Making Specific Subpopulations of Granule and Periglomerular Neurons in the Olfactory Bulb. *J. Neurosci.* **25,** 6997–7003 (2005).

108. Colak, D. *et al.* Adult Neurogenesis Requires Smad4-Mediated Bone Morphogenic Protein Signaling in Stem Cells. *J. Neurosci.* **28,** 434–446 (2008).

109. Hack, M. A. *et al.* Neuronal fate determinants of adult olfactory bulb neurogenesis. *Nat. Neurosci.* **8,** 865–872 (2005).

110. Parras, C. M. *et al.* Mash1 specifies neurons and oligodendrocytes in the postnatal brain. *EMBO J.* **23,** 4495–4505 (2004).

111. Ramírez-Castillejo, C. *et al.* Pigment epithelium-derived factor is a niche signal for neural stem cell renewal. *Nat. Neurosci.* **9,** 331–339 (2006).

112. Jackson, E. L. *et al.* PDGFRα-Positive B Cells Are Neural Stem Cells in the Adult SVZ that Form Glioma-like Growths in Response to Increased PDGF Signaling. *Neuron* **51,** 187–199 (2006).

113. Young, K. M., Merson, T. D., Sotthibundhu, A., Coulson, E. J. & Bartlett, P. F. p75 Neurotrophin Receptor Expression Defines a Population of BDNF-Responsive Neurogenic Precursor Cells. *J. Neurosci.* **27,** 5146–5155 (2007).

114. Balordi, F. & Fishell, G. Hedgehog Signaling in the Subventricular Zone Is Required for Both the Maintenance of Stem Cells and the Migration of Newborn Neurons. *J. Neurosci.* **27,** 5936–5947 (2007).

115. Sakaguchi, M. *et al.* A carbohydrate-binding protein, Galectin-1, promotes proliferation of adult neural stem cells. *Proc. Natl. Acad. Sci.* **103,** 7112–7117 (2006).

116. Wurmser, A. E. *et al.* Cell fusion-independent differentiation of neural stem cells to the endothelial lineage. *Nature* **430,** 350–356 (2004).

117. Chen, S. *et al.* Interrogating cellular fate decisions with high-throughput arrays of multiplexed cellular communities. *Nat. Commun.* **7,** 1–8 (2016).

118. Brooks, E. R. & Wallingford, J. B. Multiciliated Cells. *Curr. Biol.* **24,** R973–R982 (2014).

119. Fliegauf, M., Benzing, T. & Omran, H. When cilia go bad: Cilia defects and ciliopathies. *Nat. Rev. Mol. Cell Biol.* **8,** 880–893 (2007).

120. Rock, J. R. & Hogan, B. L. M. Epithelial Progenitor Cells in Lung Development, Maintenance, Repair, and Disease. *Annu. Rev. Cell Dev. Biol.* **27,** 493–512 (2011).

121. Stannard, W. & O'Callaghan, C. Ciliary function and the role of cilia in clearance. *J. aerosol Med.* **19,** 110–115 (2006).

122. Spassky, N. & Meunier, A. The development and functions of multiciliated epithelia. *Nat. Rev. Mol. Cell Biol.* **18,** 423–436 (2017).

123. Wang, Y. A., Yu, X., Silverman, P. M., Harris, R. L. & Edward, H. NIH Public Access. **385,** 22–29 (2010).

124. Egg Transport in the Rabbit Oviduct : The Roles of Cilia and Muscle Author (s): S . A . Halbert , P . Y . Tam and R . J . Blandau Published by : American Association for the Advancement of Science Stable URL : http://www.jstor.org/stable/1741428 digitiz. **191,** 1052–1053 (2018).

125. Lyons, R. A. *et al.* Fallopian tube ciliary beat frequency in relation to the stage of menstrual cycle and anatomical site. *Hum. Reprod.* **17,** 584–588 (2002).

126. Crow, J., Amso, N. N., Lewin, J. & Shaw, R. W. Morphology and infrastructure of Fallopian tube epithelium at different stages of the menstrual cycle and menopause. **9,** 2224–2233 (1994).

127. Norwood, T. & Anderson, G. W. on the Tips for Ovum of Oviduct in situ ' Pickup of Texas charges membranes Sodium. **791,** 788–791 (1980).

128. Holt, W. V. & Fazeli, A. Sperm Storage in the Female Reproductive Tract. *Annu. Rev. Anim. Biosci.* **4,** 291–310 (2016).

129. Sullivan, R. & Mieusset, R. The human epididymis: Its function in sperm maturation. *Hum. Reprod. Update* **22,** 574–587 (2016).

130. WINET, H. On the Mechanism for Flow in the Efferent Ducts. *J. Androl.* **1,** 304–311 (1980).

131. Del Bigio, M. R. The ependyma: A protective barrier between brain and cerebrospinal fluid. *Glia* **14,** 1–13 (1995).

132. Hirota, Y. *et al.* Planar polarity of multiciliated ependymal cells involves the anterior migration of basal bodies regulated by non-muscle myosin II. *Development* **137,** 3037–3046 (2010).

133. Meletis, K. *et al.* Spinal cord injury reveals multilineage differentiation of ependymal cells. *PLoS Biol.* **6,** 1494–1507 (2008).

134. Ren, Y. *et al.* Ependymal cell contribution to scar formation after spinal cord injury is minimal, local and dependent on direct ependymal injury. *Sci. Rep.* **7,** 1–16 (2017).

135. Satir, P. CILIA: Before and after. *Cilia* **6,** 1–11 (2017).

136. Higginbotham, H., Bielas, S., Tanaka, T. & Gleeson, J. G. Transgenic mouse line with green-fluorescent protein-labeled Centrin 2 allows visualization of the centrosome in living cells. *Transgenic Res.* **13,** 155–164 (2004).

137. Hart, P. E. *et al.* Characterization of the X-linked murine centrin Cetn2 gene. *Gene* **264,** 205–213 (2001).

138. Errabolu, R., Sanders, M. a & Salisbury, J. L. Cloning of a cDNA encoding human centrin, an EF-hand protein of centrosomes and mitotic spindle poles. *J. Cell Sci.* **107 (Pt 1,** 9–16 (1994).

139. Azimzadeh, J. *et al.* hPOC5 is a centrin-binding protein required for assembly of full-length centrioles. *J. Cell Biol.* **185,** 101–114 (2009).

140. Graser, S. *et al.* Cep164, a novel centriole appendage protein required for primary cilium formation. *J. Cell Biol.* **179,** 321–330 (2007).

141. Tsukita, S. *et al.* Coordinated ciliary beating requires Odf2-mediated polarization of basal bodies via basal feet. *Cell* **148,** 189–200 (2012).

142. Herawati, E. *et al.* Multiciliated cell basal bodies align in stereotypical patterns coordinated by the apical cytoskeleton. *J. Cell Biol.* **214,** 571–586 (2016).

143. Clare, D. K. *et al.* Basal foot MTOC organizes pillar MTs required for coordination of beating cilia. *Nat. Commun.* **5,** 4888 (2014).

144. Werner, M. E. *et al.* Actin and microtubules drive differential aspects of planar cell polarity in multiciliated cells. *J. Cell Biol.* **195,** 19–26 (2011).

145. Ruat, M., Roudaut, H., Ferent, J. & Traiffort, E. Hedgehog trafficking, cilia and brain functions. *Differentiation* **83,** S97–S104 (2012).

146. Mirzadeh, Z., Han, Y., Soriano-navarro, M., García-, J. M. & Alvarez-buylla, A. NIH

Public Access. **30,** 2600–2610 (2010).

147. Dawe, H. R., Farr, H. & Gull, K. Centriole/basal body morphogenesis and migration during ciliogenesis in animal cells. *J. Cell Sci.* **120,** 7–15 (2006).

148. Marcet, B. *et al.* Control of vertebrate multiciliogenesis by miR-449 through direct repression of the Delta/Notch pathway. *Nat. Cell Biol.* **13,** 693–701 (2011).

149. Bray, S. J. Notch signalling: A simple pathway becomes complex. *Nat. Rev. Mol. Cell Biol.* **7,** 678–689 (2006).

150. Kessler, M. *et al.* The Notch and Wnt pathways regulate stemness and differentiation in human fallopian tube organoids. *Nat. Commun.* **6,** 1–11 (2015).

151. Chevalier, B. *et al.* MiR-34/449 control apical actin network formation during multiciliogenesis through small GTPase pathways. *Nat. Commun.* **6,** (2015).

152. Ben-Shushan, E., Feldman, E. & Reubinoff, B. E. Notch signaling regulates motor neuron differentiation of human embryonic stem cells. *Stem Cells* **33,** 403–15 (2015).

153. Arbi, M. *et al.* GemC1 controls multiciliogenesis in the airway epithelium. *EMBO Rep.* **17,** 400–413 (2016).

154. Terré, B. *et al.* GEMC1 is a critical regulator of multiciliated cell differentiation. *EMBO J.* **35,** 942–60 (2016).

155. Pefani, D. E. *et al.* Idas, a novel phylogenetically conserved geminin-related protein, binds to geminin and is required for cell cycle progression. *J. Biol. Chem.* **286,** 23234–23246 (2011).

156. Ma, L., Quigley, I., Omran, H. & Kintner, C. Multicilin drives centriole biogenesis via E2f proteins. *Genes Dev.* **28,** 1461–1471 (2014).

157. He, Q., Johnston, J., Zeitlinger, J., City, K. & City, K. HHS Public Access. *Clin Psychol Rev.* **33,** 395–401 (2015).

158. Tan, F. E. *et al.* Myb promotes centriole amplification and later steps of the multiciliogenesis program. *Development* **140,** 4277–86 (2013).

159. Kyrousi, C. *et al.* Mcidas and GemC1/Lynkeas are key regulators for the generation of multiciliated ependymal cells in the adult neurogenic niche. *Development* dev.126342 (2015). doi:10.1242/dev.126342

160. Jacquet, B. V *et al.* Specification of a Foxj1-dependent lineage in the forebrain is required for embryonic-to-postnatal transition of neurogenesis in the olfactory bulb. *J. Neurosci.* **31,** 9368–9382 (2011).

161. Yu, X., Ng, C. P., Habacher, H. & Roy, S. Foxj1 transcription factors are master regulators of the motile ciliogenic program. *Nat. Genet.* **40,** 1445–1453 (2008).

162. Weidemann, M. *et al.* CFAP157 is a murine downstream effector of FOXJ1 that is specifically required for flagellum morphogenesis and sperm motility. *Development* **143,** 4736–4748 (2016).

163. You, Y. *et al.* Role of f-box factor foxj1 in differentiation of ciliated airway epithelial cells. *Am. J. Physiol. Lung Cell. Mol. Physiol.* **286,** L650–L657 (2004).

164. Pan, J., You, Y., Huang, T. & Brody, S. L. RhoA-mediated apical actin enrichment is required for ciliogenesis and promoted by Foxj1. *J. Cell Sci.* **120,** 1868–1876 (2007).

165. Stubbs, J., Oishi, I., Kintner, C. & Diego, S. HHS Public Access. **40,** 1454–1460 (2015).

166. Balestrini, A., Cosentino, C., Errico, A. & Garner, E. GEMC1 is a TopBP1 interacting protein required for chromosomal DNA replication. *Nat. Cell Biol.* **12,** 484–491 (2010).

167. Kyrousi, C., Lalioti, M.-E., Skavatsou, E., Lygerou, Z. & Taraviras, S. Mcidas and GemC1/Lynkeas specify embryonic radial glial cells. *Neurogenesis* **3,** e1172747 (2016).

168. Kyrousi, C., Lygerou, Z. & Taraviras, S. How a Radial Glial Cell Decides to Become a Multiciliated Ependymal Cell. 1–11 (2017). doi:10.1002/glia.23118

169. Wallmeier, J. *et al.* Mutations in CCNO result in congenital mucociliary clearance disorder with reduced generation of multiple motile cilia. *Nat. Genet.* **46,** 646–651

(2014).

170. Zhou, F. *et al.* Gmnc Is a Master Regulator of the Multiciliated Cell Differentiation Program. *Curr. Biol.* **25,** 3267–3273 (2015).

171. Al Jord, A. *et al.* Centriole amplification by mother and daughter centrioles differs in multiciliated cells. (2014). doi:10.1038/nature13770

172. Boutin, C. *et al.* A dual role for planar cell polarity genes in ciliated cells. *Proc. Natl. Acad. Sci. U. S. A.* 1–10 (2014). doi:10.1073/pnas.1404988111

173. Tissir, F. *et al.* Lack of cadherins Celsr2 and Celsr3 impairs ependymal ciliogenesis, leading to fatal hydrocephalus. *Nat. Neurosci.* **13,** 700–707 (2010).

174. Guirao, B. *et al.* Coupling between hydrodynamic forces and planar cell polarity orients mammalian motile cilia. *Nat. Cell Biol.* **12,** 341–350 (2010).

175. Wallingford, J. B. NIH Public Access. **22,** 597–604 (2011).

CONCLUSIVE REMARKS AND DISCUSSION

1 Mirzadeh, Z., Merkle, F. T., Soriano-Navarro, M., Garcia-Verdugo, J. M. & Alvarez-Buylla, A. Neural Stem Cells Confer Unique Pinwheel Architecture to the Ventricular Surface in Neurogenic Regions of the Adult Brain. *Cell Stem Cell* **3,** 265–278 (2008).

2. Gao, P. *et al.* Article Deterministic Progenitor Behavior and Unitary Production of Neurons in the Neocortex. *Cell* **159,** 775–788 (2014).

3. Kyrousi, C. *et al.* Mcidas and GemC1/Lynkeas are key regulators for the generation of multiciliated ependymal cells in the adult neurogenic niche. *Development* dev.126342 (2015). doi:10.1242/dev.126342

4. Loulier, K. *et al.* Multiplex Cell and Lineage Tracking with Combinatorial Labels. *Neuron* **81,** 505–520 (2014).

5. Haas, K., Sin, W., Javaherian, A., Li, Z. & Cline, H. T. for Gene Transfer In Vivo. **29,** 583–591 (2001).

6. Al Jord. *et al.* Centriole amplification by mother and daughter centrioles differs in multiciliated cells. (2014). doi:10.1038/nature13770

7. Sawamoto, K. *et al.* New Neurons Follow theFlow of Cerebrospinal Fluidin the Adult Brain. **629,** 1–4 (2006).

8. Livet, J. *et al.* Transgenic strategies for combinatorial expression of fluorescent proteins in the nervous system. **450,** (2007).

9. Muthusamy, N., Vijayakumar, A., Cheng, G. & Ghashghaei, H. T. A Knock-in Foxj1CreERT2:: GFP mouse for recombination in epithelial cells with motile cilia. *Genesis* **52,** 350–358 (2014).

10. Belvindrah, R., Nissant, A. & Lledo, P.-M. Abnormal Neuronal Migration Changes the Fate of Developing Neurons in the Postnatal Olfactory Bulb. *J. Neurosci.* **31,** 7551–7562 (2011).

11. Jacquet, B. V. *et al.* FoxJ1-dependent gene expression is required for differentiation of radial glia into ependymal cells and a subset of astrocytes in the postnatal brain. *Development* **136,** 4021–31 (2009).

APPENDIX

© 2017. Published by The Company of Biologists Ltd | Development (2017) 144, 201-210 doi:10.1242/dev.138271

STEM CELLS AND REGENERATION

RESEARCH ARTICLE

mTORC1 signaling and primary cilia are required for brain ventricle morphogenesis

Philippe Foerster[1], Marie Daclin[1], Shihavuddin Asm[1], Marion Faucourt[1], Alessandra Boletta[2], Auguste Genovesio[1] and Nathalie Spassky[1,*]

ABSTRACT

Radial glial cells (RCGs) are self-renewing progenitor cells that give rise to neurons and glia during embryonic development. Throughout neurogenesis, these cells contact the cerebral ventricles and bear a primary cilium. Although the role of the primary cilium in embryonic patterning has been studied, its role in brain ventricular morphogenesis is poorly characterized. Using conditional mutants, we show that the primary cilia of radial glia determine the size of the surface of their ventricular apical domain through regulation of the mTORC1 pathway. In cilium-less mutants, the orientation of the mitotic spindle in radial glia is also significantly perturbed and associated with an increased number of basal progenitors. The enlarged apical domain of RGCs leads to dilatation of the brain ventricles during late embryonic stages (ventriculomegaly), which initiates hydrocephalus during postnatal stages. These phenotypes can all be significantly rescued by treatment with the mTORC1 inhibitor rapamycin. These results suggest that primary cilia regulate ventricle morphogenesis by acting as a brake on the mTORC1 pathway. This opens new avenues for the diagnosis and treatment of hydrocephalus.

KEY WORDS: Cilia, Ventricular system, mTORC1 pathway, Hydrocephalus

INTRODUCTION

The vertebrate brain forms around a ventricular cavity filled with cerebrospinal fluid (CSF) that undergoes dynamic morphological changes during development. The neural tube wall constitutes a pseudostratified epithelium composed of elongated progenitor cells called radial glial cells (RGCs) that progressively generate, directly or indirectly, all neurons and glial cells. The brain ventricular system plays crucial roles in brain development, function and homeostasis, and leads to severe neurological disorders when defective (Lehtinen and Walsh, 2011; Lowery and Sive, 2009). Deciphering the mechanisms that regulate brain ventricle morphogenesis is thus essential to understand neocortical histogenesis and identify new therapeutic targets for these common pathologies.

[1]Ecole Normale Supérieure, Institut de Biologie de l'ENS (IBENS), INSERM U1024, and CNRS UMR 8197, PSL Research University, 46 rue d'Ulm, Paris 75005, France. [2]Division of Genetics and Cell Biology, San Raffaele Scientific Institute, Milan 20132, Italy.

*Author for correspondence (nathalie.spassky@ens.fr)

N.S., 0000-0003-4722-6464

Received 7 April 2016; Accepted 5 December 2016

The cerebral cortex originates from the dorsal telencephalon and is composed of six layers, each containing different classes of neurons. Cortical neurons and glia are formed through asymmetric divisions of RGCs, which are bipolar cells that traverse the width of the epithelium, with a basal domain at the pial surface and a ciliated apical contact at the ventricular surface. The primary cilium is a microtubule-based membrane protrusion, the axoneme of which is nucleated by the basal body, a modified mother centriole. Its dynamics are intimately linked to the progression of the cell cycle; it grows during the G1 phase and is resorbed just before mitosis (Nigg and Stearns, 2011). The primary cilium is an important signaling organelle at all developmental stages and has been shown to be crucial for morphogenetic processes such as brain patterning and tissue homeostasis (Eggenschwiler and Anderson, 2007; Willaredt et al., 2008). The primary cilium is chemosensitive and detects a variety of signaling molecules that are important for development (e.g. Shh, Wnt, Pdgf) (Guemez-Gamboa et al., 2014). In the kidney, it also acts as a mechanosensor that detects shear stress, leading to the downregulation of the mTOR pathway necessary for the proper control of cell size (Boehlke et al., 2010; Orhon et al., 2016). The cerebrospinal fluid secreted by the choroid plexus provides diffusible signals that are essential for the early development of RGC (Lehtinen et al., 2011; Chau et al., 2015; Higginbotham et al., 2013). The apical localization of the primary cilium is thus optimal for detecting chemo- or mechano-sensory signals from the CSF, and thus participates in brain morphogenesis by regulating RGC physiology (Lehtinen and Walsh, 2011).

Ciliopathies are a group of genetic diseases characterized by impaired ciliary function. Common brain pathologies encountered in ciliopathy patients are neurocognitive impairments, epilepsy and hydrocephalus. Hydrocephalus is a complex multifactorial brain disorder leading to reduced cortical thickness and enlarged ventricular cavities due to the accumulation of CSF in the ventricles at postnatal stages. It is one of the most common birth defects (Zhang et al., 2006) and has been correlated with a wide range of neurodevelopmental disorders, including schizophrenia (Shenton et al., 2001). Abnormal brain ventricle enlargement often develops at early postnatal stages as a result of defects in ependymal cilia (Ibanez-Tallon et al., 2003) or the choroid plexus (Banizs et al., 2005; Del Bigio, 2010). It was also shown that postnatal hydrocephalus could result from increased apoptosis and impaired proliferation of cilium-less $NG2^+$ and PDGFR-α^+ neural progenitors (Carter et al., 2012). In this study, ventriculomegaly and hydrocephalus are defined as brain ventricular enlargement at embryonic or postnatal stages, respectively. To date, the mechanisms leading to prenatal ventriculomegaly have remained obscure.

Using conditional mouse mutants, we show that depletion of the primary cilia of RGCs from E10.5 onwards results in progressive enlargement of the lateral ventricles (ventriculomegaly) without

Development (2017) 144, 201-210 doi:10.1242/dev.138271

affecting brain patterning. This phenotype is associated with progressive enlargement of the surface area of RGC apical endfeet induced by abnormal upregulation of the mTORC1 pathway. In addition, we show that cilia depletion leads to misorientation of the RGC mitotic spindle, which is associated with an increased number of basal progenitors in the somatosensory cortex. The size of the apical endfeet, the increased number of basal progenitors and the ventricular enlargement are all rescued by rapamycin treatment. These results suggest that the mTORC1 pathway controlled by the primary cilium regulates ventricle morphogenesis and corticogenesis, and thus constitutes a new potential therapeutic target for the treatment of hydrocephalus.

RESULTS

Ventricular morphogenesis defects in ciliary mutants

During mouse brain development, neuroepithelial (NEP) cells and RGCs extend a primary cilium into the ventricles (Higginbotham et al., 2013; Fig. S1A). The dynamics are tightly correlated with the cell cycle and interkinetic nuclear migration (Kim et al., 2011; Paridaen et al., 2013). To study the role of the primary cilium in forebrain development, we generated conditional ciliary knockouts of floxed *Ift88* or *Kif3a* genes (Haycraft et al., 2007; Marszalek et al., 1999) to ablate cilia from the apical surfaces of either NEP cells (using FoxG1-Cre mice: *FoxG1-K3A*^{cKO}) or RGCs (using Nestin-Cre mice: *Nestin-K3A*^{cKO} or *Nestin-Ift88*^{cKO}, Fig. S1B-E). In *FoxG1-K3A*^{cKO} mice, cilia depletion in NEP cells leads to patterning defects and altered GLI3 processing, as previously reported (Benadiba et al., 2012; Besse et al., 2011; Higginbotham et al., 2013; Willaredt et al., 2008; Laclef et al., 2015; Fig. S1F-H). In contrast, no polarity or patterning defects were observed in Nestin-Cre conditional ciliary mutants (*Nestin-K3A*^{cKO} or *Nestin-Ift88*^{cKO}), in which Cre was expressed in the forebrain from embryonic day (E)11 onwards and recombination leads to complete cilia ablation from E14.5 (Fig. S1B-E). Indeed, both the expression patterns of Ngn2 (Neurog2; a marker of the dorsal telencephalon) and Dbx1 (a marker of the pallium-subpallium boundary), and Gli3 processing were unaltered in Nestin conditional knockout (cKO) mutant forebrains at E12.5 (Fig. S1F-H). Furthermore, the apical positions of the centrosomes (Fig. S1C and Fig. S3A,B) and thus the polarity of RGCs were normal. As previously described (Tong et al., 2014), we observed that *Nestin-K3A*^{cKO} conditional ciliary mutants show severe hydrocephalus at postnatal stages (Fig. 1). However, we noticed that at earlier stages (from E18.5 onwards), *Nestin-K3A*^{cKO} mice displayed a progressive enlargement of the lateral ventricles (Fig. 1A,B), and reduced cortical thickness (Fig. 1A,C) associated with a moderate but significant decrease in the number of post-mitotic neurons labeled with a Ctip2 antibody (a marker of early-born neurons) (Fig. 1D,E). Similar phenotypes were observed in *Nestin-Ift88*^{cKO} mice (data not shown). The enlarged ventricles and the reduced brain tissue observed in the ciliary mutants before motile cilia develop both suggest that ablation of primary cilia at E11 leads to the development of prenatal ventriculomegaly, which might initiate postnatal hydrocephalus.

Primary cilia abrogation in RGCs leads to apical domain enlargement

Primary cilia extend from the apical surface of RGCs in the brain ventricles. To further identify the cellular mechanisms leading to ventricular enlargement, we analyzed the apical domains of RGCs on whole-mount somatosensory cortical ventricular walls in *Nestin-K3A*^{cKO} ciliary mutant and control embryos (Fig. 2A) stained with an antibody against ZO-1 (Tjp1) that labels the tight junctions and delimits individual RGC apical domains (Fig. S2A,B,D). The size of the apical domains was quantified and color-coded with Packing Analyzer (Aigouy et al., 2010) and CellProfiler (Lamprecht et al., 2007) software (Fig. 2B-F). In control embryos, the mean size of the apical domains increased from E12.5 to E16.5; they were more heterogeneous at E16.5 than they were at E14.5 (Fig. 2C-F). Thus, the size of the RGC apical domain increases progressively during normal development, as previously shown (Nishizawa et al., 2007). Interestingly, the increase was significantly greater in ciliary mutants than in controls at all stages analyzed, and the difference increased with age: the relative difference in size between ciliary mutant and controls was 7% at E12.5, 35% at E14.5 and 39% at E16.5 (Fig. 2C-F). Similar results were obtained in *Nestin-Ift88*^{cKO} embryos compared with controls (Fig. S2B-C). Finally, as *Nestin* is also expressed in the lateral ganglionic eminence (LGE), we confirmed that apical domain enlargement was also present in *Nestin-K3A*^{cKO} lateral ganglionic eminence at E14.5 (Fig. S2D,E). These results suggest that cilia abrogation leads to a progressive increase in the size of RGC apical domains during forebrain development.

Apical domain enlargement during mitosis is greater in ciliary mutants than in controls

RGCs are highly polarized cells in which nuclear interkinetic migration takes place in the ventricular zone (VZ). Their nucleus is larger than the surface of their apical domain, suggesting that the size of the apical domain reflects the distance of the cell body from the ventricle and, thus, the phase of the cell cycle. To examine this possibility and determine whether the increase in the size of the apical domain in cilia mutants is correlated with a given phase of the cell cycle, whole-mount cortical ventricular walls from ciliary mutants and controls were triple-labeled with antibodies against ZO-1, 4A4 (phospho-vimentin; cytoplasmic mitotic marker) and γ-tubulin (Tubg1; marker of the pericentriolar material). Apical domains in three categories of cells were examined: interphase cells (γ-tubulin^{+}/4A4^{-}), mitotic cells (γ-tubulin^{-}/4A4^{+}) and other cells (γ-tubulin^{-}/4A4^{-}) (Fig. S3A,B, Fig. 3A-D). The size of the apical domains is significantly smaller during the interphase than during mitosis both in controls and *Nestin-K3A*^{cKO} mutants, suggesting that its size is precisely controlled as the cell cycle advances. The percentage of mitotic cells was similar in controls and mutants (Fig. 3A,B), in accordance with the observation that the number of mitotic cells in the ventricular zone was unaffected in cilium-less RGCs (see below, Fig. 3G-I). However, the size of the apical domains in both interphase and mitotic cells was greater in mutants than in controls, suggesting that cilia abrogation leads to a similar enlargement of both interphase and mitotic apical domains (Fig. S3A,B, Fig. 3C,D).

Apical endfoot enlargement in ciliary mutants is associated with spindle orientation defects

Cell shape and mechanical cues have been shown to guide division orientation in epithelia (Wyatt et al., 2015) and mitotic spindle orientation contributes to cell fate determination (Paridaen and Huttner, 2014). We therefore tested whether RGC apical domain enlargement in ciliary mutants could perturb mitotic spindle orientation. We measured anaphase spindle orientation in controls and *Nestin-K3A*^{cKO} mutants. Subtle defects in spindle orientation were observed: the median at E12.5 was 6.2° in controls but 8.7° in mutants (Fig. S3C). This defect worsened at E14.5: the median was 6.9° in controls and 10.2° in mutants (Fig. 3E,F). To test whether these defects affected other cells in the cortex, E14.5 coronal

Development (2017) 144, 201-210 doi:10.1242/dev.138271

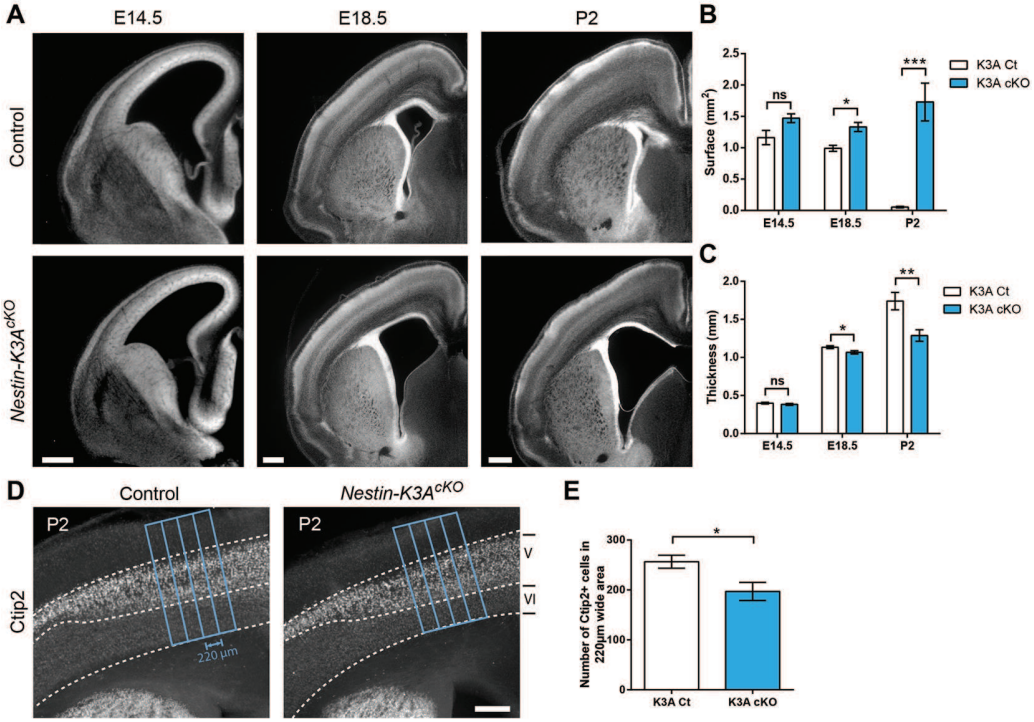

Fig. 1. Ventricular enlargement in ciliary mutants. (A) Representative coronal sections of control and *Nestin-K3A*^{cKO} mutant forebrains at E14.5, E18.5 and P2. (B,C) Concomitant increases in the area of the lateral ventricle and decreases in cortical thickness at each embryonic and postnatal stage show the progression of embryonic ventriculomegaly and postnatal hydrocephalus in the ciliary mutant (*n*=4). (D) Representative Ctip2 immunostaining on coronal sections of control and ciliary mutant forebrains at P2. The boundaries between cortical layers V and VI are indicated by dashed lines. Blue boxes show the area quantified in E. (E) Quantification of the number of Ctip2^{+} cells in the 220-µm-wide area outlined in D (*n*=6). Scale bars: 0.5 mm (A,D). ns, not significant.

sections were immunostained with antibodies against PH3 (Phc3; mitotic cells), Tbr2 (Eomes; basal progenitors, BPs) and Ctip2 (Bcl11b; early born neurons). Although the abundance of mitotic or Pax6^{+} (RGC) cells was similar in the VZ of controls and *Nestin-K3A*^{cKO} and *Nestin-Ift88*^{cKO} mutants (Fig. 3G-I, Fig. S3D-F), the number of mitotic cells increased 2-fold in the subventricular zone (SVZ) of the ciliary mutants compared with controls and was associated with a significant increase in the number of basal progenitors (Fig. 3G-K). These results suggest that cilia abrogation leads to apical domain enlargement, impaired mitotic spindle orientation, increased cell proliferation and the generation of supernumerary progenitors in the SVZ at E14.5.

Other non-ciliary effects of Kif3a or Ift88 knockout have been reported to affect microtubule dynamics, leading to spindle misorientation (Delaval et al., 2011; Kodani et al., 2013; Teng et al., 2005); ninein (Nin)$^{+}$ sub-distal appendages were absent from Kif3a embryonic knockout mouse fibroblasts (Kodani et al., 2013) and removal of ninein from the developing neocortex caused premature depletion of progenitors from the VZ (Wang et al., 2009) and enlargement of the endfoot area of apical progenitors (Shinohara et al., 2013). Here, no defects in subdistal appendages or ninein localization at the centrosome were detected in cilium-less RGCs at E14.5 (Fig. S4A,B). Similarly, no defects in polarity were observed in cortical ventricular walls labeled with adherens junction markers on *en face* views of the RGCs lacking a primary cilium, suggesting that cilia abrogation did not affect markers of apico-basal cell polarity (Fig. S4C). Thus, cilia abrogation in these ciliary mutants does not lead to the loss of sub-distal appendages. Mitotic spindle misorientation observed in *Nestin-K3A*^{cKO} ciliary mutant is probably due to increased cell size rather than impaired attachment of microtubules to the centrosome. These results, together with the similar phenotype observed in two different ciliary mutants (Kif3a and Ift88), suggest that mitotic spindle misorientation might be directly linked to cilia abrogation.

The number of Ctip2^{+} neurons at E14.5 was similar in controls and ciliary mutants (Fig. S3D-F) but it was decreased at postnatal day (P)2 (Fig. 1D,E). Interestingly, no defects in cell survival could be observed at either age in controls and *Nestin-K3A*^{cKO} mutant mice, suggesting that the decrease in Ctip2^{+} cells at P2 was not due to increased cell death. Indeed, the numbers of activated caspase-3^{+} cells (data not shown) and TUNEL^{+} cells were similar in *Nestin-K3A*^{cKO} neonatal mice (7±2 TUNEL^{+} cells per section) and controls (6±1 TUNEL^{+} cells per section). These results thus confirm previous findings that cilia abrogation in *Nestin-K3A*^{cKO} mice does not lead to increased cell death (Tong et al., 2014). To test whether thinning of the cortex could be due to tissue stretch, we quantified cell density on tissue sections at P2. However, no significant differences were observed (Fig. S4E). Altogether, these results suggest that the thinner cortex at P2 is due to premature differentiation rather than defects in cell survival or changes in cell density.

Cilia regulate RGC apical domain size through the mTORC1 pathway

In the kidney, deletion of the primary cilium by knockout of Kif3a caused cell enlargement as a result of abnormal upregulation of the mTORC1 pathway (Boehlke et al., 2010; Orhon et al., 2016). To test whether cilia regulate the size of the RGC apical domain through the mTORC1 pathway, we analyzed dorsal telencephalic lysates from controls and ciliary mutants, at E14.5, for phosphorylation of

Development (2017) 144, 201-210 doi:10.1242/dev.138271

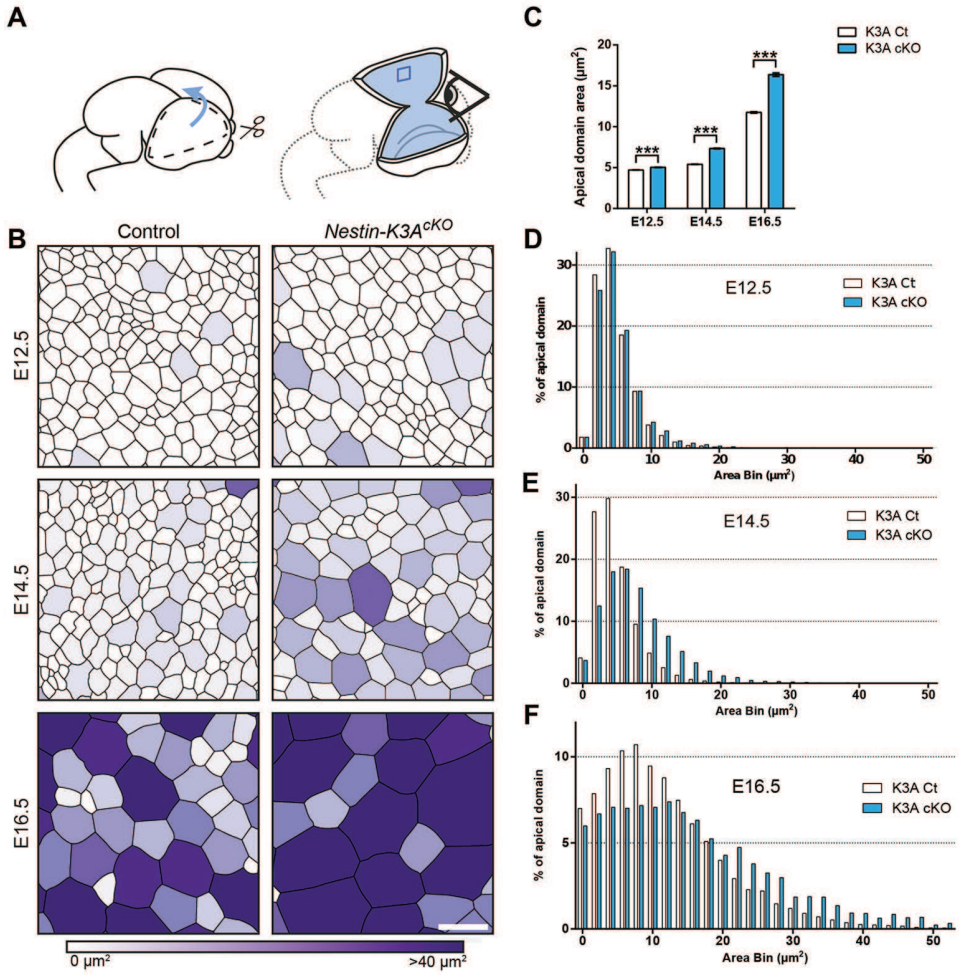

Fig. 2. Cilia abrogation leads to the progressive enlargement of RGC apical domains. (A) Schematic representation of embryonic forebrain dissection for whole mount preparations of cortical ventricular surfaces. (B) Cortical surfaces immunostained with the ZO-1 antibody shown in Fig. S2A were skeletonized to obtain segmented images of representative cortical surfaces at E12.5, E14.5 and E16.5 of controls and Kif3A ciliary mutants. The surface areas per cell are color coded from white (less than 10 μm^2) to dark purple (more than 40 μm^2). (C) Quantification of the surface area of the apical domains in controls (white) and ciliary mutants (blue) at E12.5, E14.5 and E16.5. (D,E,F) Sample distribution of apical domain areas in control (white) and Kif3a^{cKO} (blue) embryos at E12.5 (D), E14.5 (E) and E16.5 (F) (2 μm^2 bins). Numbers of apical domains measured in B at E12.5 (11805 for controls and 13329 for K3A^{cKO}, *n*=3), at E14.5 (12731 for controls and 9173 for K3A^{cKO}, *n*=3) and E16.5 (8895 for controls and 7476 for K3A^{cKO}, *n*=3). Apical domains measured in C: 100 per genotype blind to the conditions. Scale bar: 5 μm.

mTOR and its targets p70S6K, S6RP (S6 ribosomal protein) and 4E-BP1, which are established markers of mTORC1 activity. The levels of phosphorylated mTOR and downstream targets increased significantly in ciliary *Nestin-K3A^{cKO}* mutants compared with controls (Fig. 4A,B, Fig. S5A). Immunostaining of the downstream mTORC1 effector with an antibody against phosphorylated ribosomal S6 protein (p-S6RP) revealed its localization at the mother centriole of the centrosome and at the apical surface of mitotic RGCs (Fig. 4C,D). Interestingly, ciliary mutant apical domains contained more p-S6RP than controls, as shown by the increased intensity of p-S6RP fluorescence at the mutant ventricular surface (Fig. 4E).

To further examine whether the mTOR pathway regulates the size of the RGC apical domain, we injected the mTORC1 inhibitor rapamycin (6 mg/kg) or vehicle intraperitoneally at E12.5. In control embryos, rapamycin injection at E12.5 had no significant effect on the size of RGC apical domain (Fig. 5A,B, Fig. S5B). In *Nestin-K3A^{cKO}* embryos, in which the size of RGC apical domains increased by 35% compared with controls (Fig. 2C), rapamycin injection at E12.5 led to an apical domain size comparable to that observed in control embryos at E14.5 (Fig. 5A-D). These results suggest that rapamycin treatment prevents excessive apical domain enlargement at E14.5 in *Nestin-K3A^{cKO}*, which might result from ineffective downregulation of mTORC1 due to the absence of primary cilia. Interestingly, the misorientation of the mitotic spindle and the number of PH3$^+$ basal mitotic figures in the developing somatosensory cortex was also rescued in cilium-less RGCs of *Nestin-K3A^{cKO}* embryos at E14.5 after a single injection of rapamycin at E12.5 (Fig. 5E,F). These results thus show that cilia abrogation in developing RGCs leads to an abnormal increase in the size of apical domains as a result of upregulation of the mTORC1 pathway, which leads to spindle misorientation in apical mitotic cells and to an abnormal increase in the number of PH3$^+$ basal mitotic figures.

Successive rapamycin injections rescue the ventriculomegaly phenotype

Since the increase in size of the cells can be rescued by rapamycin administration, to further confirm that progressive enlargement of RGC apical domains leads to ventriculomegaly, we injected rapamycin at a low dose (1 mg/kg) once a day between E14.5 and E17.5 and analyzed the size of the lateral ventricles at E19. This low dose of rapamycin was used because we observed a high rate of mortality with consecutive treatments at higher doses. Interestingly, four successive injections of rapamycin rescued the size of the ventricle in ciliary mutants, which was not significantly different from that of control embryos injected with vehicle (Fig. 6). Furthermore, although a single injection of rapamycin had no effect on controls at E14.5 because the mean area of the apical domain was similar at E12.5 and E14.5 (4.7 μm^2 at E12.5 and 4.8 μm^2 at E14.5; Fig. 2C and Fig. 5A,B), we observed that consecutive rapamycin injections significantly decreased the size of the ventricles in control

Development (2017) 144, 201-210 doi:10.1242/dev.138271

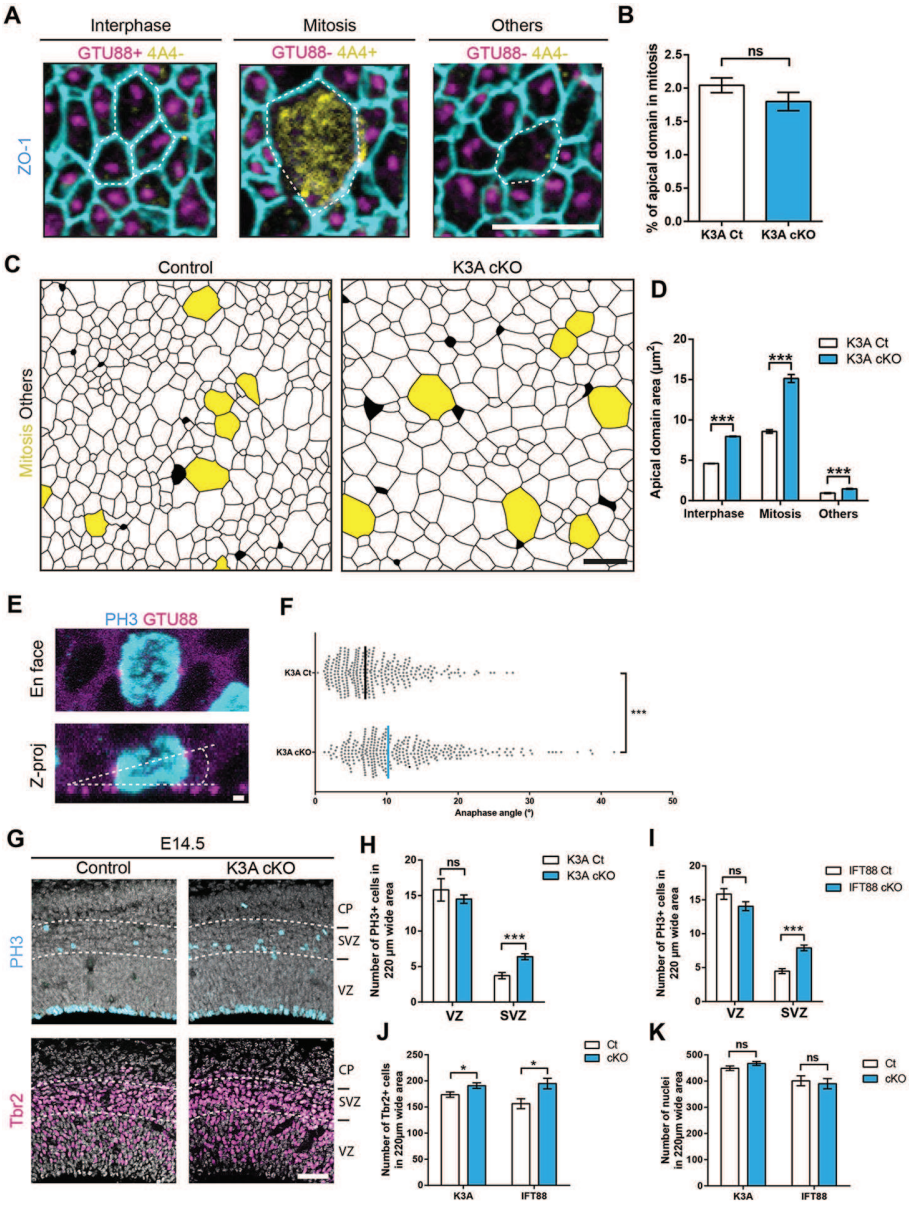

Fig. 3. Apical domain enlargement leads to corticogenesis defects. (A) Triple immunostaining with ZO1 (cell junctions in cyan), GTU88 (pericentriolar marker in magenta) and 4A4 (mitotic cells in yellow) antibodies on E14.5 whole mount cortical surfaces allowed us to classify the cells in three categories: cells in interphase (GTU88^{+}/4A4), cells in mitosis (GTU88^{-}/4A4^{+}) and other cells (GTU88^{-}/4A4^{-}). (B) Quantification in controls and *Nestin-K3A*^{cKO} mutants of the percentage of 4A4^{+} (mitotic) ventricular cells: the total number of mitotic cells contacting the ventricle (number of apical domains in mitosis) was related to the number of GTU88^{-}/4A4^{+} cells. (C) Segmented images of the immunostaining shown in Fig. S3A,B, in which mitotic 4A4^{+} cells are shown in yellow. (D) Quantification of the apical domain areas of control (white) and mutant mice (blue) in each cell category. Data are the mean±s.e.m. *n*=3 per genotype per experimental condition in B and D. Numbers of apical domains analyzed in D in interphase (20279 for controls and 12843 for *Nestin-K3A*^{cKO}), mitotic (432 for controls and 245 for *Nestin-K3A*^{cKO}) and others (604 for controls and 668 for *Nestin-K3A*^{cKO}) cells. (E) *En face* view and *Z*-projection of a cilium-less apically positioned PH3^{+} mutant cell double-immunostained with the GTU88 antibody illustrating the methodology for measuring anaphase spindle orientation. The ventricular surface is delineated by the positions of GTU88^{+} dots in neighboring PH3^{-} cells (angle between dashed lines). (F) Quantification of the angle formed by a line passing through both centrosomes of cilium-less and control PH3^{+} cells and the ventricular surface. Anaphase angles measured in L: 324 per genotype. (G) Representative images of PH3^{+} mitotic cells and Tbr2^{+} intermediate progenitors in coronal sections of the somatosensory cortex of *Nestin-K3A*^{cKO} mutant mice and controls at E14.5. (H,I) Quantification of PH3^{+} mitotic cells in the SVZ on a 220-μm-wide area from *Nestin-K3A*^{cKO} and *Nestin-Ift88*^{cKO} mice shows a significant increase in the mutants compared to the controls. (J,K) Quantification of Tbr2^{+} intermediate progenitor cells and DAPI^{+} cells in 220-μm-wide areas of *Nestin-K3A*^{cKO} and *Nestin-Ift88*^{cKO} mice and their respective controls. Data are the mean±s.e.m. in B,D,H-K or median in F (*n*=3 per genotype). Scale bars: 5 μm (A,C); 1 μm (E); 50 μm (G).

embryos (Fig. 6), suggesting that mTORC1 inhibition by rapamycin treatment acts as a brake on the enlargement of RGC apical domains but does not decrease the size of the apical domains. These results suggest that the progressive increase in RGC apical domain size during normal cortical development contributes to ventricle morphogenesis and that it is regulated by the mTOR pathway (Fig. 2), although rapamycin treatment might also affect other cell types surrounding the ventricles (Magri and Galli, 2013).

Development (2017) 144, 201-210 doi:10.1242/dev.138271

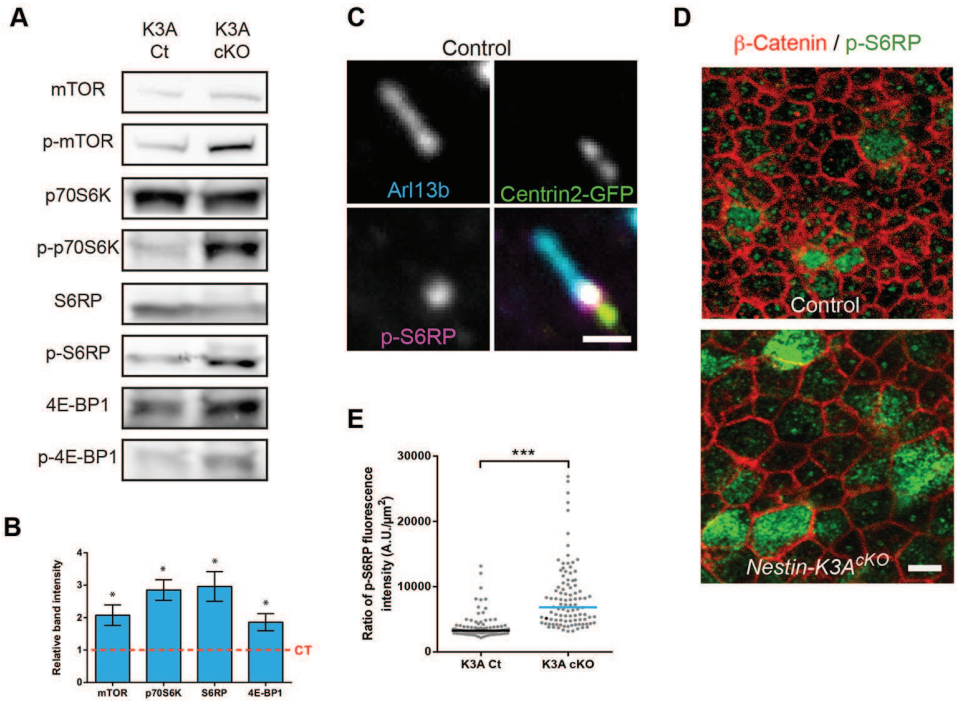

Fig. 4. Cilia abrogation leads to an increase in the mTORC1 pathway. (A) Western blot analysis of E14.5 control and cilium-less cortical lysates shows increased phosphorylation of mTOR targets in ciliary mutants compared with controls. (B) Quantification of bands from three independent experiments (A) shows that the increase in mTOR pathway activity in ciliary mutants compared with controls is significant. (C) Double immunostaining of an E14.5 Centrin-2-GFP control cortical ventricular surface with Arl13b (cilia, cyan), and phosphorylated S6RP (p-S6RP, magenta) antibodies showing p-S6RP staining at the mother centriole of the centrosome in ciliated cells. (D) Double immunostaining of E14.5 cortical surfaces from control and *Nestin-K3A*^{cKO} ciliary mutants with antibodies against β-catenin (red) and p-S6RP (green). (E) Quantification of the ratio between the intensity of p-S6RP fluorescence and the surface area of the apical domain in controls and *Nestin-K3A*^{cKO} ciliary mutants at E14.5 shows an increase in the level of p-S6RP in the mutants. Apical domains measured in E: 100 per genotype blind to the condition. Scale bars: 1 µm (C) and 5 µm (D).

DISCUSSION

In the present study, we genetically ablated the primary cilium of RGCs using Ift88 or Kif3a conditional mutant mice and observed a progressive increase in the size of their ventricular apical domains through upregulation of the mTORC1 pathway. These defects are associated with a significant perturbation of their mitotic spindle orientation, an overproduction of basal mitotic progenitors at E14.5, a decreased number of cortical neurons at later stages and progressive enlargement of the lateral ventricles, defined as ventriculomegaly. Interestingly, all these defects were attributable to an abnormal increase in mTORC1 pathway activity as they were rescued by one or several injections of the mTORC1 inhibitor rapamycin. Altogether, this study shows for the first time that the primary cilium of RGCs regulates ventricular morphogenesis through control of the size of their ventricular contact by acting as a brake on the mTORC1 signaling pathway.

Here, we used conditional knockout of ciliary genes (*Ift88* and *Kif3a*) in *Nestin-Cre* mice to deplete RGCs of their primary cilium, bypassing its role in brain patterning and the polarity of neuroepithelial cells (Benadiba et al., 2012; Besse et al., 2011; Higginbotham et al., 2013; Willaredt et al., 2008; Wilson et al., 2011). Although Nestin-Cre expression starts around E10.5 in the forebrain, cilia abrogation in the VZ was complete only at E14.5, as previously shown (Liang et al., 2012; Fig. S1A-E). The phenotypes observed at E12.5 might thus be partially due to inefficient recombination before E12.5. Moreover, Nestin is broadly expressed at later developmental stages, suggesting that some of the phenotypes observed in ciliary mutants are, in part, due to non-cell-autonomous effects.

During their development from RGCs (Spassky et al., 2005), multiciliated ependymal cells enlarge their apical domain (Mirzadeh et al., 2010). It is thus possible that the enrichment of ciliary mutants in large apical domains at a given developmental stage corresponds to premature ependymal differentiation. However, the numbers of ventricular CD24^{+}/centrin-2 (Cetn2)-GFP^{+} cells at E18.5 were similar in controls and ciliary mutants, ruling out this hypothesis (Fig. S4D). Another possibility is that depletion of cilia leads to defects in the cytoskeleton and adherens junctions, resulting in increases in ventricular cell delamination and available space at the ventricular surface, and ultimately to enlargement of the apical domains. However, no defects in either adherens junctions or actin cytoskeleton were observed by immunostaining the cortical ventricular surface during corticogenesis in mutant RGC (Fig. S4C). Altogether these observations suggest that ventriculomegaly is due to apical domain enlargement of RGC before their differentiation into ependymal cells, ruling out a contribution of ependymal dysfunction during embryogenesis. The prenatal ventriculomegaly described here precedes and might contribute to the initiation of hydrocephalus observed at postnatal stages (this study and Tong et al., 2014). Postnatal hydrocephalus can thus be caused by a variety of factors including defects in ventricular morphogenesis (this study), disturbed CSF flow due to impaired ependymal cilia function, over-production of CSF by the choroid plexus (Del Bigio, 2010) or combinations of these factors.

Development (2017) 144, 201-210 doi:10.1242/dev.138271

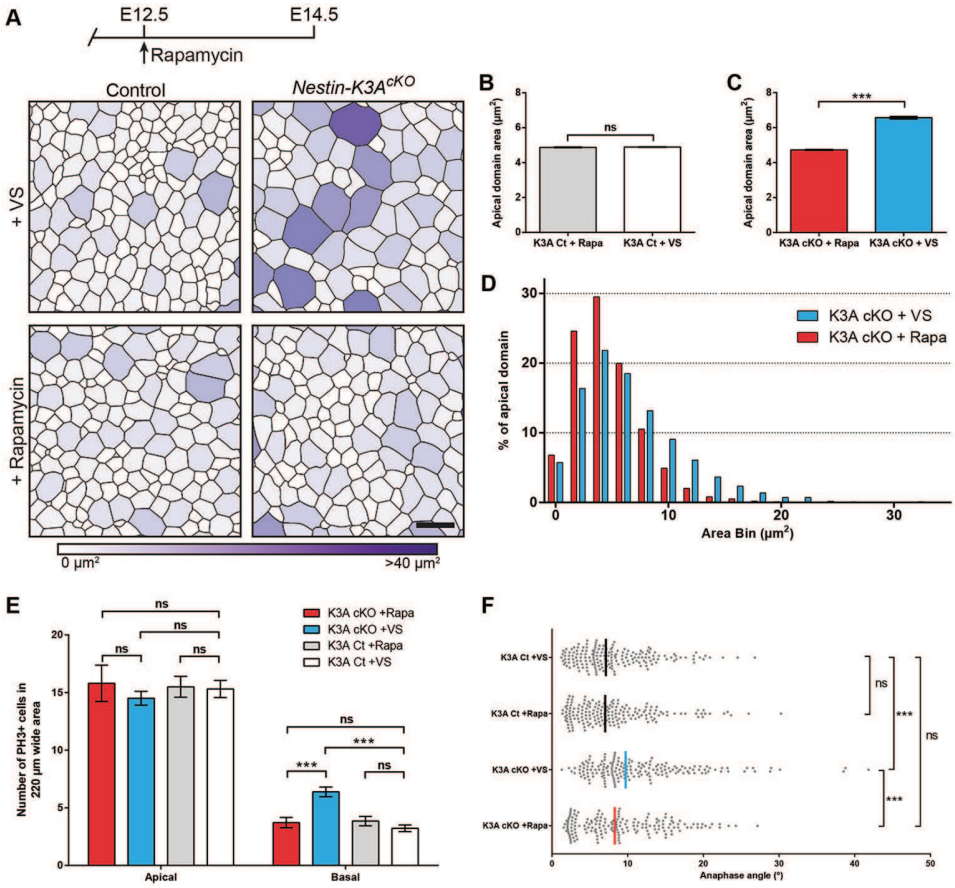

Fig. 5. Apical domain enlargement and corticogenesis defects at E14.5 are rescued by a single rapamycin injection at E12.5. (A) Cortical surfaces immunostained with ZO-1 antibody shown in Fig. S5B were skeletonized to obtain segmented images of representative cortical surfaces at E14.5 from controls and *Nestin-K3A*^{cKO} ciliary mutants injected with rapamycin or vehicle solution. Color code is as described in Fig. 2. (B,C) Quantification of apical domain areas at E14.5 shows a significant decrease in rapamycin-injected (red bar in C) compared with vehicle-injected ciliary mutants (blue bar in C); no significant difference is observed between rapamycin- and vehicle-injected controls (B). (D) Distribution of apical domain surfaces in cortices from E14.5 mutants injected with vehicle (blue) or rapamycin (red). (E) Quantification of the relative number of PH3^{+} cells in 220-µm-wide areas on coronal sections at E14.5 in rapamycin- and vehicle-injected controls and ciliary mutants shows significant rescue of the number of basally positioned PH3^{+} cells, which return to normal levels in rapamycin-injected ciliary mutants but not in controls. (F) Quantification of anaphase angles of PH3^{+} apical cells in control and ciliary mutants injected with rapamycin or vehicle show significant rescue of the mitotic spindle misorientation in rapamycin-injected ciliary mutants. Data are the mean±s.e.m. in B-E or the median in F (*n*=3 per genotype per experimental condition). Apical domain analyzed in B-D for vehicle (14040 for controls, 14001 for *Nestin-K3A*^{cKO}) and rapamycin treatment (14900 for controls, 14399 for *Nestin-K3A*^{cKO}). Anaphase angles measured in F: 180 per condition. Scale bar: 5 µm.

In control embryos, RGC apical domains are highly diverse in size at a given developmental stage. The sizes increase throughout development, leading to greater size diversity at later stages (Nishizawa et al., 2007; this study). Enlargement is also observed in ciliary mutants and is greater than in control embryos. Further studies should determine the effects of apical domain morphology, mode of division and long-term potentials on the mechanical constraints exerted by RGCs on the morphogenesis of brain ventricles. We have shown here that the enlargement of the RGC apical domain is due to rapamycin-sensitive control of localized cell growth by the primary cilium. mTORC1 signaling, the targets of which are enriched at the apical domain of RGCs, is known to control cell growth by upregulating protein synthesis (Fig. 4A). This raises the question whether local protein synthesis is involved in apical cell enlargement. Although the size of RGC apical domains has not been studied, microcephaly and ventricular enlargement have been reported in mouse mutants in which the activity of the mTOR pathway was, respectively, defective or aberrantly elevated (Cloetta et al., 2013; Way et al., 2009; Magri et al., 2011). Mechanosensory proteins polycystic kidney disease 1 (Pkd1) and Pkd2 are expressed in primary cilia of RGCs, and their ablation leads to postnatal hydrocephalus and planar cell polarity defects in mouse ventricular epithelium (Wodarczyk et al., 2009; Ohata et al., 2015). Moreover, it was shown that Pkd1 can inhibit the mTOR pathway and regulate cell size in the kidney (Distefano et al., 2009). We thus tested whether Pkd1 contributed to the control of the mTOR pathway and cell size in RGCs by measuring the size of the apical domains in *Nestin-Cre* conditional knockouts of floxed *Pkd1*. However, no difference in the surface area of RGC apical domains was observed at E14.5 (Fig. S6), suggesting that primary cilia do not regulate the size of RGCs through the mechanosensory protein Pkd1 via the mTOR pathway. Interestingly, it was recently discovered that primary cilium-dependent autophagy regulates kidney epithelial cell size through the LKB1-AMPK-mTOR signaling pathway in response to fluid flow (Orhon et al., 2016). Whether the mTOR pathway and the mechanical stress pathway are coordinated in the control of RGC size in the primary cilium-dependent autophagy pathway is an attractive hypothesis that remains to be investigated.

Development (2017) 144, 201-210 doi:10.1242/dev.138271

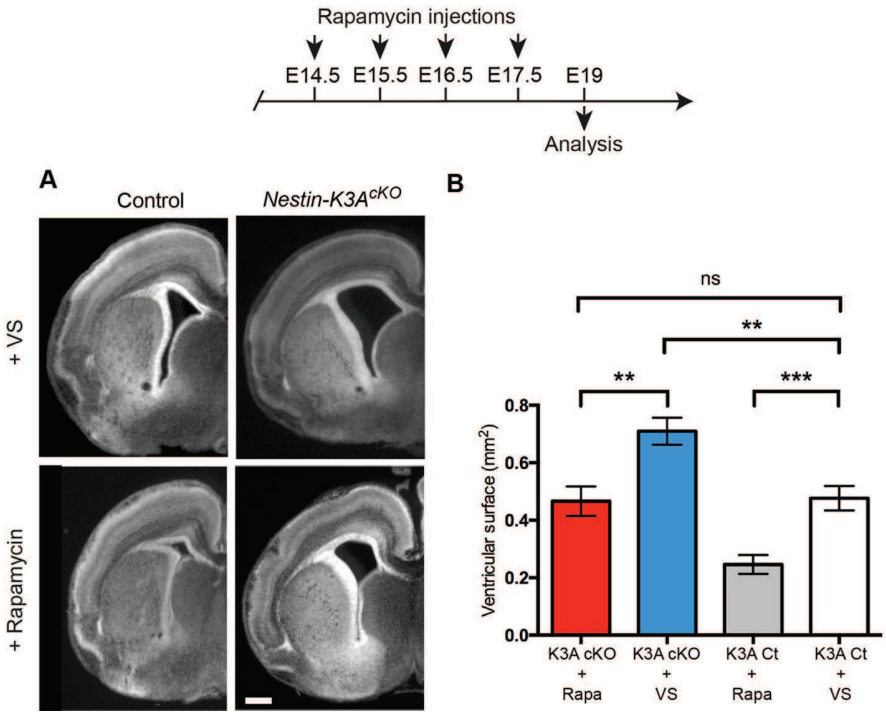

Fig. 6. Ventriculomegaly phenotype at E19 is rescued by repeated rapamycin injections from E14.5 to E17.5. (A) Representative coronal sections of control and *Nestin-K3A*^{cKO} mutant forebrains at E19. (B) Quantification of the area of the lateral ventricle in control and ciliary mutants injected with rapamycin or vehicle solution from E14.5 to E17.5 show the rescue of the ventriculomegaly phenotype after successive injections of rapamycin. Scale bar: 500 µm.

Further studies are thus required to identify the upstream signals of the mTOR pathway in these cells. Altogether, our results shed light on a new role of the primary cilium in the local control of cell growth and ventricular morphogenesis during brain development.

MATERIALS AND METHODS

Mouse strains

All animal care was in accordance with French and European legislation. All the mice used in this study were previously described: *Kif3a*^{fl}, *Kif3a*$^{ko/+}$ (Marszalek et al., 1999), *IFT88*^{fl}, *IFT88*$^{ko/+}$ (Haycraft et al., 2007), *Nestin-Cre* (Tronche et al., 1999), *FoxG1-Cre* (Hébert and McConnell, 2000), *Rosa26*^{mTmG} (Muzumdar et al., 2007), *Centrin-2-GFP* (Higginbotham et al., 2004). To produce conditional Kif3a and IFT88 mutants, we crossed *Kif3a*$^{fl/fl}$ or *IFT88*$^{fl/fl}$ mice with *Kif3a*$^{ko/+}$ *Nestin-Cre*$^{+/-}$ or *IFT88*$^{ko/+}$ *Nestin-Cre*$^{+/-}$ mice, respectively. To obtain conditional *Kif3a FoxG1* mutants, we crossed *Kif3a*$^{fl/fl}$ with *Kif3a*$^{ko/+}$ *FoxG1-Cre*$^{+/-}$. *Nestin::Cre;Kif3a*$^{ko/fl}$, *Nestin::Cre;Ift88*$^{ko/fl}$ and *Nestin::Cre;FoxG1*$^{ko/fl}$ were used as ciliary mutants, whereas *Nestin::Cre;Kif3a*$^{fl/+}$, *Nestin::Cre;Ift88*$^{fl/+}$ and *Nestin::Cre;FoxG1*$^{fl/+}$ mice were used as controls. We also crossed *Kif3a*$^{fl/fl}$ *Centrin-2*$^{GFP/GFP}$ mice with *Kif3a*$^{ko/+}$ *Nestin-Cre*$^{+/-}$ mice to generate conditional mutants with GFP^{+} centrioles. The mice were maintained on a C57Bl6/J background. E0.5 was defined as noon on the day the vaginal plug was detected.

Immunofluorescence, *en face* views and *in situ* hybridization

Mouse brains were fixed by immersion in 4% paraformaldehyde at 4°C for 4 h (embryonic brains) or overnight (postnatal brains) then washed several times in PBS. Coronal sections (80 or 100 µm) were cut on a Vibratome (S1000, Leica). For *en face* views, telencephalic hemispheres were first isolated in DMEM/F12 (Life Technologies) and fixed in 4% paraformaldehyde (PFA) in PBS for 1 h at 4°C. Tissues were then washed in PBS and immunostained as described below. Before mounting, the ventral telencephalon was removed with Pascheff–Wolff microscissors on a silicone rubber plate, and the dorsal telencephalon was flat-mounted by making a few cuts around the edge.

For immunostaining, samples were blocked for 30 min to 1 h in PBS containing 0.1% Triton X-100 and 10% fetal bovine serum, and then incubated overnight with the primary antibodies. The following antibodies were used: rabbit anti-activated caspase-3 (1:1000, Cell Signaling, 9662), rabbit anti-ZO-1 (1:100, Life Technologies, 402200), rat anti-ZO-1 (1:100, Developmental Studies Hybridoma Bank, AB2205518), rabbit anti-Ninein (gift from Michel Bornens; Mogensen et al., 2000), rabbit anti-Tbr2 (1:500, Abcam, ab23345), rabbit anti-Adenylate cyclase 3 (1:500, Santa Cruz, sc-588), mouse anti-Arl13b (1:500, NeuroMab, 75-287), mouse anti-N-cadherin (1:100, BD Biosciences, 610921), rabbit anti-phospho-Histone H3 (Ser10) (1:500, Millipore, 06-570), mouse anti-Vimentin (phospho S55) [4A4] (1:1000, Abcam, ab22651; Weissman et al., 2003), rabbit anti-Pax6 (1:1000, Millipore, AB5409), rabbit anti-Ctip2 [25B6] (1:1000, Millipore, ab18465), mouse anti-β-catenin (1:500, Millipore, 05-665), mouse anti-acetylated tubulin [6-11-B1] (1:500, Sigma-Aldrich, T6793), mouse anti-γ-Tubulin [GTU-88] (1:500, Sigma Aldrich, T6557), mouse anti-Actin (1:100, Millipore, mab1501), rabbit anti-phospho-S6 ribosomal protein (1:100, Cell Signaling, 2211), rat anti-CD24 (1:100, BD Pharmingen, 557436) and species-specific Alexa Fluor 488, 594 and 647 (1:1000, Life Technologies) secondary antibodies. Tissues were counterstained with DAPI (Sigma), mounted in Fluoromount (Southern Biotech) and examined with a confocal fluorescence microscope (SP5 Leica) or a fluorescence microscope (Zeiss Observer.Z1 with Apotome and Hamamatsu camera). For TUNEL staining, coronal cryostat or vibratome sections were labelled with In Situ Cell Death Detection Kit according to the manufacturer's instructions (Roche).

For quantification of cells expressing Ctip2, PH3, Tbr2 or Pax6, a single confocal fluorescent optical section was analyzed. A rectangle with a fixed width (220 µm) spanning the entire thickness of the cortex was placed at a 45° angle to the cortex to approximately mark the somatosensory cortex. Six regions per coronal section on a total of six sections at different rostro-caudal levels were analyzed for each condition. Quantification results are shown as indicated in graphs as a number per unit area (see Fig. 1E and Fig. 3G-J, Fig. S3E-F).

Anaphase spindle orientations were measured on reconstituted *Z*-projections from *en face* view acquisitions, using PH3 and γ-tubulin to identify anaphase and pericentriolar material, respectively. The anaphase angle was the angle between the vector connecting the two anaphase-centrosomes and the vector connecting apical surface centrosomes. For *in situ* hybridization, E12.5 mouse brains were fixed overnight in 4% PFA at 4°C. 100 µm vibratome sections were hybridized as described (López-Bendito et al., 2006) with digoxigenin-labeled *Ngn2* and *Dbx1* probes (Lu et al., 1994).

Development (2017) 144, 201-210 doi:10.1242/dev.138271

Segmentation

Semi-automated segmentation of ZO-1 was performed with Packing Analyzer software (Aigouy et al., 2010), which allows manual correction after automated detection. Segmented images were then vectorized in Illustrator CS6 (Adobe). Finally, images were analyzed with CellProfiler software (Lamprecht et al., 2007) to generate data and color-coded area maps. Edges of the picture were excluded from the analysis.

Scanning and transmission electron microscopy

For scanning electron microscopy, brain embryos were dissected in PBS and fixed in 2% PFA/2.5% glutaraldehyde. Fixed samples were treated with 2% osmium and washed several times in ultrapure water, dehydrated in a graded series of ethanol concentrations and prepared for scanning electron microscopy using the critical point procedure (CPD7501, Polaron). Their surfaces were coated with a 20 nm gold layer using a gold spattering device (Scancoat Six, Edwards). Samples were observed under a Cambridge S260 scanning electron microscope at 15 keV.

For transmission electron microscopy, dorsal E12.5 telencephalons were dissected in PBS then fixed in a 2% PFA/1% glutaraldehyde in 0.1 M phosphate buffer for 3 h. After rinsing in PBS, the tissue was postfixed in 1% osmium tetroxide for 30 min on ice, protected from light, with shaking. The tissue blocks were then dehydrated in 50% and 70% ethanol baths for 7 min each then stained in 1% uranyl acetate in methanol. After the final dehydration, the samples were immersed for 40 min in a graded series of ethanol/Epon solutions (2:1, 1:1, 1:2 ratios), then in pure Epon. The samples were mounted in Epon blocks for 48 h at 60°C to ensure polymerization. Ultrathin sections (70 nm) were cut sagittally on an ultra-microtome (Ultracut E; Leica) and analyzed with a transmission electron microscope (Technai 12, Philips).

Western blotting

Dissected dorsal E12.5 or E14.5 telencephalons were frozen in liquid nitrogen; four or five of the same genotype were pooled. Tissue was homogenized in RIPA lysis buffer (50 mM Tris-HCl pH8, 150 mM NaCl, 1% Igepal CA-630, 0.5% sodium deoxycholate, 0.1% SDS) with Complete ULTRA protease inhibitor cocktail (Roche) and PhosSTOP phosphatase inhibitor cocktail (Roche). The homogenates were centrifuged at 13,500 ***g*** for 30 min at 4°C and the clear lysates stored at −80°C until used. Total protein content was quantified with the BCA protein assay (Thermo Fisher Scientific). Samples were then diluted in 2× Laemmli SDS Sample buffer (BioRad) and boiled for 5 min at 95°C. Equal amounts of protein (50 or 100 µg) were run on precast 7.5% Mini Protean TGX Gels (BioRad) and transferred overnight at 4°C onto nitrocellulose membranes (BioRad). The membranes were blocked in 5% non-fat dry milk in TBS-T (pH 7.4 with 0.1% Tween 20) for 1 h at room temperature. Primary antibodies were diluted in 3% BSA (Sigma Aldrich) and the membranes were incubated overnight at 4°C. We used the following antibodies (1:1000 dilution, from Cell Signaling unless otherwise indicated): rabbit anti-phospho-mTOR (Ser 2448) (2971), rabbit anti-mTOR (2972), rabbit anti-p70S6 kinase (9202), rabbit anti-phospho-p70S6 kinase (9205), rabbit anti-S6 ribosomal protein (2217), rabbit anti-phospho-S6 ribosomal protein (4857), mouse 6F5 anti-Gli3 (1:500, Genentech), mouse anti-GAPDH (1:10,000, Ambion). After removing the primary antibodies, the blots were washed several times in TBS-T then incubated with horseradish peroxidase-conjugated secondary antibodies (1:10,000, Jackson ImmunoResearch). Secondary antibodies were detected by SuperSignal West Dura or West Femto Maximum Chemiluminescent substrate (Thermo Scientific). Signals were analyzed with an ImageQuant LAS 400 device (GE Healthcare). Unsaturated bands were quantified using ImageJ (http://rsb.info.nih.gov/ij).

Rapamycin treatment

Rapamycin (Merck) was dissolved in 100% ethanol, stored at −20°C and diluted in vehicle containing 5% Tween 80 and 5% PEG400 (Sigma-Aldrich) just before injection. For *in vivo* administration, pregnant E12.5 dams received an intraperitoneal injection of rapamycin (1 or 6 mg/kg) or vehicle.

Statistical analysis

For normally distributed data (data shown as the mean±s.e.m.), a two-tailed Student's *t*-test was performed. For nonparametric distributions (data shown as the median), a two-tailed Mann–Whitney test was performed. $*P<0.05$, $**P<0.01$ and $***P<0.001$.

Area of the lateral ventricle was measured by outlining the ventricle of three representative sections and the mean value plotted on the graph ($n=3$) (Figs 1 and 6).

Acknowledgements

We thank Amandine Correia and Christophe Auger (IBENS animal facility) and Benjamin Mathieu (IBENS Imaging facility) for excellent technical assistance. We wish to thank Benoit Aigouy for the Packing Analyzer software, Genentech for the anti-Gli3 antibody, Michel Bornens for the anti-Ninein antibody, Bradley Yoder, Larry Goldstein and Joseph Gleeson for their kind gifts of the IFT88-lox mutant mice, Kif3a-lox and knockout mouse lines and Centrin-2-GFP transgenic mice, respectively. We are very grateful to the members of the Morin and Spassky labs for insightful and stimulating discussions and I. Caillé for critical reading of the manuscript.

Competing interests

The authors declare no competing or financial interests.

Author contributions

Conceptualization and methodology: N.S.; Formal analysis, Investigation and validation: P.F., M.D., A.S., M.F., A.G., N.S.; Resources: A.B., N.S.; Visualization: P.F., A.S., N.S.; Supervision, funding acquisition and project administration: N.S.; Writing – original draft preparation: N.S., P.F.; Writing – review and editing: A.G., A.B., N.S.

Funding

We acknowledge the IBENS Imaging Facility, member of the national infrastructure France-BioImaging, supported by the French National Research Agency (ANR-10-INBS-04, ANR-10-LABX-54 MEMO LIFE, ANR-11-IDEX-0001-02 PSL* Research University Investments for the future) and by the 'Région Ile-de-France' (NERF N° 2011-45, DIM Cerveau et Pensée 'Alpins'), the Fondation pour la Recherche Médicale (N° DGE 20111123023) and the Fédération pour la Recherche sur le Cerveau - Rotary International France (2011). The N.S. laboratory was financed by the Institut National de la Santé et de la Recherche Médicale (INSERM), the Centre National de la Recherche Scientifique (CNRS), the Ecole Normale Supérieure (ENS), the ANR (ANR-12-BSV4-0006), the European Research Council (ERC Consolidator grant 647466), the Fondation pour la Recherche Médicale (FRM20140329547) the Canceropole-IDF (2014-1-PL BIO-11-INSERM 12-1) and the Fondation Pierre-Gilles de Gennes (FPGG03). It was supported by the program 'Investissements d'Avenir' of the French Government and implemented by the ANR (ANR-10-LABX-54 MEMOLIFE and ANR-11-IDEX-0001-02 PSL* Research University). P.F. and M.D. were supported by a doctoral grant from Sorbonne Universités and by the MEMO LIFE program (P.F.). Deposited in PMC for immediate release.

Supplementary information

Supplementary information available online at
http://dev.biologists.org/lookup/doi/10.1242/dev.138271.supplemental

References

Aigouy, B., Farhadifar, R., Staple, D. B., Sagner, A., Röper, J.-C., Jülicher, F. and Eaton, S. (2010). Cell flow reorients the axis of planar polarity in the wing epithelium of Drosophila. *Cell* **142**, 773-786.

Banizs, B., Pike, M. M., Millican, C. L., Ferguson, W. B., Komlosi, P., Sheetz, J., Bell, P. D., Schwiebert, E. M. and Yoder, B. K. (2005). Dysfunctional cilia lead to altered ependyma and choroid plexus function, and result in the formation of hydrocephalus. *Development* **132**, 5329-5339.

Benadiba, C., Magnani, D., Niquille, M., Morlé, L., Valloton, D., Nawabi, H., Ait-Lounis, A., Otsmane, B., Reith, W., Theil, T. et al. (2012). The ciliogenic transcription factor RFX3 regulates early midline distribution of guidepost neurons required for corpus callosum development. *PLoS Genet.* **8**, e1002606.

Besse, L., Neti, M., Anselme, I., Gerhardt, C., Ruther, U., Laclef, C. and Schneider-Maunoury, S. (2011). Primary cilia control telencephalic patterning and morphogenesis via Gli3 proteolytic processing. *Development* **138**, 2079-2088.

Boehlke, C., Kotsis, F., Patel, V., Braeg, S., Voelker, H., Bredt, S., Beyer, T., Janusch, H., Hamann, C., Gödel, M. et al. (2010). Primary cilia regulate mTORC1 activity and cell size through Lkb1. *Nat. Cell Biol.* **12**, 1115-1122.

Carter, C. S., Vogel, T. W., Zhang, Q., Seo, S., Swiderski, R. E., Moninger, T. O., Cassell, M. D., Thedens, D. R., Keppler-Noreuil, K. M., Nopoulos, P. et al. (2012). Abnormal development of NG2+PDGFR-α+ neural progenitor cells leads to neonatal hydrocephalus in a ciliopathy mouse model. *Nat. Med.* **18**, 1797-1804.

Chau, K. F., Springel, M. W., Broadbelt, K. G., Park, H.-Y., Topal, S., Lun, M. P., Mullan, H., Maynard, T., Steen, H., LaMantia, A. S. et al. (2015). Progressive differentiation and instructive capacities of amniotic fluid and cerebrospinal fluid proteomes following neural tube closure. *Dev. Cell* **35**, 789-802.

Cloetta, D., Thomanetz, V., Baranek, C., Lustenberger, R. M., Lin, S., Oliveri, F., Atanasoski, S. and Ruegg, M. A. (2013). Inactivation of mTORC1 in the developing brain causes microcephaly and affects gliogenesis. *J. Neurosci.* **33**, 7799-7810.

Del Bigio, M. R. (2010). Ependymal cells: biology and pathology. *Acta Neuropathol.* **119**, 55-73.

Delaval, B., Bright, A., Lawson, N. D. and Doxsey, S. (2011). The cilia protein IFT88 is required for spindle orientation in mitosis. *Nat. Cell Biol.* **13**, 461-468.

Distefano, G., Boca, M., Rowe, I., Wodarczyk, C., Ma, L., Piontek, K. B., Germino, G. G., Pandolfi, P. P. and Boletta, A. (2009). Polycystin-1 regulates extracellular signal-regulated kinase-dependent phosphorylation of tuberin to control cell size through mTOR and its downstream effectors S6K and 4EBP1. *Mol. Cell. Biol.* **29**, 2359-2371.

Eggenschwiler, J. T. and Anderson, K. V. (2007). Cilia and developmental signaling. *Annu. Rev. Cell Dev. Biol.* **23**, 345-373.

Guemez-Gamboa, A., Coufal, N. G. and Gleeson, J. G. (2014). Primary cilia in the developing and mature brain. *Neuron* **82**, 511-521.

Haycraft, C. J., Zhang, Q., Song, B., Jackson, W. S., Detloff, P. J., Serra, R. and Yoder, B. K. (2007). Intraflagellar transport is essential for endochondral bone formation. *Development* **134**, 307-316.

Hébert, J. and McConnell, S. (2000). Targeting of cre to the Foxg1 (BF-1) locus mediates loxP recombination in the telencephalon and other developing head structures. *Dev.Biol.* **222**, 296-306.

Higginbotham, H., Bielas, S., Tanaka, T. and Gleeson, J. G. (2004). Transgenic mouse line with green-fluorescent protein-labeled Centrin 2 allows visualization of the centrosome in living cells. *Transgenic Res.* **13**, 155-164.

Higginbotham, H., Guo, J., Yokota, Y., Umberger, N. L., Su, C.-Y., Li, J., Verma, N., Hirt, J., Ghukasyan, V., Caspary, T. et al. (2013). Arl13b-regulated cilia activities are essential for polarized radial glial scaffold formation. *Nat. Neurosci.* **16**, 1000-1007.

Ibanez-Tallon, I., Heintz, N. and Omran, H. (2003). To beat or not to beat: roles of cilia in development and disease. *Hum. Mol. Genet.* **12**, R27-R35.

Kim, S., Zaghloul, N. A., Bubenshchikova, E., Oh, E. C., Rankin, S., Katsanis, N., Obara, T. and Tsiokas, L. (2011). Nde1-mediated inhibition of ciliogenesis affects cell cycle re-entry. *Nat. Cell Biol.* **13**, 351-360.

Kodani, A., Sirerol-Piquer, M. S., Seol, A., Garcia-Verdugo, J.-M. and Reiter, J. F. (2013). Kif3a interacts with Dynactin subunit p150Glued to organize centriole subdistal appendages. *EMBO J.* **32**, 597-607.

Laclef, C., Anselme, I., Besse, L., Catala, M., Palmyre, A., Baas, D., Paschaki, M., Pedraza, M., Métin, C., Durand, B. et al. (2015). The role of primary cilia in corpus callosum formation is mediated by production of the Gli3 repressor. *Hum. Mol. Genet.* **24**, 4997-5014.

Lamprecht, M. R., Sabatini, D. M. and Carpenter, A. E. (2007). CellProfiler™: free, versatile software for automated biological image analysis. *BioTechniques* **42**, 71-75.

Lehtinen, M. K. and Walsh, C. A. (2011). Neurogenesis at the brain–cerebrospinal fluid interface. *Annu. Rev. Cell Dev. Biol.* **27**, 653-679.

Lehtinen, M. K., Zappaterra, M. W., Chen, X., Yang, Y. J., Hill, A. D., Lun, M., Maynard, T., Gonzalez, D., Kim, S., Ye, P. et al. (2011). The cerebrospinal fluid provides a proliferative niche for neural progenitor cells. *Neuron* **69**, 893-905.

Liang, H., Hippenmeyer, S. and Ghashghaei, H. T. (2012). A Nestin-cre transgenic mouse is insufficient for recombination in early embryonic neural progenitors. *Biol. Open* **1**, 1200-1203.

López-Bendito, G., Cautinat, A., Sánchez, J. A., Bielle, F., Flames, N., Garratt, A. N., Talmage, D. A., Role, L. W., Charnay, P., Marín, O. et al. (2006). Tangential neuronal migration controls axon guidance: a role for neuregulin-1 in thalamocortical axon navigation. *Cell* **125**, 127-142.

Lowery, L. A. and Sive, H. (2009). Totally tubular: the mystery behind function and origin of the brain ventricular system. *BioEssays* **31**, 446-458.

Lu, S., Wise, T. L. and Ruddle, F. H. (1994). Mouse homeobox gene Dbx: sequence, gene structure and expression pattern during mid-gestation. *Mech. Dev.* **47**, 187-195.

Magri, L. and Galli, R. (2013). mTOR signaling in neural stem cells: from basic biology to disease. *Cell. Mol. Life Sci.* **70**, 2887-2898.

Magri, L., Cambiaghi, M., Cominelli, M., Alfaro-Cervello, C., Cursi, M., Pala, M., Bulfone, A., Garcia-Verdugo, J. M., Leocani, L., Minicucci, F. et al. (2011). Sustained activation of mTOR pathway in embryonic neural stem cells leads to development of tuberous sclerosis complex-associated lesions. *Cell Stem Cell*, **9**, 447-462.

Marszalek, J. R., Ruiz-Lozano, P., Roberts, E., Chien, K. R. and Goldstein, L. S. B. (1999). Situs inversus and embryonic ciliary morphogenesis defects in mouse mutants lacking the KIF3A subunit of kinesin-II. *Proc. Natl. Acad. Sci. USA* **96**, 5043-5048.

Mirzadeh, Z., Han, Y.-G., Soriano-Navarro, M., Garcia-Verdugo, J. M. and Alvarez-Buylla, A. (2010). Cilia organize ependymal planar polarity. *J. Neurosci.* **30**, 2600-2610.

Mogensen, M. M., Malik, A., Piel, M., Bouckson-Castaing, V. and Bornens, M. (2000). Microtubule minus-end anchorage at centrosomal and non-centrosomal sites: the role of ninein. *J. Cell Sci.* **113**, 3013-3023.

Muzumdar, M. D., Tasic, B., Miyamichi, K., Li, L. and Luo, L. (2007). A global double-fluorescent Cre reporter mouse. *Genesis* **45**, 593-605.

Nigg, E. A. and Stearns, T. (2011). The centrosome cycle: centriole biogenesis, duplication and inherent asymmetries. *Nat. Cell Biol.* **13**, 1154-1160.

Nishizawa, Y., Imafuku, H., Saito, K., Kanda, R., Kimura, M., Minobe, S., Miyazaki, F., Kawakatsu, S., Masaoka, M., Ogawa, M. et al. (2007). Survey of the morphogenetic dynamics of the ventricular surface of the developing mouse neocortex. *Dev. Dyn.* **236**, 3061-3070.

Ohata, S., Herranz-Pérez, V., Nakatani, J., Boletta, A., Garcia-Verdugo, J. M. and Alvarez-Buylla, A. (2015). Mechanosensory genes Pkd1 and Pkd2 contribute to the planar polarization of brain ventricular epithelium. *J. Neurosci.* **35**, 11153-11168.

Orhon, I., Dupont, N., Zaidan, M., Boitez, V., Burtin, M., Schmitt, A., Capiod, T., Viau, A., Beau, I., Kuehn, E. W. et al. (2016). Primary-cilium-dependent autophagy controls epithelial cell volume in response to fluid flow. *Nat. Cell Biol.* **18**, 657-667.

Paridaen, J. T. and Huttner, W. B. (2014). Neurogenesis during development of the vertebrate central nervous system. *EMBO Rep.* **15**, 351-364.

Paridaen, J. T. M. L., Wilsch-Bräuninger, M. and Huttner, W. B. (2013). Asymmetric inheritance of centrosome-associated primary cilium membrane directs ciliogenesis after cell division. *Cell* **155**, 333-344.

Shenton, M. E., Dickey, C. C., Frumin, M. and McCarley, R. W. (2001). A review of MRI findings in schizophrenia. *Schizophr. Res.* **49**, 1-52.

Shinohara, H., Sakayori, N., Takahashi, M. and Osumi, N. (2013). Ninein is essential for the maintenance of the cortical progenitor character by anchoring the centrosome to microtubules. *Biol. Open* **2**, 739-749.

Spassky, N., Merkle, F. T., Flames, N., Tramontin, A. D., Garcia-Verdugo, J. M. and Alvarez-Buylla, A. (2005). Adult ependymal cells are postmitotic and are derived from radial glial cells during embryogenesis. *J. Neurosci.* **25**, 10-18.

Teng, J., Rai, T., Tanaka, Y., Takei, Y., Nakata, T., Hirasawa, M., Kulkarni, A. B. and Hirokawa, N. (2005). The KIF3 motor transports N-cadherin and organizes the developing neuroepithelium. *Nat. Cell Biol.* **7**, 474-482.

Tong, C. K., Han, Y.-G., Shah, J. K., Obernier, K., Guinto, C. D. and Alvarez-Buylla, A. (2014). Primary cilia are required in a unique subpopulation of neural progenitors. *Proc. Natl. Acad. Sci. USA* **111**, 12438-12443.

Tronche, F., Kellendonk, C., Kretz, O., Gass, P., Anlag, K., Orban, P. C., Bock, R., Klein, R. and Schütz, G. (1999). Disruption of the glucocorticoid receptor gene in the nervous system results in reduced anxiety. *Nat. Genet.* **23**, 99-103.

Wang, X., Tsai, J.-W., Imai, J. H., Lian, W.-N., Vallee, R. B. and Shi, S.-H. (2009). Asymmetric centrosome inheritance maintains neural progenitors in the neocortex. *Nature* **461**, 947-955.

Way, S. W., McKenna, J., Mietzsch, U., Reith, R. M., Wu, H. C. J. and Gambello, M. J. (2009). Loss of Tsc2 in radial glia models the brain pathology of tuberous sclerosis complex in the mouse. *Hum. Mol. Genet.* **18**, 1252-1265.

Weissman, T., Noctor, S. C., Clinton, B. K., Honig, L. S. and Kriegstein, A. R. (2003). Neurogenic radial glial cells in reptile, rodent and human: from mitosis to migration. *Cereb. Cortex* **13**, 550-559.

Willaredt, M. A., Hasenpusch-Theil, K., Gardner, H. AR., Kitanovic, I., Hirschfeld-Warneken, V. C., Gojak, C. P., Gorgas, K., Bradford, C. L., Spatz, J., Wolfl, S. et al. (2008). A crucial role for primary cilia in cortical morphogenesis. *J. Neurosci.* **28**, 12887-12900.

Wilson, S. L., Wilson, J. P., Wang, C., Wang, B. and McConnell, S. K. (2011). Primary cilia and Gli3 activity regulate cerebral cortical size. *Dev. Neurobiol.* **72**, 1196-1212.

Wodarczyk, C., Rowe, I., Chiaravalli, M., Pema, M., Qian, F. and Boletta, A. (2009). A novel mouse model reveals that polycystin-1 deficiency in ependyma and choroid plexus results in dysfunctional cilia and hydrocephalus. *PLoS ONE* **4**, e7137.

Wyatt, T. P. J., Harris, A. R., Lam, M., Cheng, Q., Bellis, J., Dimitracopoulos, A., Kabla, A. J., Charras, G. T. and Baum, B. (2015). Emergence of homeostatic epithelial packing and stress dissipation through divisions oriented along the long cell axis. *Proc. Natl. Acad. Sci. USA* **112**, 5726-5731.

Zhang, J., Williams, M. A. and Rigamonti, D. (2006). Genetics of human hydrocephalus. *J. Neurol.* **253**, 1255-1266.

SUPPLEMENTARY FIGURES

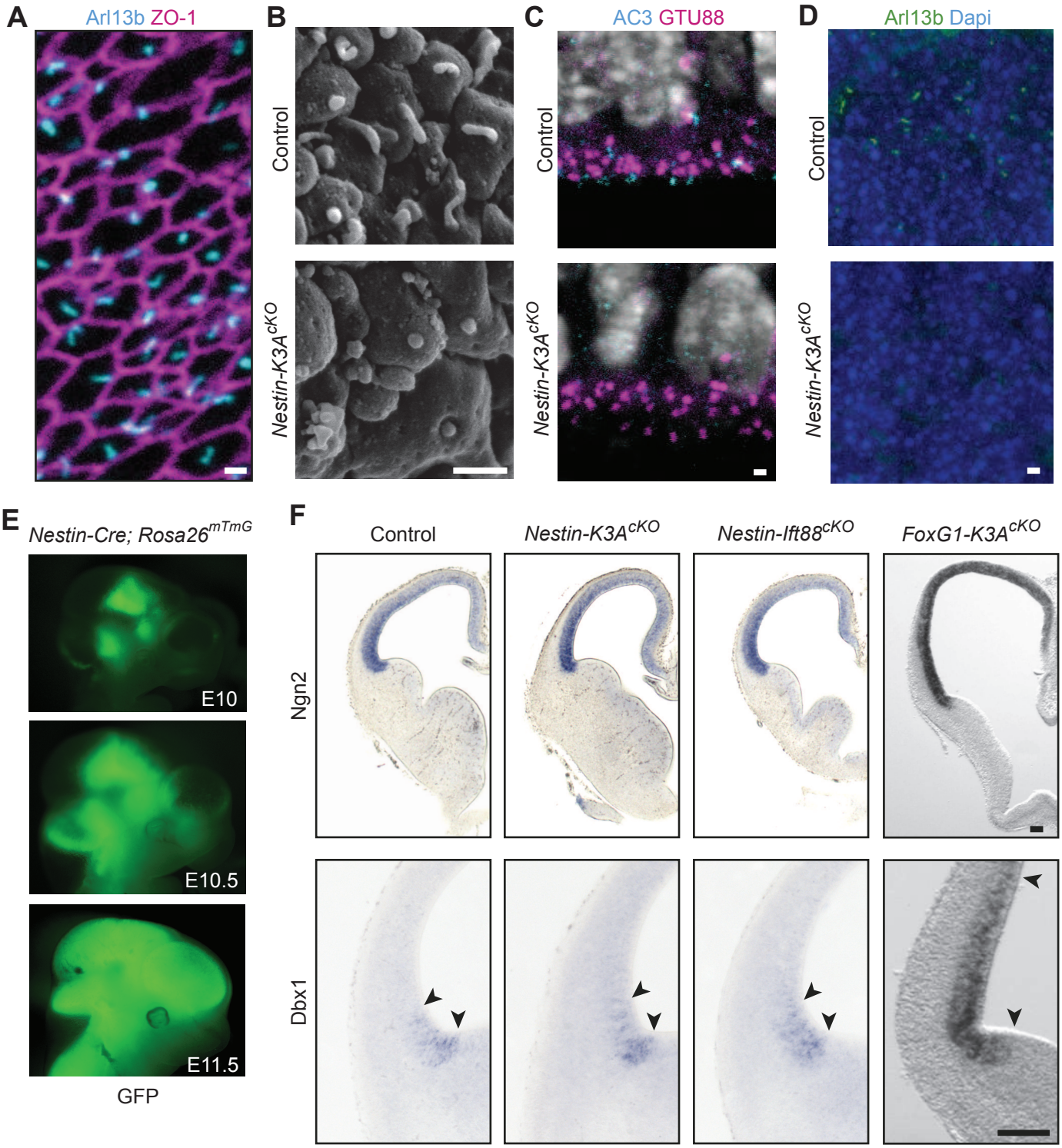

Figure S1: Patterning defects are observed in *FoxG1-cre* but not *Nestin-cre* conditional ciliary mutants. (A) Ventricular surface of the somatosensory cortex at E14.5 double immunostained with Arl13b (primary cilium, cyan) and ZO-1 (cell junctions, magenta) antibodies showing that most cells extend a primary cilium toward the ventricle. (B) Scanning electron micrographs of control and ciliary mutant cortical ventricular surfaces at E14.5 showing the absence of cilia in the mutant. (C) Double immunostaining with adenylate cyclase 3 (AC3, primary cilium, cyan) and GTU88 (pericentriolar material, magenta) antibodies counterstained with DAPI (gray) on coronal sections of the somatosensory cortex of control and *Nestin-K3A*^{cKO} mutant at E14.5 showing the apical localization of basal bodies in ciliary mutants despite the absence of cilia. (D) Immunostaining with Arl13b (green) antibody counterstained with DAPI (blue) on coronal sections of control and *Nestin-K3A*^{cKO} mutant at E14.5 showing the absence of primary cilia in the subventricular zone of the somatosensory cortex, (E) Side view of *Nestin-Cre; Rosa26*^{mTmG} at E10, E10.5 and E11.5 showing that GFP expression is induced from E11 in the telencephalon. (F) *In situ* hybridization with Ngn2 and Dbx1 probes on coronal sections of *Nestin-Ift88*^{cKO}, *Nestin-K3A*^{cKO}, *FoxG1-K3a*^{cKO} conditional mutants and controls at E12.5. Patterning defects are observed in *FoxG1-K3a*^{cKO} mutants, but not in *Nestin-K3A*^{cKO} ciliary mutants or controls. (F) Western blots of cortical lysates from *Nestin-K3A*^{cKO}, *Nestin-Ift88*^{cKO}, *FoxG1-K3a*^{cKO} mutants and their controls at E12.5. The Gli3A- and Gli3R-immunoreactive bands migrate at 190 and 83 kDa, respectively. (G) Quantification of the Gli3A:Gli3R ratio in control and ciliary mutants shows no significant differences among the genotypes except in *FoxG1-K3a*^{cKO} mice in which Gli3A is significantly more abundant compared to Gli3R. Data are the mean ± s.e.m (C). Scale bars: 1 μm in (A-D), 100 μm in (F).

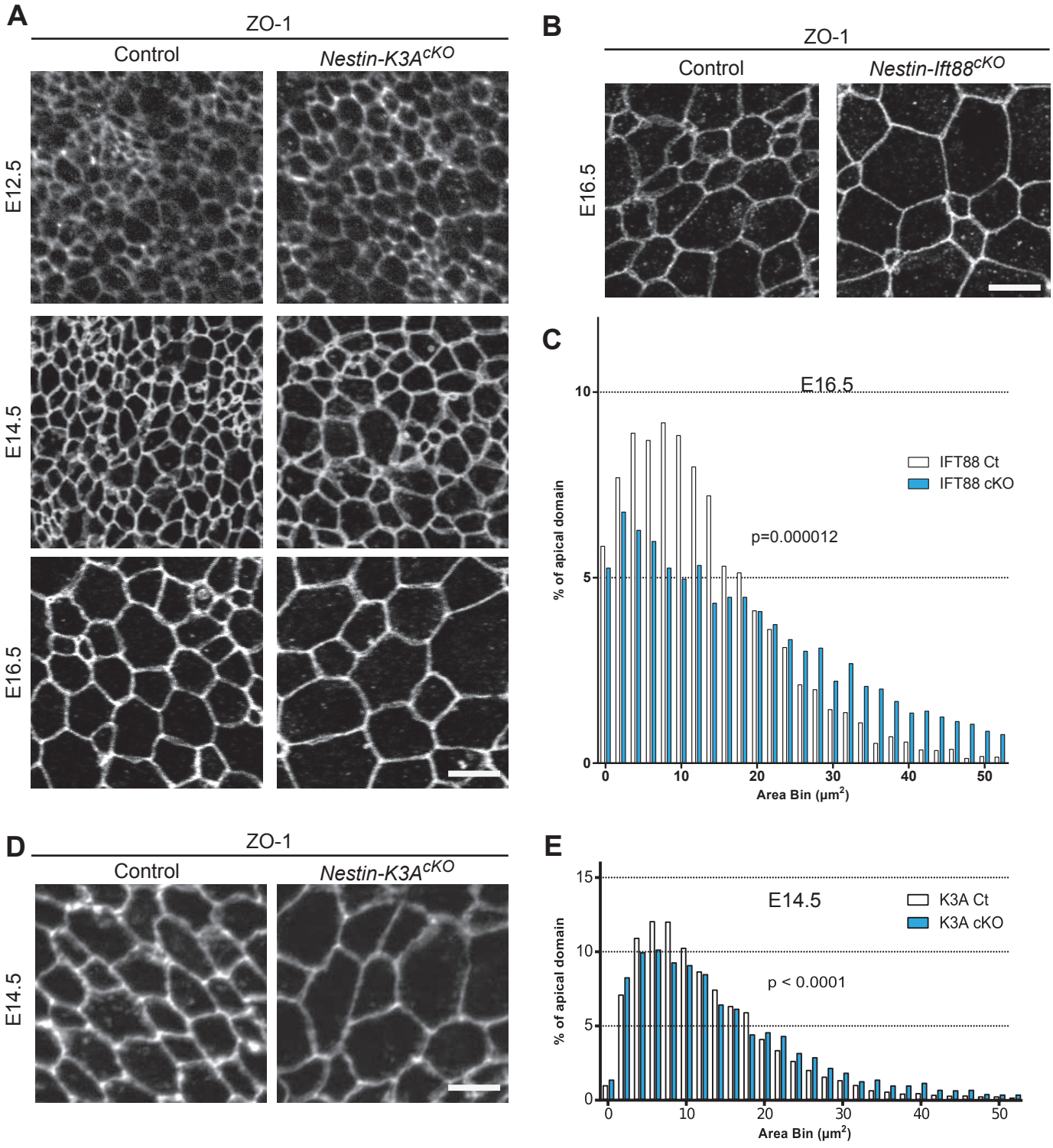

Figure S2: Cilia abrogation leads to RGC apical domain enlargement in the somatosensory cortex and in the LGE. (A) Immunostaining with ZO-1 antibody on ventricular surfaces from whole mounts of the somatosensory cortex of a control and *Nestin-K3A*^{cKO} ciliary mutant at the indicated stages. Corresponding segmented images are shown in Figure 2B. (B) Immunostaining with ZO-1 antibody on ventricular surfaces from whole mounts of control and *Nestin-Ift88*^{cKO} mice at E16.5. (C) Distribution of apical domain surfaces from control (white) and *Nestin-Ift88*^{cKO} (blue) embryos at E16.5 (2 µm^2 bins). (D) Immunostaining with the ZO-1 antibody on ventricular surfaces from whole mounts of the LGE of a control and a *Nestin-K3A*^{cKO} ciliary mutant at E14.5. (E) Distribution of apical domain surfaces of the LGE from control (white) and *Nestin-K3A*^{cKO} (blue) embryos at E14.5 (2 µm^2 bins). Scale bars: 5 µm.

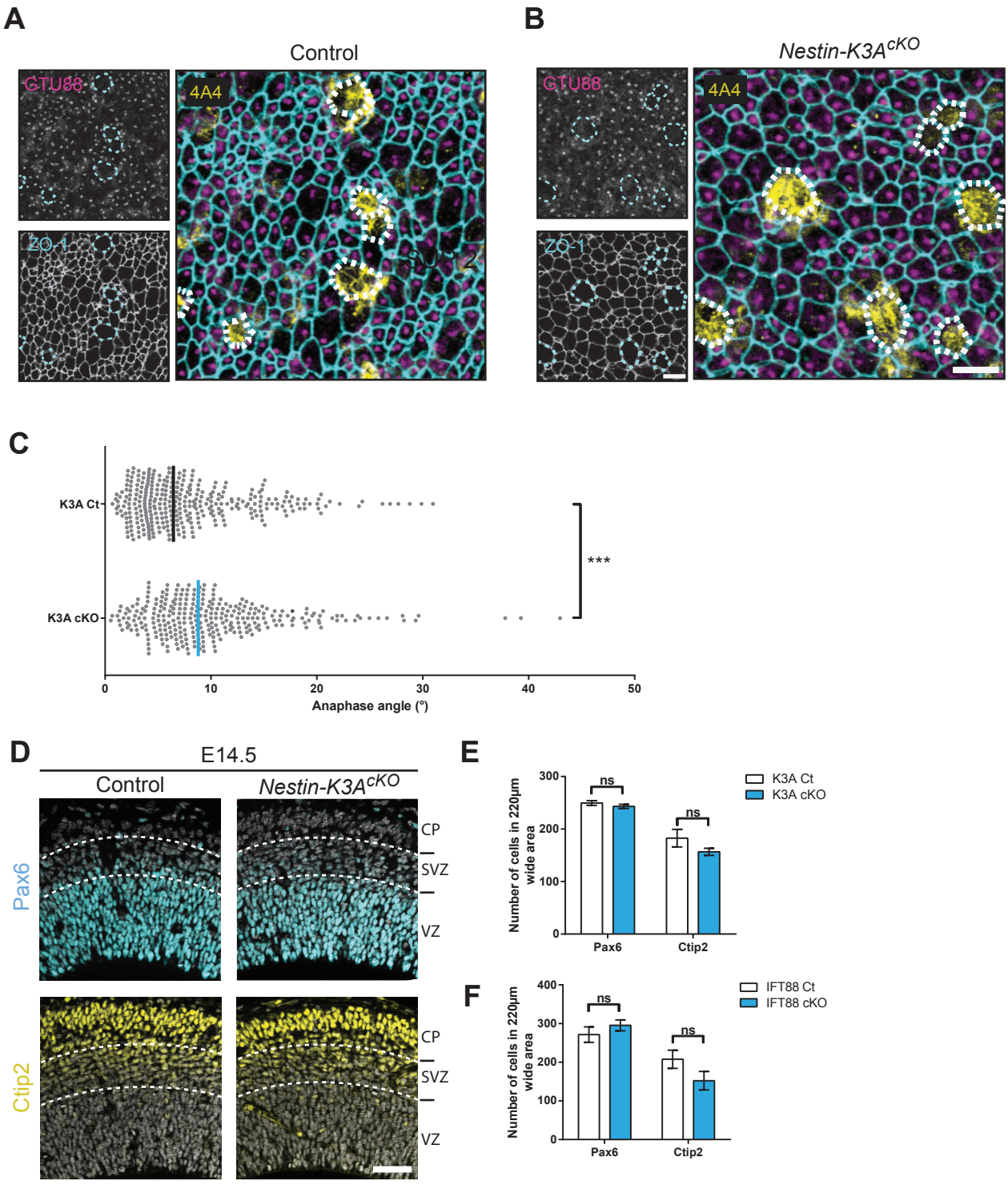

Figure S3: Characterization of cortical cell types in controls and ciliary mutants.

(A-B) Triple immunostaining with ZO-1 (cell junctions, cyan), GTU88 (pericentriolar materials, magenta) and 4A4 (mitotic cells, yellow) antibodies on whole mounts of control (A) and ciliary mutant (B) cortical ventricular walls at E14.5. Corresponding segmented images are shown in Figure 3C. Apical cell contacts of $GTU88^{-}/4A4^{+}$ mitotic cells are outlined by white dotted lines. (C) Quantification of mitotic spindle orientation at E12.5 showing a 31% increase in ciliary mutants compared to controls. Anaphase angles measured: 344 per genotype. (D) Immunostaining with Pax6 (RGC, cyan) or Ctip2 (early-differentiated neurons, yellow) antibodies on E14.5 coronal sections from a control and a $Kif3a^{cKO}$ ciliary mutant. The boundaries between the layers (ventricular zone, VZ; subventricular zone, SVZ; cortical plate, CP) are indicated by white dotted lines. (E, F) Quantification of the numbers of $Pax6^{+}$ and $Ctip2^{+}$ cells in *Nestin-K3A*^{cKO} and *Nestin-Ift88*^{cKO} mutants and their respective controls. Scale bars: 5 µm in A, B and 50 µm in D.

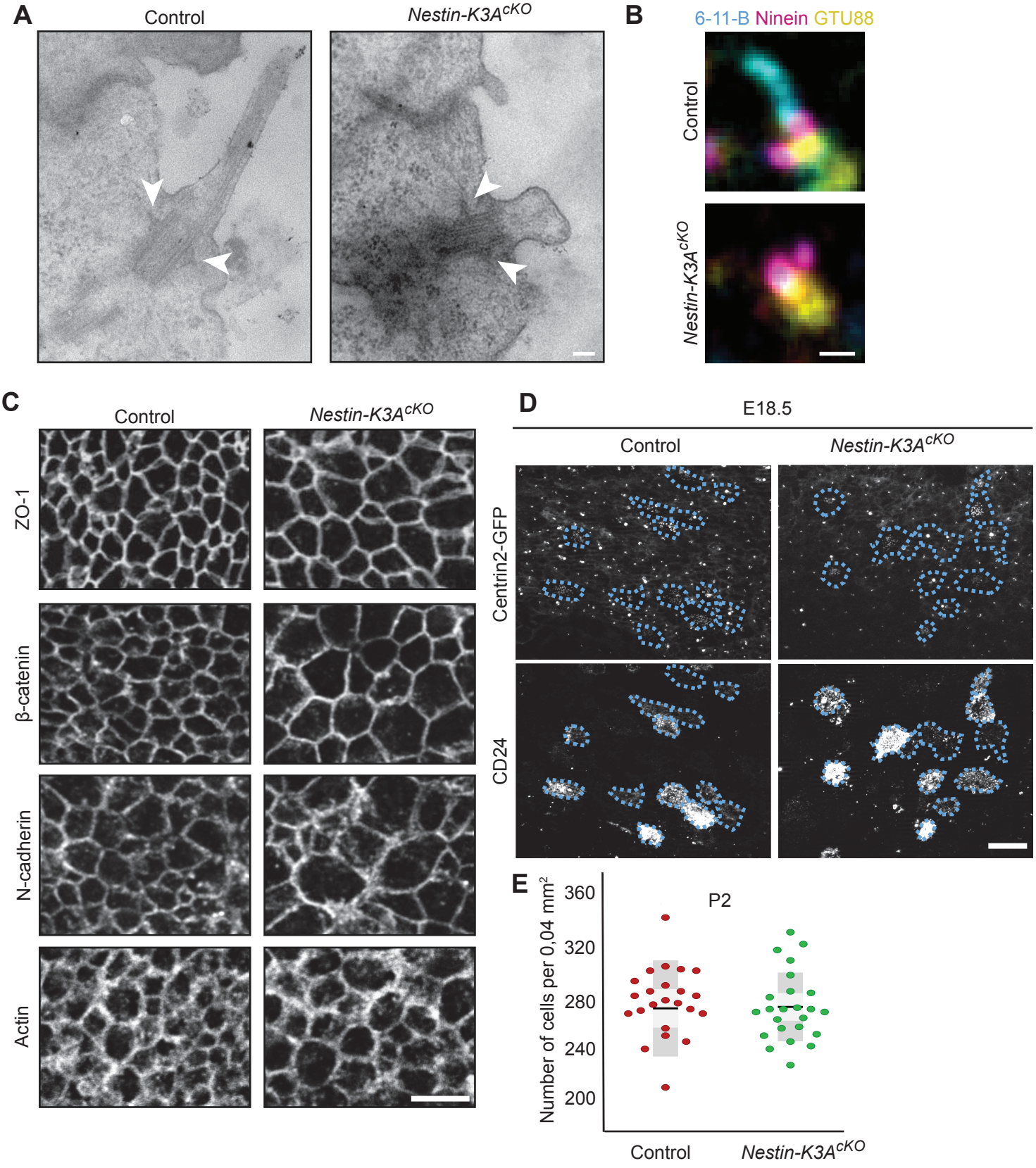

Figure S4: Depletion of the primary cilium from radial glia does not affect cell junctions, centriolar appendage formation or ependymal specification. (A) Transmission electron micrograph of control and ciliary mutant apical domains at E14.5 showing normal formation of subdistal appendages (arrowheads). (B) Triple immunostaining of E14.5 control and mutant cortical ventricular surfaces with 6-11-B (cilia, cyan), ninein (subdistal appendages, magenta) and GTU88 (pericentriolar materials, yellow) antibodies showing similar ninein staining in the control and the mutant despite depletion of primary cilia. (C) Immunostaining with ZO-1, β-catenin, N-cadherin (adherens junctions) or F-actin antibodies on E14.5 WM cortical ventricular surface shows no defects in cell junctions or actin cytoskeleton in ciliary mutants compared to controls. (D) Immunostaining with the CD24 antibody (magenta) on whole mounts of *Centrin2-GFP; Kif3a*^{cKO} mutants or *Centrin2-GFP* control cortices at E18.5; cells specified for the ependymal lineage are recognized by the multiple *Centrin2-GFP*$^{+}$ dots in the cytoplasm and circled with blue dotted lines; similar staining with the CD24 antibody and *centrin2-GFP* transgene show no premature differentiation of multiciliated ependymal cells in the ciliary mutant compared to the control. (E) Quantification of DAPI^{+} cells per 0.04 mm^{2} in the cortex of controls and ciliary mutants at P2. Scale bars: 100 µm in (A), 0.5 µm in (B), 5 µm in (C) and 50 µm in (D).

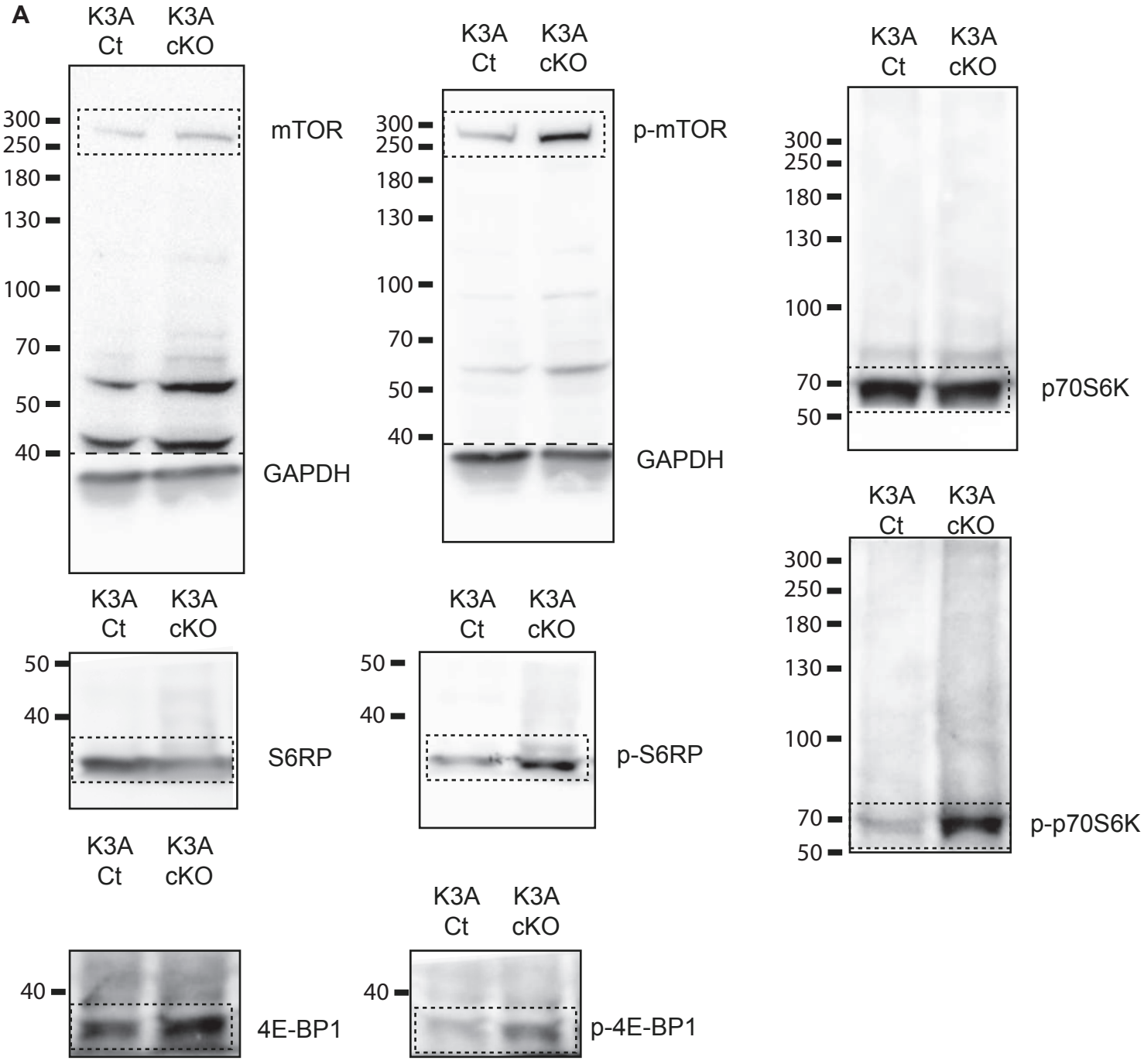

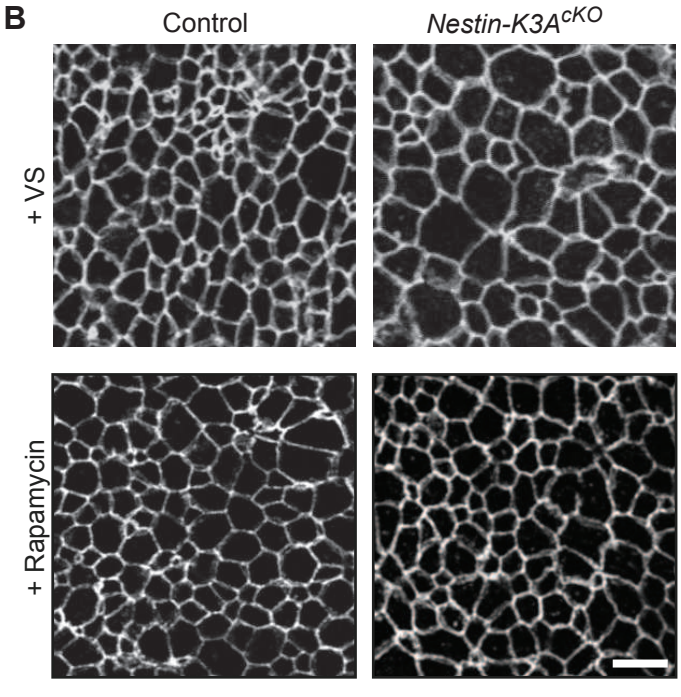

Figure S5: Increased mTORC1 signaling in cilium-less RGC leads to enlargement of the RGC apical domain, which can be rescued by rapamycin treatment. (A) Uncropped images of the western blots shown in Figure 4A. (B) Immunostaining with the ZO-1 antibody of ventricular surfaces on whole mounts of E14.5 control and ciliary mutants injected with vehicle or rapamycin at E12.5. Corresponding segmented images are shown in Figure 4F. Scale bar: 5 µm.

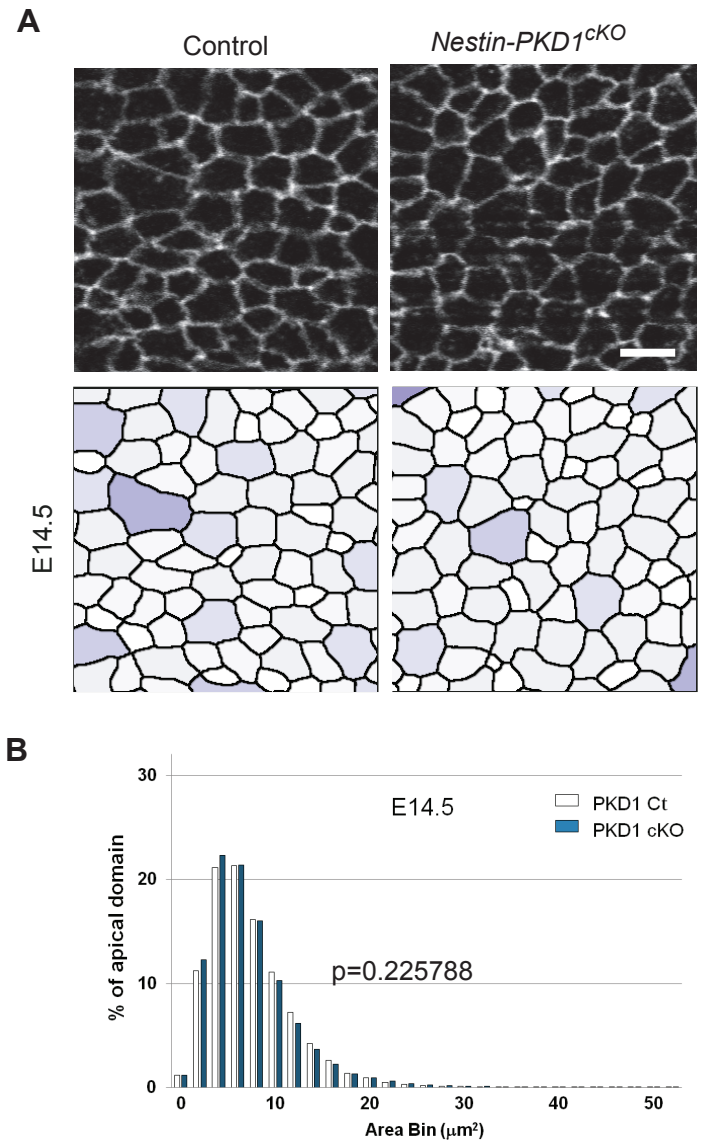

Figure S6: Pkd1 disruption in Nestin-cre derivatives does not lead to enlargement of the RGC apical domain.

(A) Immunostaining with the ZO-1 antibody and corresponding segmented images of ventricular surfaces on whole mounts of an E14.5 control and Pkd1 conditional mutant. (B) Distribution of apical domain surfaces from control (white) and *Nestin-Pkd1*^{cKO} (blue) embryos at E14.5 (2 μm^2 bins). Scale bar: 5 μm.

Résumé

Les cellules épendymaires sont des cellules multiciliées qui tapissent les parois de toutes les cavités du cerveau. Une fois différenciées, ces cellules ne se divisent plus au cours de la vie. Le battement de ces multiples cils motiles joue un rôle important pour maintenir un flux constant de liquide cérébrospinal à travers toutes les cavités cérébrales. Les cellules épendymaires assurent également des fonctions critiques d'échanges moléculaires avec le liquide cérébrospinal. Dans son ensemble, l'implication des cellules épendymaires et de leurs cils motiles s'avère d'une importance majeure dans le maintien des circuits neuraux ainsi que dans le fonctionnement plus global du cerveau. Récemment, une nouvelle caractéristique des cellules épendymaires a été identifiée ; elles font partie d'un micro-environnement appelé une « niche » centrée autour de cellules souches neurales dans le cerveau du rongeur adulte. Ces cellules souches neurales adultes sont capables de produire de nouveaux neurones qui migreront vers le bulbe olfactif des rongeurs adultes.

Concernant leur origine, il a été montré que les cellules épendymaires multiciliées dérivent des cellules souches neurales durant les stades tardifs embryonnaires. Ces mêmes cellules souches peuvent d'ailleurs donner naissance à la plupart des différents types de cellules du cerveau. Cependant, les mécanismes par lesquels les cellules souches décident de leur destin cellulaire restent largement méconnus. Dans ce projet, nous étudions quel type de division donne naissance à des cellules épendymaires et nous nous intéressons également au lignage épendymaire. Nos données suggèrent que les cellules épendymaires ne migrent pas après leur dernière division et qu'elles restent à proximité de l'endroit où elles ont été produites. Chose particulièrement intéressante, nous montrons que les cellules épendymaires peuvent être générées par division symétrique ou asymétrique. Nos résultats révèlent aussi que les cellules souches neurales embryonnaires se divisent de manière asymétrique pour donner naissance à la fois à une cellule épendymaire et à une cellule souche neurale adulte. Ces données viennent s'ajouter à la connaissance actuelle que nous avons du développement du cerveau. De plus, elles pourraient contribuer à ouvrir de nouvelles perspectives et stratégies thérapeutiques pour soigner les maladies neurodégénératives à beaucoup plus long terme.

Mots Clés

Cellules épendymaires, développement du cerveau, cellules de glie radiaire, neurogénèse adulte, cils

Abstract

Ependymal cells are multiciliated cells lining the walls of all brain cavities. Once they are mature, they do not divide during life. Their motile ciliary beating endorses a crucial role in maintaining a proper flow of cerebrospinal fluid throughout all brain cavities. Ependymal cells also ensure critical molecular exchanges of the cerebrospinal fluid. On the whole, the involvement of ependymal cells and their multiple motile cilia in the maintenance of the neural circuits and more globally in the well-functioning of the entire brain have proven paramount. More recently, a new characteristic of ependymal cells has been brought to light. Namely, they are part of a microenvironment so-called a "niche" surrounding adult neural stem cells in the adult rodent brain. Noteworthy, these adult neural stem cells are capable of producing new neurons that will migrate to the olfactory bulb of rodents.

In terms of their origin, it was shown that multiciliated ependymal cells derive from neural stem cells during late embryonic stages. Besides, the same stem cells can give rise to most cell types of the brain. However, little is known about how fate-decision is made in neural stem cells. In this project, we tackle more particularly how multiciliated ependymal cells arise from the neural stem cells. Most specifically, we address the type of cell division and the ependymal cell lineage. We find that ependymal cells are not migrating subsequent to their last division, but rather stay where they were first produced. Most interestingly, they can be generated through both symmetric and asymmetric cell division. We also show that embryonic neural stem cells divide asymmetrically to give rise to both an ependymal cell and an adult stem cell. We are confident that these data bring major new insights in the current understanding of neural development. Additionally, these findings could contribute in opening new therapeutic perspectives and strategies to cure neurodegenerative diseases in a much longer term.

Keywords

Ependymal cells, brain development, radial glial cells, adult neurogenesis, cilia